

RESPONSE OF COASTAL ICHTHYOPLANKTON ASSEMBLAGES OFF
NORTHERN CALIFORNIA TO SEASONAL OCEANOGRAPHIC AND CLIMATE
VARIABILITY

By

Blair Mansfield Winnacott

A Thesis Presented to

The Faculty of Humboldt State University

In Partial Fulfillment of the Requirements for the Degree

Master of Science in Natural Resources: Fisheries

Committee Membership

Dr. Eric Bjorkstedt, Committee Chair

Dr. Andrew Kinziger, Committee Member

Dr. Jose Marin Jarrin, Committee Member

Dr. Erin Kelly, Program Graduate Coordinator

December 2021

ABSTRACT

RESPONSE OF COASTAL ICHTHYOPLANKTON ASSEMBLAGES OFF NORTHERN CALIFORNIA TO SEASONAL OCEANOGRAPHIC AND CLIMATE VARIABILITY

Blair Mansfield Winnacott

This study analyzed samples collected along the Trinidad Head Line (41°N) to characterize variability in the ichthyoplankton assemblage in coastal waters off northern California from late 2007 through 2019, a period during which a major marine heatwave (MHW; late 2014-16) strongly perturbed the ecosystem. I augmented visual identification with genetic techniques to resolve the species composition of visually cryptic larval rockfishes (*Sebastes* spp.). While taxonomic composition off northern California was largely similar to studies off Oregon and Washington, and cross-shelf structure and seasonal patterns in species' abundance were generally consistent with the distribution and phenology of parental stocks, interannual variability in assemblage structure responded strongly to basin scale climate forcing. Specifically, a sharp and persistent increase in the overall abundance of larval fishes (despite declines in a few species with cool-water affinities) and species richness coincided with the unprecedented late 2014-16 MHW that manifested first with the arrival of the "Warm Blob" in coastal waters in late 2014 and was subsequently reinforced by a strong El Niño event in 2015-16. During this event, several rare or previously unrecorded taxa occurred in our collections. Our

observations suggest onshore advection of larvae of oceanic species and reduced offshore dispersion of coastal species' larvae, but the starkest changes in assemblage structure appear to be associated with poleward shifts in the spawning distribution of adult stocks marked by the appearance (at high abundance) of several species that typically spawn well to the south of our sampling region (e.g., *Genyonemus lineatus*, *Merluccius productus*, and *Sardinops sagax*). Resolving aggregate *Sebastes* to species highlights similar patterns, including the arrival of new species (e.g., *Sebastes jordani*) with the 2015-16 El Niño that would have otherwise gone undetected. These results lay the foundation for extending the use of larval fish assemblages as indicators of ecosystem responses to climate forcing in this important transitional region of the California Current.

ACKNOWLEDGEMENTS

I would like to thank my advisor, Dr. Eric Bjorkstedt, for giving me guidance throughout my master's degree and investing an incredible amount of time into developing me as a scientist. I have a profound respect for Eric as both a scientist and mentor and I hope to emulate these qualities throughout my career. I am also deeply grateful for the support from Dr. Andrew Kinziger who provided me with his expertise and guidance to conduct genetic sequencing as well as access to lab space and equipment. I would also like to thank Dr. Jose Marin Jarrin for his advice on analyzing community data as well as conversations about early life history stages of marine fishes in the California Current. Finally, I would like to thank Dr. Andrew Thompson for providing materials and useful guidance on genetic identifications of larval rockfishes.

This research would not have been possible without the help of those that have been key in sampling along the Trinidad Head Line. Roxanne Robertson, Phil White, Abby Johnson, Kathryn (Crane) Meyer, Abby White, and Ashok Sadrozinski have played lead roles in sampling along the Trinidad Head Line. I would like to thank the captain and crew of the *R/V Coral Sea*, and the legions of student volunteers who have supported the sampling program. Erin Damm, Halle Shauer, Caymin Ackerman, Spencer Hitzeroth, Olivia Giovanetti, and Sage Roy dedicated an incredible amount of time helping extract and analyze larval fishes from plankton samples.

This research would also not have been possible without funding from several sources. Sampling along the Trinidad Head Line has been supported by NOAA's

Southwest Fisheries Science Center in collaboration with Humboldt State University through the Cooperative Institute for Marine Ecosystems and Climate (CIMEC) and the Cooperative Institute for Marine, Earth, and Atmospheric Sciences (CIMEAS). Funding from the California State University Council on Ocean Affairs, Science, and Technology (COAST) and the Malcolm Oliphant Scholarship in Marine Science is gratefully acknowledged.

Finally, I am greatly indebted to my parents Neal and Marguerite Winnacott and my partner Natasha Ficzytz for the endless love and support. I would not have been able to do it without their help.

TABLE OF CONTENTS

ABSTRACT.....	ii
ACKNOWLEDGEMENTS	iv
TABLE OF CONTENTS.....	vi
LIST OF TABLES	x
LIST OF FIGURES	xii
LIST OF APPENDICES	xxi
INTRODUCTION	1
Sampling Designs and Utility of Monitoring Ichthyoplankton	2
Assemblage Patterns of Ichthyoplankton in the CCE.....	4
Taxonomic Limitations in Ichthyoplankton Surveys.....	5
Oceanographic Dynamics of the California Current System (CCS)	6
Dynamics and structure of the California Current	6
Regional differences of climatology in the CCS	7
Inter-annual variation.....	8
Cross-shelf Structure During Upwelling and its Influence on Ichthyoplankton	11
Recent Climate Variability	14
Trinidad Head Line.....	17
Research Questions and Objectives	19
MATERIALS AND METHODS.....	20
Ethics Statement	20
Ichthyoplankton Collection.....	20

Species Identification.....	21
Ichthyoplankton Count Data Standardization.....	22
Ichthyoplankton Classification	23
Oceanographic Data.....	23
Local hydrographic variables.....	24
Spiciness	24
Sea level anomalies	25
Coastal upwelling index.....	25
Data Structure	26
Statistical Analysis.....	28
Cross-shelf and seasonal patterns	29
Inter-annual patterns	30
Non-metric multidimensional scaling analysis (NMDS).....	32
Oceanographic-assemblage correlations.....	33
Comparative community analysis.....	35
RESULTS	37
General Assemblage Composition.....	37
Visual assemblage.....	37
Rockfish assemblage.....	38
Cross-shelf and Seasonal Assemblage Patterns.....	44
Visual assemblage.....	44
Rockfish assemblage.....	50
Interannual Variability	58

Local environmental conditions.....	58
Visual assemblage.....	63
Rockfish assemblage.....	69
Temporal Patterns of Rare Taxa and Corresponding Biogeographic Assemblages	75
Visual assemblage.....	75
Rockfish assemblage.....	79
Species Richness and Shannon-Weiner Diversity	81
Visual assemblage.....	81
Rockfish assemblage.....	81
Nonmetric Multidimensional Scaling Analysis	86
Visual assemblage.....	86
Rockfish assemblage.....	94
Assemblage-Oceanographic Correlations.....	98
Canonical correspondence analysis (CCA)	98
Delta generalized additive models	102
Pairwise regression: assemblage-temperature correlations.....	106
Effects of Parsing Rockfishes to Species on Measures of Assemblage Structure.....	114
Assemblage composition	114
Cross-shelf, seasonal, and taxonomic contrasts	116
Nonmetric multidimensional scaling analysis	119
Species richness and Shannon-Weiner diversity contrasts	125
Pairwise regression: assemblage-temperature correlations.....	129
DISCUSSION	132

Caveats and Sampling Biases	133
Taxonomic Comparisons to Elsewhere in the CCE.....	134
Cross-shelf Patterns	135
Seasonal Patterns	138
Responses of Ichthyoplankton to Climate Variability: Patterns and Mechanisms.....	139
Late 2014-15 warm ‘blob’ impacts.....	140
2015-16 El Niño impacts	142
Comparisons to the late 2009-10 and late 2018-19 El Niño	145
Other patterns and mechanisms	146
Value of Genetic Identification for Resolving Assemblage Variability in Response to Climate Forcing	147
Ecosystem Implications	148
Motivations for Future Work.....	149
REFERENCES	151
APPENDIX A.....	165
APPENDIX B	169
APPENDIX C	177
APPENDIX D.....	181
APPENDIX E	190

LIST OF TABLES

Table 1. Taxonomic list of common larval fishes within the visual assemblage, including corresponding adult biogeographic ranges in ‘()’ (latitudinal: coastwide [CW], northern [N], and southern [S]; cross-shelf: oceanic [O] and coastal [C]), mean areal density (No./m²), total areal density, percent of total areal density, maximum observed areal density in a sample, and percent positive tow. Total areal density is calculated as the areal density summed across all samples. Percent positive tow is calculated as the number of tows in which a species was observed over the total number of tows. Mean areal density is calculated as the total areal density over the total number of tows. Percent of total density is calculated as the total areal density of an individual taxon over the total aggregate larval density summed across all samples. The number of rare taxa included within coastwide, northern, and southern assemblages are indicated in ‘()’. Abbreviations represent taxon names used in ordination. See Appendix B for list of rare taxa. 39

Table 2. Taxonomic list of larval rockfishes within the rockfish assemblage, including corresponding adult biogeographic ranges in ‘()’ (latitudinal: coastwide [CW], northern [N], and southern [S]), mean areal density (No./m²), mean areal density, total areal density, percent of total areal density, maximum observed areal density in a sample, and percent positive tow. Total areal density is calculated as the areal density summed across all samples. Percent positive tow is calculated as the number of tows in which a species was observed over the total number of tows. Mean areal density is calculated as the total areal density over the total number of tows. Maximum catch is the largest areal density observed in a tow. Percent of total density is calculated as the total areal density of an individual taxon over the total aggregate larval density summed across all samples. Abbreviations represent taxon names used in ordination. The “WEVZ” complex includes *S. wilsoni* (Pygmy rockfish), *S. emphaeus* (Puget Sound rockfish), *S. variegatus* (Harlequin rockfish), and *S. zacentrus* (Sharpchin rockfish). The “MyDi” complex includes *S. mystinus* (Blue rockfish) and *S. diaconus* (Deacon rockfish). 41

Table 3. Results of Permutational Analysis of Variance (PERMANOVA) and indicator species analysis (ISA) for station and seasonal differences in composition of common taxa within the visual assemblage. Seasonal clusters are based on visually distinct monthly clusters from hierarchical cluster analysis performed on months (See Figure 4). Significance of indicator taxa ($p < 0.05$) for each factor level are listed with their associated indicator value (%). 47

Table 4. Results of Permutational Analysis of Variance (PERMANOVA) and indicator species analysis (ISA) for station and seasonal differences in composition of common species or species complexes within the rockfish assemblage. Seasonal clusters are based on results of hierarchical cluster analysis performed on months (See Figure 8).

Significance of indicator taxa ($p < 0.05$) for each factor level are listed with their associated indicator value (%).	54
---	----

Table 5. List of common taxa included in the unresolved (<i>Sebastes</i> spp. larvae in aggregate) and resolved (<i>Sebastes</i> spp. larvae resolved to species) larval assemblages. 115	
---	--

LIST OF FIGURES

Figure 1. Basin-scale climate indices. Panels from top to bottom represent: Multivariate ENSO Index (MEI), North Pacific Gyre Oscillation (NPGO), Pacific Decadal Oscillation (PDO).....	16
Figure 2. Trinidad Head Line off northern California. Stations (circles) are TH01 (most inshore) to TH05 (most offshore) and overlaid on bathymetry (contours in m). Landmarks are Point St. George, Trinidad Head, and Cape Mendocino.....	18
Figure 3. Cross-shelf distributions of common larval taxa within the visual assemblage aggregated over the entire time series. Cross-shelf distributions are represented as relative abundance (scaled by size of bubble) based on areal density (No./m ²) at stations (x-axis) 5 (TH05; offshore) to 1 (TH01; nearshore). See Table 1 for full taxon names corresponding to abbreviations.	45
Figure 4. Cross-shelf and seasonal dendrograms resulting from hierarchical cluster analysis performed on common taxa within the visual assemblage. Top panel: cross-shelf dendrogram performed on stations. Bottom panel: seasonal dendrogram performed on individual months. Different letters indicate results of pairwise PERMANOVA analysis indicating significant pairwise differences ($p < 0.05$) using a Bonferroni correction.	46
Figure 5. Seasonal distributions of common larval taxa within the visual assemblage aggregated over all cruises within each month. Seasonal distributions of each species are represented as relative abundance (scaled by size of bubble) based on areal density (No./m ²) during each month (x-axis). See Table 1 for full taxon names corresponding to abbreviations.	49
Figure 6. Taxon dendrogram from hierarchical cluster analysis performed on common taxa within the visual assemblage. Ecologically interpretable clusters are labelled.....	50
Figure 7. Cross-shelf distributions of common species or species complexes within the rockfish assemblage aggregated over the entire time series. Cross-shelf distributions of each species are represented as relative abundance (scaled by size of bubble) based on areal density (No./m ²) at stations (x-axis) 5 (TH05; offshore) to 1 (TH01; nearshore). See Table 2 for full taxon names corresponding to abbreviations.....	52
Figure 8. Cross-shelf and seasonal dendrograms resulting from hierarchical cluster analysis performed on common species or species complexes within the rockfish assemblage. Top panel: cross-shelf dendrogram performed on stations. Bottom panel: seasonal dendrograms performed on months. Different letters indicate results of pairwise	

PERMANOVA analysis indicating significant pairwise differences ($p < 0.05$) using a Bonferroni correction.....	53
Figure 9. Seasonal distributions of common species or species complexes within the rockfish assemblage aggregated over all cruises within each month. Seasonal distributions of each species are represented as relative abundance (scaled by size of bubble) based on areal density (No./m ²) during each month (x-axis). See Table 1 for full taxon names corresponding to abbreviations.....	56
Figure 10. Taxon dendrogram from hierarchical cluster analysis performed on common species or species complexes within the rockfish assemblage. Ecologically interpretable clusters are labelled.....	57
Figure 11. Intra-annual variability in local environmental conditions in the upper 0-10 m of the water column aggregated across all stations within a cruise. Panels from top to bottom: temperature (°C), salinity (PSU), and log ₁₀ (chlorophyll <i>a</i> concentration + 1) (mg m ⁻³) by day of year (x-axis). Black line (± SE in gray) represents a generalized additive model fit to environmental observations. Symbol numbers correspond to the observation year. Symbol color corresponds to a temperature anomaly from a seasonal climatology (see methods for calculation of anomaly product).....	59
Figure 12. Local hydrographic conditions observed along the TH-line time series at station TH03 (41°03.50 N, 124°20.50 W, 140 m). From top to bottom: temperature (°C), salinity (PSU), and log ₁₀ (chlorophyll <i>a</i> concentration + 1) (mg m ⁻³) by depth (m; y-axis) and time (x-axis).	61
Figure 13. Regional oceanographic indices. Panels from top to bottom represent: cumulative sea level anomaly (calculated from daily values at 40.76°N from Jan 1 to Dec 31), average monthly sea level anomaly (red and blue bars), cumulative Coastal Transport Upwelling Index (CUTI; m ² s ⁻¹ , calculated from daily values at 41°N from Jan. 1 to Dec.31), and average monthly CUTI at 41°N. Monthly Sea level anomalies extending below zero (blue) indicate a negative anomaly and values extending above zero (red) indicate a positive anomaly.....	62
Figure 14. Mean areal density (No./m ² ; y-axis) of common taxa within the visual assemblage and aggregate rare taxa across all stations by cruise date (x-axis). Gray bars indicate extended observation gaps.	64
Figure 15. Mean areal density (No./m ² ; y-axis) of common larval taxa within the visual assemblage aggregated over all cruises within each year (x-axis). “Other” represents the remaining common taxa (<i>Artedius</i> spp., <i>G. zachirus</i> , <i>Liparis</i> spp, <i>P. crockeri</i> , <i>P. vetulus</i>) in aggregate.	66

Figure 16. Boxplots comparing mean areal density (No./m²; y-axis) of common taxa within the visual assemblage aggregated by cruise between pre-MHW (November 2007-July 2014), MHW (August 2014-May 2017), and post-MHW (June 2017-December 2019) time periods (x-axis). Significant differences ($p < 0.05$) were tested using the non-parametric Kruskal-Wallis test. Pairwise comparisons were tested using Dunn's multiple comparisons test with a Bonferroni correction and the significance level set at: * = $p < 0.05$, ** = $p < 0.01$, *** = $p < 0.001$, **** = $p < 0.0001$. The y-axis indicates areal density on a log-transformed scale. 68

Figure 17. Mean areal density (No./m²; y-axis) of common species or species complexes within the rockfish assemblage across all stations by cruise date (x-axis). Gray bars indicate extended observation gaps. 70

Figure 18. Mean log-transformed areal density ($\log_{10}[\text{No./m}^2 + 1]$; y-axis) of common species or species complexes within the rockfish assemblage aggregated over all cruises within each year (x-axis). Top panel: spring, summer, and fall-spawning rockfishes. Bottom panel: winter-spawning rockfishes. Ethanol-preserved samples were not collected during winter months in 2012 and summer months in 2010, 2011, and 2012. 72

Figure 19. Boxplots comparing mean areal density (No./m²; y-axis) of common species or species complexes within the rockfish assemblage aggregated by cruise between pre-MHW (November 2007-July 2014), MHW (August 2014-May 2017), and post-MHW (June 2017-December 2019) time periods (x-axis). Significant differences ($p < 0.05$) were tested using the non-parametric Kruskal-Wallis test. Pairwise comparisons were tested using Dunn's multiple comparisons test with a Bonferroni correction and the significance level set at: * = $p < 0.05$, ** = $p < 0.01$, *** = $p < 0.001$, **** = $p < 0.0001$. The y-axis indicates areal density on a log-transformed scale. 74

Figure 20. Inter-annual variability in species richness and log-transformed areal density ($\log_{10}[\text{No./m}^2 + 1]$) of rare taxa grouped by adult biogeographic ranges. Panels from top to bottom: species richness and areal density of aggregate rare coastwide, northern, and southern adult spawning assemblages (y-axis) by cruise date (x-axis). Symbol and line color corresponds to coastal (blue) or oceanic (red) adult spawning assemblages. Lines indicate loess smooth (tuned to capture interannual trends) fit to observations. Gray bars indicate extended observation gaps. 76

Figure 21. Time series variability in areal density (No./m²) of notable rare taxa within the visual assemblage by cruise date (x-axis) and station (y-axis). Circles scale with areal density. Gray shading indicates extended observation gaps. 78

Figure 22. Time series variability in areal density (No./m²) of notable rare species within the rockfish assemblage by cruise date (x-axis) and station (y-axis). Circles scale with areal density. Gray shading indicates extended observation gaps. 80

Figure 23. Intra-annual variability in Shannon-Weiner diversity (top panel; y-axis) and species richness (bottom panel; y-axis) within the visual assemblage by day of year (x-axis). Black line (\pm SE in gray) represents a generalized additive model fit to each biodiversity index. Symbol number correspond to the observation year. Symbol color corresponds to a temperature anomaly from a seasonal climatology (see methods for calculation of anomaly product). 82

Figure 24. Inter-annual variability in Shannon-Weiner diversity (top panel; y-axis) and species richness (bottom panel; y-axis) within the visual assemblage by cruise date (x-axis). Black line (\pm SE in gray) represents a loess smooth (tuned to capture interannual trends) fit to observations. Symbol color corresponds to a temperature anomaly from a seasonal climatology (see methods for calculation of anomaly product). Gray bars indicate extended observation gaps. 83

Figure 25. Intra-annual variability in Shannon-Weiner diversity (top panel; y-axis) and species richness (bottom panel; y-axis) within the rockfish assemblage by day of year (x-axis). Black line (\pm SE in gray) represents a generalized additive model fit to each biodiversity index. Symbol number corresponds to the observation year. Symbol color corresponds to a temperature anomaly from a seasonal climatology (see methods for calculation of anomaly product). 84

Figure 26. Inter-annual variability in Shannon-Weiner diversity (top panel; y-axis) and species richness (bottom panel; y-axis) within the rockfish assemblage by cruise date (x-axis). Black line (\pm SE in gray) represents a loess smooth (tuned to capture interannual trends) fit to observations. Symbol color corresponds to a temperature anomaly from a seasonal climatology (see methods for calculation of anomaly product). Gray bars indicate extended observation gaps. 85

Figure 27. Nonmetric multidimension scaling ordination plots depicting community structure of common taxa within the visual assemblage along axis 1 and axis 2. Top panel: Cross-shelf structure with symbols and colors corresponding to stations. Bottom panel: seasonal structure with symbols and colors corresponding to seasonal clusters. Ellipses represent the standard deviation of each factor level in ordination space. Species labels (see Table 1 for names corresponding to abbreviations) represent the centroids of their scores. See Appendix C for ellipses and points corresponding to each individual month. 87

Figure 28. Intra-annual cycle of mean NMDS axis scores (y-axis) performed on common taxa within the visual assemblage aggregated across stations within a cruise by day of year (x-axis). From top to bottom: NMDS 1, NMDS2, and NMDS3. Black line (\pm SE in gray) represents a generalized additive model fit to NMDS scores. Symbol number correspond to the observation year. Symbol color corresponds to a temperature anomaly from a seasonal climatology (see methods for calculation of anomaly product). 88

Figure 29. Intra-annual cycle of mean NMDS axis scores (y-axis) performed on common taxa within the visual assemblage for each sampling station by day of year (x-axis). From left to right: NMDS1, NMDS2, and NMDS3. From top to bottom: stations TH01, TH02, TH03, TH04, and TH05. Black line (\pm SE in gray) represents a generalized additive model fit to NMDS scores. Symbol number correspond to the observation year. Symbol color corresponds to a temperature anomaly from a seasonal climatology (see methods for calculation of anomaly product)..... 90

Figure 30. Time series of mean residuals from NMDS performed on common taxa within the visual assemblage aggregated over all stations within a cruise. From top to bottom: NMDS 1, NMDS2, and NMDS3 axis score residuals (y-axis) by cruise date (x-axis). See methods for description of residual product. 92

Figure 31. Time series of mean residuals from NMDS performed on common taxa within the visual assemblage for each sampling station. From left to right: NMDS1, NMDS2, and NMDS3 (y-axis) by cruise date (x-axis). From top to bottom: TH01, TH02, TH03, TH04, and TH05. See methods for description of residual product. 93

Figure 32. Nonmetric multidimension scaling ordination plots depicting community structure of common species or species complexes within the rockfish assemblage along axis 1 and axis 2. Top panel: seasonal structure with symbols and colors corresponding to seasonal clusters. Bottom panel: Cross-shelf structure with symbols and colors corresponding to stations. Ellipses represent the standard deviation of each factor level in ordination space. Species labels (see Table 2 for names corresponding to abbreviations) represent the centroids of their scores. See Appendix C for ellipses and points corresponding to each individual month..... 95

Figure 33. Intra-annual cycle of mean NMDS axis scores (y-axis) performed on the rockfish assemblage aggregated across stations within a cruise by day of year (x-axis). Top panel: NMDS1. Bottom panel: NMDS2. Black line (\pm SE in gray) represents a generalized additive model fit to NMDS scores. Symbol number correspond to the observation year. Symbol color corresponds to a temperature anomaly from a seasonal climatology (see methods for calculation of anomaly product)..... 96

Figure 34. Intra-annual cycle of mean NMDS axis scores (y-axis) performed on the rockfish assemblage for each sampling station by day of year (x-axis). Left panels: NMDS1. Right panels: NMDS2. From top to bottom: stations TH01, TH02, TH03, TH04, and TH05. Black line (\pm SE in gray) represents a generalized additive model fit to NMDS scores. Symbol number correspond to the observation year. Symbol color corresponds to a temperature anomaly from a seasonal climatology (see methods for calculation of anomaly product). 97

Figure 35. Canonical correspondence analysis depicting structure of common taxa within the visual assemblage in relation to significant oceanographic variables ($p < 0.01$).

Temp10 = temperature anomaly in the upper 0-10 m. Sp10 = spiciness anomaly in the upper 0-10 m. SL14 = sea level anomaly averaged over 14-days prior to a cruise. CUTI14 = coastal upwelling transport index anomaly averaged over 14-days prior to a cruise. See Table 1 for full names of each taxon corresponding to abbreviations. The first two axes (CCA1 and CCA2; eigenvectors) account for approximately 89% of the variability explained by the CCA and approximately 5.5% of the total variability in the data. 99

Figure 36. Canonical correspondence analysis depicting structure of common species or species complexes within the rockfish assemblage in relation to significant oceanographic variables ($p < 0.01$). Top panel: winter-spawning rockfishes. Bottom panel: summer-spawning rockfishes. Temp10 = temperature anomaly measured in the upper 0-10 m. Sal10 = salinity anomaly measured in the upper 0-10 m. Chla10 = log-transformed chlorophyll *a* anomaly measured in the upper 0-10 meters. Sp10 = spiciness anomaly measured in the upper 0-10 m. SL14 = sea level anomaly averaged over 14-days prior to a cruise. See Table 2 for full names of each taxon corresponding to abbreviations. The first two axes (CCA1 and CCA2; eigenvectors) account for approximately 83% (94%) of the variability explained by the CCA within winter-spawning rockfishes (summer-spawning rockfishes) and approximately 11% (9%) of the total variability in the data. 101

Figure 37. Fitted lines (solid) and 95% confidence intervals (dashed) for the additive effect of a seasonally corrected temperature anomaly in the upper 0-10 m from the binomial (top panels) and lognormal (bottom panels) GAMs for common taxa included within the visual assemblage. Taxa are grouped by shared relationships for each model. The significance of the added effect of the temperature anomaly smooth term in each model is indicated by each taxon name (see Table 1 for full names) and set at: * = $p < 0.05$, ** = $p < 0.01$, *** = $p < 0.001$ 103

Figure 38. Fitted lines (solid) and 95% confidence intervals (dashed) for the additive effect of a seasonally corrected temperature anomaly in the upper 0-10 m from the binomial (top panels) and lognormal (bottom panels) GAMs for common species or species complexes included within the rockfish assemblage. Taxa are grouped by shared relationships for each model. The significance of the added effect of the temperature anomaly smooth term in each model is indicated by each taxon name (see Table 2 for full names) and set at: * = $p < 0.05$, ** = $p < 0.01$, *** = $p < 0.001$ 105

Figure 39. Fitted lines (blue) and 95% confidence intervals (shaded gray) resulting from pairwise regression for the relationship between a seasonally corrected temperature anomaly in the upper 0-10 m of the water column and species richness anomaly and Shannon-Weiner diversity anomaly within the visual assemblage. Each biodiversity index was analyzed using all available data (all months). Species richness was further analyzed by distinct periods of the year (August-March and April-July). The results of each pairwise linear model are indicated by the coefficient of determination (R^2) and the

significance of the temperature anomaly term (n.s. = $p > 0.05$, * = $p < 0.05$, ** = $p < 0.01$, *** = $p < 0.001$). 107

Figure 40. Fitted lines (blue) and 95% confidence intervals (shaded gray) resulting from pairwise regression for the relationship between a seasonally corrected temperature anomaly and seasonally corrected residuals from each NMDS axis within the visual assemblage. Each axis was analyzed using all available data (all months). NMDS2 was further analyzed by different seasons (August-March and April-July). The results of each pairwise linear model are indicated by the coefficient of determination (R^2) and the significance of the temperature anomaly term (n.s. = $p > 0.05$, * = $p < 0.05$, ** = $p < 0.01$, *** = $p < 0.001$). 109

Figure 41. Fitted lines (blue) and 95% confidence intervals (shaded gray) resulting from pairwise regression for the relationship between a seasonally corrected temperature anomaly and species richness anomaly (left-hand column) and Shannon-Weiner diversity anomaly (right-hand column) within the rockfish assemblage. Each biodiversity index was analyzed using all available data (all months) and by different seasons (January-February and March-December). The results of each pairwise linear model are indicated by the coefficient of determination (R^2) and the significance of the temperature anomaly term (n.s. = $p > 0.05$, * = $p < 0.05$, ** = $p < 0.01$, *** = $p < 0.001$). 111

Figure 42. Fitted lines (blue) and 95% confidence intervals (shaded gray) resulting from pairwise regression for the relationship between a seasonally corrected temperature anomaly and seasonally corrected residuals from each NMDS axis within the rockfish assemblage. Each axis was analyzed using all available data (all months). NMDS axis 1 was further analyzed by different seasons (January-February and March-December). The results of each pairwise linear model are indicated by the coefficient of determination (R^2) and the significance of the temperature anomaly term (n.s. = $p > 0.05$, * = $p < 0.05$, ** = $p < 0.01$, *** = $p < 0.001$). 113

Figure 43. Taxon dendrograms from hierarchical cluster analysis performed on common taxa within the unresolved (*Sebastes* spp. larvae in aggregate) and resolved (*Sebastes* spp. larvae resolved to species) larval assemblages. Ecologically interpretable clusters are labelled. 117

Figure 44. Cross-shelf and seasonal dendrograms from hierarchical cluster analysis performed on common taxa within the unresolved (left-hand columns; *Sebastes* spp. larvae in aggregate) and resolved (right-hand columns; *Sebastes* spp. larvae resolved to species) larval assemblage. Top panels: Cross-shelf dendrogram performed on stations. Bottom panels: seasonal dendrograms performed on months. 118

Figure 45. Nonmetric multidimension scaling ordination plots depicting community structure of common taxa within the unresolved (top panel; *Sebastes* spp. in aggregate) and resolved (bottom panel; *Sebastes* spp. larvae resolved to species) assemblage along

axis 1 and axis 2. Symbols and colors correspond to stations. Ellipses represent the standard deviation of each factor level in ordination space. Species labels (see Table 1 and Table 2 for names corresponding to abbreviations) represent the centroids of their scores..... 120

Figure 46. Nonmetric multidimension scaling ordination plots depicting community structure of common taxa within the unresolved (top panel; *Sebastes* spp. larvae in aggregate) and resolved (bottom panel; *Sebastes* spp. larvae resolved to species) assemblage along axis 2 and axis 3. Symbols and colors correspond to seasonal clusters (see Figure 44 for definition of clusters). Ellipses represent the standard deviation of each factor level in ordination space. Species labels (see Table 1 and Table 2 for names corresponding to abbreviations) represent the centroids of their scores..... 122

Figure 47. Intra-annual cycle of mean NMDS axis scores (y-axis) performed on common taxa within the unresolved (left-hand columns; *Sebastes* spp. larvae in aggregate) and resolved (right-hand columns; *Sebastes* spp. larvae resolved to species) larval assemblages by day of year (x-axis). Panels from top to bottom: NMDS1, NMDS2, and NMDS3. Black line (\pm SE in gray) represents a generalized additive model fit to NMDS scores. Symbol number correspond to the observation year. Symbol color corresponds to a temperature anomaly from a seasonal climatology (see methods for calculation of anomaly product). 124

Figure 48. Time series of mean residuals from NMDS performed on common taxa within the unresolved (left-hand columns; *Sebastes* spp. larvae in aggregate) and resolved (right-hand columns; *Sebastes* spp. larvae resolved to species) larval assemblages. From top to bottom: NMDS1, NMDS2, and NMDS3 axis score residuals (y-axis) by cruise date (x-axis). See methods for description of residual product. 125

Figure 49. Intra-annual variability in Shannon-Weiner diversity (top panels; y-axis) and species richness (bottom panels; y-axis) within the unresolved (left-hand columns; *Sebastes* spp. larvae in aggregate) and resolved (right-hand columns; *Sebastes* spp. larvae resolved to species) larval assemblages by day of year (x-axis). Black line (\pm SE in gray) represents a generalized additive model fit to each biodiversity index. Symbol number correspond to the observation year. Symbol color corresponds to a temperature anomaly from a seasonal climatology (see methods for calculation of anomaly product). 126

Figure 50. Inter-annual variability in Shannon-Weiner diversity (top panels; y-axis) and species richness (bottom panels; y-axis) within the unresolved (left-hand columns; *Sebastes* spp. larvae in aggregate) and resolved (right-hand columns; *Sebastes* spp. larvae resolved to species) larval assemblages by cruise date (x-axis). Black line (\pm SE in gray) represents a loess smooth (tuned to capture interannual trends) fit to observations. Symbol color corresponds to a temperature anomaly from a seasonal climatology (see methods for calculation of anomaly product). Gray bars indicate extended observation gaps. 128

Figure 51. Fitted lines (blue) and 95% confidence intervals (shaded gray) resulting from pairwise regression for the relationship between a seasonally corrected temperature anomaly and species richness anomaly and Shannon-Weiner diversity anomaly within the unresolved (left-hand columns; *Sebastes* spp. larvae in aggregate) and resolved (right-hand columns; *Sebastes* spp. larvae resolved to species) larval assemblages. Each biodiversity index was analyzed using all available data (all months) and by different seasons (August-March and April-July). The results of each pairwise linear model are indicated by the coefficient of determination (R^2) and the significance of the temperature anomaly term (n.s.= $p > 0.05$, * = $p < 0.05$, ** = $p < 0.01$, *** = $p < 0.001$). 130

Figure 52. Fitted lines (blue) and 95% confidence intervals (shaded gray) resulting from pairwise regression for the relationship between a seasonally corrected temperature anomaly and seasonally corrected residuals from each NMDS axis within the unresolved (left-hand columns; *Sebastes* spp. larvae in aggregate) and resolved (right-hand columns; *Sebastes* spp. larvae resolved to species) larval assemblages. Each biodiversity index was analyzed using all available data (all months) and by different seasons (August-March and April-July). The results of each pairwise linear model are indicated by the coefficient of determination (R^2) and the significance of the temperature anomaly term (n.s.= $p > 0.05$, * = $p < 0.05$, ** = $p < 0.01$, *** = $p < 0.001$). 131

LIST OF APPENDICES

Appendix A: Detailed methods for conducting genetic sequencing and identification on ethanol-preserved larval rockfishes (*Sebastes* spp.). 165

Appendix B. Taxonomic list of rare larval fishes within the visual assemblage, including corresponding adult biogeographic ranges in ‘()’, mean areal density (No./m²), total areal density, percent of total areal density, maximum observed areal density in a sample, and percent positive tow. Adult spawning ranges are defined as: (C) coastal (typically occupy and spawn in habitat inshore of the upper slope), or (O) oceanic (mostly spawn offshore of the upper slope), crossed with species latitudinal ranges defined as: (CW) coastwide (typically found and spawn throughout the CCS), (N) northern (adults spawn mostly Monterey Bay and north), or (S) southern (adults spawn mostly Monterey Bay and south). Total areal density is calculated as the areal density summed across all samples. Percent positive tow is calculated as the number of tows in which a species was observed over the total number of tows. Mean areal density is calculated as the total areal density over the total number of tows. Percent of total density is calculated as the total areal density of an individual taxon over the total aggregate larval density summed across all samples..... 169

Appendix C. Ordination plots depicting (A) seasonal structure within the visual assemblage by individual months along NMDS1 and NMDS2, (B) assemblage structure within the visual assemblage along NMDS2 and NMDS3, and (C) seasonal structure within the rockfish assemblage by individual months along NMDS1 and NMDS2. In figures A and C, points and ellipses are color coded by the month a sample was collected. See Table 1 for species names corresponding to abbreviations in figure B. 177

Appendix D. Fitted lines (solid) and 95% confidence intervals (dashed) for the additive effect of a seasonally corrected temperature anomaly in the upper 0-10 m of the water-column on larval abundance based on delta generalized additive models (delta-GAM) for common taxa included within the (A) visual assemblage and (B) rockfish assemblage. The binomial model (OCC; left hand column) estimates the probability of larval occurrence in relation to a temperature anomaly. The lognormal model (log₁₀(No./m²) | OCC; right hand column) estimates the magnitude of abundance for positive counts in relation to a temperature anomaly. Explanatory variables used to model both presence and abundance of positive counts were station, day of year, and a seasonally corrected temperature anomaly between 0 and 10 m (see methods for anomaly calculations). The significance of the temperature anomaly smooth term within each model is indicated for each taxon and set at: * = $p < 0.05$, ** = $p < 0.01$, *** = $p < 0.001$, and n. s. = not significant..... 181

Appendix E. Interannual variability in cross-shelf distributions and seasonal occurrence. Plots depict interannual variation in cross-shelf distributions by cruise date (x-axis) and station (y-axis) for common taxa within the (A) visual assemblage and (B) rockfish assemblage. Also included is interannual variation in seasonal occurrence by year (x-axis) and day of year (y-axis) for common taxa within the (C) visual assemblage and (E) rockfish assemblage. Circles scale with areal density (No./m ²). Gray shading indicates extended observation gaps.	190
---	-----

INTRODUCTION

Monitoring the distributions and spawning behavior of adult fish stocks and their responses to climate forcing can be difficult and costly. Fortunately, most marine fishes have a planktonic larval phase (i.e., ichthyoplankton) that co-occur with other species in space and time and are easily captured in the upper 100 m of the water column, and thus offer a way to monitor several aspects of the adult spawning stock for multiple species simultaneously (Koslow and Wright 2016). More importantly, ichthyoplankton are sensitive indicators of environmental perturbations, and long-term monitoring can provide useful information on the effects of climate change on marine ecosystems (Hsieh et al. 2005, Brodeur et al. 2008).

The factors that regulate the distribution, abundance, and composition of ichthyoplankton at a given time are dependent on both biological and physical processes. When and where larvae occur and larval abundance is closely tied to spawning characteristics and strategies of the adult stock, such as their phenology (Doney et al. 2012, Asch 2015), spawning distributions and habitat (Ralston et al. 2003, Hitchman et al. 2012, Thompson et al. 2016), and the size and condition of the spawning stock (Ralston et al. 2003, Harvey 2005, Ralston and MacFarlane 2010). After spawning, larvae are subject to their physical environment, which can influence survival through food availability and predation (Checkley 1982, Houde 1987, Houde 2008, Hare 2014) and ocean currents and other hydrographic processes (e.g., transport, fronts, eddies) involved in the horizontal distribution of larvae (Bjorkstedt et al. 2002, Woodson et al.

2012, Morgan 2014). Therefore, spatial and temporal variability in the abundance and composition of ichthyoplankton assemblages is a consequence of the behavior and condition of the adult stock modified by oceanographic processes (e.g., transport) that regulate horizontal distributions and influence survival (Brodeur et al. 2008, Koslow et al. 2013, Koslow and Wright 2016, Auth et al. 2018).

Of particular interest is the utility of plankton dynamics and the distribution of both assemblages and individual species as robust indicators of ecosystem state and response to climate forcing in upwelling systems (Hooff and Peterson 2006, Brodeur et al. 2008, Keister et al. 2011, Koslow et al. 2017, Lilly and Ohman 2018). Larval fish assemblages, by virtue of being robust indicators of the distribution of adult spawning stocks (Ralston et al. 2003, Ralston and MacFarlane 2010, Hitchman et al. 2012, Thompson et al. 2016), can serve a similar purpose and also provide information on other elements of the ecosystem (Auth et al. 2011, Brodeur et al. 2008, Koslow et al. 2017). In this thesis, I analyze the distribution, abundance, and composition of ichthyoplankton assemblages off northern California with the intent of characterizing how the assemblage changes over the course of 12-years (late 2007-2019) that were marked by substantial oceanographic variability.

Sampling Designs and Utility of Monitoring Ichthyoplankton

In the California Current Ecosystem (CCE), most programs (California Cooperative Oceanic Fisheries Investigation [CalCOFI] and the Newport Hydrographic Line [NH]) have utilized oblique (Bongo) plankton tows to sample early life history

stages and other planktonic forms. The Bongo net has been standard for sampling ichthyoplankton to depths of 20 m (NH; Brodeur et al. 2008) or 210 m (CalCOFI; Kramer et al. 1972, McClatchie et al. 2014), as most ichthyoplankton reside in the upper 100 m of the water column (Moser 1996, Sakuma et al. 1999, Bjorkstedt et al. 2002, Auth and Brodeur 2006). A typical survey calls for conducting a Bongo tow at pre-determined stations along a cross-shelf transect. Surveys typically take two main forms; low frequency (CalCOFI) and high frequency surveys (NH). Low frequency surveys typically cover large areas and are useful for understanding spatial dynamics of plankton but sampling occasions are infrequent and poorly resolve phenology and seasonal patterns. High frequency surveys typically have less spatial coverage (e.g., occupy a single cross-shelf transect) but sample year-round and capture variability in plankton ecosystems at higher frequency (Bjorkstedt and Peterson 2015).

Bongo nets tend to capture very young larval fishes (i.e., preflexion stages; only a few days old [Hitchman et al. 2012]), which supports their use as a source of ichthyoplankton data suitable for providing information on adult stocks (Koslow and Wright 2016). Older larvae are less abundant due to high levels of mortality during egg and larval stages (Houde 2002, 2008), and become less susceptible to capture as detection and swimming capabilities develop (McGurk 1992, Fuiman 2002). Thus, the abundance of early larval stages has not yet been entirely decoupled from adult production and can therefore indicate spawning patterns and processes of the adult stock (Ralston et al. 2003, Koslow and Davison 2015, Koslow and Wright 2016, Thompson et al. 2016). More importantly, several aspects of ichthyoplankton data are utilized as indicators of

ecosystem state and provide a tool to monitor trends in ocean conditions. For example, winter ichthyoplankton biomass is used as an indicator of future juvenile salmon foraging success (Daly et al. 2013), whereas shifts in assemblage composition, the presence of distinct indicator taxa, or short-term dominance of rare species can provide information on ecosystem state (Brodeur et al. 2008, Auth et al. 2018, Nielsen et al. 2020, Weber et al. 2021).

Assemblage Patterns of Ichthyoplankton in the CCE

Much of our understanding of factors that regulate the distribution and abundance of ichthyoplankton in the CCE is based on surveys of ichthyoplankton in the northern California Current off coastal Oregon and Washington (Doyle et al. 2002, Auth and Brodeur 2006, Auth 2008, Brodeur et al. 2008, Auth et al. 2011) and in the Southern California Bight (SCB; Hsieh et al. 2009, Koslow et al. 2013, Thompson et al. 2014, Koslow et al. 2017). In coastal waters (between the inner shelf and just beyond the upper slope), surveys characterize ichthyoplankton into distinct cross-shelf biogeographic assemblages, such as coastal and oceanic assemblages. Osmerids (smelts), cottids (sculpins), some pleuronectids, such as *Psettichthys melanostictus* (sand sole), and liparids (snailfishes) tend to form a distinct coastal assemblage (Doyle et al. 2002, Auth and Brodeur 2006, Sadrozinski 2008), which closely reflects the shallow coastal spawning areas of adults. Oceanic assemblages typically reflect the spawning location of deep-water pleuronectids and mesopelagic fishes, such as *Protomyctophum crockeri* (California flashlightfish) and *Tarletonbeania crenularis* (blue lanternfish; Doyle et al.

2002, Auth and Brodeur 2006, Sadrozinski 2008). Latitudinal variation in ichthyoplankton assemblages, on average, tends to mirror alongshore distributions of adult populations (Doyle et al. 2002, Williams and Ralston 2002, Auth and Brodeur 2006, Ralston et al. 2013, Thompson et al. 2014). These patterns are apparent at coast-wide scales, over which ichthyoplankton composition reflects differences in the biogeographic affinity of fishes within the CCE (Thompson et al. 2014).

Ichthyoplankton assemblages in the coastal waters off northern California are poorly understood and have been characterized in a handful of short-term studies (Doyle 2002, Sadrozinski 2008, Auth 2008, 2009). Comparative analysis of ichthyoplankton data collected in the northern and southern regions of the CCE indicate substantial differences in assemblage structure and limited coherence in how these assemblages vary over time (Thompson 2014). Information on the composition and variability of ichthyoplankton assemblages in the extensive spatial gap between existing surveys is needed to support comprehensive understanding of patterns and processes that influence larval fish assemblage dynamics throughout the CCE.

Taxonomic Limitations in Ichthyoplankton Surveys

Limitations on taxonomic resolution have historically constrained insights from ichthyoplankton survey data in the California Current. While most taxa can be resolved to species, several groups can be resolved only to genus or family level when present in the earliest stages of larval development (i.e., preflexion or flexion): sanddabs (*Citharichthys* spp.), thornyheads (*Sebastolobus* spp.), snailfishes (*Liparis* spp.), and several genera of

sculpins (*Artedius* spp., cottids, etc.) or at all stages of larval development; rockfishes (*Sebastes* spp.) and smelts (Osmeridae). Such ambiguity is especially problematic in the case of the speciose genus *Sebastes*. In aggregate, rockfishes are one of the most commonly observed groups of ichthyoplankton in the CCE (Doyle et al. 2002, Auth and Brodeur 2006, Auth 2011, Thompson et al. 2016, 2017) and few species can be identified at the larval stage using visual markers (Moser et al. 2000, Johansson et al. 2018). Thus, few published studies have been able to resolve spatial and temporal patterns in larvae of individual species within the genus *Sebastes*. Recently, this problem has been resolved using genetic techniques, which have enabled identifications of previously unknown larval fishes, and have been particularly useful in parsing *Sebastes* larvae to species or species complexes (Taylor et al. 2004, Taylor 2004, Thompson et al. 2016, 2017, Johansson et al. 2018). Following Thompson et al. (2016), this study augments visual identifications with genetic techniques to resolve the species composition of visually cryptic larval rockfishes (*Sebastes* spp.), a first application of this approach off northern California.

Oceanographic Dynamics of the California Current System (CCS)

Dynamics and structure of the California Current

The CCS, along the U.S. west coast, is an eastern boundary current system marked by seasonal and latitudinal variability in the consistency and intensity of wind-driven upwelling (Checkley and Barth 2009). Upwelling is driven by strong equatorward winds in combination with the rotation of the earth's surface (Coriolis Effect) that cause

the surface mixed layer to be transported offshore (Ekman Transport), while cold, deep, nutrient-rich waters are upwelled towards the coast (Checkley and Barth 2009, Jacox and Edwards 2012). Coastal upwelling is highly seasonal, occurring more strongly during the spring and summer when winds are predominantly coming from the north. In contrast, during fall and winter months, southerly winds or weak northerly winds drive the poleward transport of the surface mixed layer, which in turn is deflected onshore (i.e., downwelling). As a result, the direction and strength of cross-shelf currents are dependent on the seasonality and direction of wind. In addition, the CCS is composed of several alongshore flowing water masses that vary in strength and direction. The most notable is the California Current, which is part of the North Pacific Gyre and flows equatorward, transporting cold, nutrient-rich subarctic waters into the CCE. Its strength and direction is regulated by equatorward winds and coastal upwelling that generate southern coastal jets (Checkley and Barth 2009).

Regional differences of climatology in the CCS

More specifically, the context of this study takes place in the coastal waters off northern California, which lies in a transitional region, where bathymetry, hydrographic features, and oceanographic processes strongly differ from other parts of the CCS (Checkley and Barth 2009). In the southern California region, upwelling is not as strong and is present year-round (Checkley and Barth 2009, García-Reyes and Largier 2012), whereas areas off Washington and Oregon exhibit strong seasonal upwelling (April-September) and downwelling along a mostly linear coastline (Hickey and Banas 2009). Off southern Oregon and northern California (between Cape Blanco and Cape

Mendocino) upwelling reaches a maximum intensity relative to the rest of the coast. Upwelling favorable winds in this region persist throughout the spring and summer, become weak in the fall, and often are disrupted by southerly winds and winter storms. Due to the position of the Cape Mendocino headland (off northern California), winds tend to have a strong onshore component, and circulation patterns in this area can at times be relatively sluggish despite regions just to the south that experience intense upwelling (Largier et al. 1993). In addition, coastal headlands (e.g., Cape Blanco and Cape Mendocino) and bathymetric features in this region can favor the development of mesoscale oceanographic features (e.g., eddies, upwelling jets, fronts, and retention zones; Largier et al. 1993, Barth et al. 2000), which can influence transport and retention of planktonic organisms (Keister et al. 2011, Morgan et al. 2011, 2012) and spatial patterns of ichthyoplankton (Bjorkstedt et al. 2002, Nishimoto and Washburn 2002, Sadrozinski 2008, Woodson et al. 2012). Alongshore flow in this region fluctuates seasonally, with enhanced equatorward flow in the spring and summer and weak equatorward or poleward flow in the fall and winter (Largier et al. 1993). Freshwater discharge during winter and early spring from major rivers (e.g., the Klamath/Trinity and Eel) and smaller coastal watersheds off northern California and Oregon can also influence coastal waters in this area.

Inter-annual variation

Much of the interannual variation in physical (e.g., off- and along-shore transport and wind-driven upwelling) and biological (e.g., primary production) conditions within the CCS is linked to basin-scale modes of climate variability. The three most widely

recognized climate indices that have the strongest signature on physical and biological variability within the CCS include the Pacific Decadal Oscillation (PDO), North Pacific Gyre Oscillation (NPGO), and the El Niño Southern Oscillation (ENSO). While these indices are considered basin scale-modes of variability, they have a strong influence on variability in alongshore transport, upwelling, and productivity in the CCS, each in turn having important consequences for the dynamics of plankton ecosystems and the productivity of adult fish stocks. Here I focus on how each index manifests in the CCS and its implications.

The PDO and NPGO capture variability in the dominant oceanic gyres of the North Pacific at low frequency time scales (10-20 years), having the strongest influence on the strength and source of alongshore transport in the California Current and the timing and strength of upwelling at local scales in the CCS (Chhak and Di Lorenzo 2007, Di Lorenzo et al. 2008, Chenillat et al. 2012, Di Lorenzo et al. 2013). Changes in the source and strength of alongshore flow and upwelling in the California Current can have important consequences for the ecosystem. During a cool phase (negative PDO and positive NPGO), equatorward flow in the California Current is enhanced and upwelling occurs earlier in the year, resulting in cooler and more productive conditions. The opposite is true for a positive phase of the PDO and negative phase of the NPGO.

In contrast to the low-frequency oscillations of the PDO and NPGO, dynamics in the equatorial Pacific typically trigger El Niño and La Niña events at intervals of 2-7 years (Di Lorenzo et al. 2013). While an El Niño event originates in the tropics, strong events can impact the northern CCS through atmospheric teleconnections and oceanic

signals (coastally trapped Kelvin waves), typically during fall through winter (Bjorkstedt et al. 2010, Jacox et al. 2015). The poleward propagation of coastally trapped Kelvin waves can result in a depression of the thermocline and reduce the efficiency of upwelling, which in turn reduces primary productivity (Chavez et al. 2002, Di Lorenzo et al. 2013, Jacox et al. 2015). Through atmospheric teleconnections, ENSO events can disrupt the strength of winds that drive upwelling and equatorward flow in the CCS (Di Lorenzo et al. 2013). Disruptions to upwelling favorable winds and a weakening of the California Current can lead to the intrusion of warm, saline waters from southern and offshore sources into coastal areas of the CCS. The CCS responds in an opposite way during La Niña events.

Climate events can impact several aspects of the ecosystem, which in turn can influence the factors that regulate the distribution and abundance of ichthyoplankton. Altered oceanographic conditions such as anomalous warming can shift the distribution of adult fish populations (Pinsky et al. 2013, Cavole et al. 2016), while changes in primary productivity can inhibit energy consumption and productivity of adult stocks (Harvey 2005). In addition, changes in primary production can influence mortality and survival of larvae, although this thesis does not directly investigate these dynamics.

Plankton ecosystems are sensitive indicators of anomalous advection associated with interannual (El Niño) or decadal climate variability (PDO and NPGO; Hooff and Peterson 2006, Keister et al. 2011, Lilly and Ohman 2018). This is supported by generally strong associations between water mass types and distinct biogeographic assemblages, indicator species, or short-term dominance of rare taxa (Hooff and Peterson

2006, Keister et al. 2005, 2011). For example, copepods in the CCS are characterized into biogeographic assemblages based on oceanic or neritic and cold or warm-water affinities (Hooff and Peterson 2006). During warm water events (e.g., positive PDO or El Niño), copepod assemblages in the northern CCS shift from consistent representation of taxa with cool-water or sub-arctic affinities to dominance of taxa with oceanic and warm-water sources, indicating anomalous onshore and poleward advection. In the southern CCS, zooplankton community structure responds similarly to variability in water mass characteristics linked to inter-annual and seasonal changes in temperature (Brinton and Townsend 2003, Mackas et al. 2006, Lilly and Ohman 2018). For example, euphausiid assemblage composition off Southern California shifts to an assemblage dominated by warm water and offshore species associated with enhanced representation of warm offshore waters in the study area (Brinton and Townsend 2003, Lilly and Ohman 2018). This study will assess whether similar patterns are present in ichthyoplankton assemblages off northern California, and examine the role that transport variability plays in driving these patterns, providing important context for understanding population and community responses to climate forcing (Auth et al. 2011, McClatchie et al. 2018).

Cross-shelf Structure During Upwelling and its Influence on Ichthyoplankton

Upwelling presents a tradeoff between productivity fueled by upwelled nutrients and offshore transport (Parrish et al. 1981, Fisher et al. 2007). For example, ichthyoplankton that enter the peak upwelling season (e.g., spring and summer) are likely to benefit from highly productive conditions when upwelling is at its maximum intensity,

but are also subject to losses when transport across the shelf is strongest (Parrish et al. 1981). This tradeoff can however be offset by larval behavior and structure generated through upwelling processes, such as fronts and eddies, which can retain and accumulate larvae and in turn help larvae avoid displacement into unfavorable habitat and close life cycle processes (Bjorkstedt et al. 2002, Nishimoto and Washburn 2002, Woodson et al. 2012, Morgan 2014).

During sustained upwelling, larvae inhabiting surface waters are typically transported offshore until they reach a front, which separates colder upwelled water nearshore from warmer offshore waters (Bjorkstedt 1998, Bjorkstedt et al. 2002, Sadrozinski 2008). Downwelling fronts, separating well-mixed waters inshore from stratified offshore waters, often reduce offshore transport which in turn force warm offshore surface waters underneath cooler inshore waters (Austin and Lentz 2002). Both upwelling and downwelling fronts, as well as any ichthyoplankton accumulating at such fronts, can be displaced offshore during wind forcing (Austin and Lentz 2002). Fronts can also form during significant freshwater input from coastal rivers, where less dense freshwater meets denser offshore waters.

Upwelling and in turn hydrographic structure varies across the shelf. Due to changes in wind forcing, bathymetry, and stratification across the shelf, upwelling occurs more diffusely over the shelf rather than in a consistent predictable location (Jacox and Edwards 2011, 2012). Thus, exchange between water masses associated with upwelling doesn't always occur right at the coast where most coastal larvae are produced. For example, exchange can occur offshore of where coastal species' larvae are found, such as

those produced in the coastal boundary layer, wherein larvae inshore are exposed to slower currents than those found further offshore, therefore reducing dispersal distance and favoring retention of coastal taxa (Nickols et al. 2012, 2013). Retention can also be achieved by the development of structure associated with upwelling that can isolate the inner shelf and reduce mixing of inshore waters from those found further offshore (Jacox and Edwards 2011, 2012).

Depth regulation by larvae can promote nearshore retention and decrease the likelihood of being advected offshore during pulses of upwelling (Morgan 2014, Satterthwaite et al. 2021). Since the strength and direction of currents vary throughout the water column, the direction and extent to which larvae are carried depends on their occupied depth. During pulses of upwelling, larvae occupying near surface currents are more likely to be advected offshore and those occupying greater depths are more likely to be retained nearshore (Morgan and Fisher 2010, Miller and Morgan 2013).

The phenology of most marine fishes in the CCS and the subsequent seasonal occurrence of ichthyoplankton is closely tied to the seasonal timing of upwelling. Upwelling reaches maximum intensity during spring and summer months, driving peaks in primary productivity but intensifying offshore and equatorward transport (Jacox and Edwards 2012). During late fall and winter months when winds become southwesterly and upwelling ceases, alongshore flow of surface waters are directed poleward and offshore waters are transported onshore (Hickey 1979, Huyer 1983). To replenish adult populations, many coastal species reproduce in the winter (e.g., *Sebastes* spp. [rockfishes] and osmerids [smelts]) to promote life cycle closure when offshore and equatorward

transport is weakest (Parrish et al. 1981, Doyle et al. 2002, Fisher et al. 2007, Brodeur et al. 2008).

Recent Climate Variability

Oceanographic conditions within the CCE have varied substantially over the last 12 years (2008-2019), including a period of unprecedented warm water anomalies. Basin scale climate indices (PDO, NPGO, and MEI) between late 2007 and early 2013 reflected relatively cool and productive conditions, save for a brief period of warming during the mild 2009-10 El Niño (Figure 1). A transition to warmer and less productive ocean conditions occurred in late 2013, when basin-scale climate patterns underwent a phase shift. Coinciding with this climate shift, the CCE experienced an unprecedented marine heatwave (MHW) that persisted between late 2014-16, causing extensive physical and biological changes throughout the Northeast Pacific (Bond et al. 2015, Di Lorenzo and Mantua 2016). In late 2013, a region of anomalously warm sea surface temperatures (SST) developed in the North Pacific (known as the warm ‘blob’) due to weak storm activity and relaxation in water column mixing (Bond et al. 2015). Warm water anomalies, exceeding 4°C in some parts of the CCE, first appeared in early 2014 as the ‘blob’ drifted east with prevailing currents and eventually arrived at the coast in fall 2014 (Bond et al. 2015, Gentemann et al. 2017). Following a brief upwelling season in mid-2015, the CCE continued to experience warm water anomalies in 2015-16 associated with one of the strongest El Niño events on record (Di Lorenzo et al. 2016, Jacox et al. 2016, Gentemann et al. 2017). Together these events produced a record breaking MHW

and one of the warmest recorded 3-year periods in the CCE (Hobday et al. 2018, Jacox et al. 2018a). While conditions in the central and southern CCS had returned to near normal by winter 2016-17, in the northern CCS recovery from the MHW was slower and had not recovered until spring 2017 (Wells et al. 2017). Apart from a return to cool and productive conditions in early 2018, warming in the CCE persisted in winter 2018-19 with the development of a mild El Niño (Thompson et al. 2019). Despite a brief upwelling season in mid-2019, the CCE again experienced a brief MHW that developed in the Gulf of Alaska in May and impinged on coastal areas in summer 2019 and continued into fall 2019 (Amaya et al. 2020).

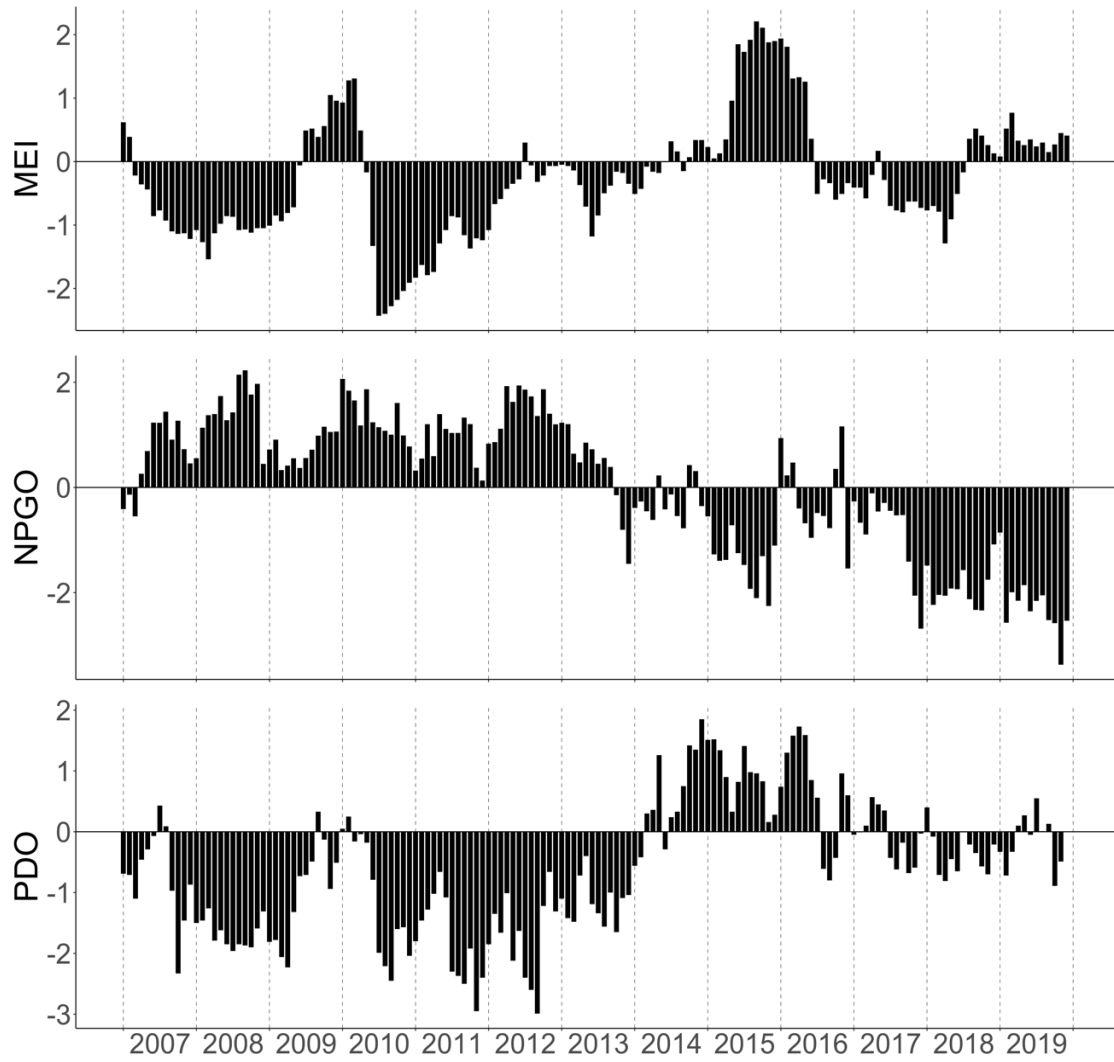


Figure 1. Basin-scale climate indices. Panels from top to bottom represent: Multivariate ENSO Index (MEI), North Pacific Gyre Oscillation (NPGO), Pacific Decadal Oscillation (PDO).

Trinidad Head Line

The Trinidad Head Line (TH-line; 41.05° N) is a high-frequency coastal transect (Bjorkstedt and Peterson 2015) that has been supporting ocean observations in coastal waters off northern California since late 2007 (Figure 2). The TH-line samples a section of the northern California Current, and is bound by two major headlands (Cape Blanco and Cape Mendocino). This region is characterized by strong seasonal forcing, with intense upwelling in the spring and summer and downwelling, storm activity, and riverine input in the winter. Zooplankton and hydrographic data have been collected at approximately monthly intervals since late 2007. The transect initially occupied six stations, three of which are located over the continental shelf and the additional three stations are occupied just offshore of the shelf break. Station 1 (TH01) is located approximately 4.8 km offshore at a depth of 35 m and station 5 (TH05) is located 37 km offshore at a depth of 780 m. Sampling is conducted during 12-hour cruises on Humboldt State University's *R/V Coral Sea*. Stations occupied over the shelf were first sampled at night prior to 2014, but are now sampled during the day due to ease of navigational challenges associated with crab gear. Offshore stations have been consistently sampled after sundown.

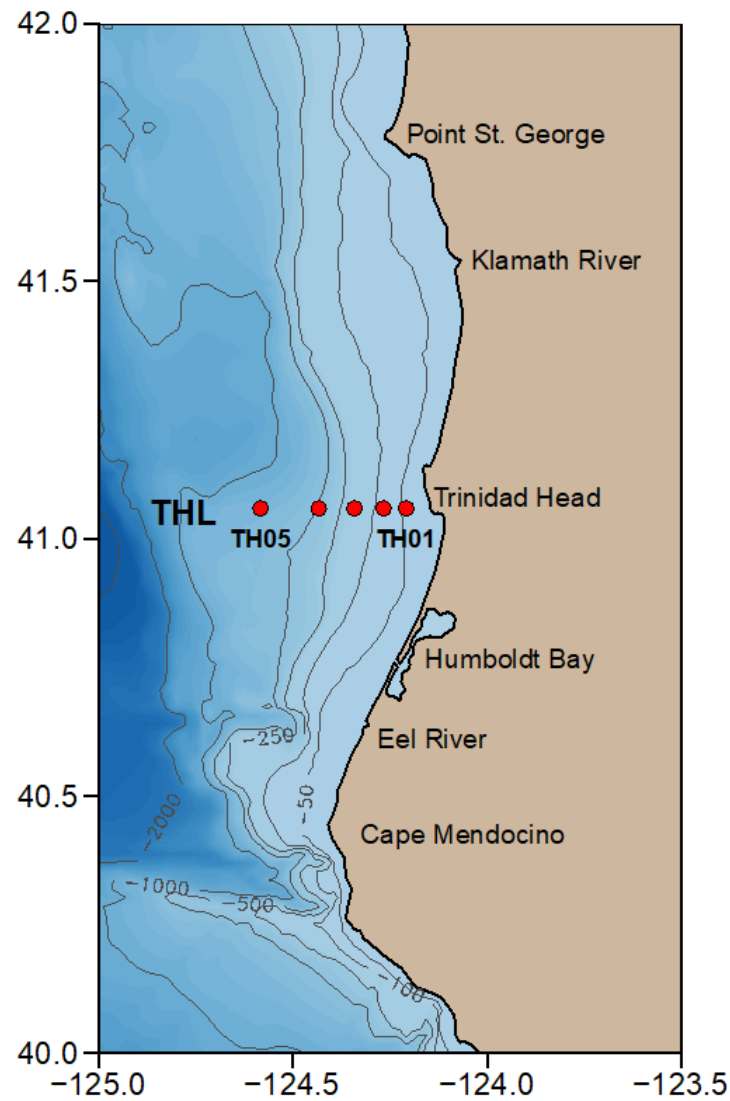


Figure 2. Trinidad Head Line off northern California. Stations (circles) are TH01 (most inshore) to TH05 (most offshore) and overlaid on bathymetry (contours in m). Landmarks are Point St. George, Trinidad Head, and Cape Mendocino.

Research Questions and Objectives

My analysis is structured around three questions that focus on understanding variability in ichthyoplankton assemblage structure and the response to oceanographic variability in the context of large-scale climate forcing. Additionally, this study resolves the challenge of visually identifying larval rockfishes (*Sebastes* spp.) by applying genetic identification techniques and to then use this information to augment the power of the broader analysis of ichthyoplankton assemblage structure and variability off northern California. The three questions are structured as:

Q1. How does ichthyoplankton assemblage structure vary on temporal (e.g., seasonal and interannual) and spatial (e.g., cross-shelf) scales?

Q2. How is assemblage variability linked to seasonal and climate related changes in oceanographic conditions, including marine heatwaves?

Q3. What species of rockfish are present and how does resolving this structure contribute to our understanding of variability in ichthyoplankton assemblages?

This study seeks to do this by (1) characterizing variability in ichthyoplankton assemblages off the northern California coast from November 2007 through December 2019 and (2) linking assemblage variability to seasonal and climate related changes in oceanographic conditions.

MATERIALS AND METHODS

Ethics Statement

All specimens and tissues used in this study are from archived collections obtained in accordance with guidelines of the Institutional Animal Care and Use Committee (IACUC) protocols 05/06.ML.41-A, 09/10.F.03-A, 13/14.M.117.A, and 15/16.M.102-A.

Ichthyoplankton Collection

Ichthyoplankton used in this study were extracted from archived zooplankton samples between November 2007 and December 2019. These samples were collected with a 0.7 m diameter Bongo net fitted with both a 505 μm dyed mesh on one side (Bongo A) and 335 μm dyed mesh on the other (Bongo B), towed obliquely from a depth of 5 meters above the sea floor at shallow stations (TH01-TH02) and to 100 meters at deeper stations (TH03-TH05). Each net is fitted with a General Oceanics flowmeter to estimate the volume of water filtered. At sea, zooplankton contents from each net are immediately preserved in either 5% buffered formalin (Bongo A) or 95% ethanol (Bongo B) after collection. In lab and within 48 hours, samples preserved in 95% ethanol are drained and re-preserved in fresh 95% ethanol.

In lab, zooplankton samples were rinsed and transferred to freshwater and all larval fishes were extracted from whole samples under a dissecting microscope with 10x

magnification. From each individual sample, larval fishes were extracted and put into 70% (Bongo A) or 95% (Bongo B) ethanol. For each sample from the ethanol-preserved net (Bongo B), individuals within the genus *Sebastes* were separated from all other larval fishes and placed into their own vial with 95% ethanol for later genetic identifications.

Although sampling along the TH-line has occurred approximately at monthly intervals since 2007, variability in the sampling intervals and occasional gaps in the record reflect missed cruises or truncated data due to foul weather. A substantial gap from May through November 2010 followed loss-at-sea of our Bongo net. No ethanol-preserved samples are available between June 2011 and early September 2012.

Species Identification

All larval fishes from the formalin-preserved samples were examined under 10x magnification with a dissecting microscope and identified to the lowest possible taxonomic level based on visual characteristics based on print references (Matarese et al. 1989, Moser 1996). Larvae were also scored for developmental stage, measured, and enumerated, although stage and size data are not rigorously analyzed here.

Larvae of only six species of rockfish in our study location can be reliably identified to species based on morphological characters (*S. aurora*, *S. diploproa*, *S. jordani*, *S. levis*, *S. paucispinis*, and *S. saxicola*; Matarese et al. 1989, Laidig et al. 1996, Moser 1996, Moser et al. 2000). All other rockfish larvae are not identifiable to species based on visual assessments and were identified using genetic techniques (i.e., DNA barcoding; Hebert et al. 2003) by comparison of 625 base pair sequences of the

cytochrome *b* gene to an existing reference database of adult rockfish sequences (see detailed methods in Appendix A). A subset of the six visually distinct species listed above were sequenced to confirm visual identifications.

For the rare samples containing >100 unknown rockfish larvae, subsets of larvae were selected as follows for genetic identification. All rockfish larvae that could not be identified to species by visual analysis were sorted into two categories based on the presence or absence of dorsal pigment. On average, 90% of unknown individuals lacked dorsal pigment. All unknown individuals with dorsal pigment were sequenced and roughly half of those lacking dorsal pigment were sequenced. Proportions of individuals from each species lacking dorsal pigment were expanded by extrapolation to the total remaining unknown rockfish larvae.

Ichthyoplankton Count Data Standardization

To account for differences in the vertical extent of the sampled water column, larval abundance is expressed as areal density (Nm^{-2}) at each station, with the caveat that net tows at offshore stations (i.e., stations TH03-TH05) are not sampling the full water column. At each station, counts of larval fish were combined with estimates of the volume of water filtered and the depth of the water column sampled to yield areal density. The volume of water filtered at each station was calculated as a product of the number of flow meter counts, the area of the mouth of the Bongo net, and a calibration coefficient.

Ichthyoplankton Classification

In this study, I define common taxa as those occurring in greater than 5% of samples. Taxa that did not meet this criterion are considered rare. Rare taxa are further distinguished into two different categories based on patterns of occurrence: 1) those that occur infrequently, sporadically, and in low abundance throughout the time series and 2) those that occur in substantial numbers, over a narrow, coherent period. Several rare taxa that meet the latter definition will be discussed separately where appropriate.

To support more comprehensive analysis of biogeographic patterns in the response of the larval assemblage, I categorized all identifiable ichthyoplankton taxa into one of six biogeographic assemblages based on adult spawning distributions using published studies throughout the CCS (Moser et al. 1993, 1994, Love et al. 2000, Williams and Ralston 2002, Hsieh et al. 2005, Allen et al. 2006, Froese and Pauly 2010). Adult spawning distributions were: (1) coastal (typically occupy and spawn in habitat inshore of the upper slope), or (2) oceanic (mostly spawn offshore of the upper slope), crossed with species latitudinal distributions defined as: (1) coastwide (typically found and spawn throughout the CCS), (2) northern (adults spawn mostly Monterey Bay and north), or (3) southern (adults spawn mostly Monterey Bay and south).

Oceanographic Data

As metrics of local and regional oceanographic conditions, several oceanographic variables were selected to characterize variability in the physical environment

experienced by larval fish assemblages throughout the study period. Local oceanographic variables considered were sea surface temperature, salinity, chlorophyll *a* concentration, and spiciness. Regional oceanographic variables considered were a sea level anomaly and the Coastal Upwelling and Transport Index (CUTI).

Local hydrographic variables

In conjunction with collection of zooplankton at each station, hydrographic data (i.e., temperature, salinity, fluorescence) were collected to characterize local hydrographic conditions in the context of local forcing and basin-scale climate variability. Hydrographic data were collected with a Sea Bird Electronics (SBE) model 19 plus V2 CTD, which is cast to 5 m above the seafloor at shallow stations and up to 500 m at deeper stations. At each station, a seasonally corrected temperature anomaly was calculated between 0 and 10 m to represent variability in temperature over the study period. At each station, I fit a generalized additive model (GAM) relating temperature to the day of year using a cyclic cubic spline to ensure continuity across the December-January transition and extracted the model's residuals as seasonally corrected anomalies (deviations from the expected conditions for a given day of year). Where appropriate, temperature anomalies were aggregated by individual cruises to produce a single value across each cruise.

Spiciness

Spiciness (Flament 2002) was examined as an index of variability in water masses present along the TH-line that might influence larval assemblage structure. Values of spiciness increase with increasing temperature and salinity (spicy water) and decrease

with cooler and fresher waters (minty water). Spiciness was measured between 0-10 m and calculated as a seasonally corrected anomaly by regressing spiciness by day of year using a GAM and extracting the model's residuals to represent anomalies (deviations from the expected) based on a cyclic cubic spline

Sea level anomalies

Sea level anomalies are an index for transport along the coast, wherein increased equatorward flow is represented by negative anomalies and weak equatorward or poleward flow is represented by positive anomalies (Chelton et al. 1982). I obtained daily sea level height for the north spit, Humboldt Bay tide gauge (40°76.7'N, 124°21.7'W), from the University of Hawaii sea level center (<http://uhslc.soest.hawaii.edu/>). Sea level height was seasonally corrected by fitting a GAM to the available daily source data (1977-2019) using the day of year as a predictor. Residuals extracted from the GAM model represent daily anomalies and were averaged to produce monthly values. Cumulative sea level anomalies were calculated using daily values from January 1st to December 31st.

Coastal upwelling index

CUTI is an approximate index for the strength of vertical transport near the coast (i.e., upwelling and downwelling) in the CCS (Jacox et al. 2018b). Centered around zero, positive CUTI values indicate upwelling conditions and negative values indicate weak upwelling or downwelling, respectively. Daily and monthly CUTI values were obtained for the time period 2007-2019 for a grid cell centered around 41°N

(<http://mjacox.com/upwelling-indices/>). Cumulative CUTI values were calculated using daily values from January 1 to December 31.

Data Structure

The larval fish data analyzed in this study are drawn from samples collected from November 2007 to December 2019 and organized into two data sets. Each dataset consists of a measure of the abundance (Nm^{-2} in the upper 100 m of the water column) for each species (or lowest taxonomic level) at each station occupied on each cruise. The first dataset, herein referred to as the “visual assemblage” is based on visual identifications of larvae from formalin-preserved samples. The second dataset, herein referred to as the “rockfish assemblage”, is based on visual and genetic identifications of rockfish larvae from ethanol-preserved samples. Discontinuities between the formalin- and ethanol-preserved samples hindered joining the two datasets. I present and analyze larval fish data from the visual and rockfish assemblages separately but in concert.

In addition, a separate analysis of a limited “joint” dataset was conducted to evaluate the added effects of resolving ambiguity in larval rockfish identifications on spatial and temporal variability of the broad larval fish assemblage off northern California. Here, a comparative community analysis was conducted between two limited datasets. The first dataset, referred to as the “unresolved assemblage”, encompasses all larval taxa from the visual assemblage with rockfish larvae limited to the genus *Sebastes*. The second dataset, referred to as the “resolved assemblage”, encompasses all larval taxa from the visual assemblage including individuals from the genus *Sebastes* resolved to

species using genetic and visual techniques. The datasets have a gap between June 2011 and early September 2012, arising from a lack of ethanol-preserved samples, which prevented genetic identification of rockfishes during this time period.

For the comparative analysis, genetically identified larval rockfishes were incorporated into the visual larval fish time series as follows. The initial step was sample-to-sample extrapolation, which consisted of taking the proportion of individuals from each genetically identified rockfish species within an individual sample and extrapolating that to the total number of unknown larval rockfishes within the corresponding sample from the visual assemblage. In cases where no rockfish larvae were present in a corresponding ethanol-preserved sample, assignment of species to rockfish larvae in the visual time series was based on genetic identifications from the neighboring samples (i.e., stations). For example, estimates of species composition at TH04 would be based on average percent species composition from TH05 and TH03 (from the same cruise). If genetically identified larval rockfishes were unavailable for an entire cruise, species composition from each station within the nearest cruise (< 14 days) was used as the basis for species composition to be extrapolated into each station that contained larval rockfishes within the dataset lacking genetic identifications. Eleven samples for which there was inadequate information to inform species composition of larval rockfishes within the visual assemblage were excluded from the analysis.

Statistical Analysis

All data analysis was performed in R (version 4.0.3; R Core Team 2020). All multivariate methods (NMDS, hierarchical cluster, PERMANOVA, and CCA) were applied to the data using functions in the R package ‘Vegan’ (Oksanen 2020). Indicator species analysis was performed using functions in the R package ‘indicspecies’ (De Caceres and Legendre 2009). GAMs were fit using the R package ‘mgcv’ (Wood 2017). All figures were created using the R package ‘ggplot2’ (Wickham 2016).

In general, analysis was focused at the level of individual samples to capture variability in both space (cross-shelf) and time. When appropriate, data or results are aggregated by cruise (i.e., averaged across stations within a cruise) to more effectively capture or illustrate inter-annual patterns and relationships to climate. Transformations of the data (i.e., log and 4th root) are applied when appropriate, as indicated below for each analysis applied to the data.

A suite of multivariate methods was used to explore how the larval fish community off northern California was structured and to identify oceanographic variables that correlate with species abundance or measures of assemblage structure over time or space as an indicator of factors influencing ichthyoplankton off northern California. Analyses (each indicated below) was performed at the level of individual stations using a sample (each net tow) by species matrix. Only common taxa were used in these analyses and samples where no larval fish were captured were removed. Removal of rare taxa was considered appropriate as rare taxa would bias results from multivariate analyses.

Abundance data for each taxon was 4th root transformed prior to the analysis to reduce the influence of samples with very high abundances (Clarke and Warwick 2001).

Cross-shelf and seasonal patterns

Hierarchical cluster analysis was used to identify cross-shelf, monthly, and taxonomic assemblages. Taxonomic clusters were created to determine which species grouped together and shared similar patterns over the time series. Each dendrogram was computed using group-averaged clustering from a Bray-Curtis ranked similarities matrix on 4th root transformed larval fish densities (Clarke and Warwick 2001). Each dendrogram was cut to produce ecologically interpretable clusters when they were visually apparent.

Permutational Analysis of Variance (PERMANOVA) was performed on the sample-by-species matrix using a Bray-Curtis dissimilarity index to test for significant differences in species composition across the transect (i.e., stations) and across seasons (i.e., months). Levels within each variable hypothesized to influence community variability were defined as: 1) station (TH01-TH05) and 2) and month (January-December). PERMANOVA is a nonparametric multivariate analysis that uses permutation techniques to test for differences in species composition among different groups (Clarke and Warwick 2001). When the PERMANOVA test was found to be significant ($p < 0.05$, $N=999$ permutations), permutational pairwise tests (using a Bonferroni correction) were conducted for each level of the factor variable station ($n=5$) or month ($n=12$) to identify where significant ($p < 0.05$, $N=9999$ permutations) contrasts existed. When PERMANOVA indicated distinct groups, an indicator species analysis

(ISA) was applied to identify taxa that were significant indicators of those groups based on an indicator value. Indicator values are a product of the relationship between a taxon's fidelity (e.g., the proportion of total abundance found within a particular group) and specificity (e.g., the proportion of total occurrence within a particular group), which is then tested for statistical significance ($p < 0.05$) using Monte Carlo simulations with 5000 random restarts (Cáceres and Legendre 2012). For the factor variable station, each taxon was allowed to be identified as an indicator of up to a combination of two stations. Instead of identifying indicator taxa for a single month, taxa were set as indicators for distinct seasonal periods. These seasonal periods were defined based on sets of months that clustered together in hierarchical cluster analysis.

Inter-annual patterns

To examine how abundance of individual larval taxa changed through time, I compared cruise averaged densities of common taxa between three time periods defined by pre-MHW (November 2007- July 2014), MHW (August 2014- May 2017), and post-MHW (June 2017- December 2019) conditions. I defined these time periods *a priori* based on climate conditions that generally favored cooler conditions during the first half of the time series, anomalous warming during the MHW, and a return to somewhat normal conditions post-MHW. To account for strong seasonal patterns of occurrence, each taxon was subset by their primary seasonal occurrence by calculating a mean day of year weighted by density (No./m²) and using two standard deviations, centered around this mean value, to define their primary seasonal extent. Several taxa that were present year-round (*Liparis* spp., *P. crockeri*, and *T. crenularis*) were not subset for a particular

seasonal period. Non-parametric Kruskal-Wallis tests were used to test the null hypothesis that abundance of common taxa did not differ significantly between time periods marked by substantial oceanographic change. In cases where the null hypothesis was rejected, Dunn's multiple comparisons test (using a Bonferroni correction) was used to identify significant ($p < 0.05$) contrasts. Larval concentrations were $\log_{10}(\text{Nm}^{-2} + 1)$ transformed prior to the analysis.

Temporal variability in ichthyoplankton diversity and species richness were examined at seasonal and interannual time scales in the context of a seasonally corrected temperature anomaly (see oceanographic data in methods for description of anomaly calculation). This analysis was performed on the cruise-aggregated data using all identifiable taxa. Larval diversity was measured by the Shannon-Weiner diversity index (H'), which calculates a diversity value using the number of species sampled and their relative abundances (Shannon and Weaver 1949). Higher Shannon-Weiner diversity corresponds to either a greater number of species sampled or where abundance is evenly distributed among species. Indices for species richness was expressed as the total number of unique taxa present within each cruise.

To assess the contribution of rare species to assemblage variability and to support more rigorous analysis, I examined temporal variability in cruise aggregates of species richness and log-transformed larval density ($\text{No.}/\text{m}^2$) at seasonal and interannual time scales for each biogeographic assemblage. Indices for species richness was expressed as the total number of unique taxa present within each cruise.

Non-metric multidimensional scaling analysis (NMDS)

Non-metric multidimensional scaling analysis (NMDS) was conducted to visualize how spatial and temporal variables structure the larval fish community from the TH-line. NMDS reduces the many dimensions of ecological data into just a few using a Bray-Curtis dissimilarity matrix and is followed by ordination to visualize and interpret assemblage structure. For this analysis, the same species-by-sample matrix used in earlier multivariate methods formed the matrix used here in NMDS. Candidate spatial variables were defined as station (TH01-TH05) and candidate temporal variables were defined based on resulting monthly clusters from hierarchical cluster analysis. The number of dimensions (axes) for the final ordination was based on the stress level (measure of goodness of fit). A smaller stress values indicates a better representation of the data, where a value below 0.1 provides an excellent representation of the data and a value greater than 0.2 is deemed a poor representation (Clarke and Warwick 2001). The smallest number of dimensions that maintained a stress level below 0.15 was selected as the final solution for ordination.

To analyze temporal variability in NMDS, values from each of the axes were extracted and plotted at seasonal and interannual time scales. Values extracted from NMDS serve as an index of community composition and can be used to identify patterns and community changes over the time series. This analysis was conducted at both the station level and as cruise aggregates. Analysis of values from each NMDS axis at the seasonal scale (day of year) were examined in the context of a seasonally corrected temperature anomaly (see oceanographic data in methods for description of anomaly

calculation). To examine interannual patterns, seasonal patterns were removed by fitting a GAM relating NMDS values to the day of year using a cyclic cubic spline to ensure continuity across the December-January transition and extracted the model's residuals as seasonally corrected values (deviations from the expected conditions for a given day of year) to plot over the time series.

Oceanographic-assemblage correlations

To assess and visualize how oceanographic variables were correlated with community structure I used canonical correspondence analysis (CCA). The assumption of unimodal relationships between candidate environmental variables and taxon abundances was broadly satisfied. Local environmental variables considered in this analysis were temperature, salinity, chlorophyll *a* concentration (transformed as $\log_{10}([\text{chl } a] + 1)$), and spiciness measured near the surface (0-10 m) and represented as anomalies. Regional variables considered were sea level and CUTI represented by anomalies and averaged 14-days prior to a cruise. Only common taxa were used in this analysis and samples where no larval fish were captured were removed. Larval densities were transformed as $\log_{10}(\text{Nm}^{-2} + 1)$ prior to the analysis. Forward stepwise selection of explanatory variables was carried out using the Monte Carlo permutation test. The significance of each environmental variable was assessed using permutations ($n=999$) and the significance level set at the $\alpha=0.05$ level. Only significant ($p < 0.05$) environmental variables were fit and displayed in ordination. The result for each oceanographic variable is a vector fit onto ordination space where strong predictors have longer arrows than weaker predictors.

The significance ($p < 0.05$) of the model and each of the canonical axes were tested using permutations ($n=999$).

To compliment results from analyses based on larval assemblage variability in the context of climate forcing, delta-GAMs were used to characterize species-specific patterns in occurrence and density (Nm^{-2}) conditional on occurrence in the context of a seasonally corrected temperature anomaly. This analysis was conducted at the scale of individual stations. The delta GAM method is used when the data contains a large proportion of zeroes and accounts for this by fitting two independent models, wherein the first model estimates the probability of occurrence and the second estimates the magnitude of abundance when present (Welsh et al. 1996). The first model estimating the probability of occurrence is fit using a GAM with a binomial distribution and the second model is fit using a gaussian distribution after log-transforming abundances of each taxon. Effects of station, day of year, and a seasonally corrected temperature anomaly (scale of individual stations; see oceanographic data in methods for description of anomaly calculation) were included in the model to isolate correlations with seasonally corrected temperature anomalies. The significance of the temperature anomaly smooth term within each model was evaluated against $\alpha=0.05$. No model selection criteria were applied.

To assess the null hypothesis that patterns in several important indices of larval fish biodiversity and assemblage structure (Species richness, Shannon-Weiner diversity, and NMDS) are related to oceanographic variability, pairwise linear regression was used to evaluate the relationship between a seasonally corrected temperature anomaly and

indices of larval fish biodiversity and assemblage structure. This analysis was performed on the cruise aggregate scale and used species richness, Shannon-Weiner diversity, and values of NMDS analyzed earlier as the response variables. To remove seasonal cyclical patterns, which might affect interpretations of regression analysis, each index was calculated as an anomaly. Anomalies were estimated as residuals from a GAM linking each index of larval fish biodiversity and assemblage structure to day of year, based on a cyclic cubic spline to ensure continuity across the December-January transition.

Relationships between each index and a temperature anomaly (see oceanographic data in methods for description of anomaly calculation) was analyzed during all months (i.e., using all available data) and by separate seasons if it was visually apparent that the effect of temperature on each index varied by season. The assumptions of linear regression (i.e., normality, linear relationships, homogeneity of variance) were broadly satisfied. The significance of the temperature anomaly term in each regression analysis was set at the $\alpha=0.05$ level.

Comparative community analysis

For both the unresolved and resolved datasets, hierarchical cluster analysis and NMDS were performed on separate sample-by-species matrices using a Bray-Curtis dissimilarity measure to compare differences in cross-shelf, monthly, and taxonomic assemblages. This analysis was performed on common taxa and samples where no larval fish occurred were removed. Larval densities (Nm^{-2}) were 4th root transformed to reduce the influence of samples with very high or very low abundances. In addition, temporal variability in NMDS values was analyzed at seasonal and interannual time scales.

Temporal variability in Shannon-Weiner diversity and species richness were compared between unresolved and resolved assemblages at seasonal and interannual time scales in the context of a seasonally corrected temperature anomaly (aggregated by cruise; see oceanographic data in methods for description of anomaly calculation). This analysis was conducted based on all identifiable collected taxa at the cruise aggregate level.

To assess whether resolving rockfishes to species within the broad assemblage had an effect on the relationship between a temperature anomaly (aggregated by cruise; see oceanographic data in methods for description of anomaly calculation) and indices of larval fish biodiversity and assemblage structure (Species richness, Shannon-Weiner diversity, and NMDS), I compared results of pairwise linear regression between the unresolved and resolved larval assemblages. To remove seasonal cyclical patterns, which might affect interpretations of regression analysis, each index was calculated as an anomaly. Anomalies were estimated as residuals from a GAM linking each index of larval fish biodiversity and assemblage structure (aggregated by cruise) to day of year, based on a cyclic cubic spline to ensure continuity across the December-January transition. The assumptions of linear regression (i.e., normality, linear relationships, homogeneity of variance) were broadly satisfied. The significance of the temperature anomaly term in each regression analysis was evaluated against $\alpha=0.05$.

RESULTS

General Assemblage Composition

Visual assemblage

This dataset includes 16,600 larvae representing 115 taxa collected from 558 formalin-preserved samples over the course of 128 cruises (Table 1). Most of the collected larvae were in pre-flexion (75%) or flexion (18%) stages of development. Of the 115 collected taxa, 102 were resolved to species, 8 are resolved to genus, and 5 were resolved to family. Taxa limited to the genus or family level within this dataset included the sanddabs (*Citharichthys* spp.), thornyheads (*Sebastolobus* spp.), snailfishes (*Liparis* spp.), several genera of sculpins (*Artedius* spp., cottids, etc.), rockfishes (*Sebastes* spp.), smelts (Osmeridae), and several rare taxa not listed ($n = 7$; see Appendix B). Infrequent observations of larger individuals of *Citharichthys* spp. can however be identified to species, with most representing *C. sordidus* (Pacific sanddab) and *C. stigmaeus* (speckled sanddab). At the family level, Cottidae and Pleuronectidae were each represented by the greatest number of species ($n = 16$), followed by the family Myctophidae ($n = 15$), and the family Bathylagidae ($n = 6$). Fifteen taxa are considered common and collectively account for 94% of the total larval concentration (by combined areal density). The three most numerically abundant taxa, *Stenobranchius leucopsarus*, aggregate *Sebastes* spp., and *Citharichthys* spp., accounted for 71.5% of the total larval concentration and 76% of the total concentration of the 15 common taxa. Of the common taxa in our collections,

most have coastwide ($n = 7$) or northern ($n = 6$) distributions in the CCS. Only two common species in our collections (*Engraulis mordax* and *Merluccius productus*) typically spawn further to the south in the CCS. Eleven of the common taxa are considered coastal and four are considered oceanic.

Rockfish assemblage

This dataset includes 3,382 individual larval rockfishes (*Sebastes* spp.) captured in 473 ethanol-preserved samples across 109 cruises. The rockfish dataset includes 32 species and two species complexes that cannot be rigorously differentiated even with the addition of species' biogeographic distributions (Table 2): the WEVZ complex (*Sebastes wilsoni* [Pygmy rockfish], *Sebastes emphaeus* [Puget Sound rockfish], *Sebastes variegatus* [Harlequin rockfish], *Sebastes zacentrus* [Sharpchin rockfish]) and the MyDi complex (*Sebastes mystinus* [Blue rockfish] and *Sebastes diaconus* [Deacon rockfish]). Of the 34 species or species complexes, 16 are considered common. The majority of these larvae are in the pre-flexion (90%) stage of development. Approximately one-third of the rockfish larvae ($n = 1,136$) could be identified visually, and most of the remaining larvae ($n = 2,246$) were successfully identified using genetic sequencing. Sequencing failed for 87 individuals (a 4% failure rate). The four most abundant species or species complexes (*S. saxicola*, *S. entomelas*, *S. jordani*, and MyDi) accounted for 72% of the total larval concentration. Of the common species or complexes in our collections, most have coastwide ($n = 7$) or northern ($n = 7$) distributions in the CCS. Only two common species in our collections (i.e., *Sebastes jordani* and *Sebastes goodei*) have a southern distribution in the CCS.

Table 1. Taxonomic list of common larval fishes within the visual assemblage, including corresponding adult biogeographic ranges in ‘()’ (latitudinal: coastwide [CW], northern [N], and southern [S]; cross-shelf: oceanic [O] and coastal [C]), mean areal density (No./m²), total areal density, percent of total areal density, maximum observed areal density in a sample, and percent positive tow. Total areal density is calculated as the areal density summed across all samples. Percent positive tow is calculated as the number of tows in which a species was observed over the total number of tows. Mean areal density is calculated as the total areal density over the total number of tows. Percent of total density is calculated as the total areal density of an individual taxon over the total aggregate larval density summed across all samples. The number of rare taxa included within coastwide, northern, and southern assemblages are indicated in ‘()’. Abbreviations represent taxon names used in ordination. See Appendix B for list of rare taxa.

Taxa	Common Name	Family	Abbreviation	Mean density	Total density	Percent of total density	Percent Positive Tow
<i>Stenobranchius leucopsarus</i> (CW-O)	Northern lampfish	Myctophidae	Sleuc	4.26	2373	31.6	54.9
<i>Sebastes</i> spp. (CW-C)	Rockfishes	Sebastidae	Sebas	4.077	2270.8	30.3	60.5
<i>Citharichthys</i> spp. (CW-C)	Sanddabs	Paralichthidae	Citha	1.297	722.3	9.63	26.2
<i>Bathylagus ochotensis</i> (CW-O)	Popeye blacksmelt	Bathylagidae	Bocho	0.621	345.6	4.61	31.8
Osmerids (N-C)	Smelts	Osmeridae	Osmer	0.512	284.9	3.8	9.9
<i>Merluccius productus</i> (S-C)	Pacific hake	Merrlucidae	Mprod	0.453	252.1	3.36	7.9
<i>Lyopsetta exilis</i> (CW-C)	Slender sole	Pleuronectidae	Lexil	0.37	205.8	2.74	23
<i>Tarletonbeania crenularis</i> (N-O)	Blue lanternfish	Myctophidae	Tcren	0.343	191	2.55	32.5
<i>Protomyctophum crockeri</i> (CW-O)	California flashlightfish	Myctophidae	Pcroc	0.155	86.6	1.15	19.9
<i>Psettichthys melanostictus</i> (N-C)	Sand sole	Pleuronectidae	Pmela	0.154	86	1.15	7
<i>Parophrys vetulus</i> (CW-C)	English sole	Pleuronectidae	Pvetu	0.097	53.8	0.72	8.3
<i>Engraulis mordax</i> (S-C)	Northern anchovy	Engraulidae	Emord	0.093	51.6	0.69	7

Taxa	Common Name	Family	Abbreviation	Mean density	Total density	Percent of total density	Percent Positive Tow
<i>Liparis</i> spp. (N-C)	Snailfishes	Liparidae	Lipar	0.084	46.7	0.62	12.2
<i>Artedius</i> spp. (N-C)	Artedius sculpins	Cottidae	Arted	0.062	34.3	0.49	9.2
<i>Glyptocephalus zachirus</i> (N-C)	Rex sole	Pleuronectidae	Gzach	0.046	25.4	0.34	6.6
Rare Coastwide (n=35)				0.399	217.6	2.88	100
Rare Northern (n=45)				0.293	163.6	2.18	98.2
Rare Southern (n=20)				0.16	89.3	1.19	23.3

Table 2. Taxonomic list of larval rockfishes within the rockfish assemblage, including corresponding adult biogeographic ranges in ‘()’ (latitudinal: coastwide [CW], northern [N], and southern [S]), mean areal density (No./m²), mean areal density, total areal density, percent of total areal density, maximum observed areal density in a sample, and percent positive tow. Total areal density is calculated as the areal density summed across all samples. Percent positive tow is calculated as the number of tows in which a species was observed over the total number of tows. Mean areal density is calculated as the total areal density over the total number of tows. Maximum catch is the largest areal density observed in a tow. Percent of total density is calculated as the total areal density of an individual taxon over the total aggregate larval density summed across all samples. Abbreviations represent taxon names used in ordination. The “WEVZ” complex includes *S. wilsoni* (Pygmy rockfish), *S. emphaeus* (Puget Sound rockfish), *S. variegatus* (Harlequin rockfish), and *S. zacentrus* (Sharpchin rockfish). The “MyDi” complex includes *S. mystinus* (Blue rockfish) and *S. diaconus* (Deacon rockfish).

Species	Common Name	Abbreviation	Mean density	Total density	Percent of total density	Percent Positive Tow
<i>Sebastes saxicola</i> (CW)	Stripetail rockfish	saxi	0.889	410	22.8	13.9
<i>Sebastes entomelas</i> (N)	Widow rockfish	ento	0.845	389.6	21.7	11.7
<i>Sebastes jordani</i> (S)	Shortbelly rockfish	jord	0.591	272.3	15.2	7.6
“MyDi” complex (CW)	MyDi	MyDi	0.48	221.5	12.3	12
<i>Sebastes goodei</i> (S)	Chilipepper rockfish	good	0.281	129.6	7.21	8.5
"WEVZ" complex (CW)	WEVZ	WEVZ	0.2	92	5.12	14.8
<i>Sebastes diploproa</i> (CW)	Splitnose rockfish	dipl	0.179	82.5	4.59	13
<i>Sebastes flavidus</i> (N)	Yellowtail rockfish	flav	0.095	43.6	2.43	3.3
<i>Sebastes crameri</i> (N)	Darkblotched rockfish	cram	0.074	34.2	1.9	5.7
<i>Sebastes elongatus</i> (CW)	Greenstriped rockfish	elon	0.042	19.5	1.09	4.6
<i>Sebastes melanops</i> (N)	Black rockfish	mela	0.035	16.2	0.9	3.7
<i>Sebastes pinniger</i> (N)	Canary rockfish	pinn	0.026	11.8	0.66	3.5

Species	Common Name	Abbreviation	Mean density	Total density	Percent of total density	Percent Positive Tow
<i>Sebastes aurora</i> (CW)	Aurora rockfish	auro	0.022	10.3	0.57	3
<i>Sebastes proriger</i> (N)	Redstripe rockfish	pror	0.022	9.92	0.55	2.6
<i>Sebastes maliger</i> (N)	Quillback rockfish	mali	0.02	9.3	0.52	2.2
<i>Sebastes caurinus</i> (CW)	Copper rockfish	caur	0.014	6.53	0.36	2.2
<i>Sebastes rufus</i> (S)	Bank rockfish		0.013	5.93	0.33	1.3
<i>Sebastes helvomaculatus</i> (N)	Rosethorn rockfish		0.012	5.4	0.3	1.3
<i>Sebastes rosaceus</i> (S)	Rosy rockfish		0.011	5.11	0.28	0.9
<i>Sebastes paucispinis</i> (CW)	Bocaccio		0.009	4.36	0.24	1.3
<i>Sebastes miniatus</i> (S)	Vermillion rockfish		0.005	2.45	0.14	1.1
<i>Sebastes auriculatus</i> (CW)	Brown rockfish		0.005	2.42	0.13	0.9
<i>Sebastes ruberrimus</i> (N)	Yelloweye rockfish		0.005	2.2	0.12	0.9
<i>Sebastes alutus</i> (N)	Pacific Ocean Perch		0.004	1.79	0.1	0.4
<i>Sebastes chlorostictus</i> (S)	Greenspotted rockfish		0.004	1.7	0.09	0.7
<i>Sebastes ovalis</i> (S)	Speckled rockfish		0.003	1.4	0.08	0.7
<i>Sebastes serranoides</i> (S)	Olive rockfish		0.002	1.09	0.06	0.2
<i>Sebastes nebulosus</i> (N)	China rockfish		0.002	0.89	0.05	0.4
<i>Sebastes melanostomus</i> (S)	Blackgill rockfish		0.002	0.75	0.04	0.2

Species	Common Name	Abbreviation	Mean density	Total density	Percent of total density	Percent Positive Tow
<i>Sebastes levis</i> (S)	Cowcod		0.001	0.55	0.03	0.2
<i>Sebastes nigrocinctus</i> (N)	Tiger rockfish		0.001	0.43	0.02	0.2
<i>Sebastes reedi</i> (N)	Yellowmouth rockfish		0.001	0.41	0.02	0.2
<i>Sebastes hopkinsi</i> (S)	Squarespot rockfish		0.001	0.35	0.02	0.2
<i>Sebastes brevispinis</i> (N)	Silvergray rockfish		0.001	0.31	0.02	0.2

Cross-shelf and Seasonal Assemblage Patterns

Visual assemblage

Inspection of species-specific spatial distributions (aggregated over the entire time series) differentiates a nearshore assemblage concentrated at the inshore stations (TH01-TH02) from an ‘offshore’ assemblage occurring over the outer shelf and upper slope (stations TH03-TH05; Figure 3). Several taxa (e.g., *E. mordax* and *Citharichthys* spp.) were identified as being more broadly distributed along the transect. Hierarchical cluster analysis performed on stations corroborates these spatial patterns, grouping stations into a nearshore cluster (stations TH01 and TH02) and an offshore cluster (stations TH03-TH05; Figure 3). Assemblage composition differed significantly across stations (PERMANOVA, $p < 0.001$; Table 3), and corresponding pairwise tests indicate assemblage composition offshore (stations TH03-TH05) is significantly different from composition at stations found nearshore (stations TH01-TH02; Figure 4). ISA identified twelve of the fifteen common species as significant indicators of one or a combination of two stations (Table 3). Two nearshore taxa were identified as significant indicators for station TH01 (Osmeridae and *P. melanostictus*) and three taxa (*Liparis* spp., *Artedius* spp., and *P. vetulus*) were identified as significant indicators for both stations TH01 and TH02. The osmerids represented a strong indicator (52%) of station TH01, whereas weaker associations were identified among *P. melanostictus* (38%) and *P. vetulus* (34%). Seven taxa that tend to be distributed further offshore were identified as indicators of

stations TH04 and TH05, with *S. leucopsarus* (66%), *Sebastes* spp. (66%), and *T. crenularis* (60%) representing the strongest indicators of these stations.

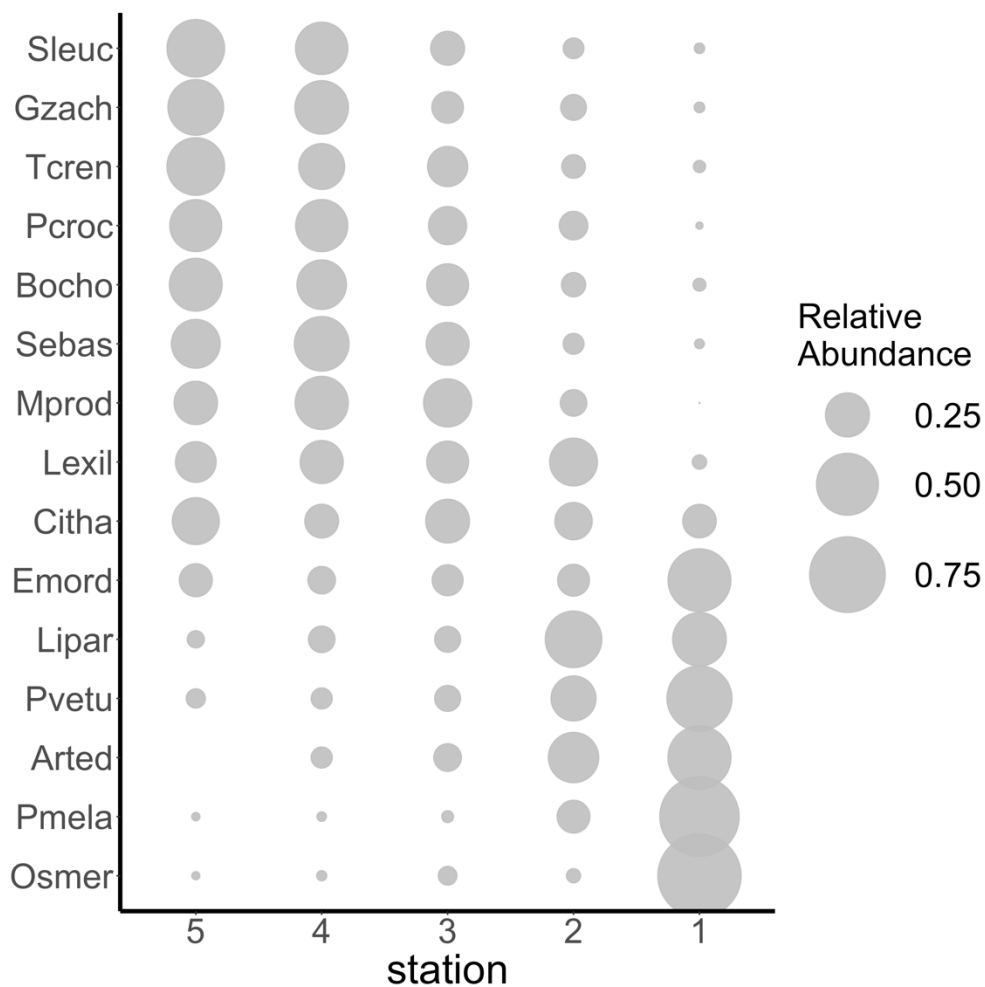


Figure 3. Cross-shelf distributions of common larval taxa within the visual assemblage aggregated over the entire time series. Cross-shelf distributions are represented as relative abundance (scaled by size of bubble) based on areal density (No./m²) at stations (x-axis) 5 (TH05; offshore) to 1 (TH01; nearshore). See Table 1 for full taxon names corresponding to abbreviations.

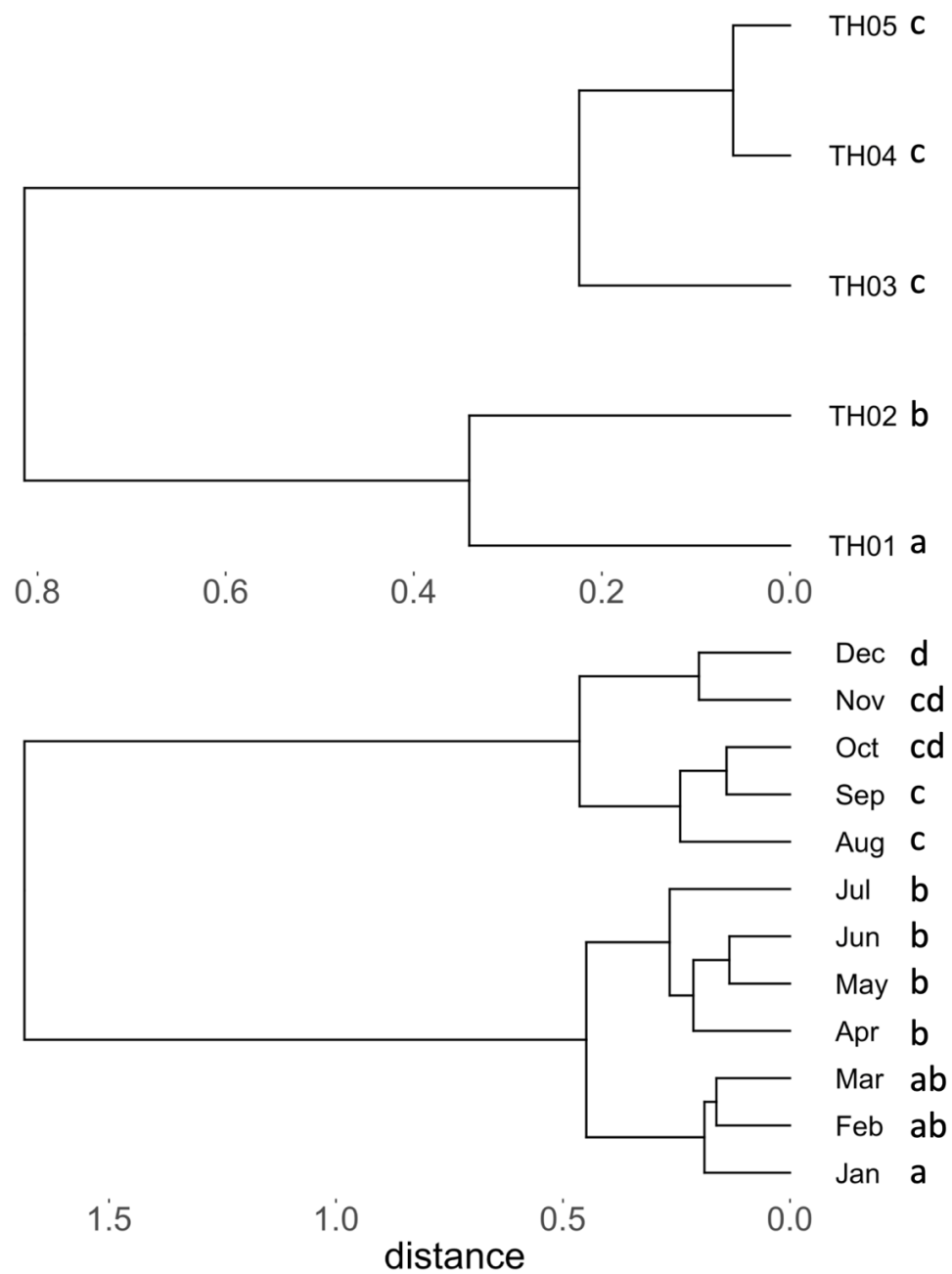


Figure 4. Cross-shelf and seasonal dendrograms resulting from hierarchical cluster analysis performed on common taxa within the visual assemblage. Top panel: cross-shelf dendrogram performed on stations. Bottom panel: seasonal dendrogram performed on individual months. Different letters indicate results of pairwise PERMANOVA analysis indicating significant pairwise differences ($p < 0.05$) using a Bonferroni correction.

Table 3. Results of Permutational Analysis of Variance (PERMANOVA) and indicator species analysis (ISA) for station and seasonal differences in composition of common taxa within the visual assemblage. Seasonal clusters are based on visually distinct monthly clusters from hierarchical cluster analysis performed on months (See Figure 4). Significance of indicator taxa ($p < 0.05$) for each factor level are listed with their associated indicator value (%).

Factor	PERMANOVA	Level	Indicator Taxa
Station	$p < 0.001$	TH01	Osmeridae (52%), <i>P. melanostictus</i> (38%)
		TH01 and TH02	<i>Liparis</i> spp. (46%), <i>Artedius</i> spp. (43%), <i>P. vetulus</i> (34%)
		TH04 and TH05	<i>S. leucopsarus</i> (66%), <i>Sebastes</i> spp. (66%), <i>T. crenularis</i> (60%), <i>B. ochotensis</i> (57%), <i>P. crockeri</i> (47%), <i>L. exilis</i> (40%), <i>G. zachirus</i> (30%)
Seasonal cluster	$p < 0.001$	January-March	<i>S. leucopsarus</i> (60%), <i>Sebastes</i> spp. (59%), <i>B. ochotensis</i> (50%), <i>M. productus</i> (35%), <i>P. vetulus</i> (26%)
		Apr-July	<i>L. exilis</i> (58%), <i>G. zachirus</i> (35%), <i>Artedius</i> spp. (27%)
		August-September	<i>Citharichthys</i> spp. (44%), <i>P. melanostictus</i> (28%)
		November-December	<i>P. crockeri</i> (41%), <i>Liparis</i> spp. (28%), Osmeridae (27%)

For most taxa within the visual assemblage, occurrence and abundance exhibited clear seasonal patterns (Figure 5). More than half of the common taxa were most frequently captured and abundant during late winter and early spring months, while several other taxa (e.g., *Citharichthys* spp. and *P. melanostictus*) were most commonly captured and abundant later in the year. A few taxa (e.g., *T. crenularis*, *P. crockeri*, and *Liparis* spp.) were captured throughout the year, without clear seasonal patterns in occurrence or abundance. Hierarchical cluster analysis corroborates these average seasonal patterns, grouping months into two distinct clusters (January-July and August-

December), which could be further differentiated into smaller seasonal clusters: winter (January-March), spring and early summer (April-July), late summer and fall (August-September), and late fall and early winter (November-December; Figure 5). Assemblage composition differed significantly across months (PERMANOVA, $p < 0.001$; Table 3). Pairwise tests indicate assemblage composition in the months of January-March were significantly different than all other months, apart from March, which was similar in composition to the months of April-July (Figure 4). Assemblage composition between months within the August-December cluster did not differ significantly, apart from December, which differed from assemblages in August and September. ISA identified thirteen of the fifteen common species as significant indicators for one of the four distinct seasonal clusters (Table 3). Corroborating seasonal patterns identified in Figure 5, January-March was assigned the most indicator taxa ($n = 5$), with *S. leucopsarus* (60%), *Sebastes* spp. (59%), and *B. ochotensis* (50%) emerging as strong indicators of this seasonal period. Three taxa were identified as significant indicators of the April-July seasonal period but were generally weak indicators, apart from *L. exilis* (58%). Similarly, most taxa identified as significant indicators of the August-September ($n = 2$) or November-December ($n = 3$) seasonal period were weak, apart from *Citharichthys* spp. (August-September; 44%) and *P. crockeri* (November-December; 41%).

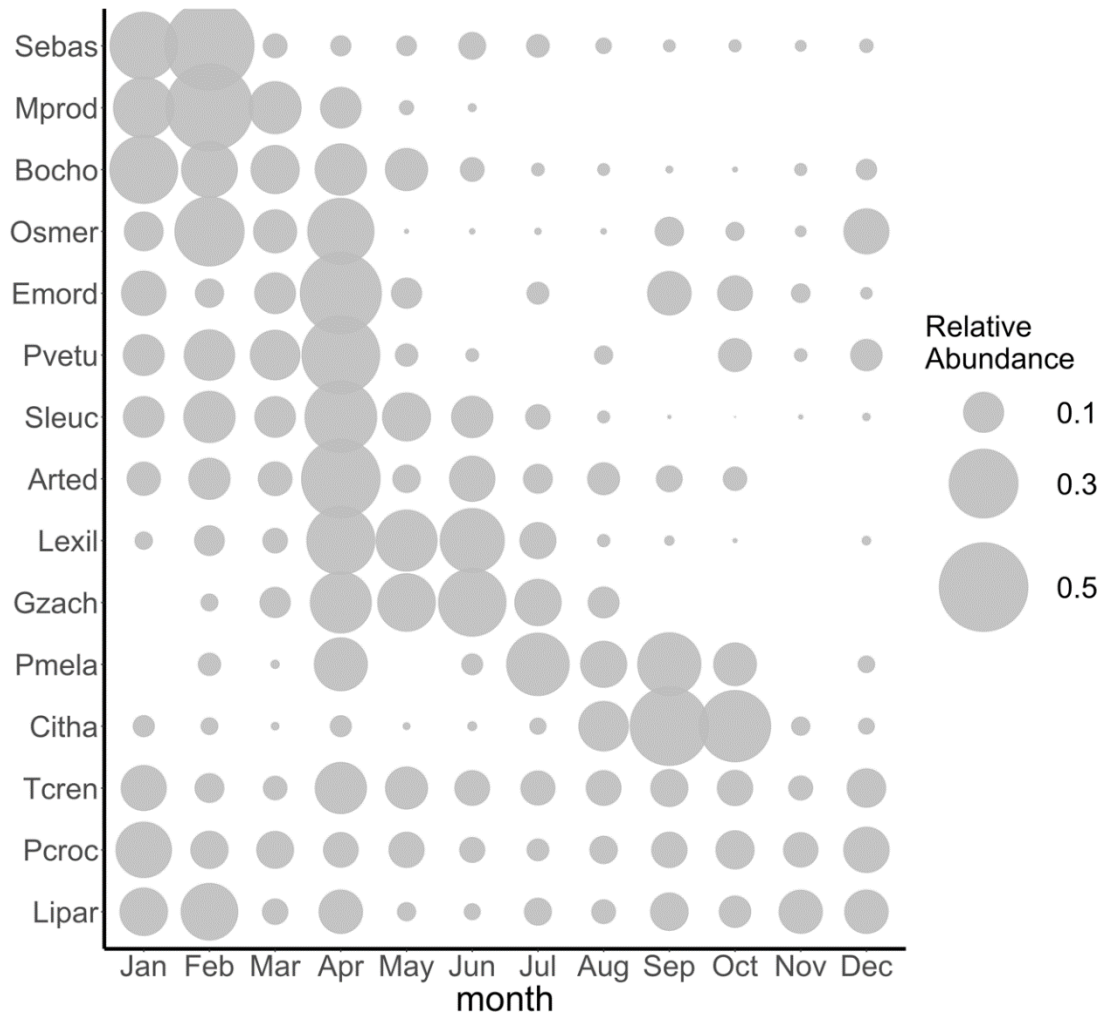


Figure 5. Seasonal distributions of common larval taxa within the visual assemblage aggregated over all cruises within each month. Seasonal distributions of each species are represented as relative abundance (scaled by size of bubble) based on areal density (No./m²) during each month (x-axis). See Table 1 for full taxon names corresponding to abbreviations.

Hierarchical cluster analysis identifies two distinct taxonomic clusters: a coastal assemblage of 5 taxa that have higher average densities at TH01 and TH02 and an offshore assemblage of the remaining 10 taxa that have higher average densities offshore (Figure 6). The taxonomic dendrogram did not appear to be explained by seasonal differences.

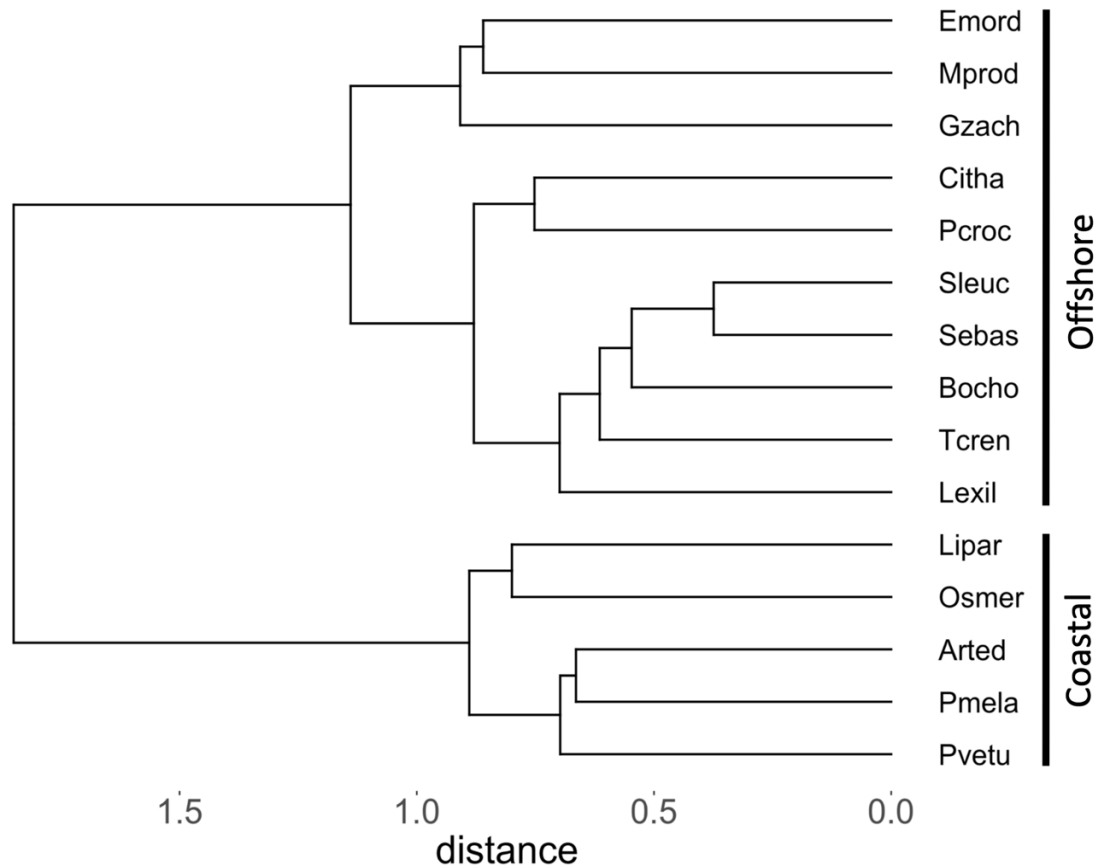


Figure 6. Taxon dendrogram from hierarchical cluster analysis performed on common taxa within the visual assemblage. Ecologically interpretable clusters are labelled.

Rockfish assemblage

Larvae of most rockfish species or species complexes were most abundant from the outer shelf (TH03) to the upper slope (TH05; Figure 7). Most species rarely occurred at stations over the mid- and inner shelf (TH02 and TH01, respectively); only 5 species were ever collected at station TH01. Two species (*S. maliger* and *S. proriger*) were identified as being more abundant over the mid- to outer-shelf (stations TH02-TH03), whereas two taxa (*S. caurinus* and the MyDi complex) were identified as being more broadly distributed along the entire transect. Hierarchical cluster analysis grouped

stations into a distinct offshore cluster (stations TH03-TH05) with high differentiation from station TH02 and even greater differentiation from station TH01 (Figure 8). Nearshore stations (TH01-TH02) were highly dissimilar and did not appear to form a distinct nearshore cluster. There were significant differences in assemblage composition across stations (PERMANOVA, $p < 0.001$; Table 4), however station TH01 was the only level where significant differentiation from the rest of the transect exists (Figure 8). Only three species were identified as significant indicators for stations (Table 4). Offshore stations were assigned *S. saxicola* (TH03 and TH04) and *S. pinniger* (TH03 and TH05), although the latter association was weak (33%). The MyDi complex was the only species or species complex identified as a significant indicator of nearshore stations (TH01 and TH02).

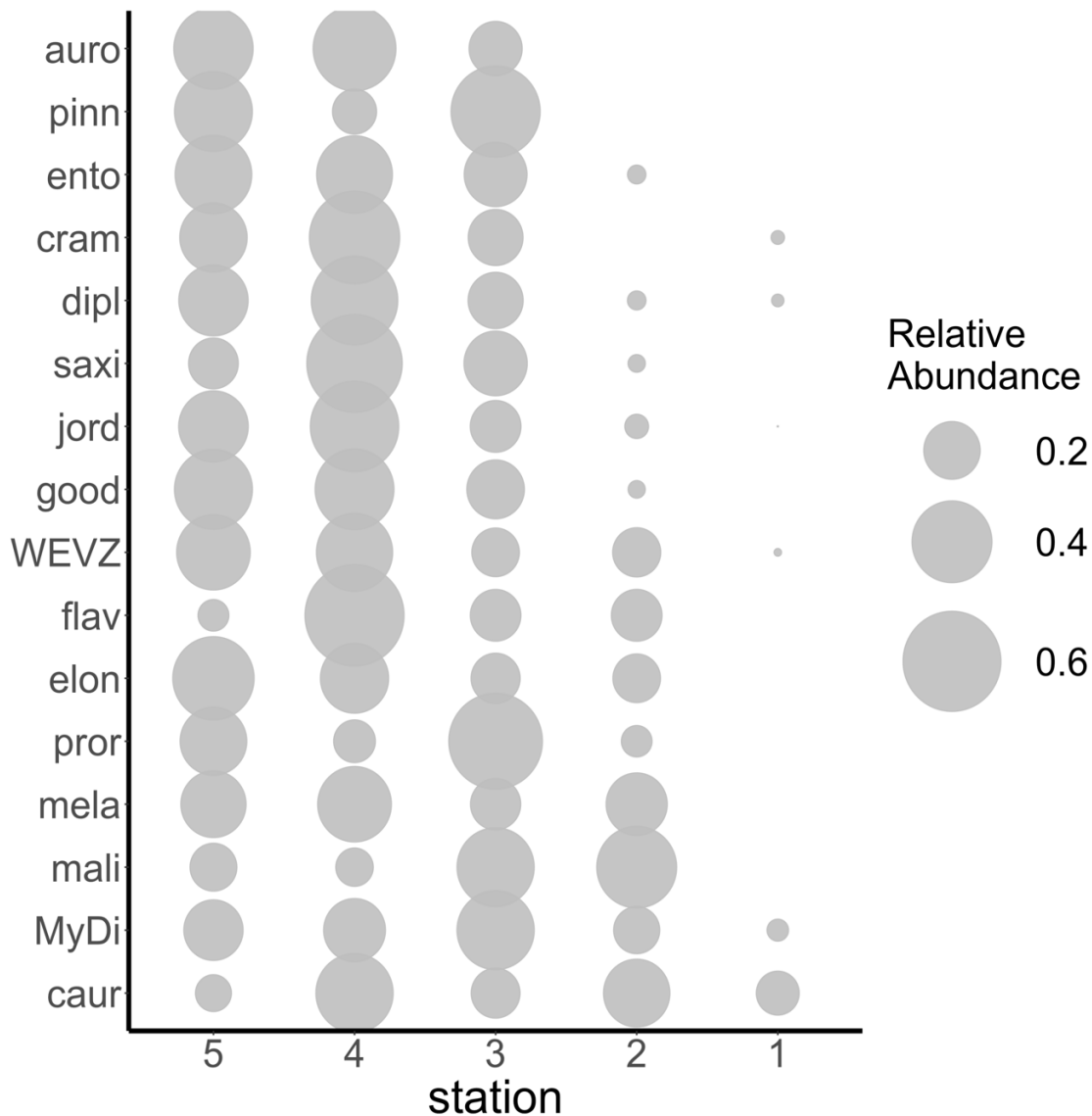


Figure 7. Cross-shelf distributions of common species or species complexes within the rockfish assemblage aggregated over the entire time series. Cross-shelf distributions of each species are represented as relative abundance (scaled by size of bubble) based on areal density (No./m²) at stations (x-axis) 5 (TH05; offshore) to 1 (TH01; nearshore). See Table 2 for full taxon names corresponding to abbreviations.

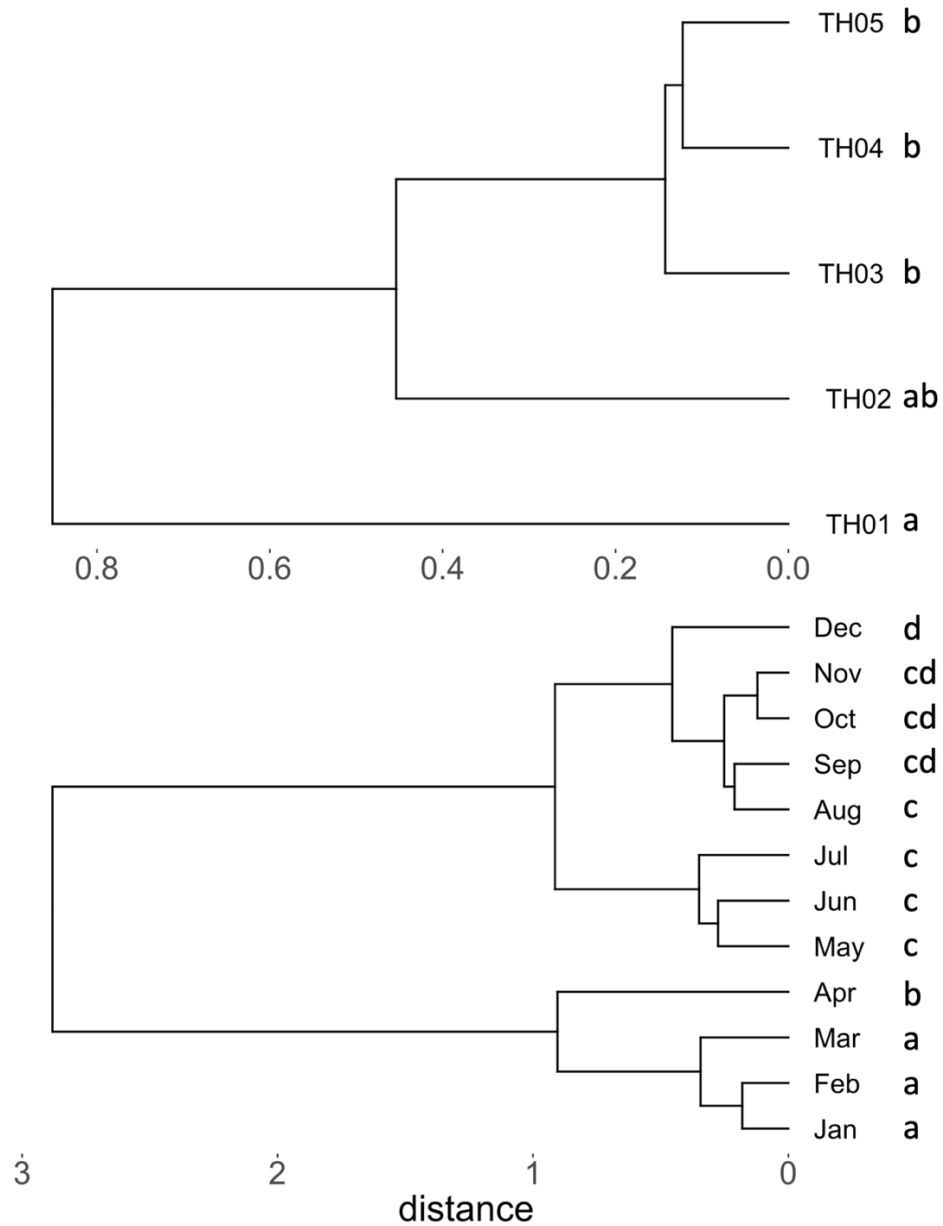


Figure 8. Cross-shelf and seasonal dendrograms resulting from hierarchical cluster analysis performed on common species or species complexes within the rockfish assemblage. Top panel: cross-shelf dendrogram performed on stations. Bottom panel: seasonal dendrograms performed on months. Different letters indicate results of pairwise PERMANOVA analysis indicating significant pairwise differences ($p < 0.05$) using a Bonferroni correction.

Table 4. Results of Permutational Analysis of Variance (PERMANOVA) and indicator species analysis (ISA) for station and seasonal differences in composition of common species or species complexes within the rockfish assemblage. Seasonal clusters are based on results of hierarchical cluster analysis performed on months (See Figure 8). Significance of indicator taxa ($p < 0.05$) for each factor level are listed with their associated indicator value (%).

Factor	PERMANOVA	Level	Indicator Taxa
Station	$p < 0.001$	TH01 and TH02	MyDi (46%)
		TH03 and TH04	<i>S. saxicola</i> (49%)
		TH03 and TH05	<i>S. pinniger</i> (33%)
Seasonal cluster	$p < 0.001$	January-March	<i>S. saxicola</i> (75%), MyDi (73%), <i>S. entomelas</i> (66%), <i>S. crameri</i> (52%), <i>S. melanops</i> (42%), <i>S. pinniger</i> (36%)
		April	<i>S. jordani</i> (47%), <i>S. maliger</i> (44%)
		May-July	<i>S. elongatus</i> (65%), <i>S. diploproa</i> (61%), <i>S. proriger</i> (51%), <i>S. aurora</i> (37%)
		December	WEVZ (46%), <i>S. goodei</i> (44%)

Larvae of most rockfish species were present during narrow, clearly defined seasonal periods (Figure 9). Several winter-spawning species were most abundant in January-March and were absent or declined substantially in April. *S. goodei* was the only winter-spawning species to be captured in December. One species (*S. maliger*) was only captured during spring and early summer months (April-June). Four species were most abundant in April-August, of which two (*S. elongatus* and *S. proriger*) had narrow seasonal distributions centered on June and July, and three others (*S. diploproa*, *S. aurora*, and the WEVZ complex) were captured more broadly throughout the year. Hierarchical cluster analysis grouped months into two distinct clusters (January-April and May-December; Figure 8). Upon further visual inspection, April was deemed strongly differentiated from January-March, while May-July appeared strongly differentiated from

August-December. Corroborating cluster analysis, assemblage composition differed significantly across months (PERMANOVA, $p < 0.001$; Table 4). Pairwise tests revealed assemblage composition between each month within the January-March cluster were similar but differed significantly from all other months (Figure 8). Assemblage composition in April was significantly different from all other months. Assemblage composition was similar in May-December apart from significant differentiation between December and the months of May-August. ISA identified fourteen of the sixteen common rockfish species or species complexes as significant indicators of one of the seasonal clusters defined from hierarchical cluster analysis (Table 4). Corroborating seasonal patterns identified in Figure 9, January-March was assigned the most indicator taxa ($n = 6$), with *S. saxicola* (75%), the MyDi complex (73%), and *S. entomelas* (66%) emerging as the strongest indicators of this seasonal period. The May-July seasonal period was assigned the second most ($n = 4$), with *S. elongatus* (65%) and *S. diploproa* (61%) emerging as the strongest indicators. Only *S. jordani* and *S. maliger* emerged as significant indicators of April. The WEVZ complex and *S. goodei* were the only two species or species complex strongly associated with December.

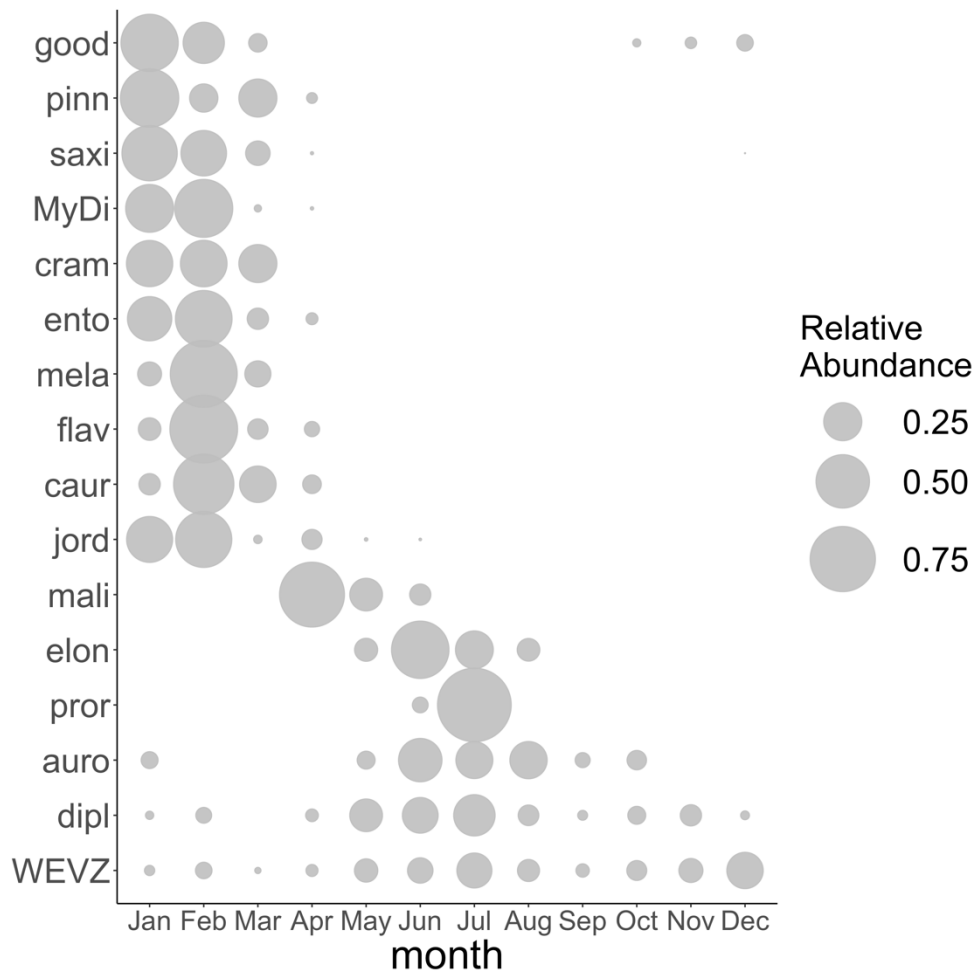


Figure 9. Seasonal distributions of common species or species complexes within the rockfish assemblage aggregated over all cruises within each month. Seasonal distributions of each species are represented as relative abundance (scaled by size of bubble) based on areal density (No./m²) during each month (x-axis). See Table 1 for full taxon names corresponding to abbreviations.

Hierarchical cluster analysis did not differentiate taxa based on spatial patterns and instead differentiate groups on the basis of seasonality (Figure 10). The taxon dendrogram separated out into two distinct clusters; a winter assemblage of 10 species and a spring and summer assemblage of 6 species.

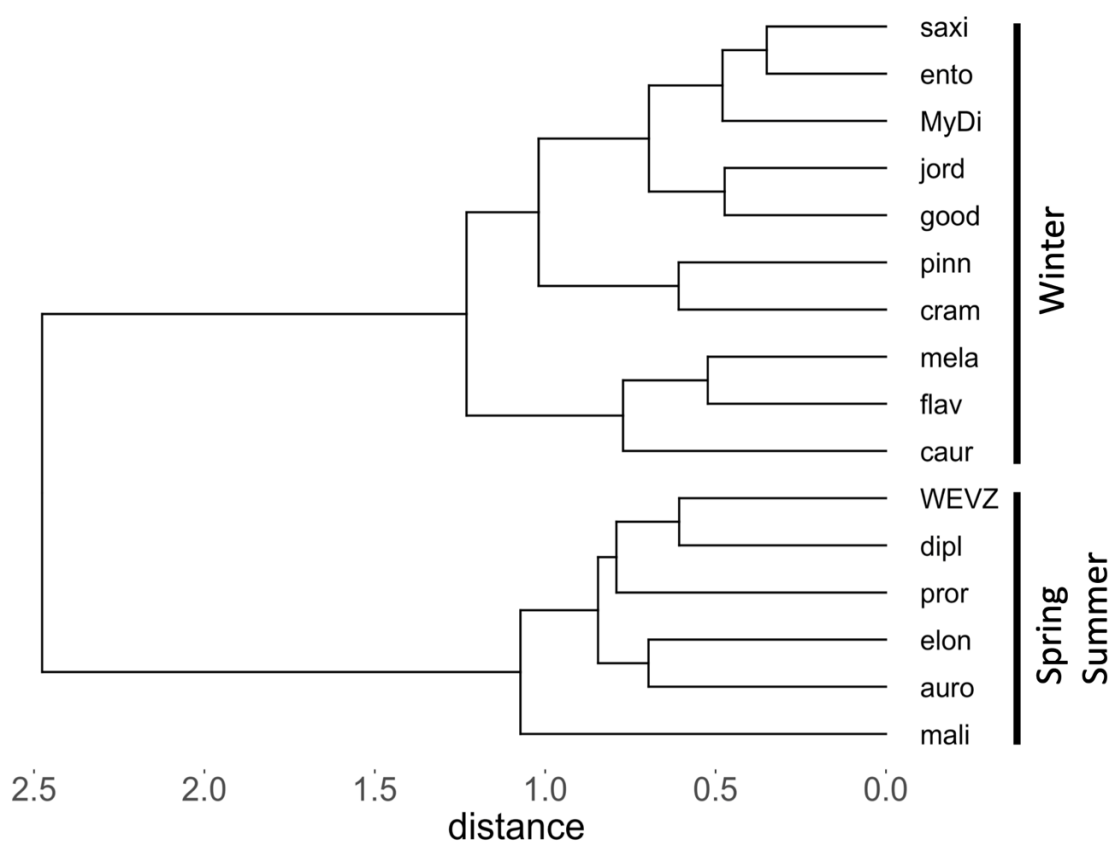


Figure 10. Taxon dendrogram from hierarchical cluster analysis performed on common species or species complexes within the rockfish assemblage. Ecologically interpretable clusters are labelled.

Interannual Variability

Local environmental conditions

Seasonal patterns in local oceanographic conditions generally correspond to dynamics characteristic of seasonal upwelling and downwelling in the CCS: cooling during spring and summer months associated with upwelling and equatorward transport followed by a transition to warmer conditions during fall and early winter months Figure 11). Seasonal patterns appeared to hold during anomalously cool and warm years, during which the greatest divergence in temperature from mean climatological conditions occurred during fall and winter months.

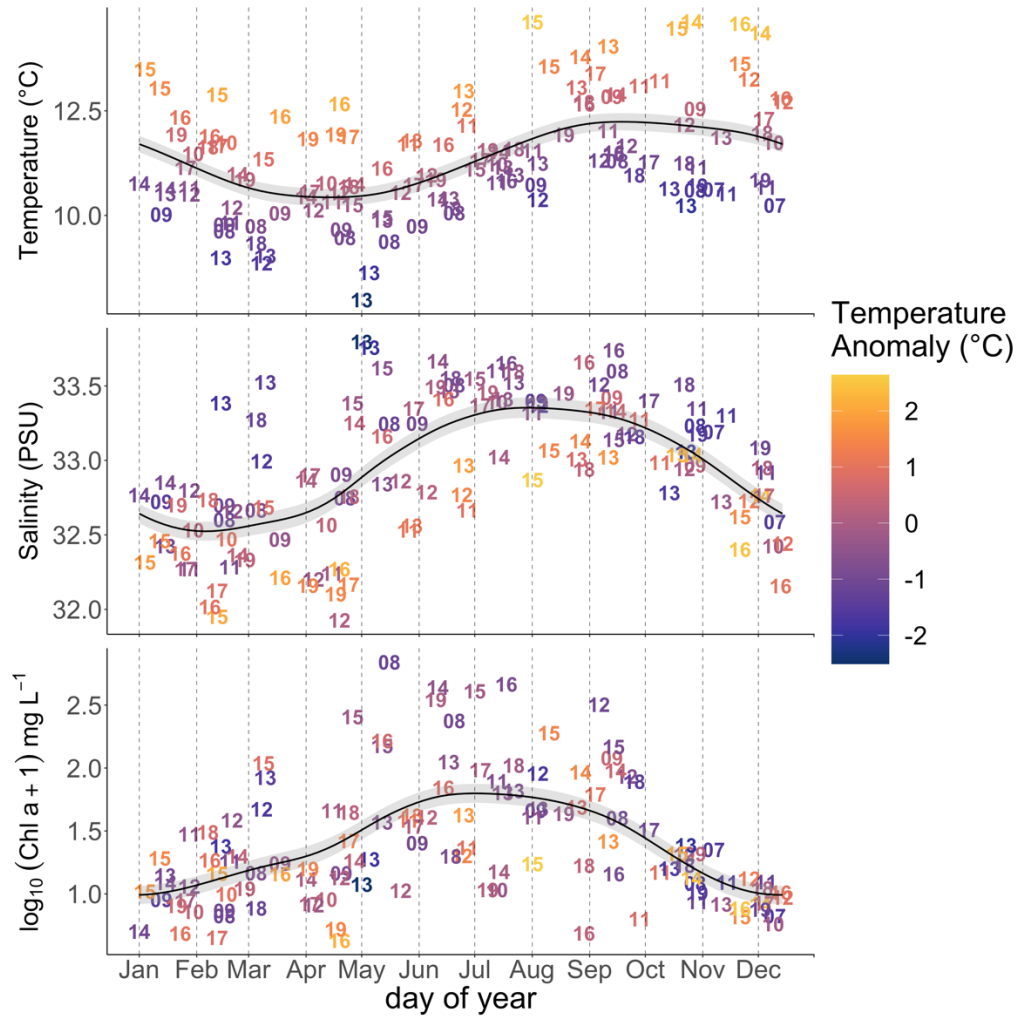


Figure 11. Intra-annual variability in local environmental conditions in the upper 0-10 m of the water column aggregated across all stations within a cruise. Panels from top to bottom: temperature (°C), salinity (PSU), and log₁₀ (chlorophyll *a* concentration + 1) (mg m⁻³) by day of year (x-axis). Black line (± SE in gray) represents a generalized additive model fit to environmental observations. Symbol numbers correspond to the observation year. Symbol color corresponds to a temperature anomaly from a seasonal climatology (see methods for calculation of anomaly product).

Interannual variability in local oceanographic conditions between late 2007 and 2019 is consistent with patterns of climate variability, with clear transitions from cooler temperatures during the early part of the record (late 2007-2009) and throughout 2011 to mid-2014, to persistent warming during climate events associated with the mild 2009-10 El Niño, the 2014-16 MHW, and a brief period of warming in winter 2018-19 (Figure 12). These patterns are consistent with variability in local indices of upwelling and sea level: positive CUTI values and negative sea level anomalies during cooler periods corresponding to enhanced upwelling and equatorward transport and negative CUTI values and positive sea level anomalies coinciding with warm climate events, most notably during the 2014-16 MHW, corresponding to reduced upwelling and poleward or weak equatorward transport (Figure 13).

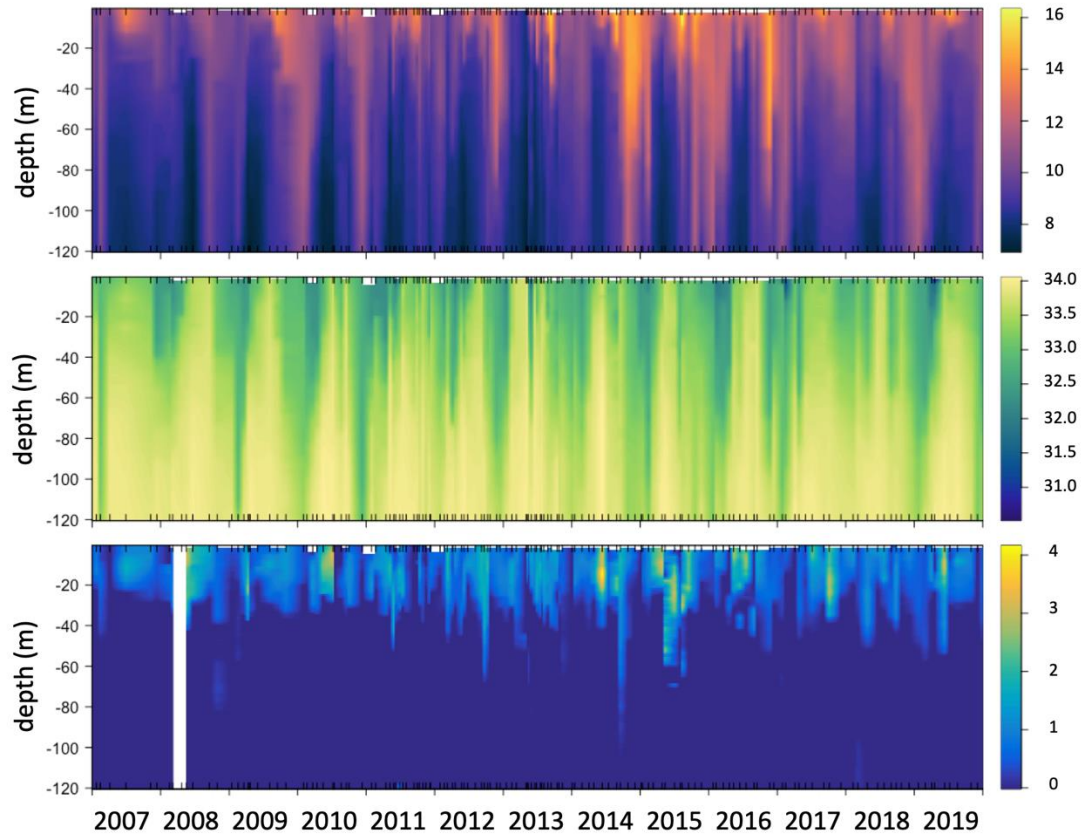


Figure 12. Local hydrographic conditions observed along the TH-line time series at station TH03 (41°03.50 N, 124°20.50 W, 140 m). From top to bottom: temperature (°C), salinity (PSU), and log10 (chlorophyll *a* concentration +1) (mg m⁻³) by depth (m; y-axis) and time (x-axis).

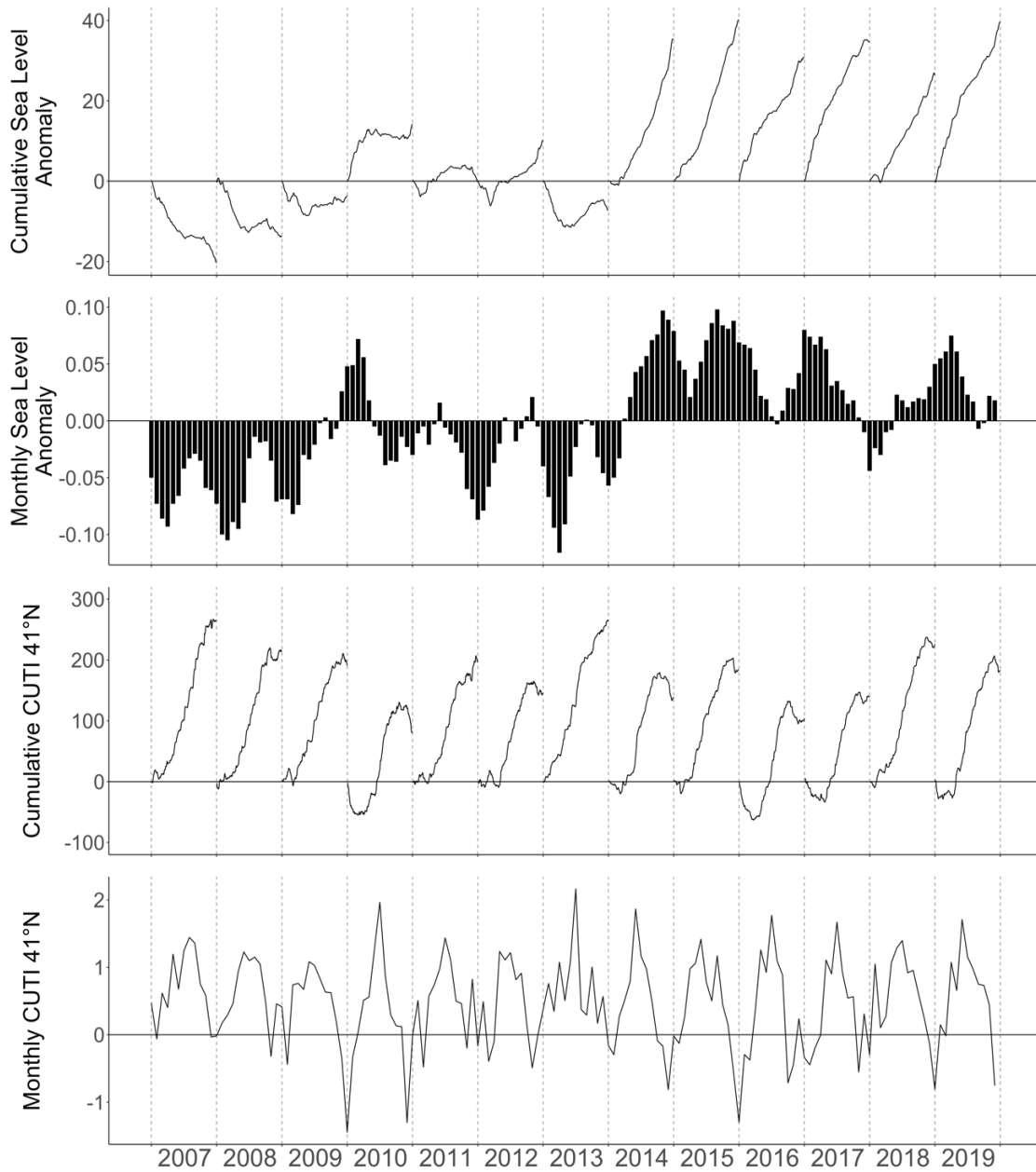


Figure 13. Regional oceanographic indices. Panels from top to bottom represent: cumulative sea level anomaly (calculated from daily values at 40.76°N from Jan 1 to Dec 31), average monthly sea level anomaly (red and blue bars), cumulative Coastal Transport Upwelling Index (CUTI; m^2s^{-1} , calculated from daily values at 41°N from Jan. 1 to Dec.31), and average monthly CUTI at 41°N. Monthly Sea level anomalies extending below zero (blue) indicate a negative anomaly and values extending above zero (red) indicate a positive anomaly.

Visual assemblage

Abundances of common larval taxa were highly variable throughout the time series (Figure 14). Several taxa that had been previously rare in the collection increased sharply in abundance following the arrival of warm water anomalies along the coast in late 2014. For example, *M. productus* and *E. mordax* were rarely observed in collections prior to late 2014 (*E. mordax*) and early 2015 (*M. productus*). Both species remained abundant during the winters of 2016 and 2017, were absent from the collection in 2018, and reappeared in early 2019, though at lower densities than during the MHW.

Abundances of *P. melanostictus*, *L. exilis*, *Sebastes* spp., and *Citharichthys* spp., during peak seasonal occurrence, also increased sharply in either late 2014 or early 2015.

Following relatively high abundances again in late 2015, *Citharichthys* spp. and *P. melanostictus* declined throughout the rest of the time series. High abundances of *L. exilis* and *Sebastes* spp. had persisted throughout the MHW and into 2017. With the exception of unusually high densities during a single cruise in early 2012, larval abundance of *B. ochotensis* was consistently highest during the winters of 2015-16. In contrast, the family Osmeridae and *S. leucopsarus* were consistently more abundant during cooler years and largely disappeared from our collections (Osmeridae) or declined in abundance (*S. leucopsarus*) just prior to warming in late 2013. Several other taxa (i.e., *Liparis* spp., *G. zachirus*, and *T. crenularis*) were consistently abundant early in the record during cooler conditions, declined sharply in early 2014-15 following the arrival of warm waters, and reappeared in high abundance in 2016.

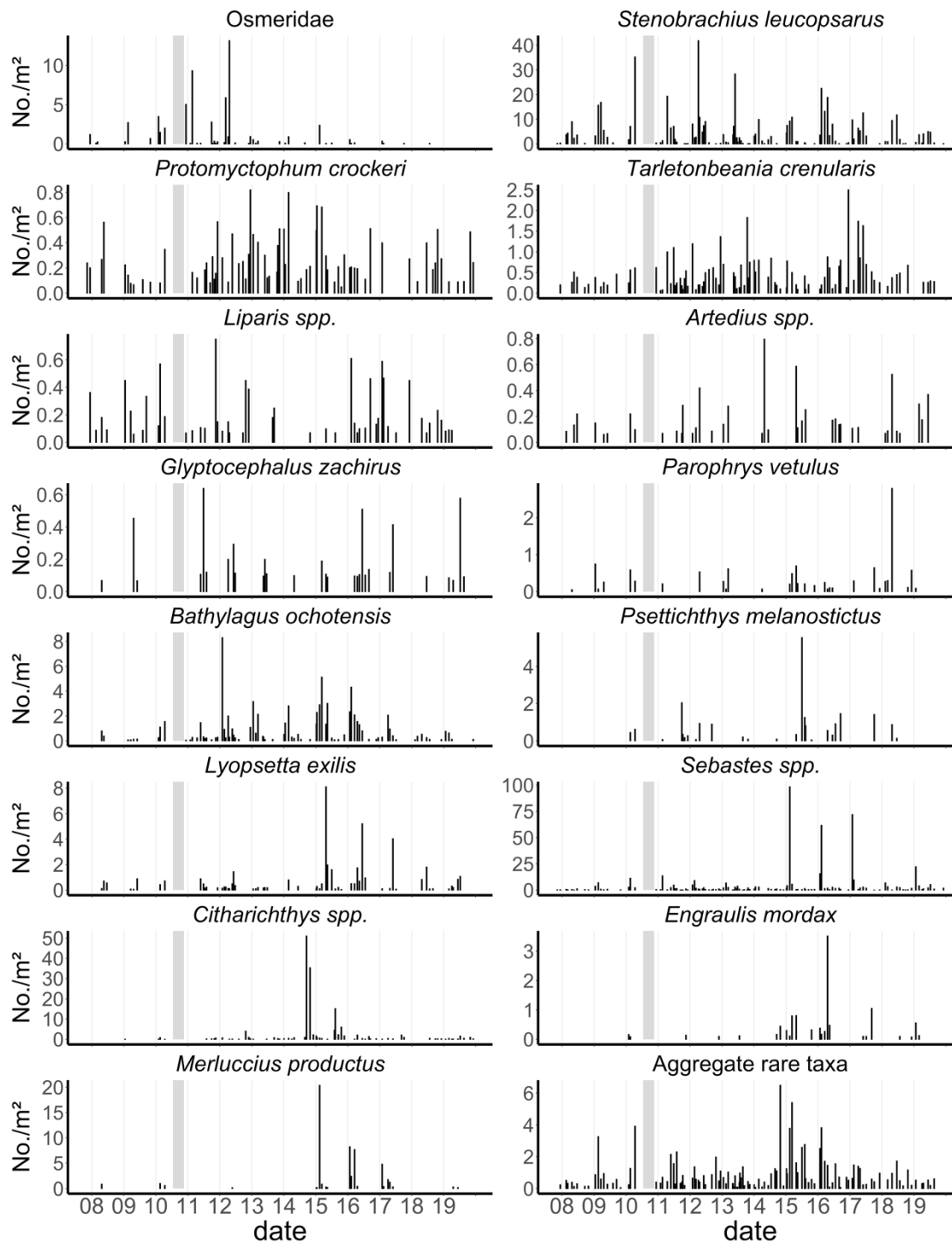


Figure 14. Mean areal density (No./m²; y-axis) of common taxa within the visual assemblage and aggregate rare taxa across all stations by cruise date (x-axis). Gray bars indicate extended observation gaps.

Aggregate abundance of rare larval taxa was generally lower during the first half of the time series with the exception of a moderate peak in response to the mild 2009-10 El Niño (Figure 14). Following early 2010, density declined and remained relatively unchanged until fall 2014, when aggregate abundance of these rare taxa increased markedly. Following consistently high densities through mid 2016, larval abundance had returned to normal for the remainder of the time series and declined substantially in 2019.

Assemblage composition of common taxa was dominated by the osmerids, *S. leucopsarus*, and *Sebastes* spp. in aggregate prior to the MHW (Figure 15). During the late 2014-16 MHW, the assemblage was dominated by a much broader suit of taxa, coinciding with the appearance of *M. productus* and *E. mordax*, sharp increases in abundance of *Citharichthys* spp., *P. melanostictus*, and *L. exilis*, and declines in *S. leucopsarus* and the osmerids.

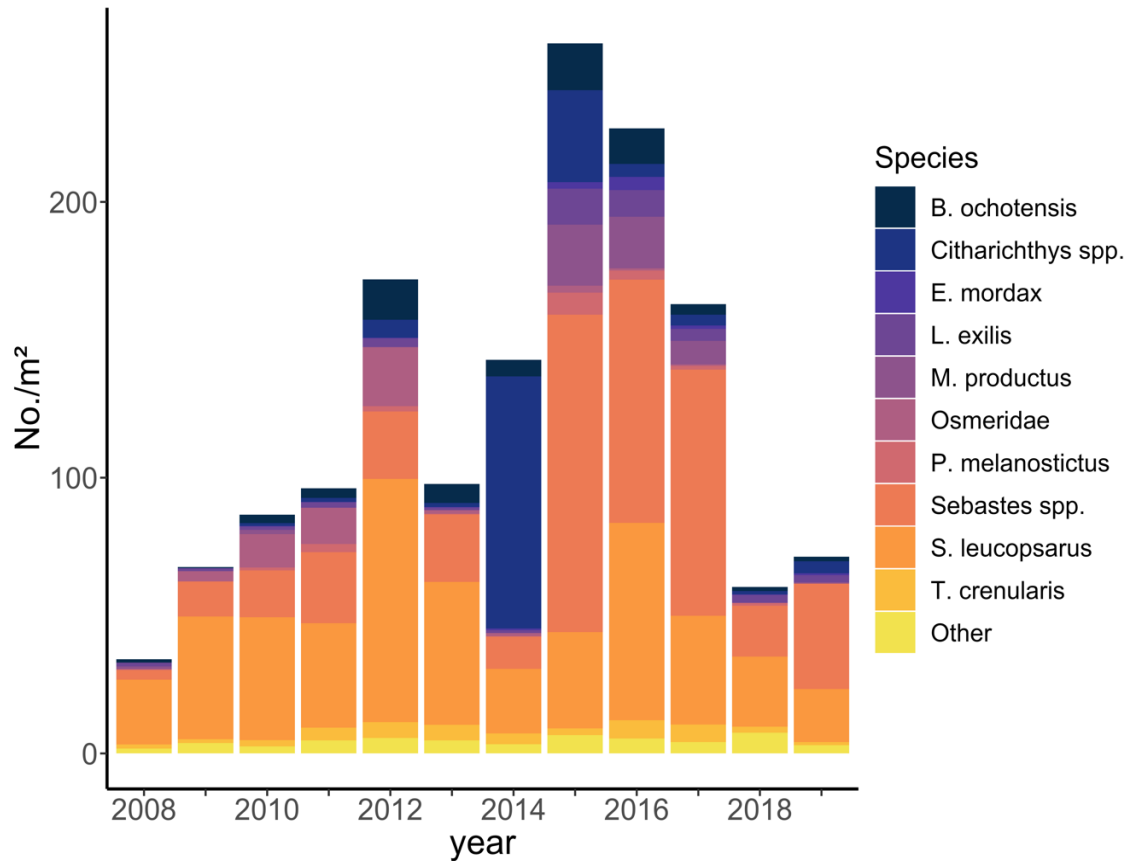


Figure 15. Mean areal density (No./m²; y-axis) of common larval taxa within the visual assemblage aggregated over all cruises within each year (x-axis). “Other” represents the remaining common taxa (*Artedius* spp., *G. zachirus*, *Liparis* spp, *P. crockeri*, *P. vetulus*) in aggregate.

Hypotheses that mean larval density differed significantly between time periods defined as pre-MHW (November 2007- July 2014), MHW (August 2014- May 2017), and post-MHW (June 2017- December 2019) were supported for 8 of the 15 common taxa (Kruskal-Wallis, $p < 0.05$; Figure 16). Osmerids were more abundant prior to the onset of the MHW than after (Dunn’s, $p < 0.05$). *M. productus*, *P. melanostictus*, and *B. ochotensis* were more abundant during the MHW than the time periods spanning pre- and post-MHW conditions (Dunn’s, $p < 0.05$). *L. exilis*, *Citharichthys* spp., and *E. mordax* were also found to be more abundant during the MHW than conditions prior (Dunn’s, $p <$

0.05), but abundance did not differ significantly from conditions following the MHW.

Although significant variability across time periods was detected for *G. zachirus* (Kruskal-Wallis, $p < 0.05$), pairwise tests were unable to detect significant variability between each time period (Dunn's, $p > 0.05$).

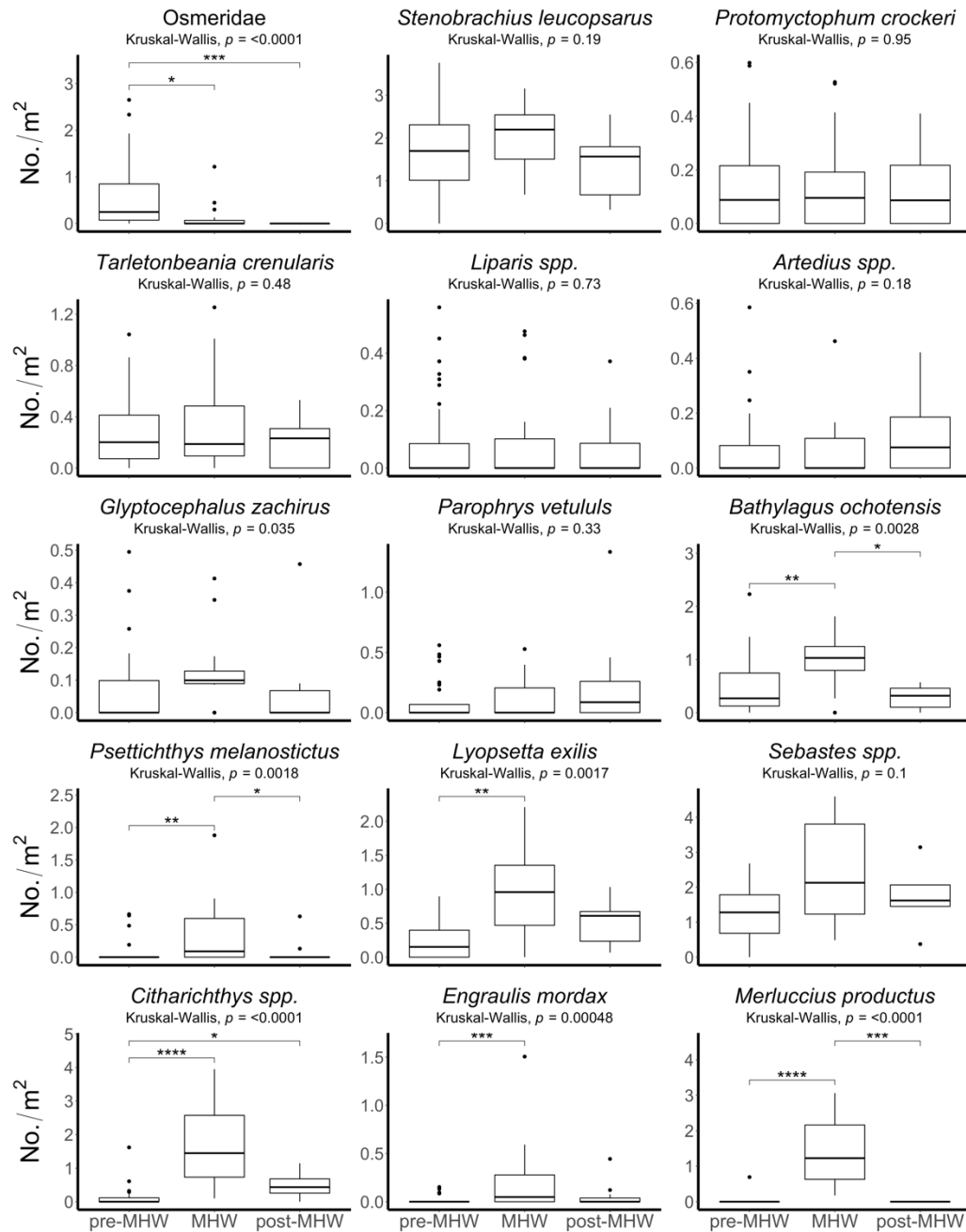


Figure 16. Boxplots comparing mean areal density (No./m²; y-axis) of common taxa within the visual assemblage aggregated by cruise between pre-MHW (November 2007-July 2014), MHW (August 2014-May 2017), and post-MHW (June 2017-December 2019) time periods (x-axis). Significant differences ($p < 0.05$) were tested using the non-parametric Kruskal-Wallis test. Pairwise comparisons were tested using Dunn's multiple comparisons test with a Bonferroni correction and the significance level set at: * = $p < 0.05$, ** = $p < 0.01$, *** = $p < 0.001$, **** = $p < 0.0001$. The y-axis indicates areal density on a log-transformed scale.

Rockfish assemblage

Larval abundance of common rockfishes varied substantially throughout the time series, with most species clearly responding to the 2015-16 El Niño (Figure 17). Most species were infrequently sampled or low in abundance in the early part of the record, save for modest increases in abundance during winter of the 2009-10 El Niño. Following the onset of the MHW, however, all winter spawning species, with the exception of *S. crameri*, were captured in unusually high abundance in 2015-17. Three winter spawning species (*S. jordani*, *S. flavidus*, *S. melanops*) occurred almost exclusively during warm years. *S. jordani* larvae were largely absent from our collections prior to high abundances in 2015. *S. jordani* larvae remained abundant throughout the MHW, were absent from our collections in 2018, and reappeared in early 2019, though at lower densities than during the MHW. Similarly, *S. flavidus* and *S. melanops* larvae were only present during the mild 2009-10 El Niño, the MHW, and in early 2019. Following a return to cooler conditions in early 2018, the abundance for most species declined with the exception of species that appear to occur in the summer and fall (e.g., WEVZ complex, *S. proriger*, *S. diploproa*, and *S. aurora*). During the brief period of warming in early 2019, larval abundance again increased sharply for several species (e.g., *S. jordani*, *S. goodei*, *S. saxicola*, MyDi complex). *S. maliger* was the only species to be completely absent during the MHW.

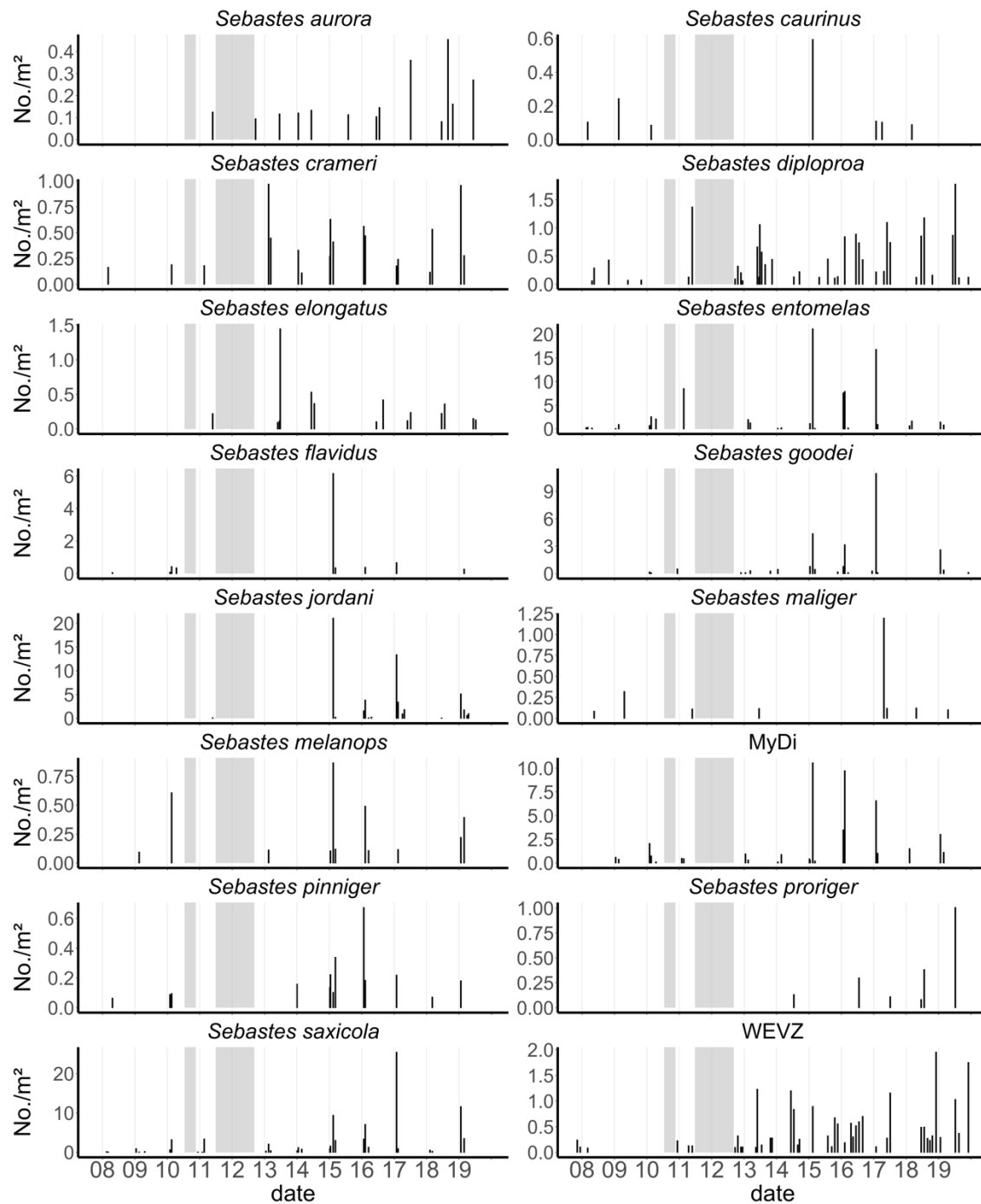


Figure 17. Mean areal density (No./m²; y-axis) of common species or species complexes within the rockfish assemblage across all stations by cruise date (x-axis). Gray bars indicate extended observation gaps.

Prior to 2015, the winter rockfish assemblage was dominated by *S. entomelas*, *S. saxicola*, and the MyDi complex (Figure 18). During warmer years (i.e., 2015-17 and 2019), the winter assemblage was dominated by a much broader suit of taxa, coinciding with the appearance of *S. jordani*, *S. flavidus*, and *S. melanops* and sharp increases in abundance of *S. goodei*. Inter-annual patterns in assemblage composition of summer spawning rockfishes were not as evident but several species were more abundant between 2016-19.

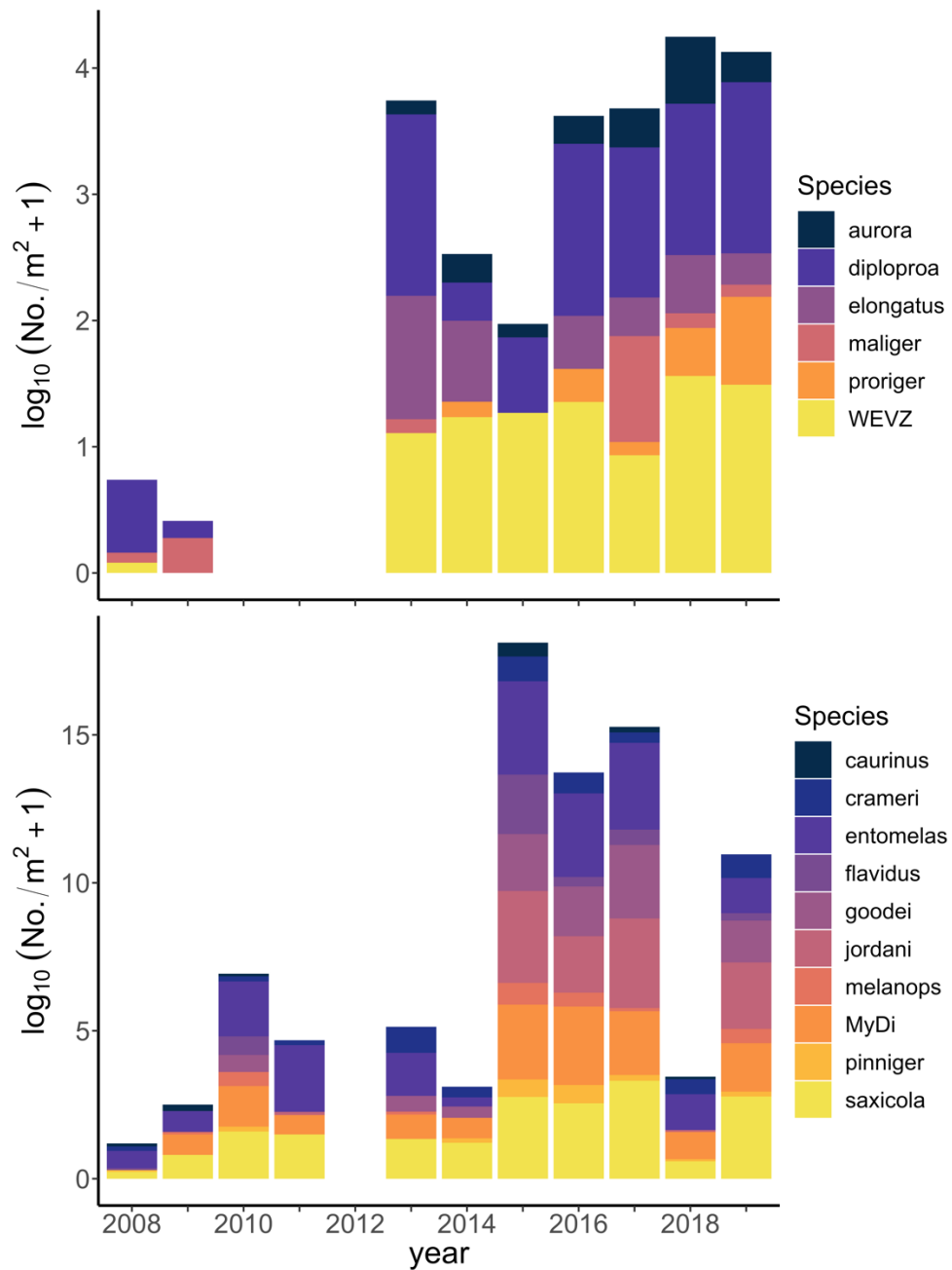


Figure 18. Mean log-transformed areal density ($\log_{10}[\text{No.}/\text{m}^2 + 1]$; y-axis) of common species or species complexes within the rockfish assemblage aggregated over all cruises within each year (x-axis). Top panel: spring, summer, and fall-spawning rockfishes. Bottom panel: winter-spawning rockfishes. Ethanol-preserved samples were not collected during winter months in 2012 and summer months in 2010, 2011, and 2012.

Hypotheses that mean larval density varied significantly between time periods defined by pre-MHW (November 2007- July 2014), MHW (August 2014- May 2017), and post-MHW (June 2017- December 2019) was supported for 6 of the 16 common rockfishes (Kruskal-Wallis, $p < 0.05$; Figure 19). Multiple comparisons test indicates that *S. goodei*, *S. jordani*, *S. pinniger*, and *S. saxicola* were more abundant during the MHW than conditions prior (Dunn's, $p < 0.05$), but abundance did not differ significantly from conditions following. There were no significant differences in larval abundance of *S. entomelas*, *S. flavidus*, and *S. proriger* (Kruskal-Wallis, $p > 0.05$), despite *S. entomelas* and *S. flavidus* being more abundant during the MHW and *S. proriger* during post-MHW conditions upon visual inspection. No species or complexes were found to have a significantly higher mean density prior to the MHW.

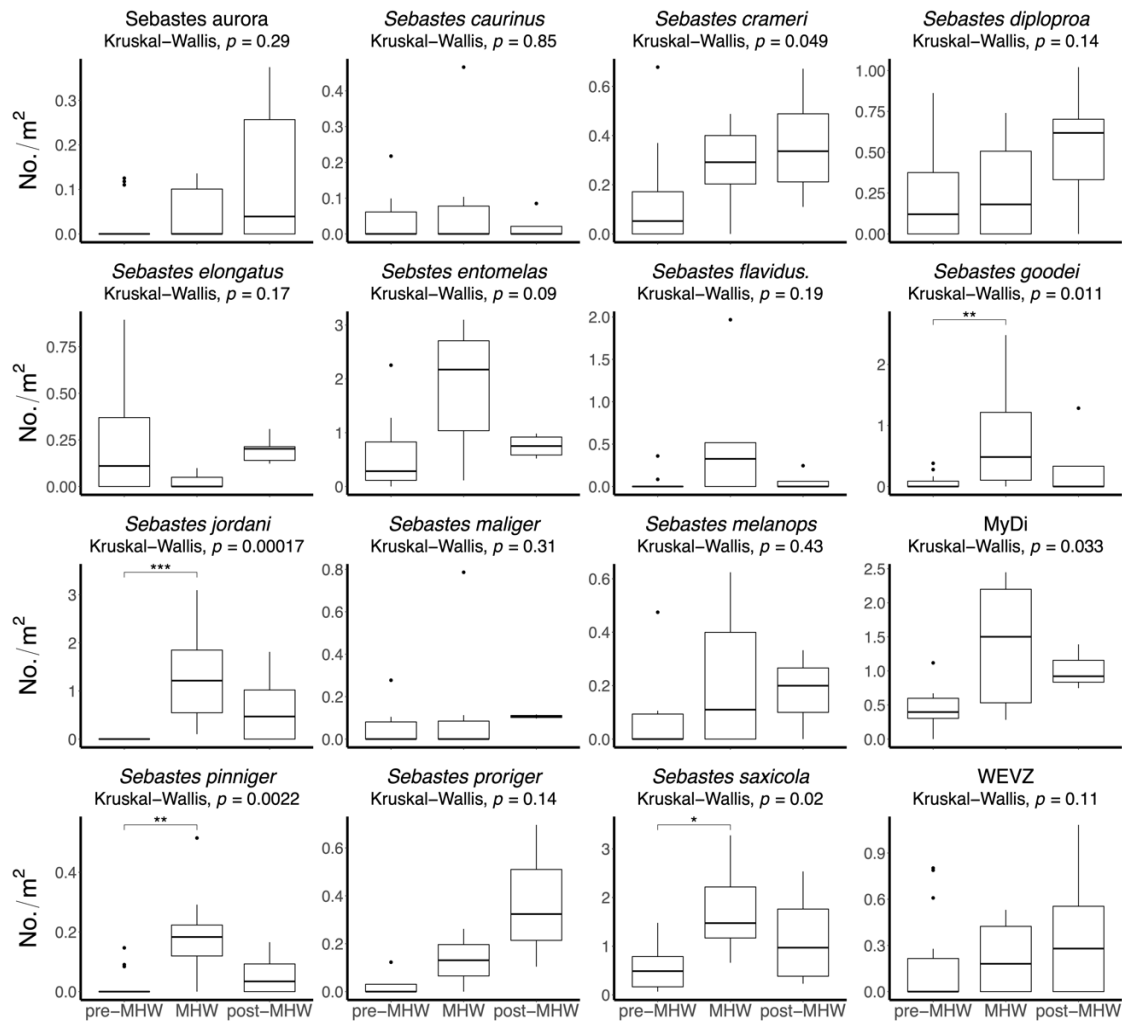


Figure 19. Boxplots comparing mean areal density (No./m²; y-axis) of common species or species complexes within the rockfish assemblage aggregated by cruise between pre-MHW (November 2007-July 2014), MHW (August 2014-May 2017), and post-MHW (June 2017-December 2019) time periods (x-axis). Significant differences ($p < 0.05$) were tested using the non-parametric Kruskal-Wallis test. Pairwise comparisons were tested using Dunn's multiple comparisons test with a Bonferroni correction and the significance level set at: * = $p < 0.05$, ** = $p < 0.01$, *** = $p < 0.001$, **** = $p < 0.0001$. The y-axis indicates areal density on a log-transformed scale.

Temporal Patterns of Rare Taxa and Corresponding Biogeographic Assemblages

Visual assemblage

Most rare taxa were assigned either northern-coastal or coastwide-oceanic affinities, whereas few taxa were assigned to southern-coastal or southern-oceanic assemblages (Appendix B). Rare coastal and oceanic taxa with southern affinities in the CCS were infrequently sampled or low in abundance throughout most of the time series apart from abrupt increases during the late 2014-2016 MHW (Figure 20). Northern coastal taxa were abundant and frequently encountered early in the time series (i.e., 2009) and again in early 2015. Rare oceanic taxa with northern affinities appeared to be present throughout most of the time series, with little variation in abundance. Oceanic and coastal taxa with coastwide affinities were abundant and frequently captured in early 2010 and 2015-16. Abundance and species richness for these biogeographic assemblages did not vary seasonally, apart from coastal taxa with northern affinities tending to be more abundant and encountered more frequently in the winter (results not shown).

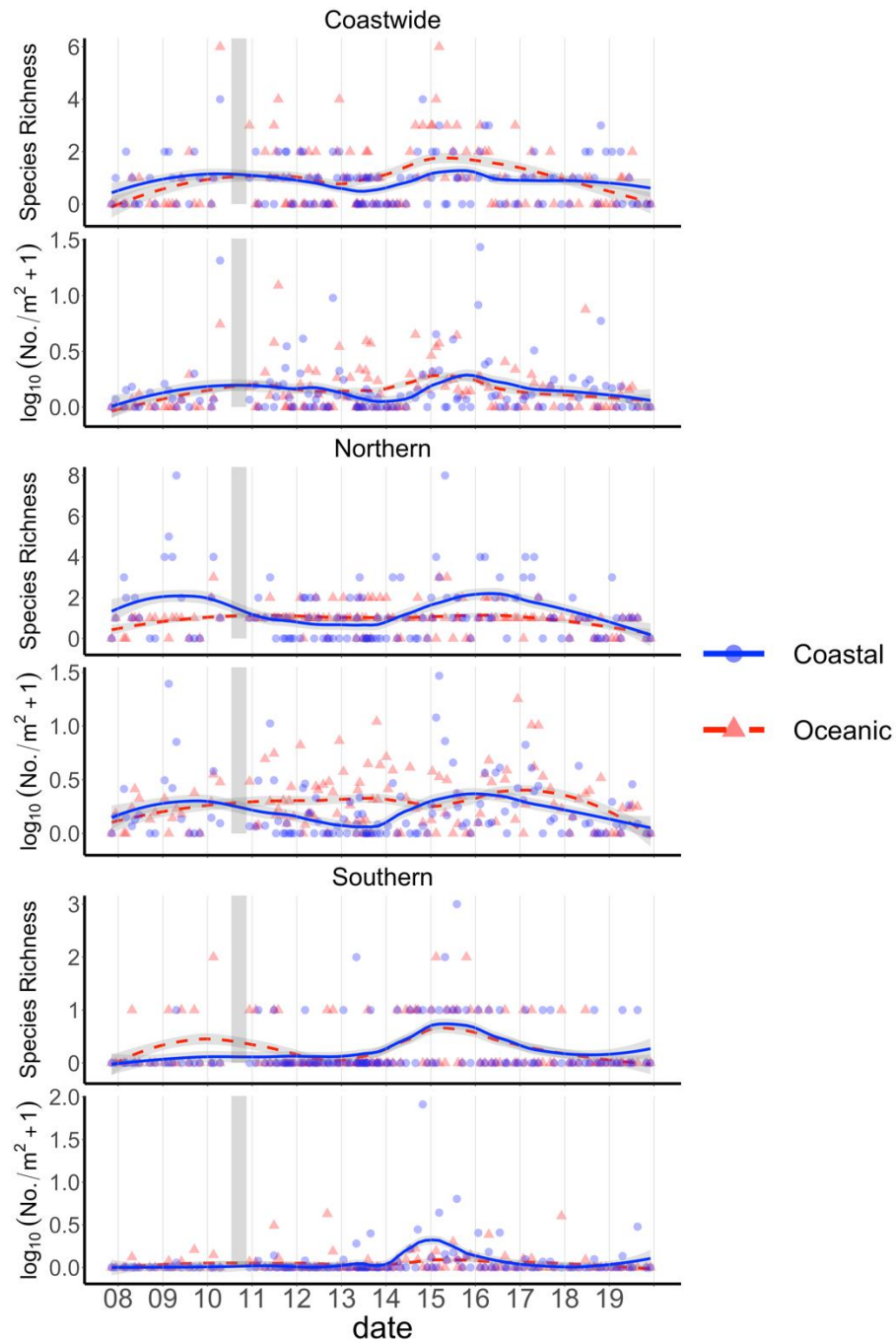


Figure 20. Inter-annual variability in species richness and log-transformed areal density ($\log_{10}[\text{No.}/\text{m}^2 + 1]$) of rare taxa grouped by adult biogeographic ranges. Panels from top to bottom: species richness and areal density of aggregate rare coastwide, northern, and southern adult spawning assemblages (y-axis) by cruise date (x-axis). Symbol and line color corresponds to coastal (blue) or oceanic (red) adult spawning assemblages. Lines indicate loess smooth (tuned to capture interannual trends) fit to observations. Gray bars indicate extended observation gaps.

The patterns described above corroborate patterns in abundance of several rare taxa that occurred coherently and in some cases in unusually high abundance during the late 2014-16 MHW (Figure 21). *Genyonemus lineatus* (white croaker), a coastal demersal species typically found off southern and central California, were absent in our collections prior to unusually high abundances in late 2014. Similarly, *Sardinops sagax* (Pacific sardine), a coastal pelagic forage species that spawns primarily off southern and central California, were rare in our collections prior to high abundances in 2015 and 2016. Several rare oceanic or deep-water taxa, such as *Sebastolobus* spp. (thornyheads), *Ichthyos lockingtoni* (medusafish), and *Embassichthys bathybius* (deepsea sole) were sampled frequently and in high abundance at various points throughout the MHW. Additionally, *Clupea palasii* (Pacific herring), although generally distributed further north in the CCS, were found in unusually high densities in early 2015 along the outer shelf (i.e., stations TH03 and TH04). Several other taxa were present in our collections only during the MHW, but in low abundance. These include several southern coastal species collected in 2015 (*Cololabis saira* [Pacific saury] and *Trachurus symmetricus* [Pacific Jack mackerel]) and 2016 (*Scomber japonicus* [Pacific mackerel]), as well as several rare oceanic and far-offshore taxa collected in late 2014 (e.g., *Loweina rara* [Laura's lanternfish] and Zoaracidae [eelpouts]) and at various points in early 2015 (e.g., *Cyclothone* spp. [bristlemouths], *Tactostoma Macropus* [longfin dragonfish], *Melamphaes* spp. [big scales]).

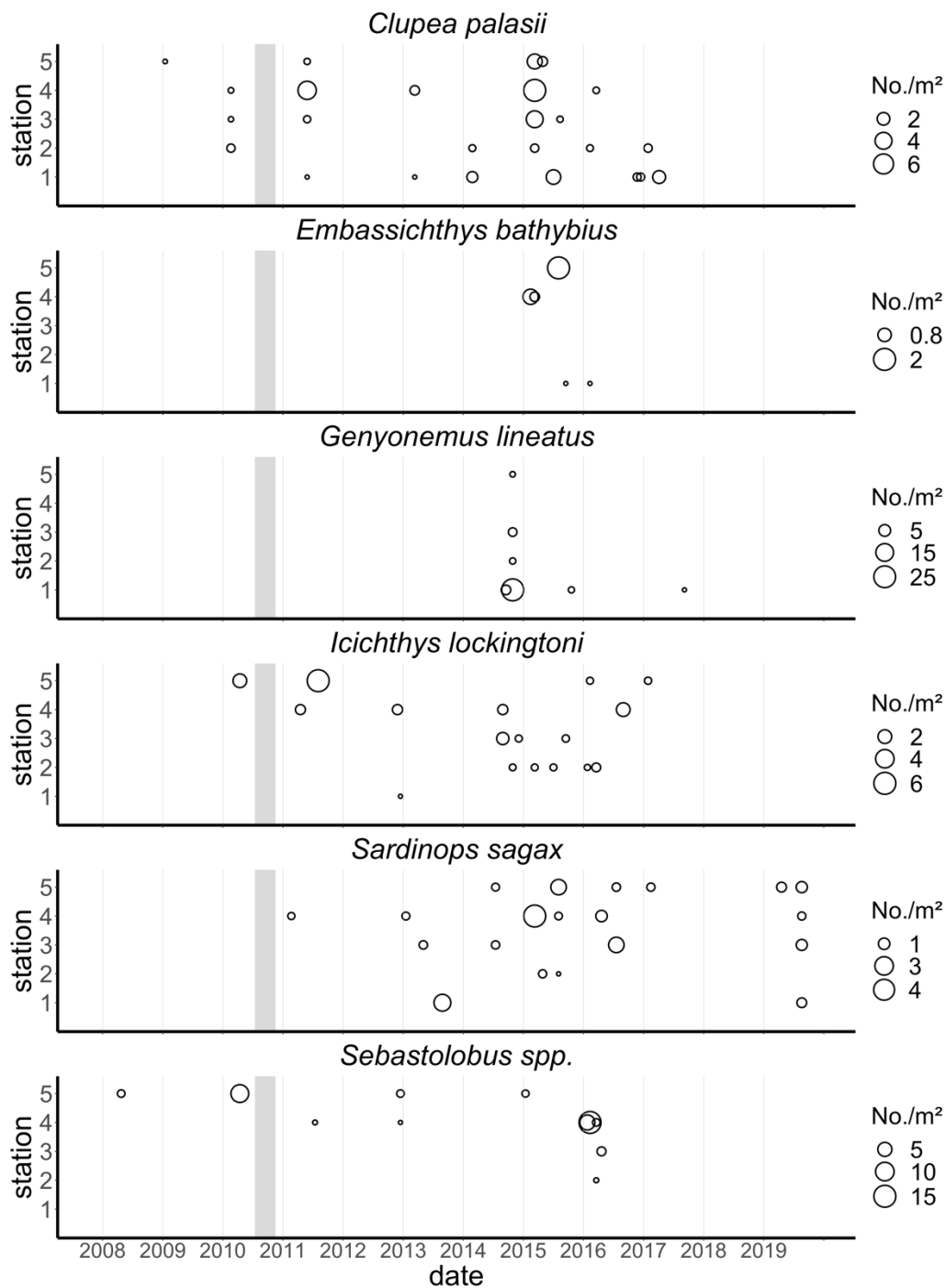


Figure 21. Time series variability in areal density (No./m²) of notable rare taxa within the visual assemblage by cruise date (x-axis) and station (y-axis). Circles scale with areal density. Gray shading indicates extended observation gaps.

Rockfish assemblage

More than half of the species within the rockfish assemblage ($n = 18$) are considered rare (Table 2). In general, trends in abundance and species richness were similar between coastwide, northern, and southern assemblages: low abundance and species richness during most of the time series apart from sharp increases throughout the MHW and in 2019 (Results not shown). Several species with northern and southern affinities within the CCS were present in our collections in high abundance during the MHW or in 2019 (Figure 22). *S. rosaceus* (rosy rockfish) and *S. rufus* (bank rockfish), the two most abundant rare southern species, were generally only present in our collection during winter months of the MHW. *S. helvomaculatus* (rosethorn rockfish), the only rare species with a northern affinity present during the MHW, was captured frequently in the spring and summer of 2016, which was followed by an absence and reappearance during a single cruise in July 2019. Several southern spawning species (*Sebastes levis* [Cowcod], *Sebastes hopkinsi* [squarespot rockfish], and *Sebastes melanostomus* [blackgill rockfish]) were only present in our collections in January 2019.

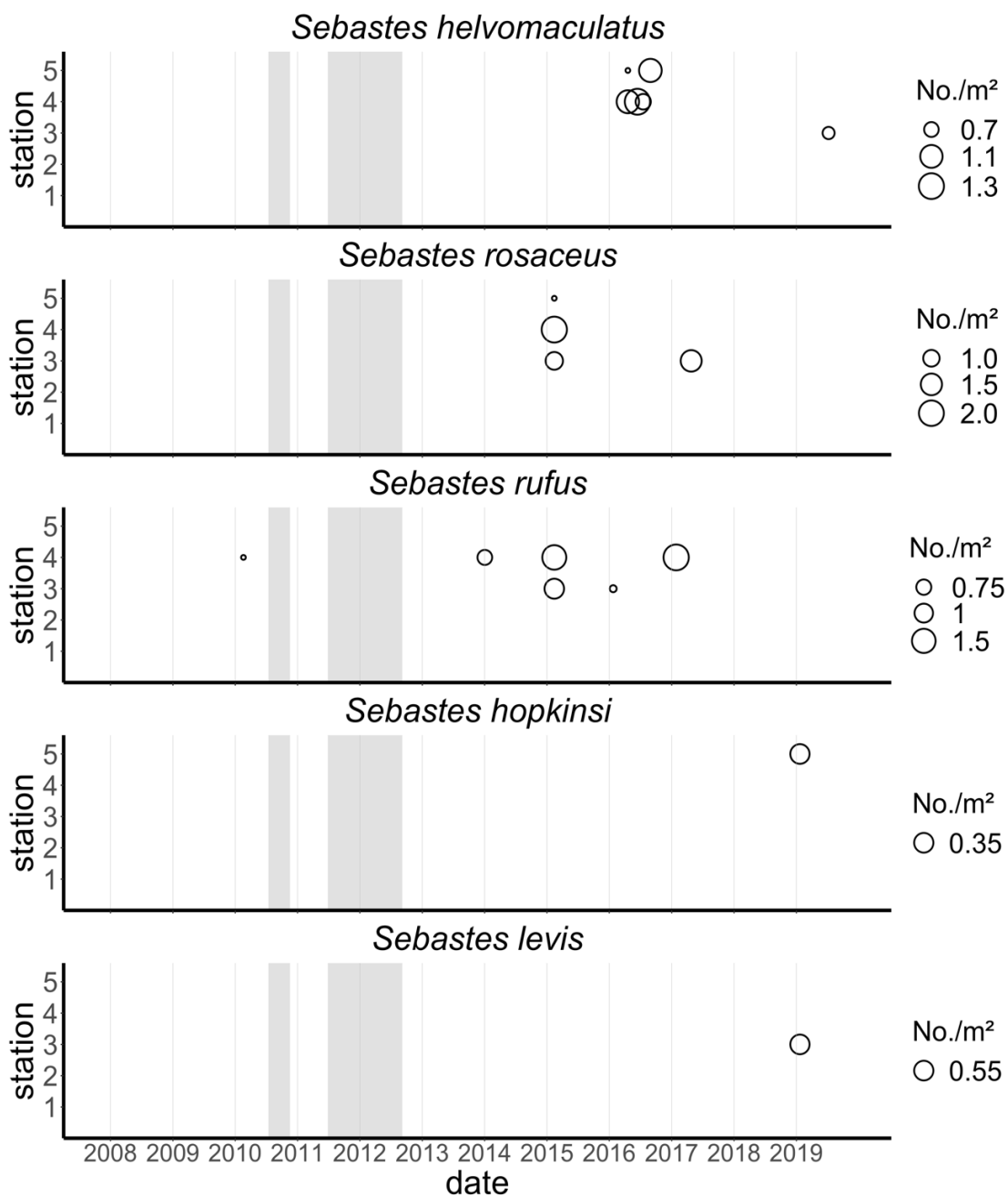


Figure 22. Time series variability in areal density (No./m²) of notable rare species within the rockfish assemblage by cruise date (x-axis) and station (y-axis). Circles scale with areal density. Gray shading indicates extended observation gaps.

Species Richness and Shannon-Weiner Diversity

Visual assemblage

Shannon-Weiner diversity varied little on intra and inter-annual scales, and variability does not appear to be linked to anomalies in temperature (Figure 23; Figure 24). In contrast, species richness varies seasonally, with increasing richness during late winter and early spring (maximum in March) and lower richness during the fall (minimum in October; Figure 23). In winter and in late summer and fall, species richness increases during warmer years, whereas species richness decreased throughout the year during anomalously cool years. Species richness was highest in early 2010 during the 2009-10 El Niño and throughout the late 2014-16 MHW (Figure 24).

Rockfish assemblage

Shannon-Weiner diversity and species richness within the rockfish assemblage varied strongly by season, and more subtly at interannual scales (Figure 25; Figure 26). Both indices exhibited similar seasonal patterns, with larger values observed in winter (e.g., Jan-March) and summer (e.g., June-July) and lower diversity and species richness in late spring (e.g., April-May) and late summer and fall months (e.g., August-December; Figure 25). During winter, species richness and Shannon-Weiner diversity were both higher during warmer years and lower during cooler years. Variability between warmer and cooler years was not detected during summer months. Patterns of inter-annual variability in Shannon-Weiner diversity and species richness were not as clear, as both indices remained relatively stable throughout the time series with the exception of

unusually high values in January and February during years affected by warm climate events (Figure 26).

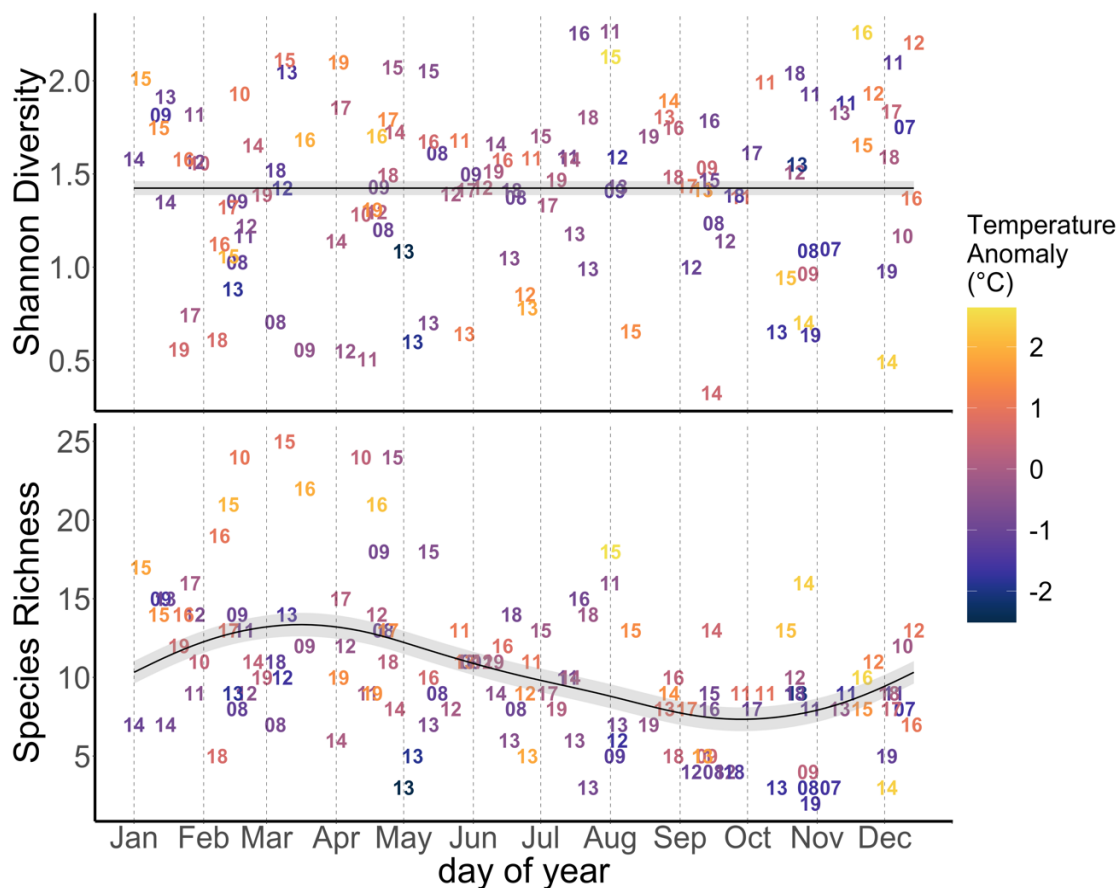


Figure 23. Intra-annual variability in Shannon-Weiner diversity (top panel; y-axis) and species richness (bottom panel; y-axis) within the visual assemblage by day of year (x-axis). Black line (\pm SE in gray) represents a generalized additive model fit to each biodiversity index. Symbol number correspond to the observation year. Symbol color corresponds to a temperature anomaly from a seasonal climatology (see methods for calculation of anomaly product).

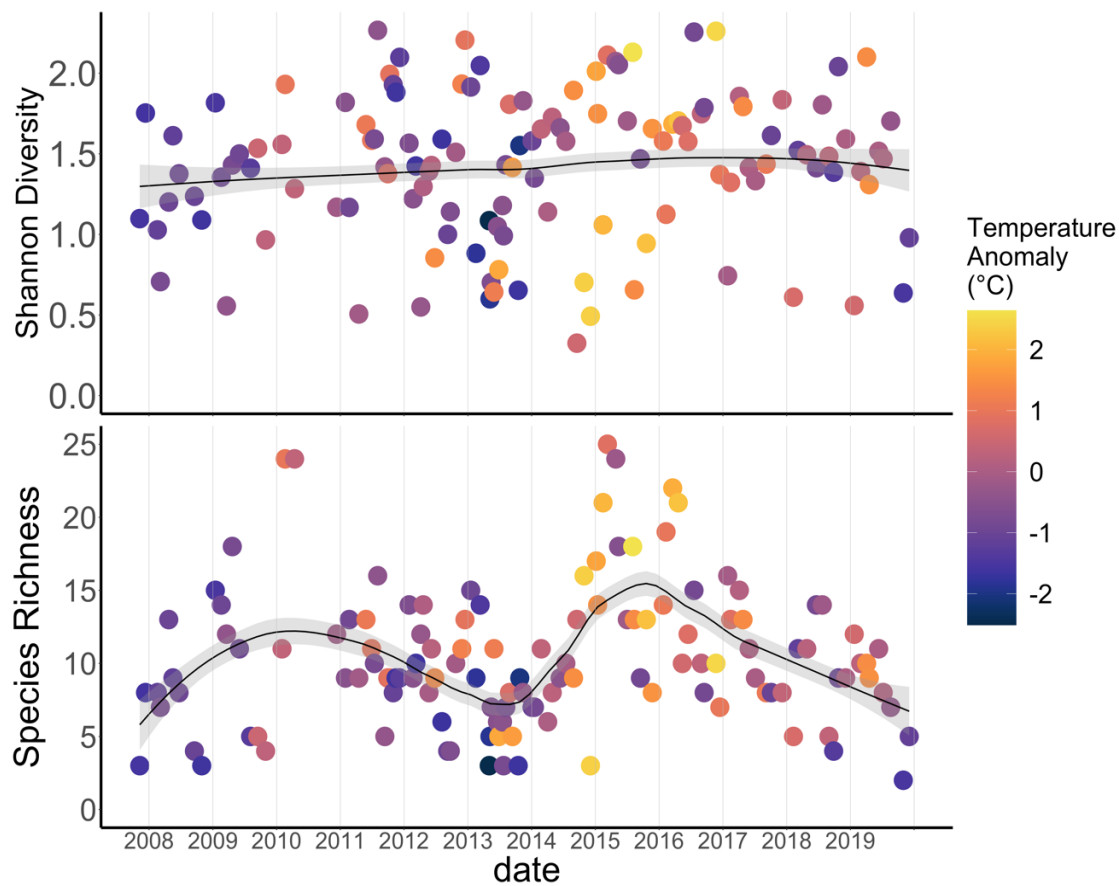


Figure 24. Inter-annual variability in Shannon-Weiner diversity (top panel; y-axis) and species richness (bottom panel; y-axis) within the visual assemblage by cruise date (x-axis). Black line (\pm SE in gray) represents a loess smooth (tuned to capture interannual trends) fit to observations. Symbol color corresponds to a temperature anomaly from a seasonal climatology (see methods for calculation of anomaly product). Gray bars indicate extended observation gaps.

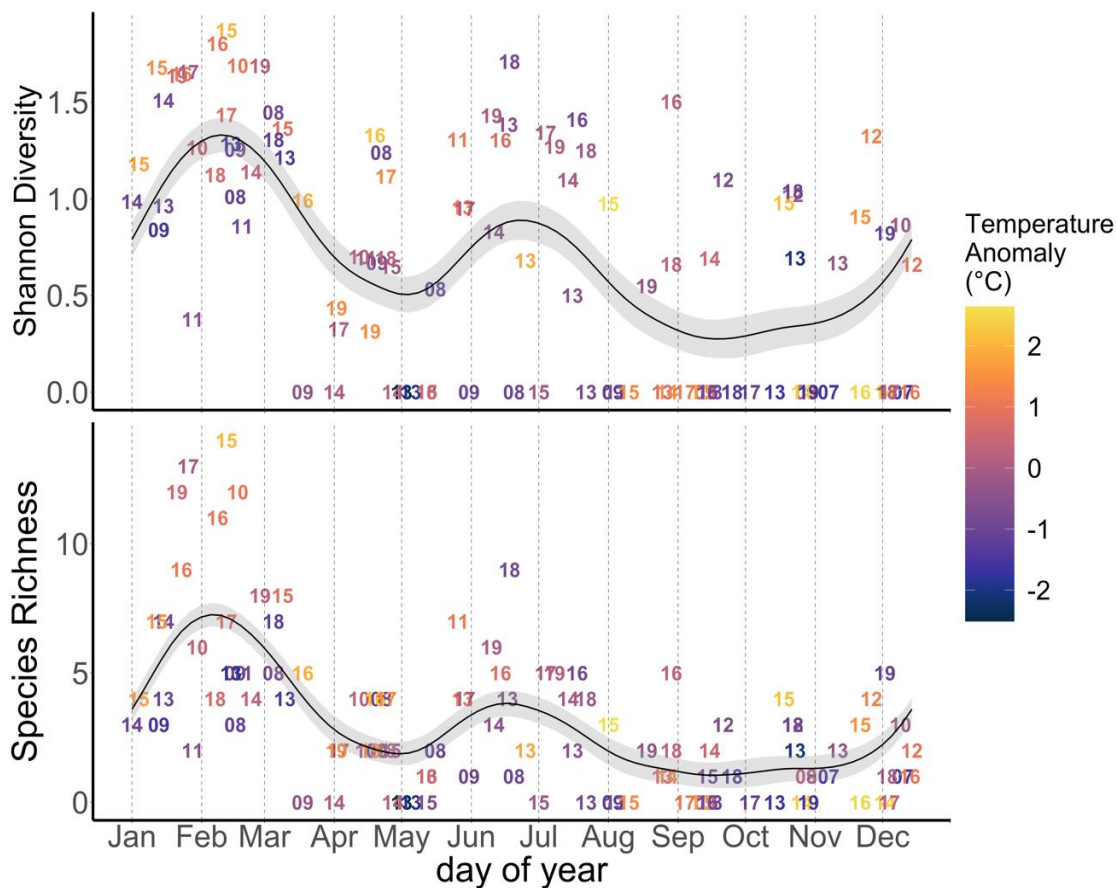


Figure 25. Intra-annual variability in Shannon-Weiner diversity (top panel; y-axis) and species richness (bottom panel; y-axis) within the rockfish assemblage by day of year (x-axis). Black line (\pm SE in gray) represents a generalized additive model fit to each biodiversity index. Symbol number corresponds to the observation year. Symbol color corresponds to a temperature anomaly from a seasonal climatology (see methods for calculation of anomaly product).

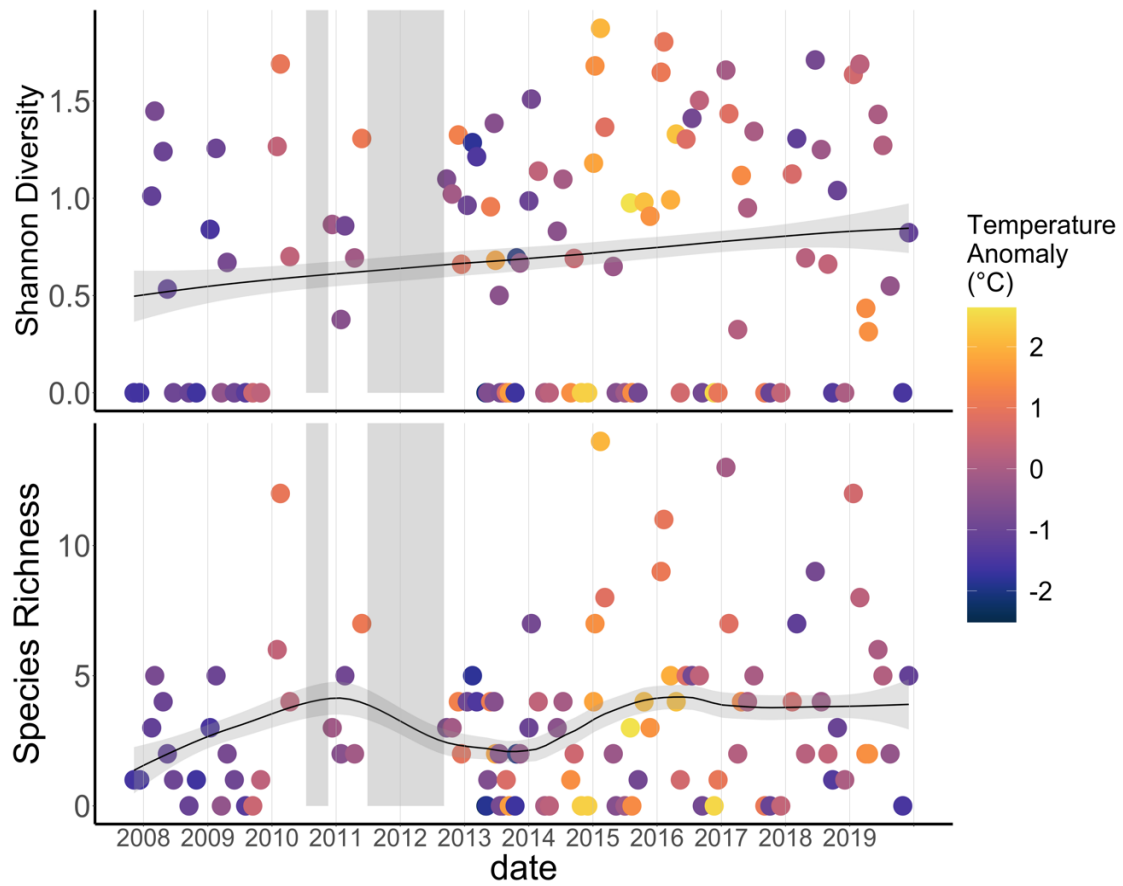


Figure 26. Inter-annual variability in Shannon-Weiner diversity (top panel; y-axis) and species richness (bottom panel; y-axis) within the rockfish assemblage by cruise date (x-axis). Black line (\pm SE in gray) represents a loess smooth (tuned to capture interannual trends) fit to observations. Symbol color corresponds to a temperature anomaly from a seasonal climatology (see methods for calculation of anomaly product). Gray bars indicate extended observation gaps.

Nonmetric Multidimensional Scaling Analysis

Visual assemblage

NMDS on three dimensions (stress=0.13) yielded an adequate and interpretable resolution of patterns in common taxa of the visual assemblage. Nearshore stations (TH01-TH02) were strongly differentiated from offshore stations (TH03-TH05) along NMDS1, consistent with species distributions across the shelf (Figure 27). No seasonal component or distinct trends were apparent along NMDS1 (Figure 28).

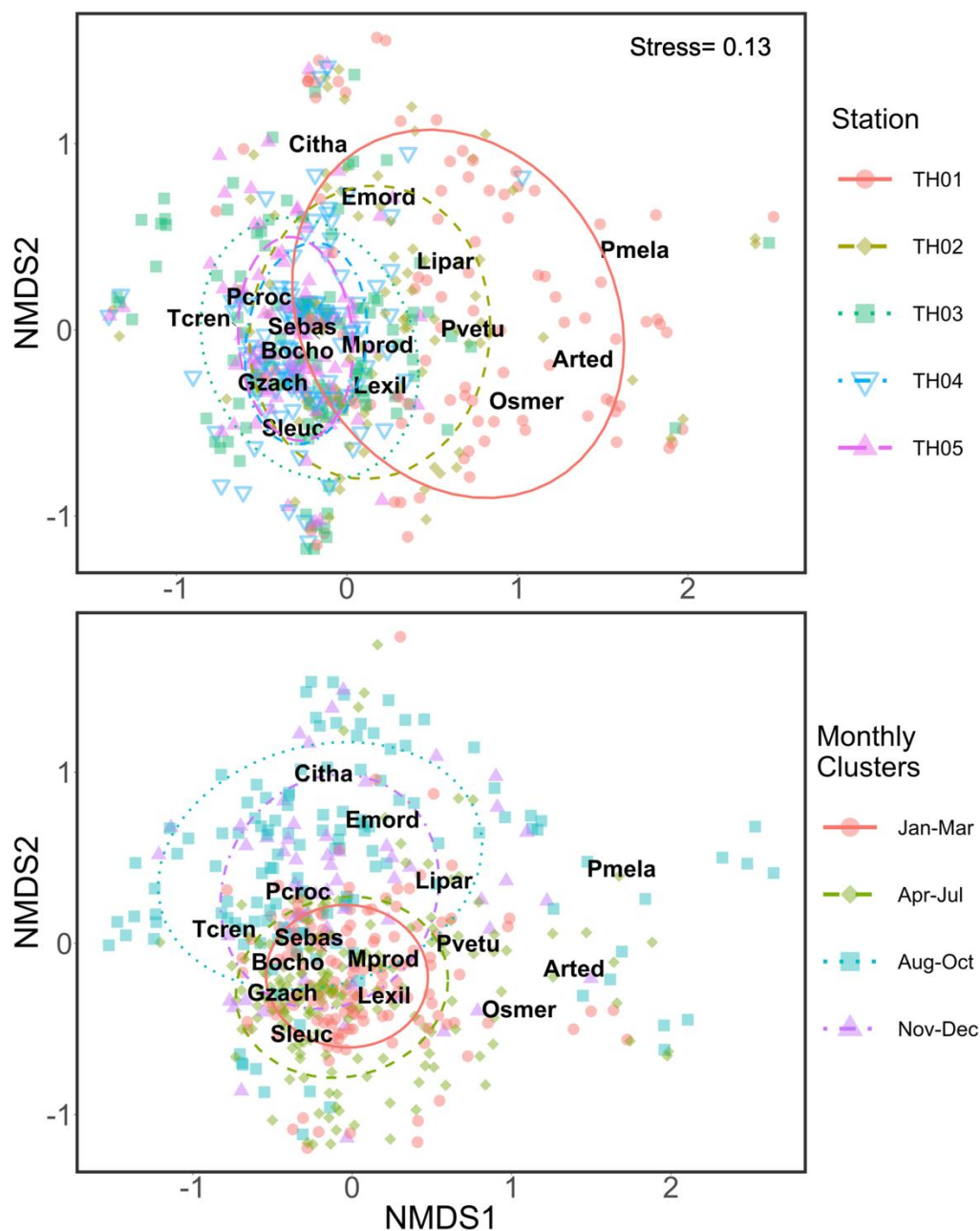


Figure 27. Nonmetric multidimension scaling ordination plots depicting community structure of common taxa within the visual assemblage along axis 1 and axis 2. Top panel: Cross-shelf structure with symbols and colors corresponding to stations. Bottom panel: seasonal structure with symbols and colors corresponding to seasonal clusters. Ellipses represent the standard deviation of each factor level in ordination space. Species labels (see Table 1 for names corresponding to abbreviations) represent the centroids of their scores. See Appendix C for ellipses and points corresponding to each individual month.

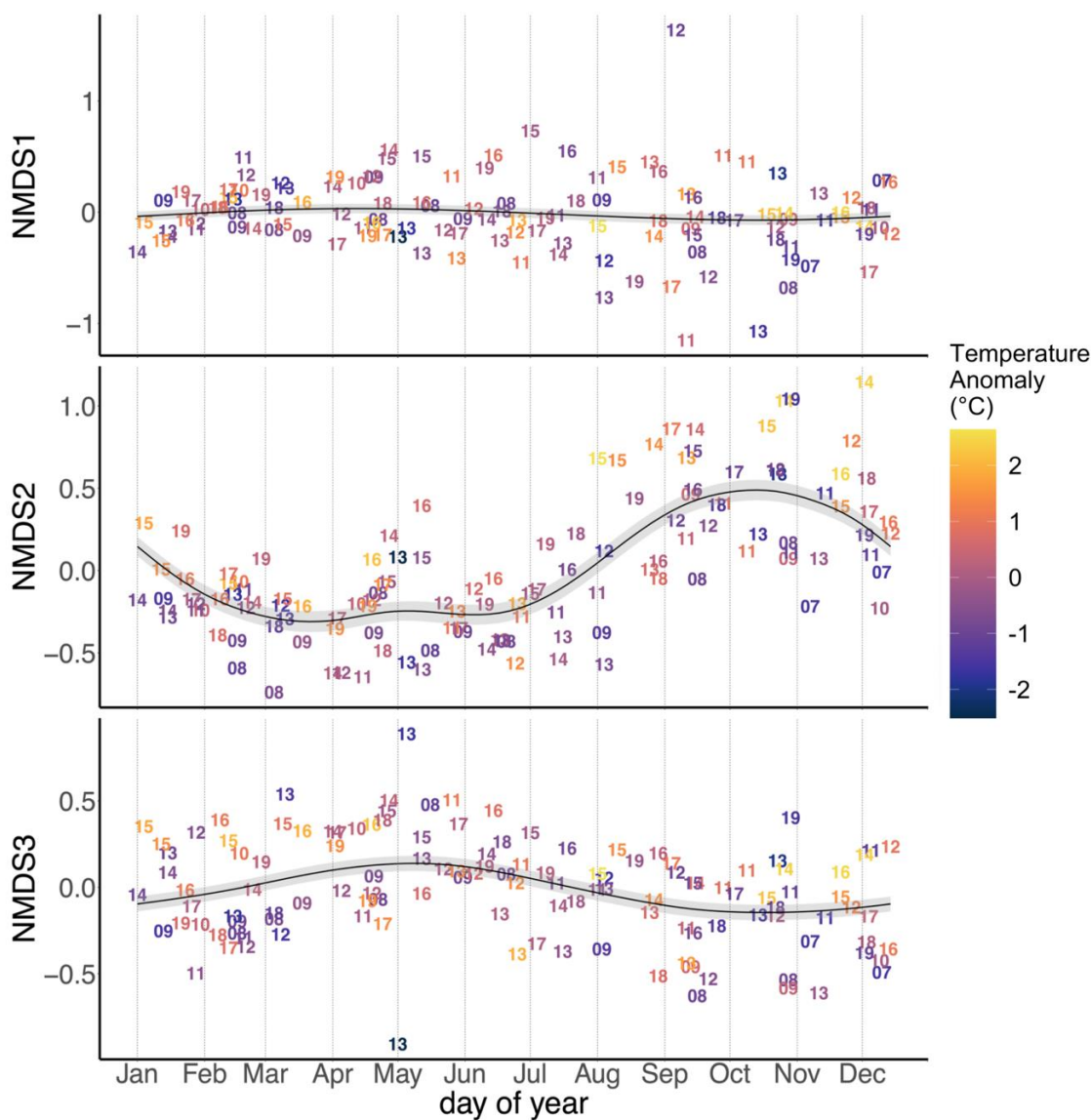


Figure 28. Intra-annual cycle of mean NMDS axis scores (y-axis) performed on common taxa within the visual assemblage aggregated across stations within a cruise by day of year (x-axis). From top to bottom: NMDS 1, NMDS2, and NMDS3. Black line (\pm SE in gray) represents a generalized additive model fit to NMDS scores. Symbol number correspond to the observation year. Symbol color corresponds to a temperature anomaly from a seasonal climatology (see methods for calculation of anomaly product).

Variation in community structure along NMDS2 reflected seasonal patterns in the assemblage and corroborated seasonal structure identified in cluster analysis (Figure 27). Samples collected in August-October and November-December were strongly differentiated from samples collected in January-March and April-July. Most taxa were associated with samples collected in January-July. *Citharichthys* spp., an indicator for samples collected in August-October, is strongly associated with samples collected in August-October along NMDS2. *E. mordax*, which was less seasonally defined, generally associated with samples collected in late summer and fall (August-December). Seasonal structure along NMDS2 was much more apparent when plotted throughout the year, further highlighting strong seasonal differentiation between samples collected in January-July from those collected in August-December (Figure 28). Seasonal patterns identified along NMDS2 were generally consistent across each cross-shelf sampling station (Figure 29).

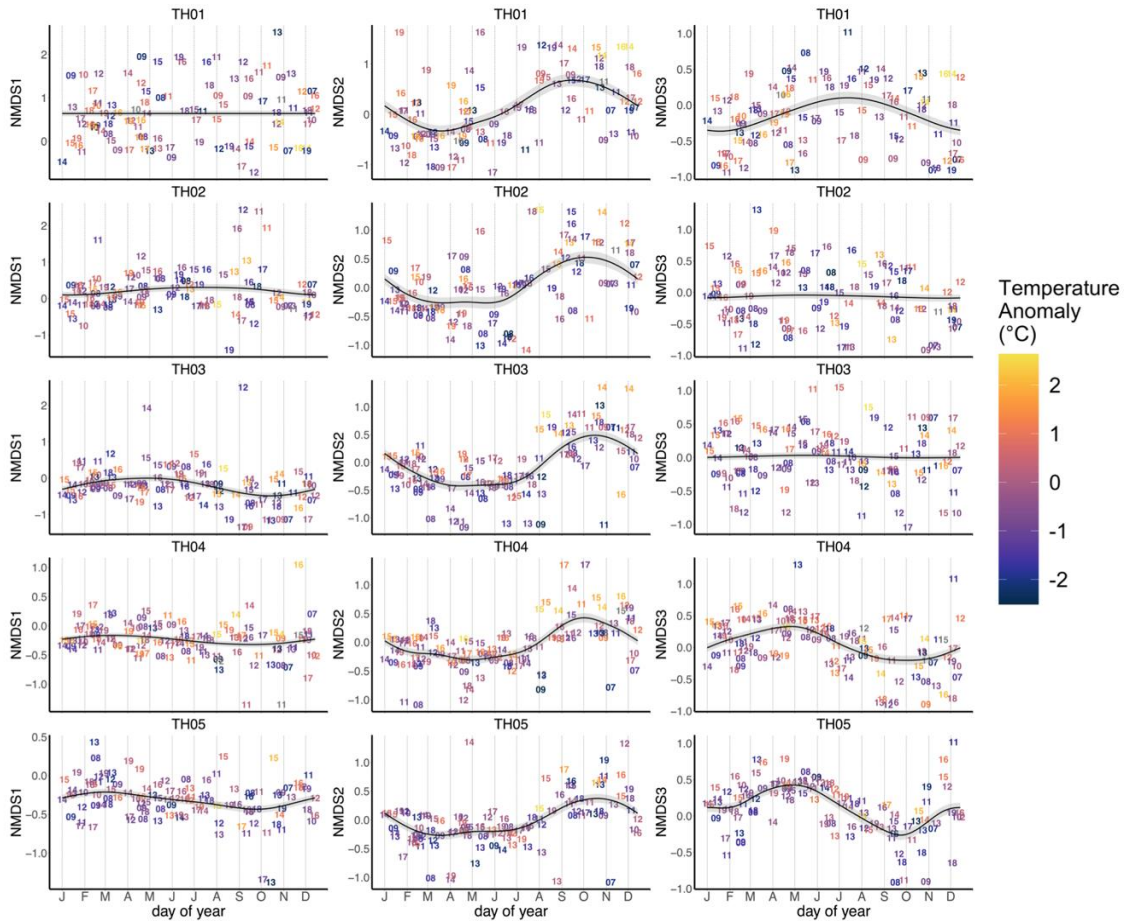


Figure 29. Intra-annual cycle of mean NMDS axis scores (y-axis) performed on common taxa within the visual assemblage for each sampling station by day of year (x-axis). From left to right: NMDS1, NMDS2, and NMDS3. From top to bottom: stations TH01, TH02, TH03, TH04, and TH05. Black line (\pm SE in gray) represents a generalized additive model fit to NMDS scores. Symbol number correspond to the observation year. Symbol color corresponds to a temperature anomaly from a seasonal climatology (see methods for calculation of anomaly product).

NMDS3 did not appear to be strongly associated with spatial or seasonal factor variables (see Appendix C for ordination results; Figure 28). Some differentiation between spring and fall is evident at offshore stations (TH04-TH05; Figure 29).

Variability along this axis appears to differentiate among assemblages that included *M.*

productus, *L. exilis*, and *B. ochotensis* from those with substantial representation of

osmerids and *Liparis* spp. at interannual scales. This pattern is consistent with opposite trends in abundance for these groups over the time series (Figure 6).

Some of the variability in NMDS2 and NMDS3 appears to be influenced by temperature anomalies (Figure 28). Much of the variability in NMDS2 around its seasonal mean occurred in August-December, during which unusually warm years (especially 2014 and 2015) were strongly differentiated from cooler years. This pattern held in January, during which values of NMDS2 in both 2015 and 2019 differed markedly from cooler years, when taxa typically representative of late summer and fall assemblages (*Citharichthys* spp. and *E. mordax*) were unusually abundant. Along NMDS3, differentiation between warm and cool years occurred primarily in January-April. In particular, warm conditions in 2015 and 2016 consistently differed from cooler years in January-April. No differentiation between warmer and cooler years was apparent throughout the remainder of the year (May-December) along NMDS3.

Analysis of seasonal anomalies highlights shifts in assemblage structure resolved on NMDS2 and NMDS3 that coincide with climate transitions (Figure 30). A shift in the assemblage along NMDS2 coincides with the late 2014-2016 MHW and is characterized by a decline in assemblages with high representation of *S. leucopsarus* and the osmerids and an increase in assemblages with high representation of *Citharichthys* spp. and *E. mordax*. Along NMDS3, a weaker but distinct signal in the time series is evident during the late 2014-16 MHW. This pattern is characterized by increased representation of assemblages that include *L. exilis*, *M. productus*, and *B. ochotensis* and a decline in assemblages with high representation of *Liparis* spp. and the osmerids. Climate signals

were most prominent at stations TH01-TH04 along NMDS2 and stations TH02-TH04 along NMDS3 (Figure 31).

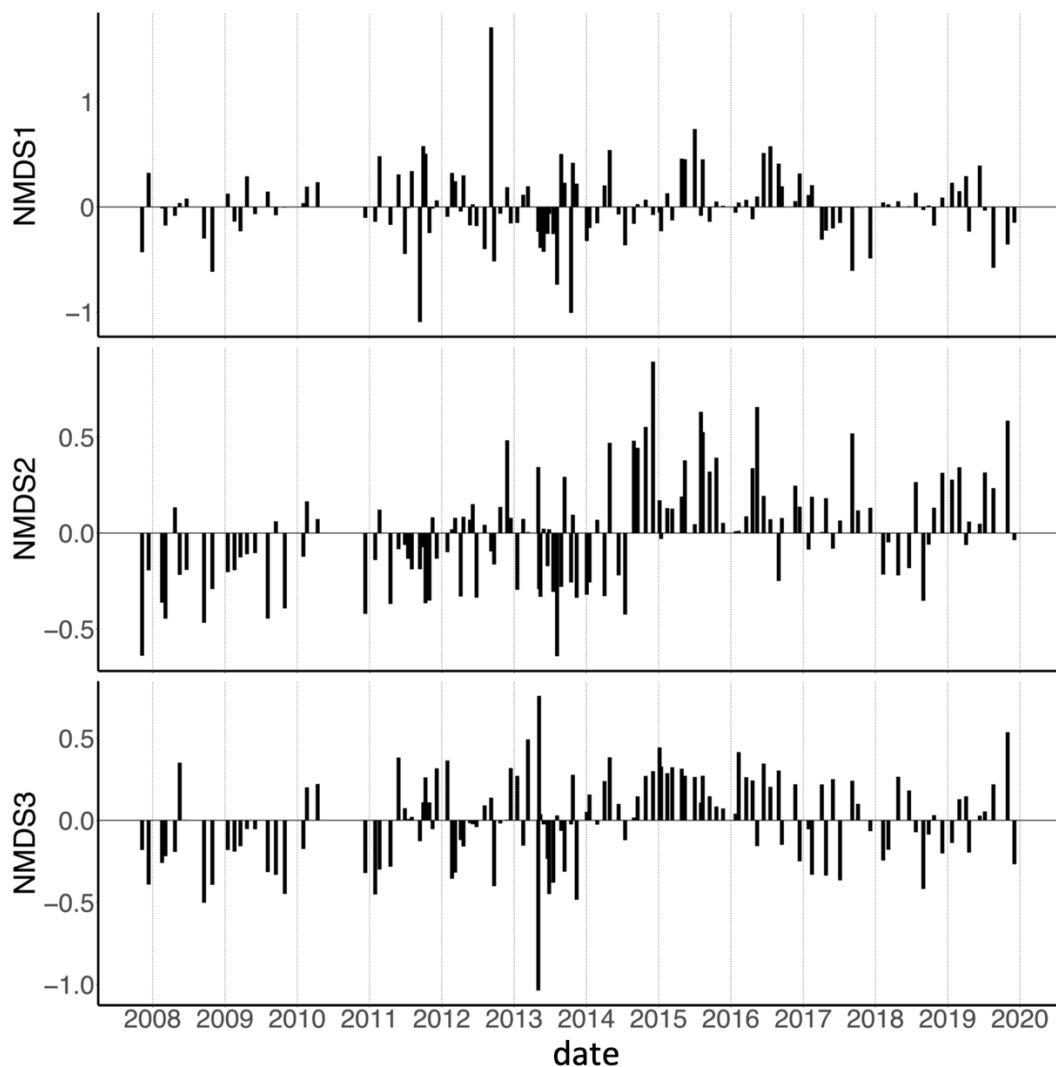


Figure 30. Time series of mean residuals from NMDS performed on common taxa within the visual assemblage aggregated over all stations within a cruise. From top to bottom: NMDS 1, NMDS2, and NMDS3 axis score residuals (y-axis) by cruise date (x-axis). See methods for description of residual product.

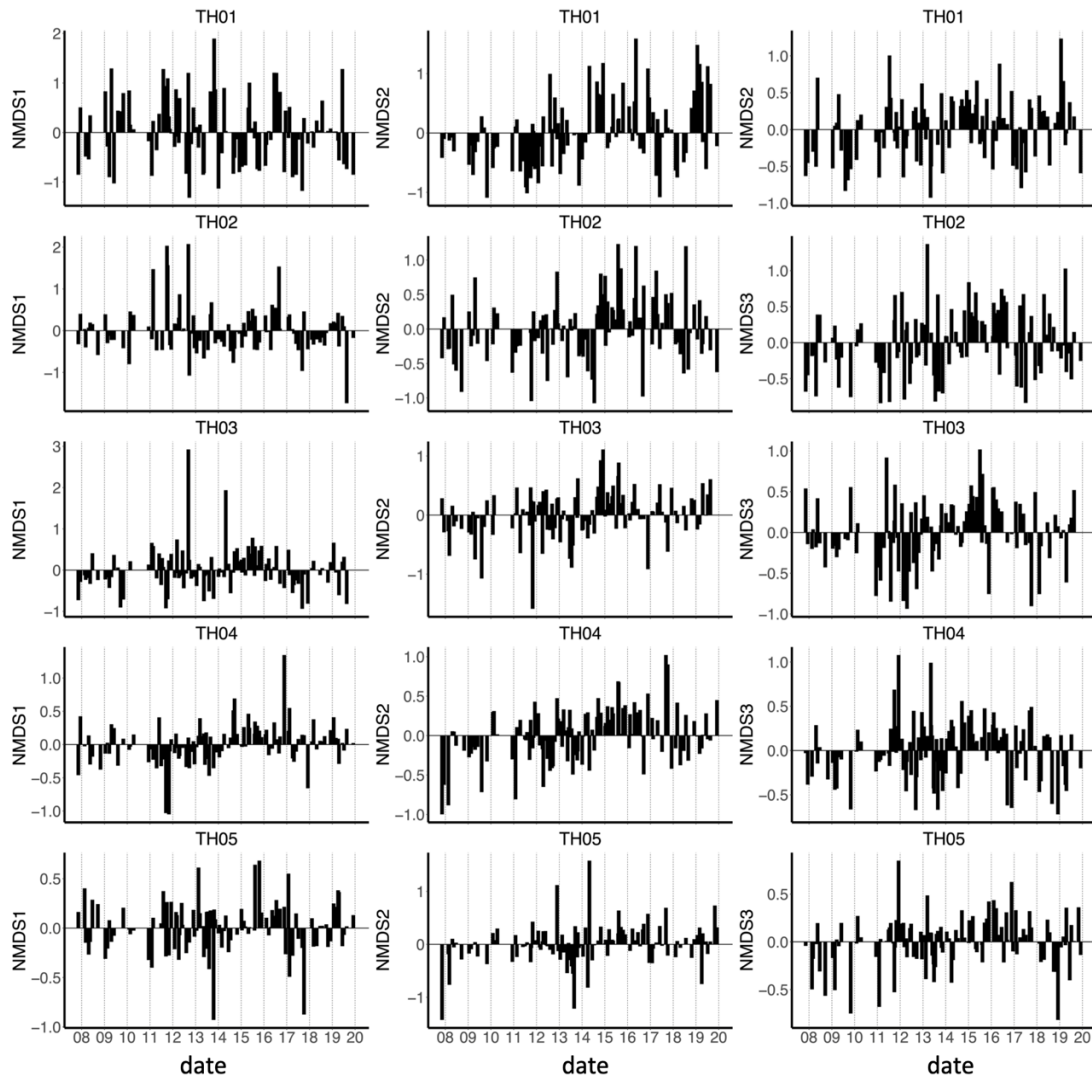


Figure 31. Time series of mean residuals from NMDS performed on common taxa within the visual assemblage for each sampling station. From left to right: NMDS1, NMDS2, and NMDS3 (y-axis) by cruise date (x-axis). From top to bottom: TH01, TH02, TH03, TH04, and TH05. See methods for description of residual product.

Rockfish assemblage

NMDS on two dimensions (stress=0.07) yielded a good and interpretable resolution of patterns in common taxa of the rockfish assemblage. Variation in community structure along NMDS1 reflected seasonal patterns in the assemblage and corroborated seasonal structure identified in cluster analysis (Figure 32). Winter months (January-March) and winter spawning species were strongly differentiated from samples and species collected during summer and fall months (May-November). Variability along NMDS1 was large in April and December, which overlapped samples collected between January-March and May-December. When plotted throughout the year, NMDS1 highlights a cyclical seasonal pattern, during which transitions between winter and summer assemblages are abrupt (Figure 33). High variability in April reflects a shift in assemblage structure from a winter-like assemblage in early April to a spring and summer-like assemblage in late April. High variability in December captures a similar shift in assemblage structure, during which both winter and summer species are present during this month. The cyclical seasonal pattern and abrupt transitions between winter and summer assemblages along NMDS1 remained consistent at each cross-shelf sampling station, although summer spawning rockfishes were typically absent from TH01 (Figure 34). Variation in community structure did not appear to be explained by spatial variables, although station TH01 was slightly differentiated from all other stations in ordination space (Figure 32).

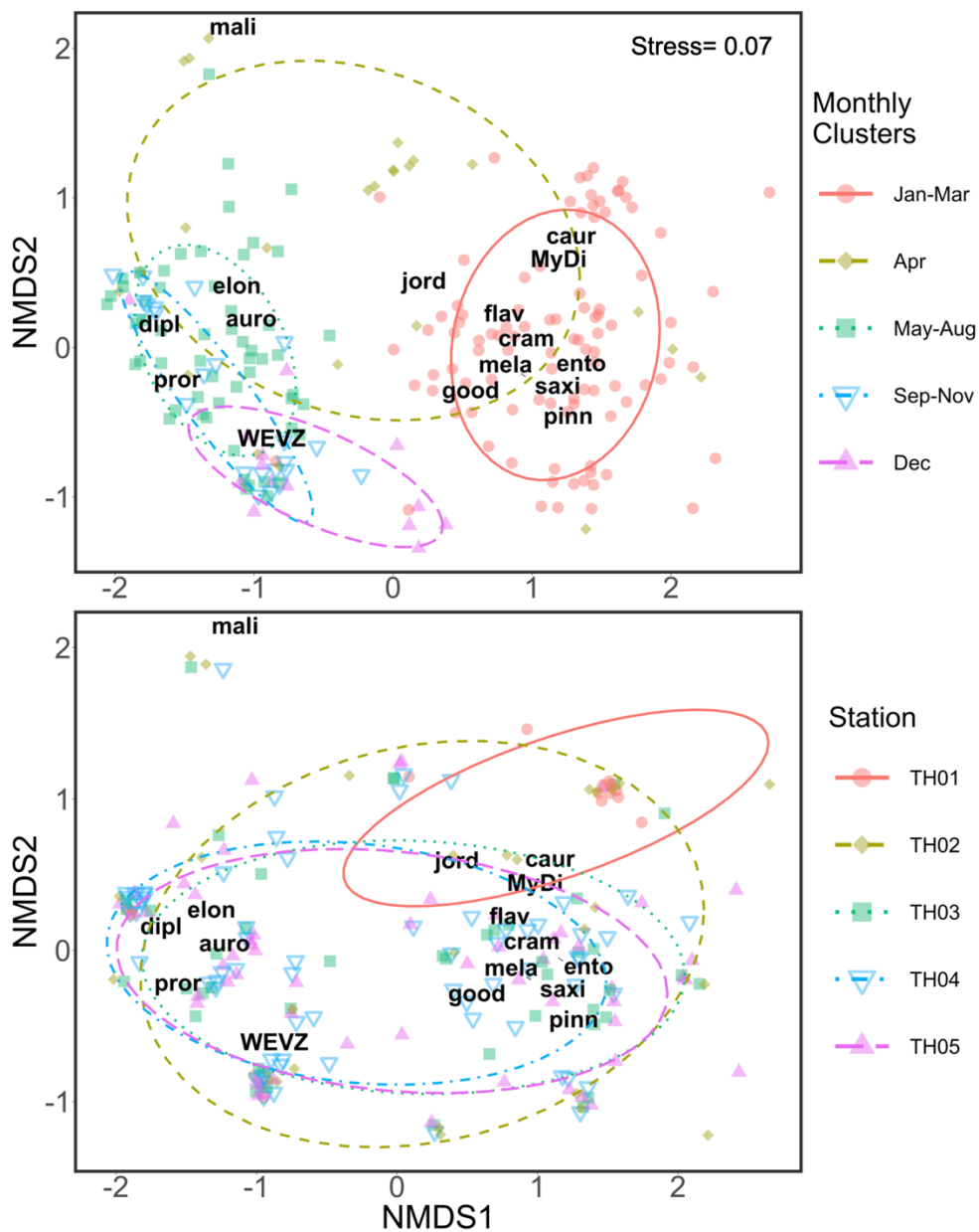


Figure 32. Nonmetric multidimension scaling ordination plots depicting community structure of common species or species complexes within the rockfish assemblage along axis 1 and axis 2. Top panel: seasonal structure with symbols and colors corresponding to seasonal clusters. Bottom panel: Cross-shelf structure with symbols and colors corresponding to stations. Ellipses represent the standard deviation of each factor level in ordination space. Species labels (see Table 2 for names corresponding to abbreviations) represent the centroids of their scores. See Appendix C for ellipses and points corresponding to each individual month.

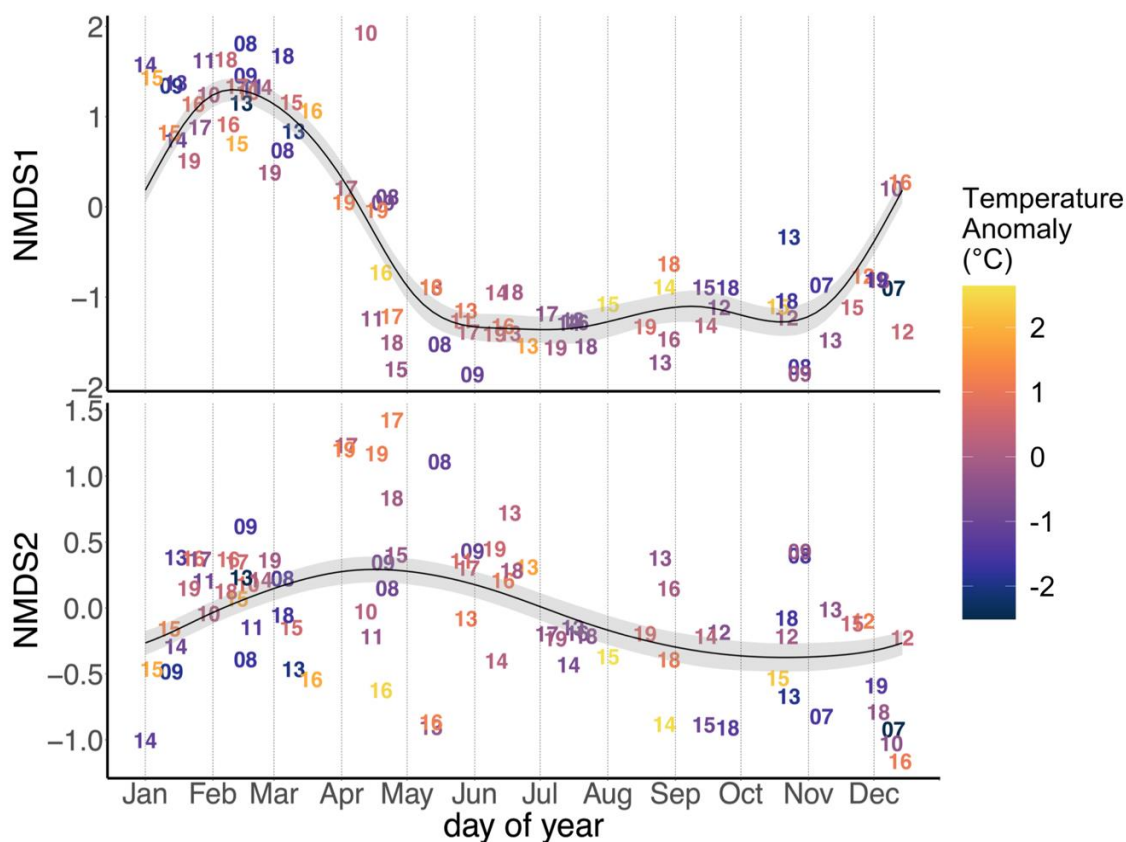


Figure 33. Intra-annual cycle of mean NMDS axis scores (y-axis) performed on the rockfish assemblage aggregated across stations within a cruise by day of year (x-axis). Top panel: NMDS1. Bottom panel: NMDS2. Black line (\pm SE in gray) represents a generalized additive model fit to NMDS scores. Symbol number correspond to the observation year. Symbol color corresponds to a temperature anomaly from a seasonal climatology (see methods for calculation of anomaly product).

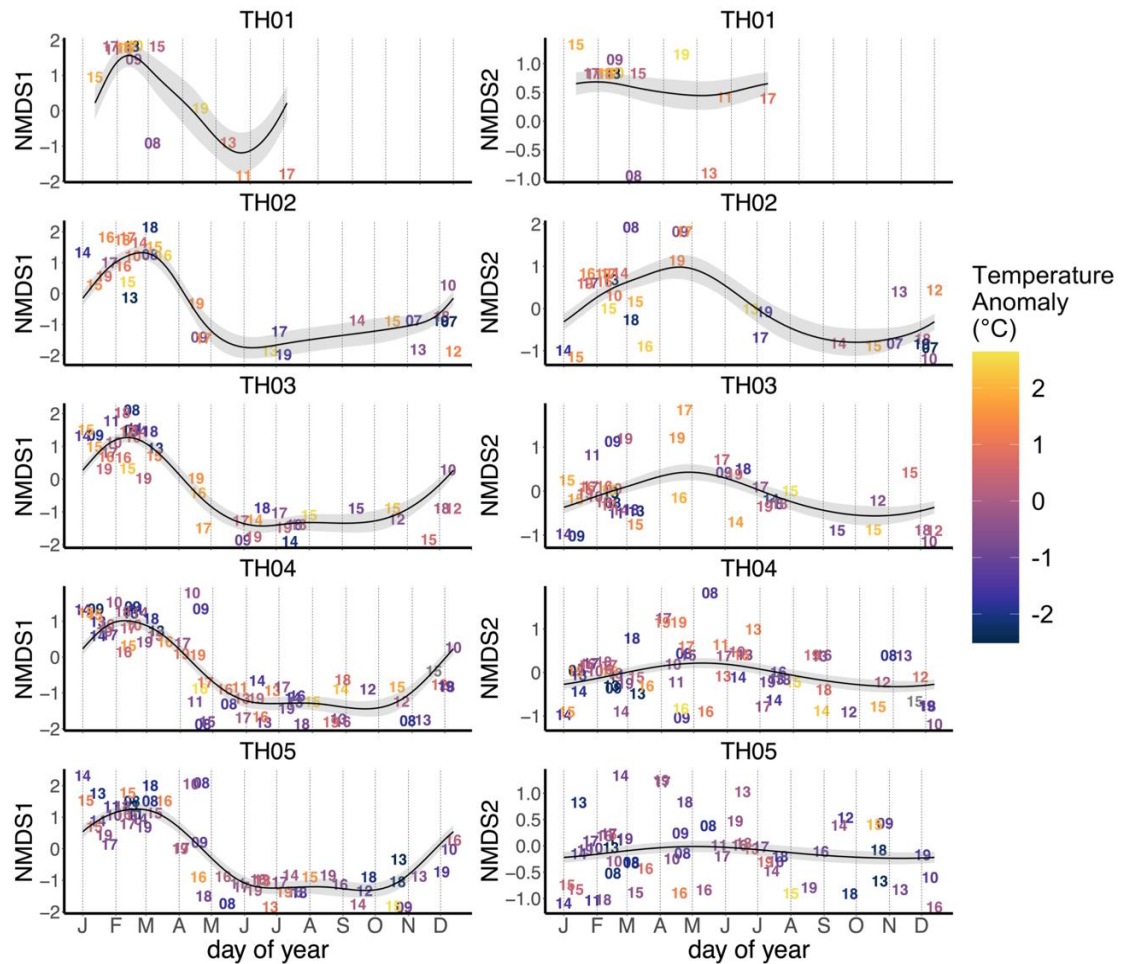


Figure 34. Intra-annual cycle of mean NMDS axis scores (y-axis) performed on the rockfish assemblage for each sampling station by day of year (x-axis). Left panels: NMDS1. Right panels: NMDS2. From top to bottom: stations TH01, TH02, TH03, TH04, and TH05. Black line (\pm SE in gray) represents a generalized additive model fit to NMDS scores. Symbol number correspond to the observation year. Symbol color corresponds to a temperature anomaly from a seasonal climatology (see methods for calculation of anomaly product).

NMDS2 did not appear to be strongly associated with spatial or seasonal factor variables (Figure 32). Variability along this axis appears to differentiate among assemblages that included *S. maliger*, which disappeared during the MHW, and assemblages in which the abundance of most other species increased.

Variability in NMDS did not appear to be strongly influenced by temperature anomalies (Figure 33), nor did analysis of seasonal anomalies highlight shifts in assemblage structure resolved on NMDS that coincide with climate transitions (results not shown). Some differentiation between warm and cool years was apparent in January-February along NMDS1.

Assemblage-Oceanographic Correlations

Canonical correspondence analysis (CCA)

Visual assemblage. Assemblage structure of larval fishes was moderately correlated with oceanographic variables (Figure 35). *E. mordax*, *M. productus*, and *Citharichthys* spp. are strongly associated with warm temperature anomalies and positive anomalies in sea level averaged over 14-days prior to a cruise. For relationships with anomalies in spiciness, larvae of *B. ochotensis* were positively correlated, whereas *G. zachirus* and the osmerids were negatively correlated. For relationships with anomalies in CUTI, *P. crockeri*, *Artedius* spp., and *L. exilis* were moderately correlated with positive anomalies, whereas liparids and *P. melanostictus* were negatively associated with CUTI. Most other taxa had weak or no relationships with oceanographic variables and clustered near the origin. Approximately 6% of the variability in assemblage structure could be attributed to anomalies in oceanographic variables, with the first two axes accounting for 89% of this explanatory power.

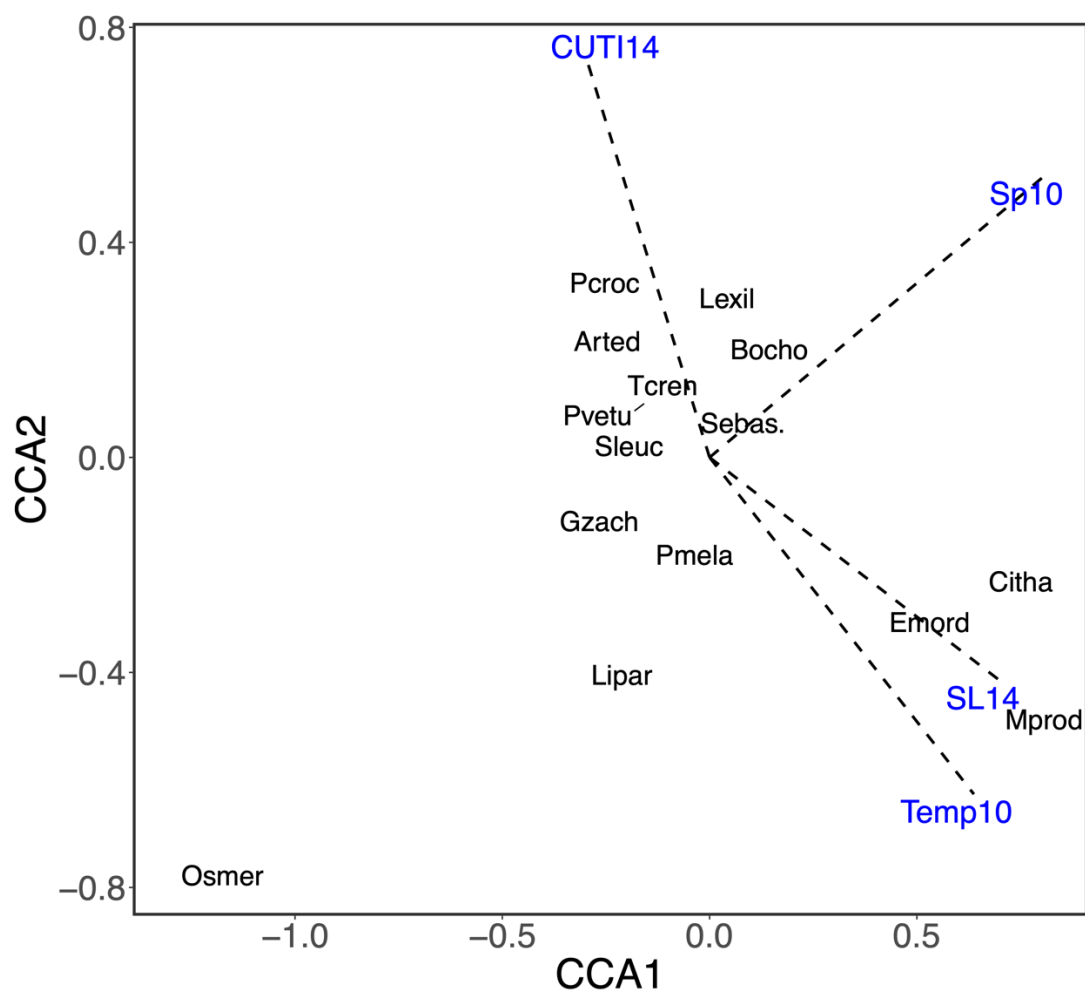


Figure 35. Canonical correspondence analysis depicting structure of common taxa within the visual assemblage in relation to significant oceanographic variables ($p < 0.01$). Temp10 = temperature anomaly in the upper 0-10 m. Sp10 = spiciness anomaly in the upper 0-10 m. SL14 = sea level anomaly averaged over 14-days prior to a cruise. CUTI14 = coastal upwelling transport index anomaly averaged over 14-days prior to a cruise. See Table 1 for full names of each taxon corresponding to abbreviations. The first two axes (CCA1 and CCA2; eigenvectors) account for approximately 89% of the variability explained by the CCA and approximately 5.5% of the total variability in the data.

Rockfish assemblage. Seasonal structure within the larval rockfish assemblage was found to be sufficiently stark to perform CCA on separate winter and summer assemblages. Results were similar to CCA performed on the visual assemblage: moderate to weak correlations between anomalies in oceanographic variables and assemblage structure, save for a few species (Figure 36). *S. jordani* and *S. flavidus* are strongly associated with warm temperature anomalies, fresher conditions, and positive sea level anomalies averaged over 14-days prior to a cruise. For relationships with anomalies in spiciness, larvae of *S. pinniger* were positively correlated, whereas *S. caurinus* and the MyDi complex were negatively correlated. Within the summer spawning rockfish assemblage, *S. proriger* was positively associated with higher-than-normal chlorophyll *a* concentration at the surface (0-10 m). The WEVZ complex was moderately correlated with positive anomalies in sea level along CCA1. Approximately 11% (9%) of the variability in the winter (summer) rockfish assemblage could be attributed to oceanographic variables, with the first two axes accounting for 83% (94%) of this explanatory power.

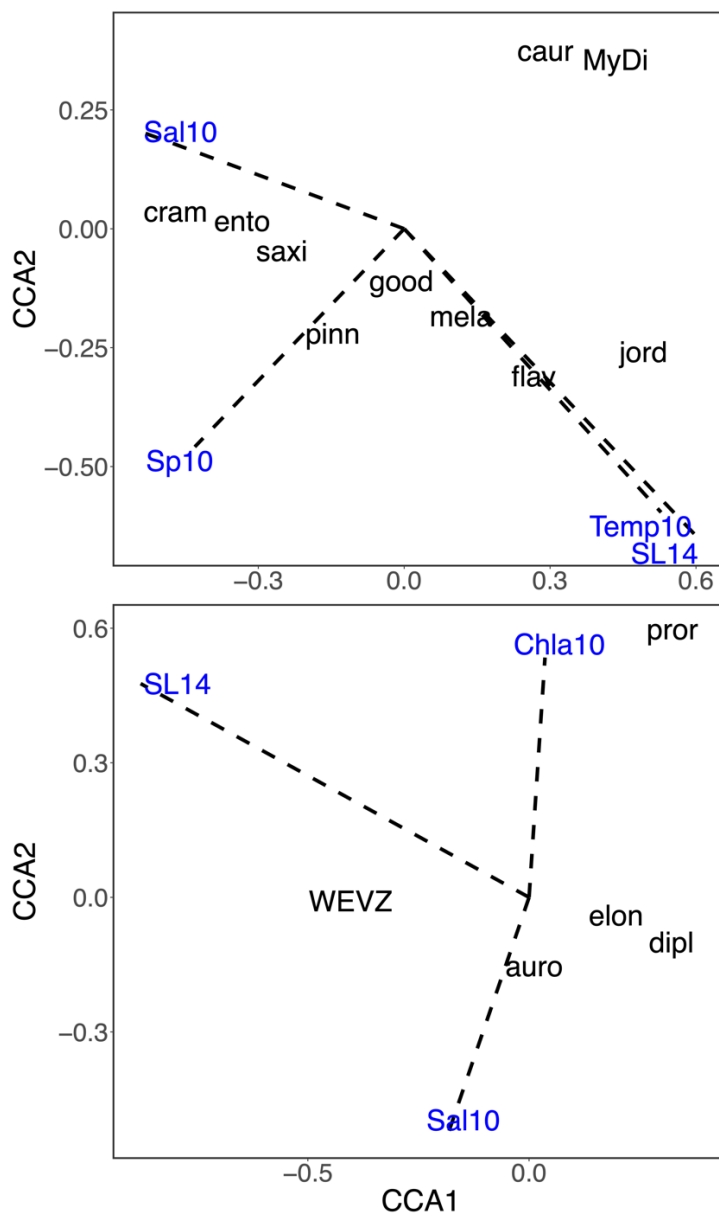


Figure 36. Canonical correspondence analysis depicting structure of common species or species complexes within the rockfish assemblage in relation to significant oceanographic variables ($p < 0.01$). Top panel: winter-spawning rockfishes. Bottom panel: summer-spawning rockfishes. Temp10 = temperature anomaly measured in the upper 0-10 m. Sal10 = salinity anomaly measured in the upper 0-10 m. Chla10 = log-transformed chlorophyll *a* anomaly measured in the upper 0-10 meters. Sp10 = spiciness anomaly measured in the upper 0-10 m. SL14 = sea level anomaly averaged over 14-days prior to a cruise. See Table 2 for full names of each taxon corresponding to abbreviations. The first two axes (CCA1 and CCA2; eigenvectors) account for approximately 83% (94%) of the variability explained by the CCA within winter-spawning rockfishes (summer-spawning rockfishes) and approximately 11% (9%) of the total variability in the data.

Delta generalized additive models

Visual assemblage. Delta-GAMs indicated that variability in terms of both occurrence and larval abundance conditional on presence was strongly related to temperature anomalies and revealed a range over which responses are observed (Figure 37; Appendix D). Within the visual assemblage, probability of occurrence for 5 species (i.e., *E. mordax*, *G. zachirus*, *Liparis* spp., *Sebastes* spp., *T. crenularis*) increased as temperature anomalies increased from -2°C and 2°C with substantial uncertainty and a slight decrease at higher temperature anomalies. In contrast, the probability of occurrence of *B. ochotensis*, *Citharichthys* spp., *L. exilis*, and *M. productus* increases markedly with increasing temperature anomalies. All other common taxa had no relationship or a slight negative relationship between probability of occurrence and temperature anomalies.

Abundance conditional on presence increases with temperature anomalies for most taxa ($n = 7$), in which 3 had significant relationships. Larval abundance of *L. exilis*, *P. crockeri*, and *Sebastes* spp. (when present) increases when warm anomalies are small (0–1°C) but decrease sharply during anomalously cool (< 1°C) and warm (> 1°C) temperatures. The remaining taxa had no relationship between abundance (when present) and temperature anomalies.

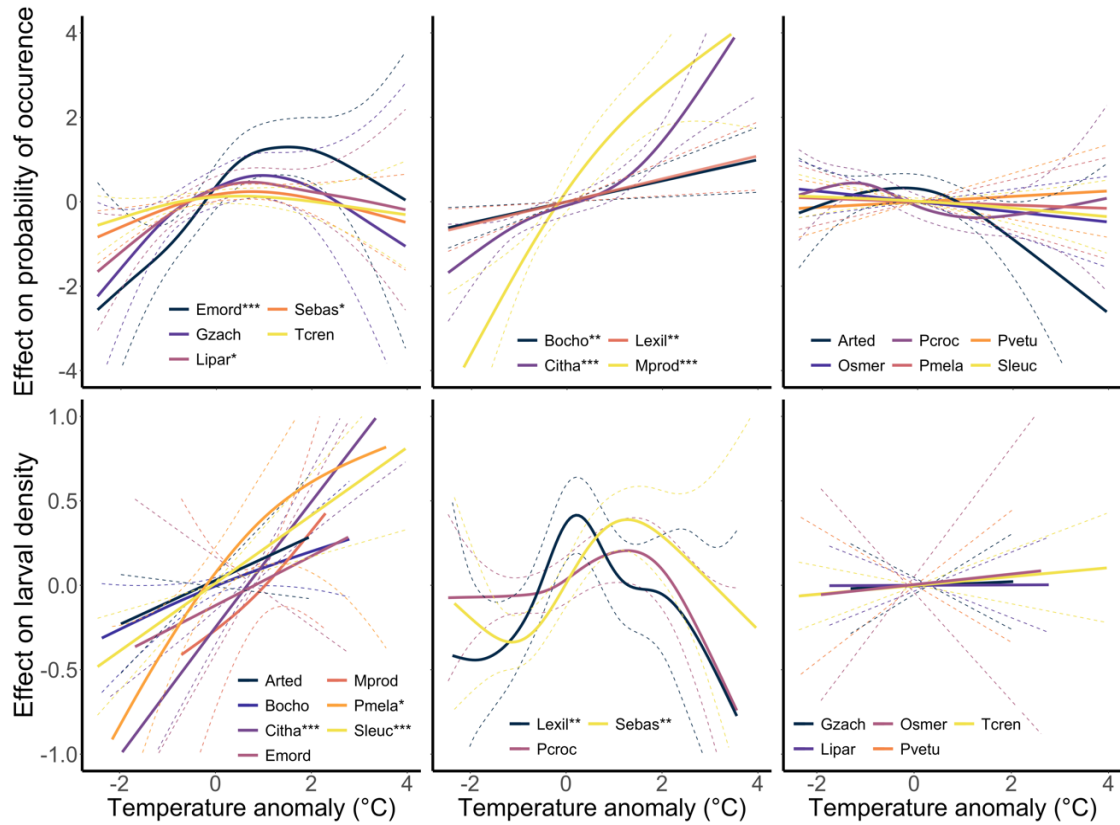
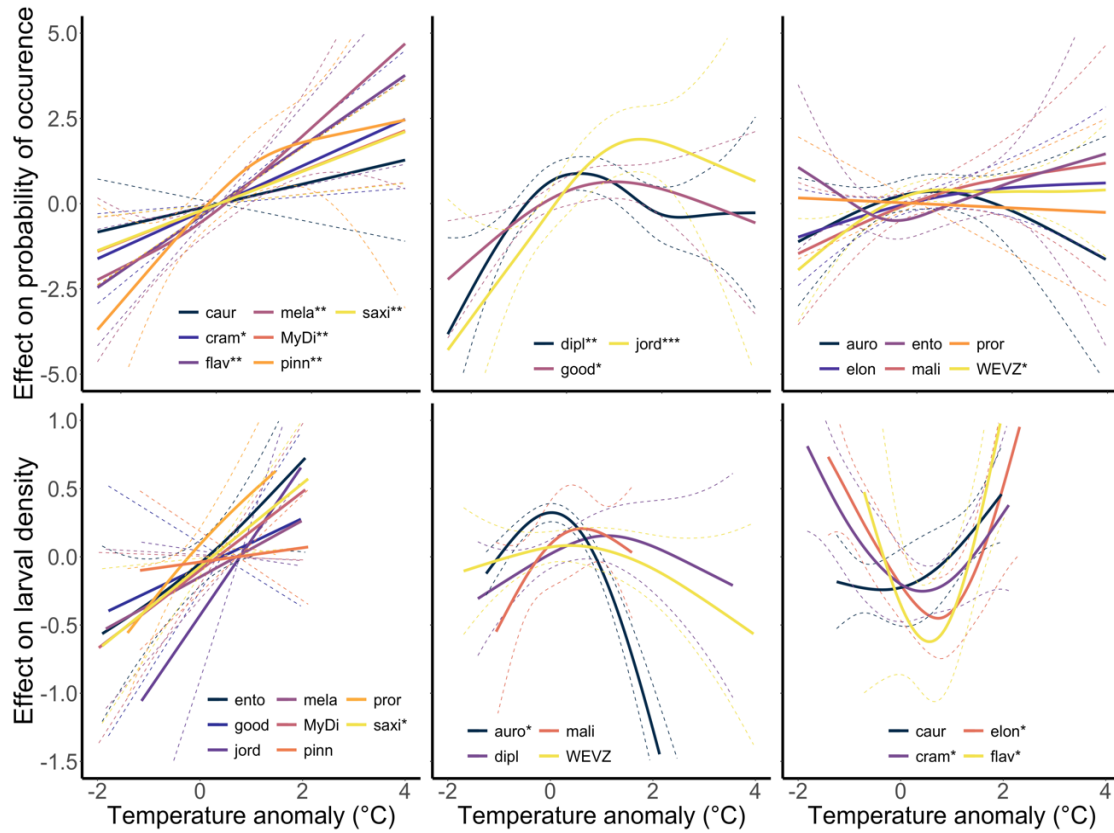


Figure 37. Fitted lines (solid) and 95% confidence intervals (dashed) for the additive effect of a seasonally corrected temperature anomaly in the upper 0-10 m from the binomial (top panels) and lognormal (bottom panels) GAMs for common taxa included within the visual assemblage. Taxa are grouped by shared relationships for each model. The significance of the added effect of the temperature anomaly smooth term in each model is indicated by each taxon name (see Table 1 for full names) and set at: * = $p < 0.05$, ** = $p < 0.01$, *** = $p < 0.001$.

Rockfish assemblage. Of the 16 common species or species complexes within the rockfish assemblage, probability of occurrence for 7 species or species complexes increased as temperature anomalies increased from -2°C and 1°C with substantial uncertainty at temperature anomalies greater than 1°C (Figure 38; Appendix D). The probability of occurrence of *S. diploproa*, *S. goodei*, and *S. jordani* increases markedly with increasing temperature anomalies, reaching an asymptote at 1°C or 2°C with great uncertainty at higher temperatures. The remaining taxa (n = 6) had no relationship or increased or decreased slightly with increasing temperatures anomalies, although uncertainty is high at values greater than 2°C. Abundance conditional on presence for 8 species or species complexes increases markedly with increasing temperature anomalies. *S. crameri*, *S. caurinus*, *S. elongatus*, and *S. flavidus* exhibited a dome-shaped relationship between abundance (when present) and temperature anomalies, increasing in abundance at unusually cool (-2°C) and warm (2°C) temperatures, whereas *S. aurora*, *S. diploproa*, *S. maliger*, and the WEVZ complex increased in abundance at normal temperatures (0°C) but declined sharply at temperatures greater and lower than 0°C.



Pairwise regression: assemblage-temperature correlations

Visual assemblage. Pairwise regression between species richness and a seasonally corrected temperature anomaly resulted in a significant positive relationship when analyzing all months together ($R^2 = 0.16$, $p < 0.001$; Figure 39) This positive relationship increased in strength when analyzing species richness in August-March ($R^2 = 0.24$, $p < 0.001$), but substantially decreased in strength in April-July ($R^2 = 0.04$, $p > 0.05$). Analysis of Shannon-Weiner diversity against a temperature anomaly did not result in a significant relationship ($R^2 = 0.004$, $p > 0.05$), nor did visual assessments indicate any seasonal variation in the effect of a temperature anomaly on Shannon-Weiner diversity (Figure 23).

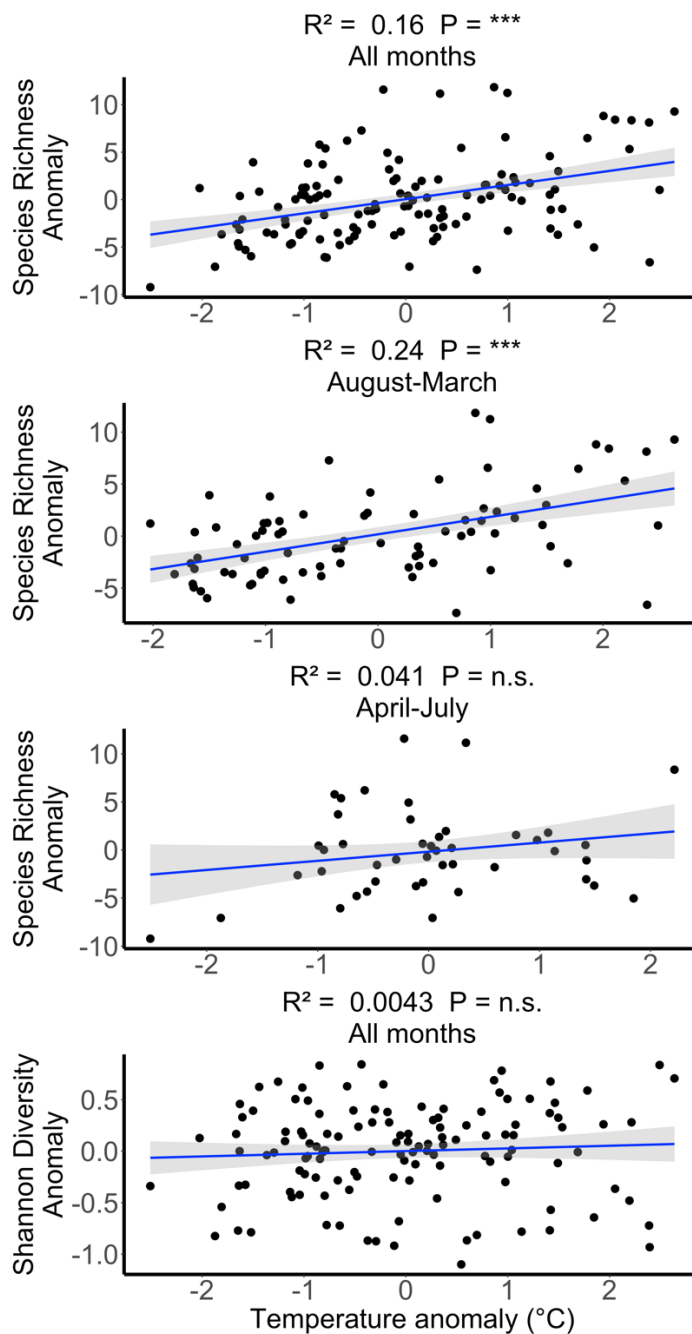


Figure 39. Fitted lines (blue) and 95% confidence intervals (shaded gray) resulting from pairwise regression for the relationship between a seasonally corrected temperature anomaly in the upper 0-10 m of the water column and species richness anomaly and Shannon-Weiner diversity anomaly within the visual assemblage. Each biodiversity index was analyzed using all available data (all months). Species richness was further analyzed by distinct periods of the year (August-March and April-July). The results of each pairwise linear model are indicated by the coefficient of determination (R^2) and the significance of the temperature anomaly term (n.s. = $p > 0.05$, * = $p < 0.05$, ** = $p < 0.01$, *** = $p < 0.001$).

Analysis of NMDS, representing an index of assemblage structure for common taxa, against a temperature anomaly resulted in a significant positive relationship along NMDS2 when including all months in the analysis (NMDS2: $R^2 = 0.18$, $p < 0.001$; Figure 40). This positive relationship increased in strength when analyzing NMDS2 in August-March ($R^2 = 0.26$, $p < 0.001$), but weakened in April-July ($R^2 = 0.035$, $p < 0.01$). NMDS is not explained by a temperature anomaly along axis 1 (NMDS1: $R^2 = 0.004$, $p > 0.05$) and axis 3 (NMDS3: $R^2 = 0.04$, $p < 0.05$), nor did visual assessments indicate any seasonal variation in the effect of a temperature anomaly on these two axes (Figure 28).

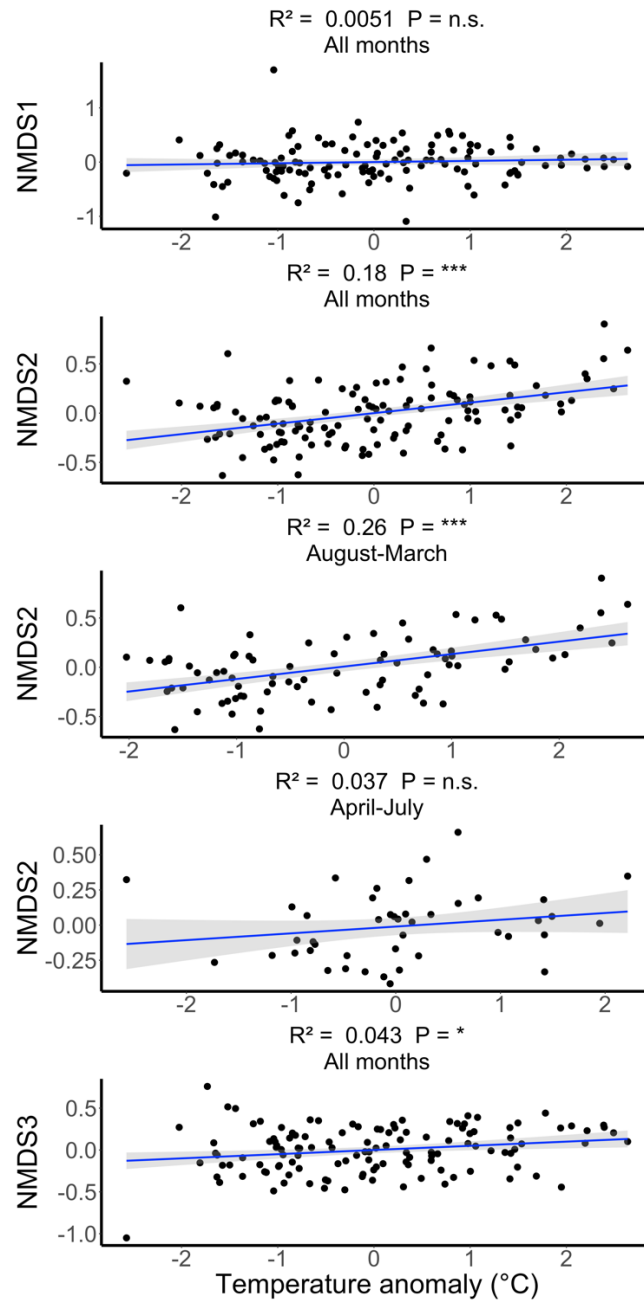


Figure 40. Fitted lines (blue) and 95% confidence intervals (shaded gray) resulting from pairwise regression for the relationship between a seasonally corrected temperature anomaly and seasonally corrected residuals from each NMDS axis within the visual assemblage. Each axis was analyzed using all available data (all months). NMDS2 was further analyzed by different seasons (August-March and April-July). The results of each pairwise linear model are indicated by the coefficient of determination (R^2) and the significance of the temperature anomaly term (n.s. = $p > 0.05$, * = $p < 0.05$, ** = $p < 0.01$, *** = $p < 0.001$).

Rockfish assemblage. Pairwise regression between species richness within the rockfish assemblage and a seasonally corrected temperature anomaly resulted in a weak but significant positive relationship when analyzing all months together ($R^2 = 0.07$, $p < 0.01$; Figure 41). A stronger positive relationship emerged when analyzing species richness and a temperature anomaly in January-February ($R^2 = 0.32$, $p < 0.01$), but this relationship breaks down in March-December ($R^2 = 0.02$, $p > 0.05$). Similarly, the relationship between Shannon-Weiner diversity and a temperature anomaly is weak but significant when analyzing all months together ($R^2 = 0.04$, $p < 0.05$). This positive relationship increases in strength when analyzing diversity against a temperature anomaly in January-February ($R^2 = 0.32$, $p < 0.01$), but breaks down in March-December ($R^2 = 0.02$, $p > 0.05$).

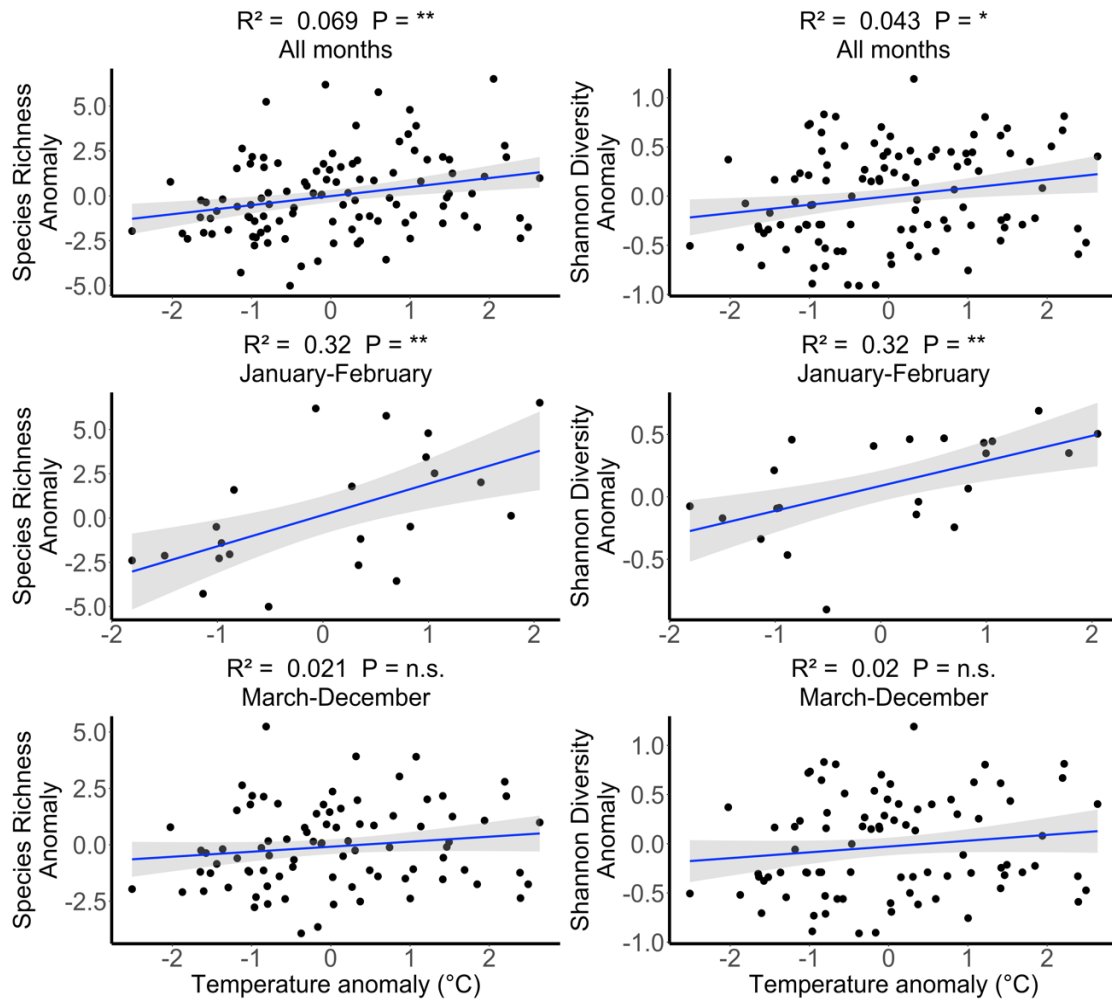


Figure 41. Fitted lines (blue) and 95% confidence intervals (shaded gray) resulting from pairwise regression for the relationship between a seasonally corrected temperature anomaly and species richness anomaly (left-hand column) and Shannon-Weiner diversity anomaly (right-hand column) within the rockfish assemblage. Each biodiversity index was analyzed using all available data (all months) and by different seasons (January-February and March-December). The results of each pairwise linear model are indicated by the coefficient of determination (R^2) and the significance of the temperature anomaly term (n.s. = $p > 0.05$, * = $p < 0.05$, ** = $p < 0.01$, *** = $p < 0.001$).

Pairwise analysis of NMDS against a temperature anomaly did not result in a significant relationship along NMDS1 and NMDS2 when including all months in the analysis (NMDS1: $R^2 = 0.004$, $p > 0.05$; NMDS2: $R^2 = 0$, $p > 0.05$; Figure 42). A slightly stronger but non-significant negative relationship emerges between NMDS1 and a temperature anomaly in January-February ($R^2 = 0.06$, $p > 0.05$), but this relationship breaks down in March-December ($R^2 = 0.001$, $p > 0.05$). Visual assessments did not indicate any seasonal variation in the effect of a temperature anomaly on NMDS2 (Figure 33).

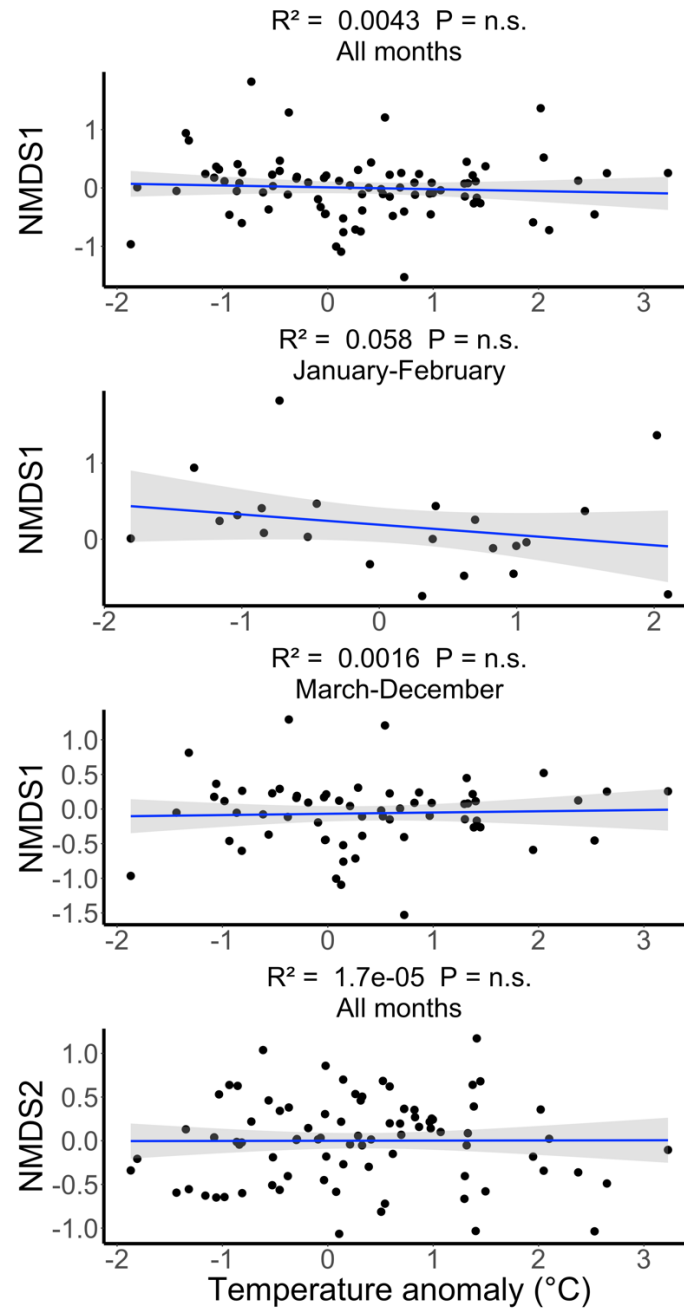


Figure 42. Fitted lines (blue) and 95% confidence intervals (shaded gray) resulting from pairwise regression for the relationship between a seasonally corrected temperature anomaly and seasonally corrected residuals from each NMDS axis within the rockfish assemblage. Each axis was analyzed using all available data (all months). NMDS axis 1 was further analyzed by different seasons (January-February and March-December). The results of each pairwise linear model are indicated by the coefficient of determination (R^2) and the significance of the temperature anomaly term (n.s. = $p > 0.05$, * = $p < 0.05$, ** = $p < 0.01$, *** = $p < 0.001$).

Effects of Parsing Rockfishes to Species on Measures of Assemblage Structure

Assemblage composition

The truncated dataset used to compare spatial and temporal assemblage variability between a fully resolved assemblage (e.g., rockfishes visually and genetically resolved) and an unresolved assemblage in which *Sebastes* is treated in aggregate contained 109 individual cruises and 523 samples. The unresolved assemblage contained the same 15 taxa analyzed earlier in the visual assemblage, whereas the resolved assemblage contained 22 common taxa (Table 5). Incorporating genetically identified larval rockfishes into the broad larval fish assemblage replaces aggregate *Sebastes* spp. with 8 common species or species complexes, which were represented by winter spawning species with the exception of *S. diploproa* and the WEVZ complex.

Table 5. List of common taxa included in the unresolved (*Sebastes* spp. larvae in aggregate) and resolved (*Sebastes* spp. larvae resolved to species) larval assemblages.

<u>Unresolved assemblage</u>		<u>Resolved assemblage</u>	
Taxa	Common Name	Taxa	Common Name
<i>Stenobranchius leucopsarus</i>	Northern lampfish	<i>Stenobranchius leucopsarus</i>	Northern lampfish
<i>Citharichthys</i> spp.	Sanddabs	<i>Citharichthys</i> spp.	Sanddabs
<i>Bathylagus ochotensis</i>	Popeye blacksmelt	<i>Bathylagus ochotensis</i>	Popeye blacksmelt
Osmeridae	Smelts	Osmeridae	Smelts
<i>Merluccius productus</i>	Pacific hake	<i>Merluccius productus</i>	Pacific hake
<i>Lyopsetta exilis</i>	Slender sole	<i>Lyopsetta exilis</i>	Slender sole
<i>Tarletonbeania crenularis</i>	Blue lanternfish	<i>Tarletonbeania crenularis</i>	Blue lanternfish
<i>Protomyctophum crockeri</i>	Calif. flashlightfish	<i>Protomyctophum crockeri</i>	Calif. flashlightfish
<i>Psettichthys melanostictus</i>	Sand sole	<i>Psettichthys melanostictus</i>	Sand sole
<i>Parophrys vetulus</i>	English sole	<i>Parophrys vetulus</i>	English sole
<i>Engraulis mordax</i>	Northern anchovy	<i>Engraulis mordax</i>	Northern anchovy
<i>Liparis</i> spp.	Snailfishes	<i>Liparis</i> spp.	Snailfishes
<i>Artedius</i> spp.	Artedius sculpins	<i>Artedius</i> spp.	Artedius sculpins
<i>Glyptocephalus zachirus</i>	Rex sole	<i>Glyptocephalus zachirus</i>	Rex sole
<i>Sebastes</i> spp.	Rockfishes	<i>Sebastes saxicola</i>	Stripetail rockfish
		<i>Sebastes entomelas</i>	Widow rockfish
		<i>Sebastes jordani</i>	Shortbelly rockfish
		"MyDi"	"MyDi" Complex
		<i>Sebastes goodei</i>	Chilipepper rockfish
		"WEVZ"	"WEVZ" complex
		<i>Sebastes diploproa</i>	Splitnose rockfish
		<i>Sebastes crameri</i>	Darkblotched rockfish

Cross-shelf, seasonal, and taxonomic contrasts

Hierarchical cluster analysis performed on the unresolved assemblage identifies two distinct taxonomic clusters: a coastal assemblage of 5 taxa that have higher average densities at TH01 and TH02 and an offshore assemblage of the remaining 10 taxa that have higher average densities offshore (Figure 43). The resolved assemblage resulted in a taxonomic dendrogram that grouped taxa into three visually distinct clusters. The winter spawning rockfishes and *M. productus* clustered together and were strongly differentiated from the remaining taxa, which were grouped into a coastal assemblage of 5 taxa and an offshore assemblage of 10 taxa. Hierarchical cluster analysis performed on stations yielded nearly identical dendrograms for both the resolved and unresolved assemblages, indicating that differences in species composition across the shelf changed little when rockfishes were resolved (Figure 44). Hierarchical cluster analysis, when performed on months, resulted in a different arrangement of months between the two assemblages. Resolving rockfishes did not result in a difference in the arrangement of months in August-December, however assemblage composition in January-March is strongly differentiated from assemblages in April-July when rockfishes are resolved.

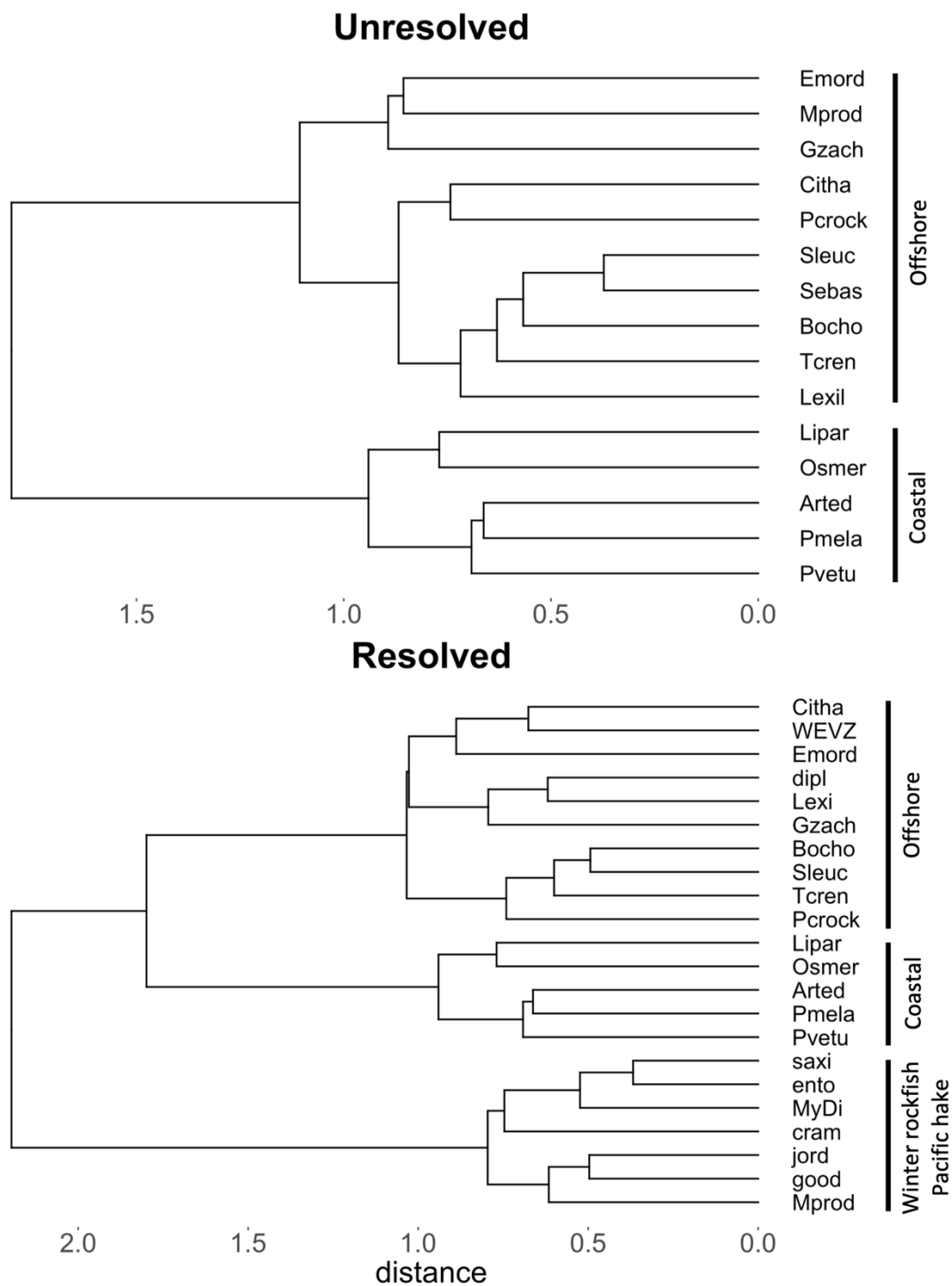


Figure 43. Taxon dendrograms from hierarchical cluster analysis performed on common taxa within the unresolved (*Sebastes* spp. larvae in aggregate) and resolved (*Sebastes* spp. larvae resolved to species) larval assemblages. Ecologically interpretable clusters are labelled.

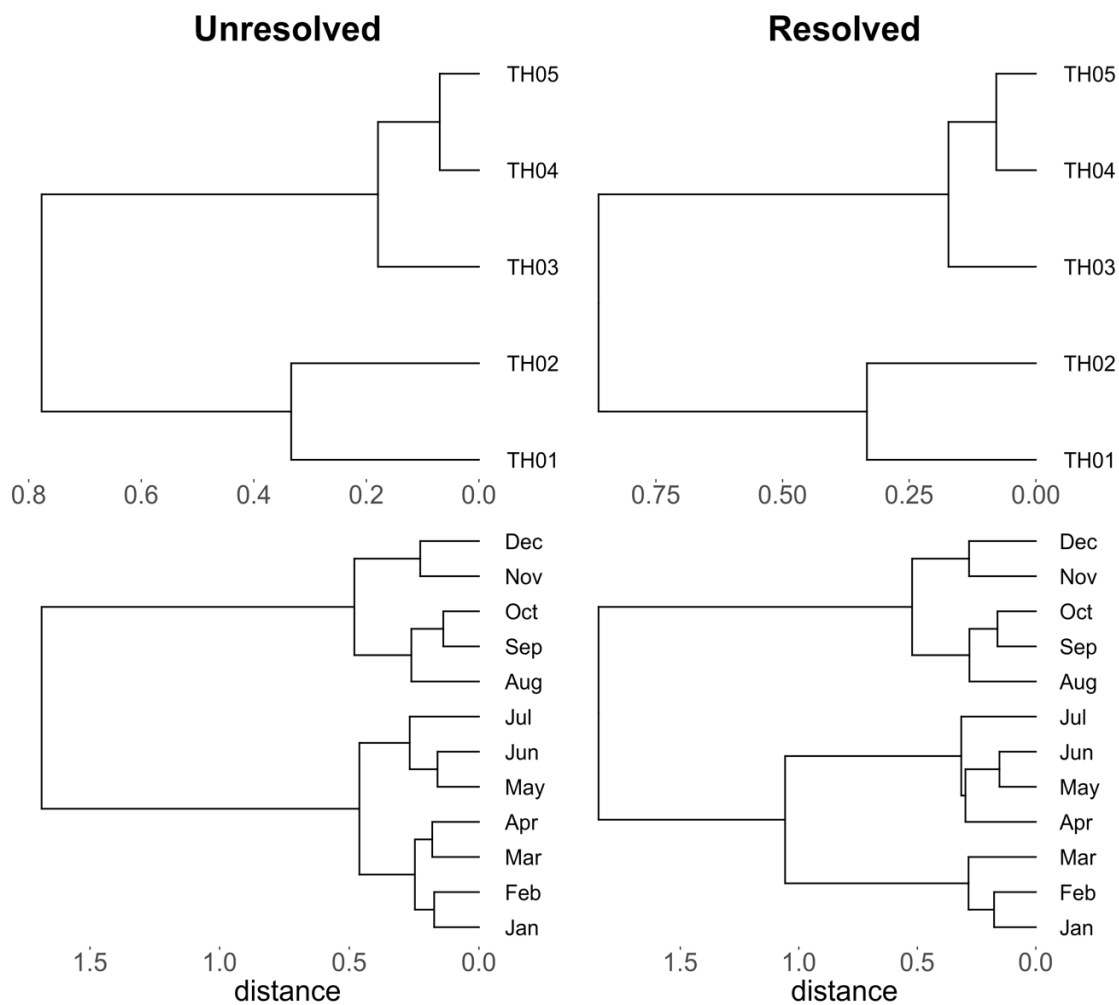


Figure 44. Cross-shelf and seasonal dendrograms from hierarchical cluster analysis performed on common taxa within the unresolved (left-hand columns; *Sebastes* spp. larvae in aggregate) and resolved (right-hand columns; *Sebastes* spp. larvae resolved to species) larval assemblage. Top panels: Cross-shelf dendrogram performed on stations. Bottom panels: seasonal dendrograms performed on months.

Nonmetric multidimensional scaling analysis

The final solutions for NMDS for both assemblages included three dimensions (stress = 0.13) and yielded adequate and interpretable resolution of patterns. The largest variation in community structure for both datasets was explained by cross-shelf differences along NMDS1 (Figure 45). Corroborating hierarchical cluster analysis performed on stations, the arrangement of taxa and samples in ordination space along NMDS1 was similar between unresolved and resolved assemblages, wherein nearshore stations (TH01-TH02) were strongly differentiated from offshore stations (TH03-TH05), consistent with species distributions across the shelf. Rockfishes included in the resolved assemblage were associated with stations TH03-TH05, although the MyDi complex was more strongly associated with stations TH01-TH02.

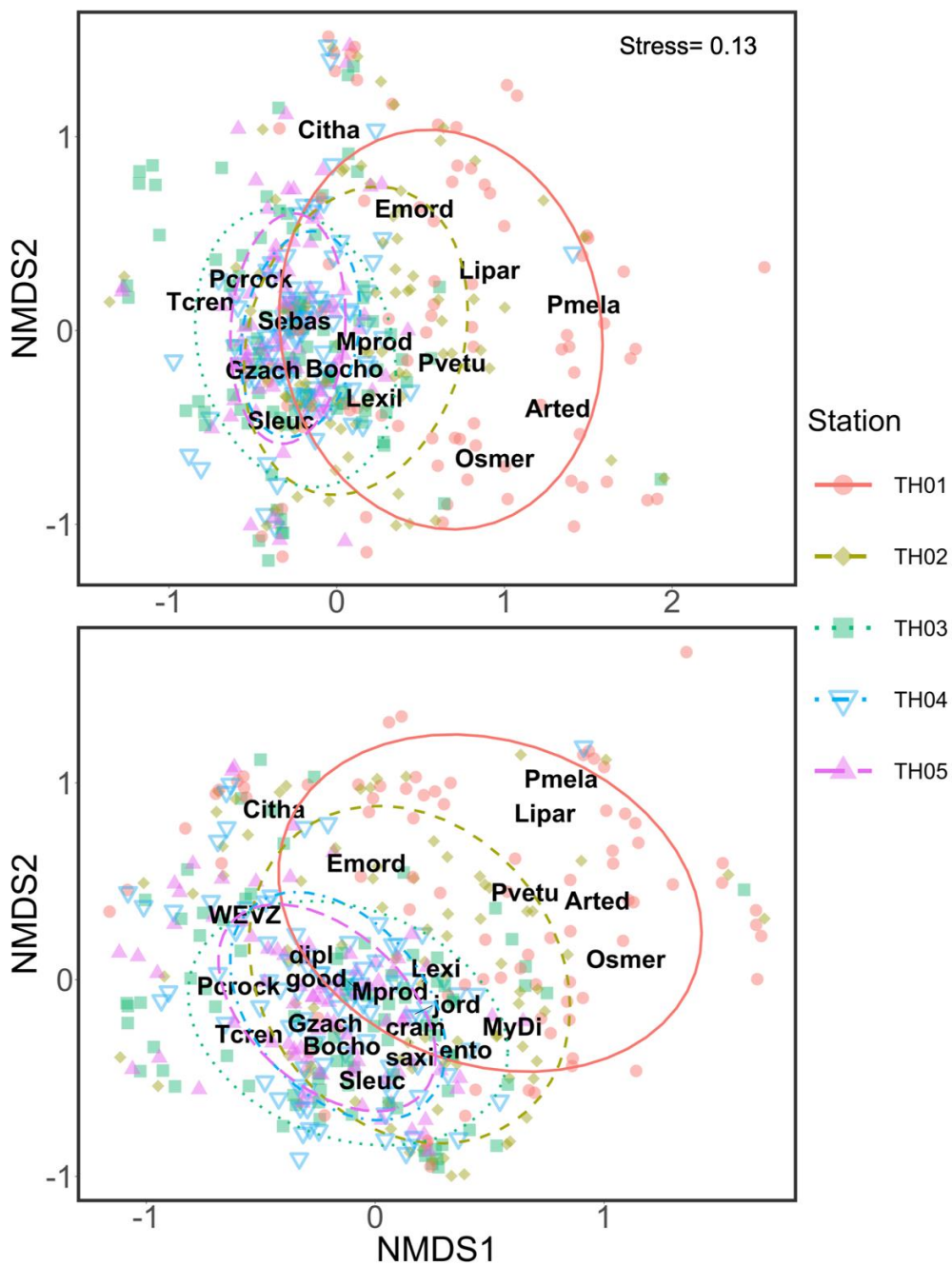


Figure 45. Nonmetric multidimension scaling ordination plots depicting community structure of common taxa within the unresolved (top panel; *Sebastes* spp. in aggregate) and resolved (bottom panel; *Sebastes* spp. larvae resolved to species) assemblage along axis 1 and axis 2. Symbols and colors correspond to stations. Ellipses represent the standard deviation of each factor level in ordination space. Species labels (see Table 1 and Table 2 for names corresponding to abbreviations) represent the centroids of their scores.

Variation in community structure along NMDS2 was similar between unresolved and resolved assemblages and reflected seasonal patterns in both assemblages (Figure 46). Corroborating hierarchical cluster analysis performed on months, NMDS2 resolved strong differentiation in assemblage structure between samples collected in August-December and samples collected in January-July for both assemblages. Along NMDS3, variation in community structure was highly dissimilar between the unresolved and resolved assemblages. Within the unresolved assemblage, variation along NMDS3 did not exhibit patterns explained by seasonality. However, variation along NMDS3 within the resolved assemblage is clearly explained by seasonal differences, differentiating among assemblages in January-March that include winter spawning rockfishes and *M. productus* from those in April-July with substantial representation of *S. diploproa*. In combination, NMDS2 and NMDS3 strongly resolve the annual cycle within the resolved assemblage and more subtly within the unresolved assemblage.

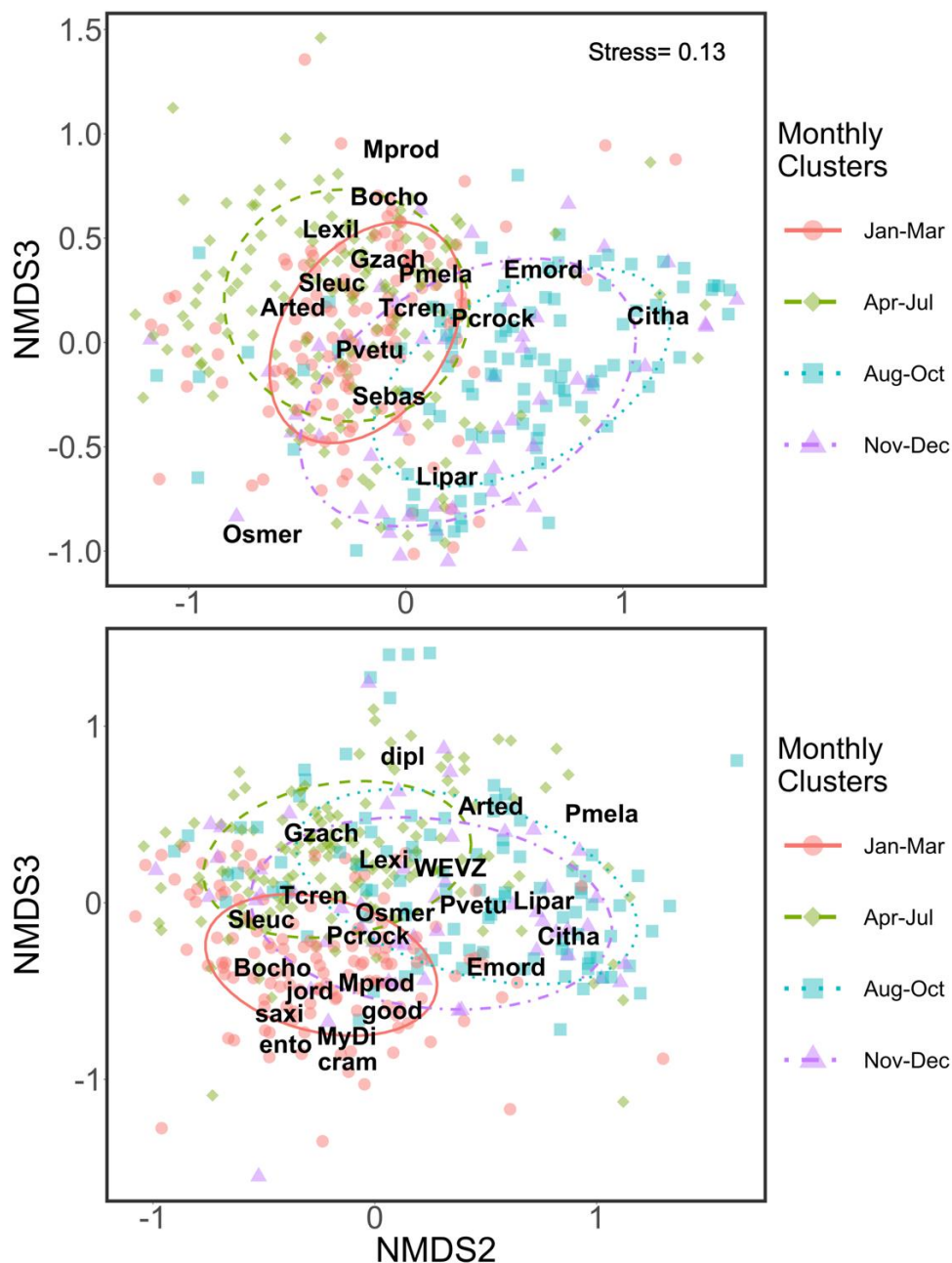


Figure 46. Nonmetric multidimension scaling ordination plots depicting community structure of common taxa within the unresolved (top panel; *Sebastes* spp. larvae in aggregate) and resolved (bottom panel; *Sebastes* spp. larvae resolved to species) assemblage along axis 2 and axis 3. Symbols and colors correspond to seasonal clusters (see Figure 44 for definition of clusters). Ellipses represent the standard deviation of each factor level in ordination space. Species labels (see Table 1 and Table 2 for names corresponding to abbreviations) represent the centroids of their scores.

Some of the variability in NMDS2 and NMDS3 appears to be influenced by temperature anomalies in both assemblages (Figure 47). Much of the variability in NMDS2 around its seasonal mean occurred in August-December for both assemblages, during which unusually warm years were strongly differentiated from cooler years. Differentiation between warmer and cooler years in January-February along NMDS2 was stronger within the resolved assemblage than compared to the unresolved assemblage. Along NMDS3, differentiation between warm and cool years occurred in January-April within the unresolved assemblage. No differentiation between warmer and cooler years was apparent throughout the year (May-December) along NMDS3 within the resolved assemblage.

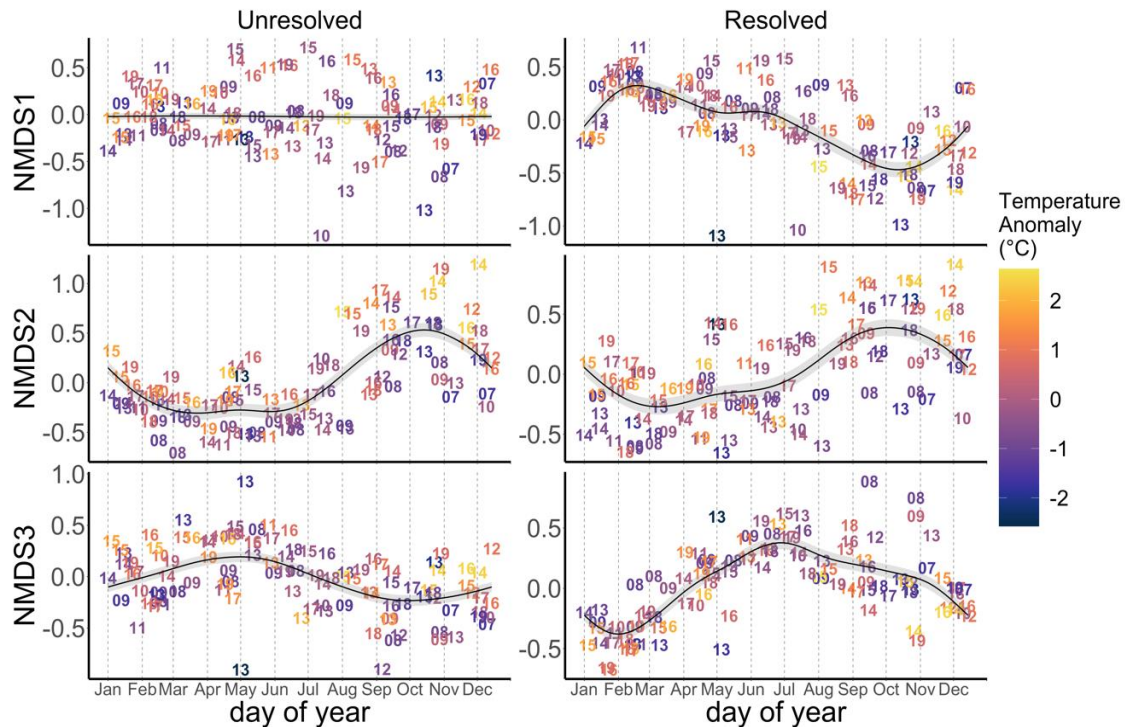


Figure 47. Intra-annual cycle of mean NMDS axis scores (y-axis) performed on common taxa within the unresolved (left-hand columns; *Sebastes* spp. larvae in aggregate) and resolved (right-hand columns; *Sebastes* spp. larvae resolved to species) larval assemblages by day of year (x-axis). Panels from top to bottom: NMDS1, NMDS2, and NMDS3. Black line (\pm SE in gray) represents a generalized additive model fit to NMDS scores. Symbol number correspond to the observation year. Symbol color corresponds to a temperature anomaly from a seasonal climatology (see methods for calculation of anomaly product).

Analysis of seasonally corrected residuals captures similar interannual trends in both unresolved and resolved assemblages along NMDS1 and NMDS2 (Figure 48).

Although no distinct interannual patterns are apparent along NMDS1, both the unresolved and resolved assemblages appear to shift in assemblage structure along NMDS2 and NMDS3 in concert with the late 2014-16 MHW.

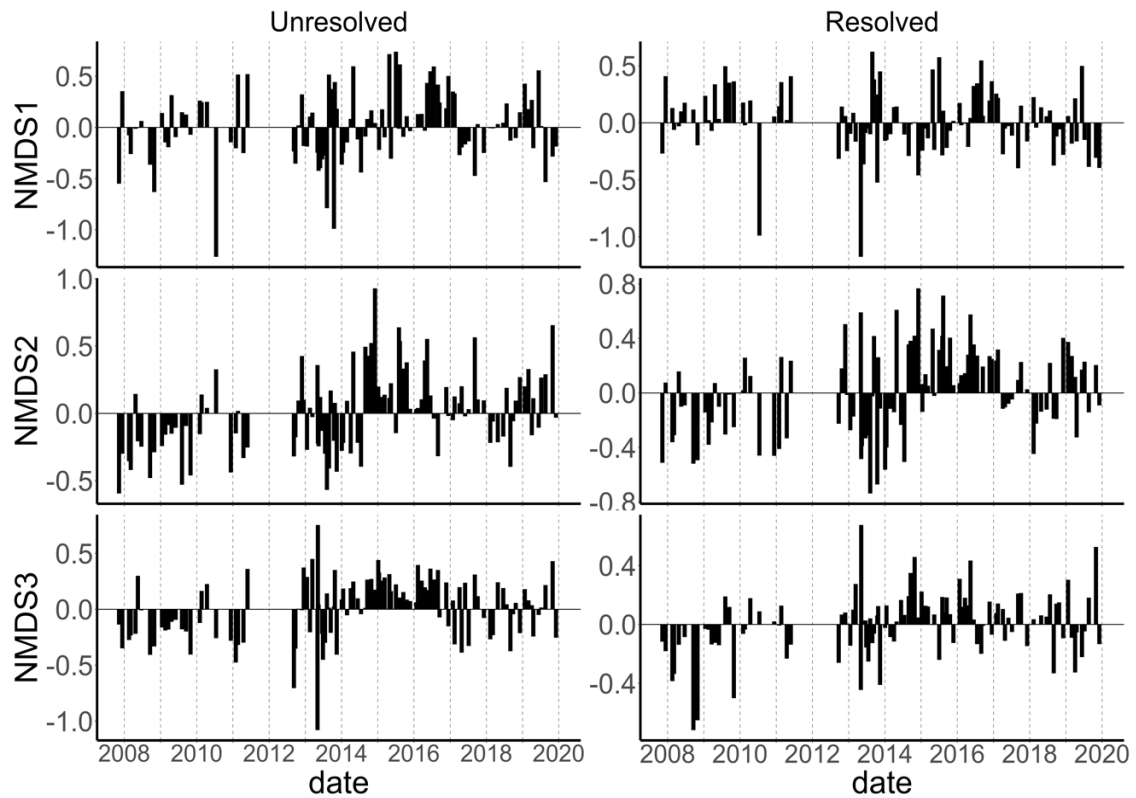


Figure 48. Time series of mean residuals from NMDS performed on common taxa within the unresolved (left-hand columns; *Sebastes* spp. larvae in aggregate) and resolved (right-hand columns; *Sebastes* spp. larvae resolved to species) larval assemblages. From top to bottom: NMDS1, NMDS2, and NMDS3 axis score residuals (y-axis) by cruise date (x-axis). See methods for description of residual product.

Species richness and Shannon-Weiner diversity contrasts

Seasonal patterns in Shannon-Weiner diversity were similar across both assemblages (Figure 49). Resolving rockfishes did not result in substantial differences in seasonal patterns in species richness, however richness peaked in March within the unresolved assemblage and in February within the resolved assemblage. Across both assemblages, species richness in January-April was exceptionally high during warmer than average years and low during cooler years. In January, this pattern was stronger within the resolved assemblage.

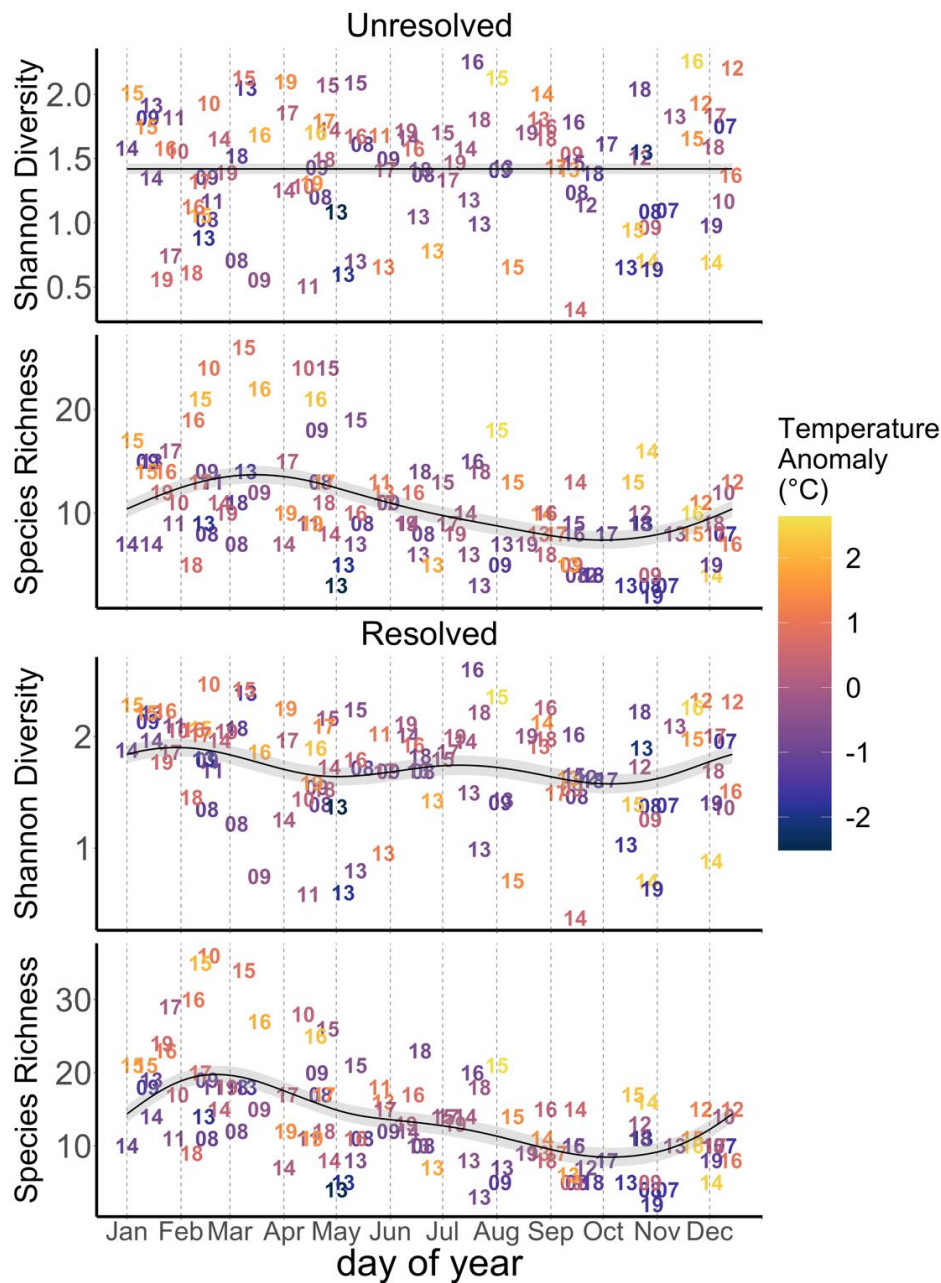


Figure 49. Intra-annual variability in Shannon-Wiener diversity (top panels; y-axis) and species richness (bottom panels; y-axis) within the unresolved (left-hand columns; *Sebastes* spp. larvae in aggregate) and resolved (right-hand columns; *Sebastes* spp. larvae resolved to species) larval assemblages by day of year (x-axis). Black line (\pm SE in gray) represents a generalized additive model fit to each biodiversity index. Symbol number correspond to the observation year. Symbol color corresponds to a temperature anomaly from a seasonal climatology (see methods for calculation of anomaly product).

Inter-annual trends in Shannon-Weiner diversity did not exhibit substantial differences between the unresolved and resolved assemblages (Figure 50). However, analysis of species richness within the resolved assemblage resulted in sharp increases in early-2017, mid-2018, and early-2019, which was not detected within the unresolved assemblage. Augmentation of rockfishes detected the largest recorded species richness over the time series in February 2010, whereas species richness within the unresolved assemblage peaked in March 2015.

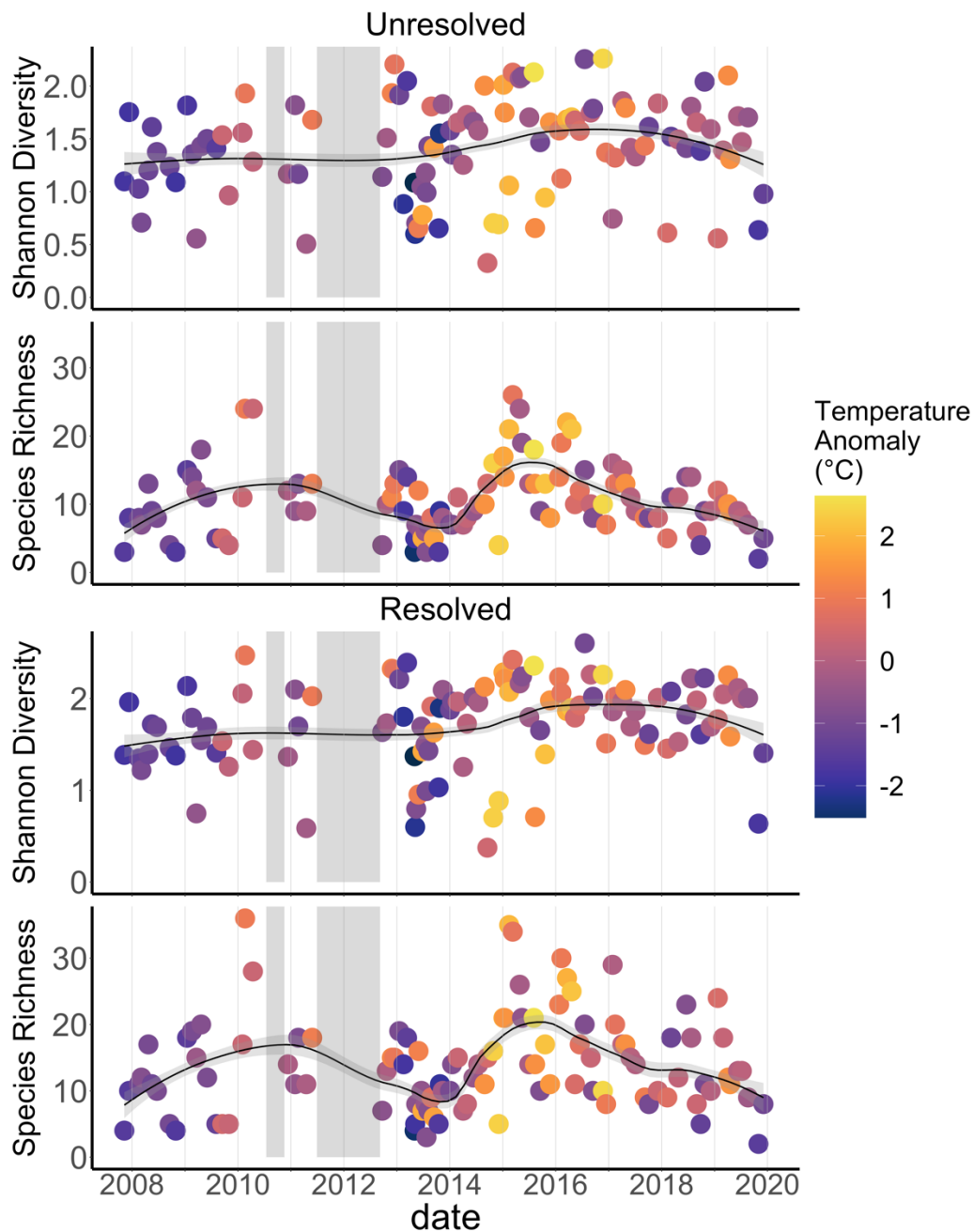


Figure 50. Inter-annual variability in Shannon-Weiner diversity (top panels; y-axis) and species richness (bottom panels; y-axis) within the unresolved (left-hand columns; *Sebastes* spp. larvae in aggregate) and resolved (right-hand columns; *Sebastes* spp. larvae resolved to species) larval assemblages by cruise date (x-axis). Black line (\pm SE in gray) represents a loess smooth (tuned to capture interannual trends) fit to observations. Symbol color corresponds to a temperature anomaly from a seasonal climatology (see methods for calculation of anomaly product). Gray bars indicate extended observation gaps.

Pairwise regression: assemblage-temperature correlations

Comparisons of results of pairwise regression between the unresolved and resolved assemblage did not result in strong differences in the relationship between a temperature anomaly and indices of biodiversity (species richness and Shannon-Weiner diversity) and assemblage structure (NMDS). The most distinguished result that emerged from this analysis is a slightly stronger positive relationship between species richness and a temperature anomaly in August-March within the unresolved assemblage (unresolved: $R^2 = 0.27, p < 0.001$; resolved: $R^2 = 0.23, p < 0.001$; Figure 51). Similar results between the two assemblages emerged from pairwise analysis of NMDS with a temperature anomaly (Figure 52). The only contrasting results between the two assemblages was a stronger positive relationship within the unresolved assemblage between NMDS2 and a temperature anomaly during all months (unresolved: $R^2 = 0.24, p < 0.001$; resolved: $R^2 = 0.18, p < 0.001$).

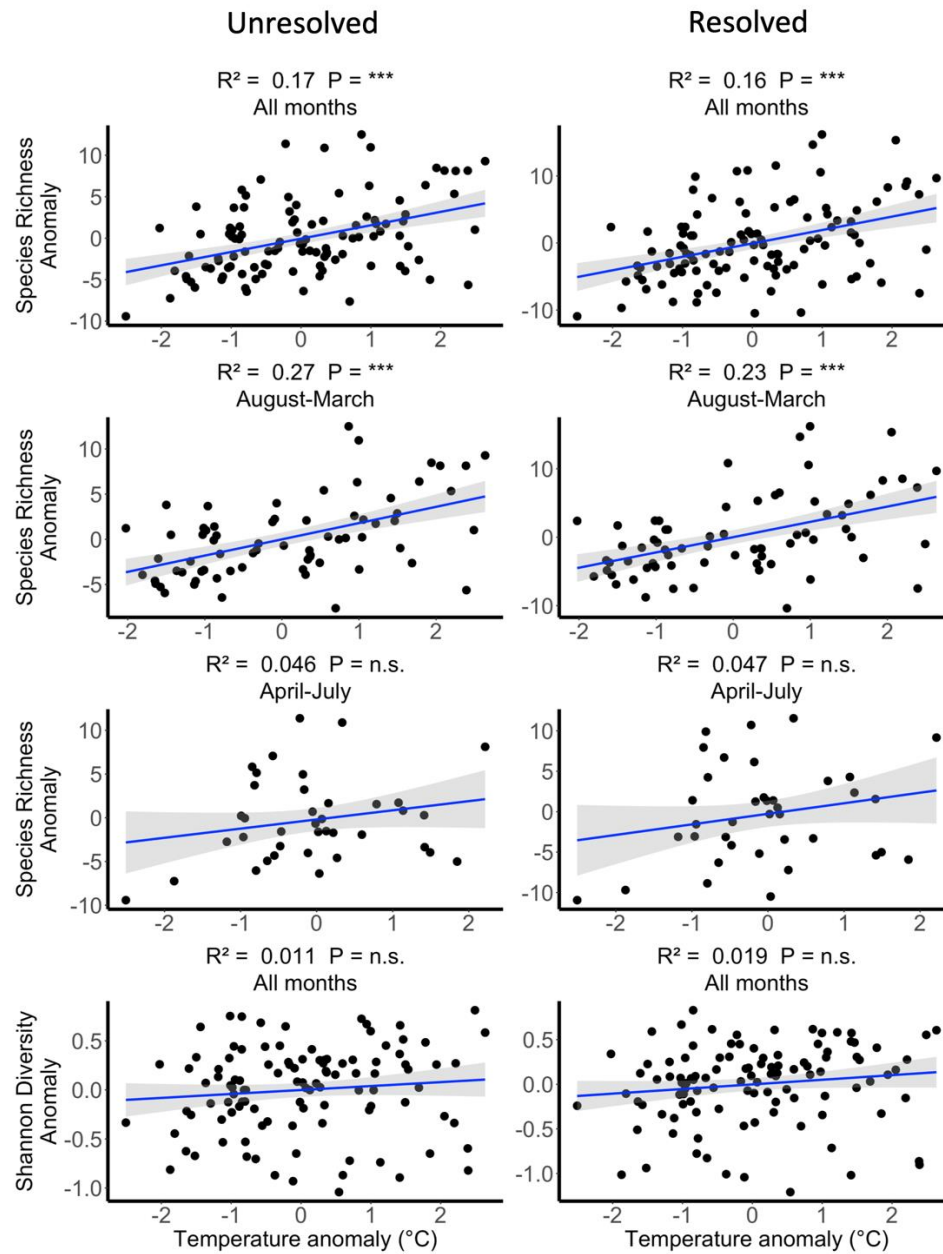


Figure 51. Fitted lines (blue) and 95% confidence intervals (shaded gray) resulting from pairwise regression for the relationship between a seasonally corrected temperature anomaly and species richness anomaly and Shannon-Weiner diversity anomaly within the unresolved (left-hand columns; *Sebastes* spp. larvae in aggregate) and resolved (right-hand columns; *Sebastes* spp. larvae resolved to species) larval assemblages. Each biodiversity index was analyzed using all available data (all months) and by different seasons (August-March and April-July). The results of each pairwise linear model are indicated by the coefficient of determination (R^2) and the significance of the temperature anomaly term (n.s. = $p > 0.05$, * = $p < 0.05$, ** = $p < 0.01$, *** = $p < 0.001$).

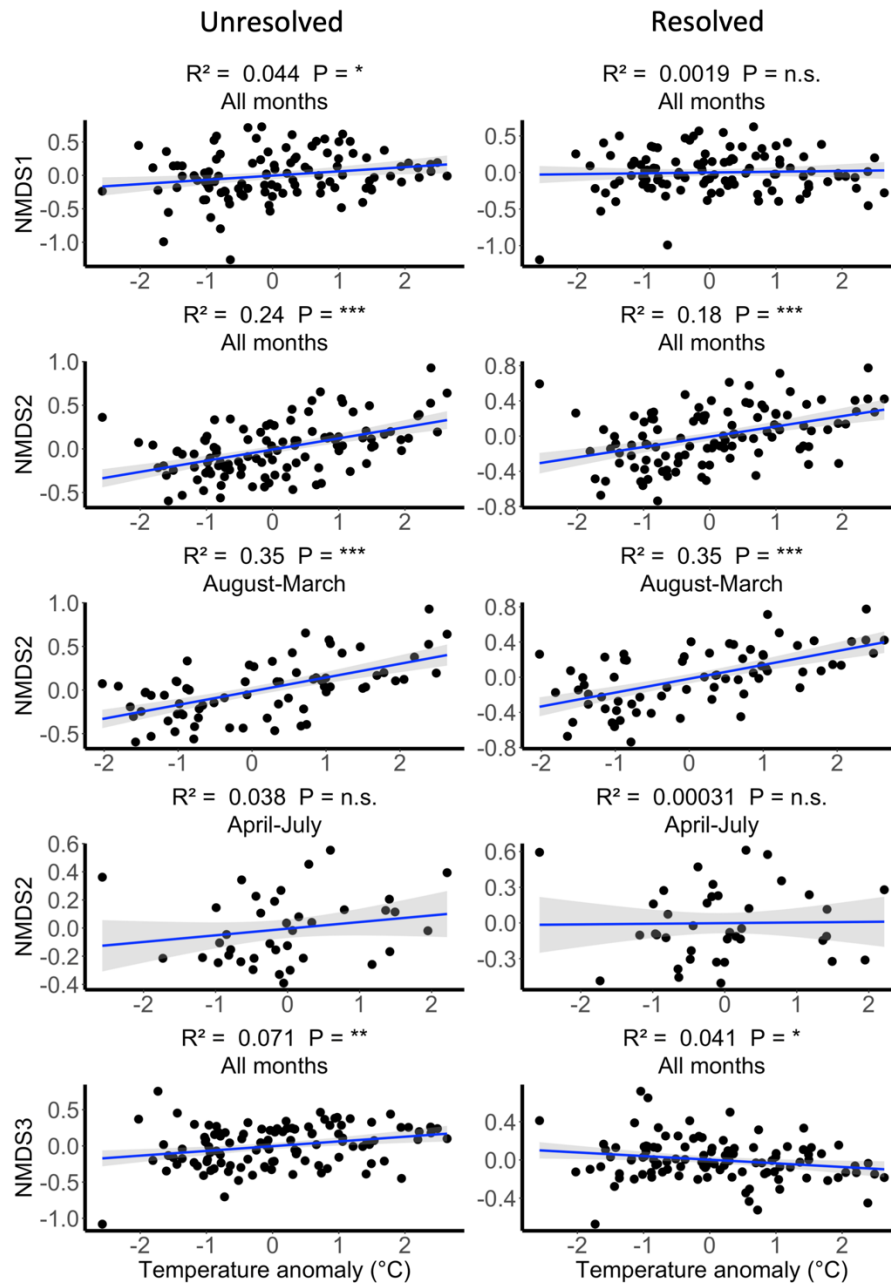


Figure 52. Fitted lines (blue) and 95% confidence intervals (shaded gray) resulting from pairwise regression for the relationship between a seasonally corrected temperature anomaly and seasonally corrected residuals from each NMDS axis within the unresolved (left-hand columns; *Sebastes* spp. larvae in aggregate) and resolved (right-hand columns; *Sebastes* spp. larvae resolved to species) larval assemblages. Each biodiversity index was analyzed using all available data (all months) and by different seasons (August-March and April-July). The results of each pairwise linear model are indicated by the coefficient of determination (R^2) and the significance of the temperature anomaly term (n.s. = $p > 0.05$, * = $p < 0.05$, ** = $p < 0.01$, *** = $p < 0.001$).

DISCUSSION

This study analyzed a 12-year time series (late 2007 through 2019) of ichthyoplankton samples collected along a cross-shelf transect off northern California to characterize variability in assemblage structure in the context of seasonal and basin-scale changes in oceanographic conditions. This work lays the foundation for extending the application of ichthyoplankton as ecosystem indicators to the region of the CCE off northern California (Brodeur et al. 2008, Daly et al. 2013, Auth et al. 2018) and demonstrates the sensitivity of this region to climate forcing (Di Lorenzo et al. 2013, Sydeman et al. 2013, Di Lorenzo and Mantua 2016).

These data enhance our understanding of larval fish dynamics within the CCS by filling a large spatial gap between surveys off southern California and off central Oregon. Moreover, this is the first study north of the Southern California Bight (SCB; Taylor et al. 2004, Thompson et al. 2016, 2017) to resolve larval rockfishes (*Sebastes* spp.) to species by applying genetic techniques to compliment the limited scope of visual identifications. This represents a substantial extension of the resolution of the larval fish assemblage, as rockfishes make up a major component of the assemblage and are a highly speciose group in the CCS (Moser et al. 2000, Love et al. 2002, Auth and Brodeur 2006, Brodeur et al. 2008, Thompson et al. 2016, 2017).

Caveats and Sampling Biases

As is the case with most surveys of pelagic ecosystems, our analysis and interpretations could be potentially confounded by several important caveats. These are reviewed below, and taken into account throughout the discussion as they affect interpretation or as they suggest hypotheses warranting further exploration.

The sampling scheme most effectively captures larvae that typically occupy the upper 100 m of the water column from the inner shelf to the upper slope. I expect the potential for larvae to occupy depths beyond 100 m to be of minor concern, as most taxa (particularly larvae of many key species of commercial and conservation interest) are rarely found below 100 meters (Auth and Brodeur 2006, Auth et al. 2007). Taxa whose larvae occur further offshore, occupy deeper habitats, or are part of distinct nearshore assemblages will be poorly represented in our collections (Marliave 1986, Taylor et al. 2004, Suntsov et al. 2012) and include a broad array of taxa that are likely to reflect synchronous patterns across the larval community as a whole (Koslow and Wright 2016).

Another potential source of bias may arise from stations that are poorly matched to patchy distributions of larvae, such as can arise from associations of larvae with hydrographic features (Bjorkstedt et al. 2002, Nishimoto and Washburn 2002). The data analyzed here are amenable to assessing such associations (Sadrozinski 2008, Bjorkstedt *unpublished results*; see Appendix E), but such fine-scale analysis goes beyond the scope of the present study. For the present study, I assume that any effects of small-scale

associations between larval fishes and oceanographic structure do not introduce systematic bias to our data and subsequent analysis.

A final source of bias stems from the practice of conducting cruises during calm conditions, which might bias our observations if rough conditions (or corresponding active upwelling or downwelling) affect the vertical or cross-shelf distributions of larvae at short time scales (Morgan et al. 2012, Morgan 2014). It is likely that several cruises were conducted during relaxation conditions, a period during which upwelling favorable winds subside (promoting safer sampling conditions) and poleward currents increase over the shelf and near surface temperatures increase (Send et al. 1987). If relaxation events promote onshore and poleward transport of larvae (Wing et al. 1995, Morgan et al. 2000) there might be some bias between our collections and what would be collected under sampling randomly with respect to ocean state. Given the consistency of cruise scheduling decisions, I expect that any such bias applies consistently across the data set.

Taxonomic Comparisons to Elsewhere in the CCE

Assemblage composition and sets of common taxa observed in this study is generally more consistent with observations off Oregon and Washington than off southern California (Auth and Brodeur 2006, Auth 2011, Thompson et al. 2014). This was not wholly surprising given what is known about adult distributions within the CCS, the closer proximity and similar structure of the TH-Line to transects within surveys off Oregon and Washington, and the presence of two biogeographic barriers (e.g., Cape Mendocino and Point Conception) between northern and southern California that

correspond to breaks in fish assemblages (Suntsov et al. 2012). Larvae of several taxa (e.g., *S. leucopsarus*, *Citharichthys* spp., and *Sebastes* spp. in aggregate) appear to be common and broadly distributed across the entire CCS. Although a large component of the assemblage in southern California is represented by *S. sagax* (Pacific sardine) and mesopelagic fishes that either spawn or are distributed in the southern California Current (Thompson et al. 2014), disparities between the CalCOFI sampling design and the TH-Line limit direct comparisons. Few differences existed in sets of dominant taxa between the TH-Line and surveys off Oregon, although some taxa with more northern distributions, such as *Ammodytes hexapterus* (Pacific sand lance) and *Isopsetta isolepis* (butter sole) appear to be abundant and sampled more frequently off Oregon and Washington (Brodeur et al. 2008).

Genetic resolution of the rockfishes further resolves biogeographic structure in the composition of larval fish assemblages of the CCE. The rockfish assemblage off northern California was mostly dominated by species that have a core distribution at higher latitudes or are found coastwide (e.g., *S. entomelas*, *S. crameri*, *S. saxicola*, *S. mystinus*/*S. deaconi* complex), and differed substantially from larval assemblages in the SCB, which are dominated by species with core distributions off southern California (Love et al. 2002, Williams and Ralston 2002, Thompson et al. 2016, 17).

Cross-shelf Patterns

The presence of distinct nearshore and offshore ichthyoplankton assemblages within the visual assemblage is consistent with previous findings in the northern

California Current (Auth and Brodeur. 2006, Sadrozinski 2008, Auth 2011). Shallow sampling stations are dominated by cottids, osmerids, liparids, and nearshore pleuronectids, reflecting the shallow coastal spawning area of adults (Miller and Lea 1972). In contrast, the rockfishes displayed limited cross-shelf variability, low abundance at nearshore stations, and consistent rarity or absence of inshore species (e.g., *S. nebulosus*, *S. auriculatus*, *S. rastrelliger*; Taylor et al. 2004, Johansson et al. 2018). As observed elsewhere in the CCS, the cross-shelf distribution of larvae for a given species generally reflects the distribution of adult habitat across the shelf (Auth and Brodeur 2006).

At the outset of this study, I expected to find higher concentrations of larvae of nearshore rockfishes and other species common as adults to coastal waters of northern California, such as species within the family Hexagrammidae. Many of the rockfishes absent from our collections include those within the subgenus *pteropodus*, a nearshore-demersal group that includes species such as *S. auriculatus* (brown rockfish) and *S. rastrelliger* (grass rockfish) that generally spawn during the spring transition when upwelling intensifies and offshore transport is strongest (Wyllie Echeverria 1987, Love et al. 2002). The rarity of such nearshore species has been reported in other larval surveys and attributed this to sampling stations being too far offshore to sample nearshore rocky reef and kelp habitat occupied by the adults (Taylor et al. 2004). I believe, in part, this pattern might also reflect species-specific adaptations within upwelling system, such as the ability of larvae to regulate their depth in stratified currents or interact with hydrographic features that enable larval retention inshore of the survey. For example,

several of these species enter the plankton and ultimately settle within the coastal boundary layer, a highly retentive zone characterized by slow alongshore currents that tend to harbor a distinct nearshore assemblage (Nickols et al. 2012, 2013). Other retentive zones can develop in regions that experience persistent upwelling (e.g., northern California), wherein circulation interacts with local topography such as headlands (e.g., Trinidad Head and Cape Mendocino) to form retentive zones on the lee side (Mace and Morgan 2006, Morgan and Fisher 2010, Morgan et al. 2011). This pattern is further consistent with the ability of larvae to regulate their depth in vertically sheared currents, which enables nearshore retention by remaining beneath strong near surface currents or only ascending at night when winds and currents have subsided (Morgan and Fisher 2010, Morgan et al. 2012, Miller and Morgan 2013, Morgan 2014). Moreover, many nearshore species (e.g., several genera of sculpin, greenlings, lingcod) have reduced larval durations and therefore reduced dispersal potential. These behaviors and strategies reduce transport, even in highly advective upwelling systems, and therefore I expect many nearshore species are retained inshore of the survey.

Shifts in species-specific cross-shelf distributions were consistent with the influence of cross-shelf transport (see Appendix E). These patterns were consistent with our observations that offshore taxa were displaced onshore during weak upwelling or downwelling and nearshore taxa were pushed offshore during strong upwelling. Some oceanic taxa however (e.g., *S. leucopsarus*) were generally more cosmopolitan in distribution, consistent with previous findings that larvae of mesopelagic taxa deep in the water column can be vertically displaced nearshore and entrained in onshore currents at

depth during strong upwelling (Smith et al. 1999), particularly in areas with a narrow continental shelf (Sabatès and Masò 1990, Bjorkstedt 1998, Sadrozinski 2008).

Seasonal Patterns

Abundances of most taxa and species richness were highest in winter and early spring, which is consistent with other findings in the northern California Current (Parrish et al. 1981, Brodeur et al. 2008, Auth et al. 2011, Thompson et al. 2014). Seasonal structure in the larval rockfish assemblage was similar to that observed for the visual assemblage, with distinct peaks and sets of species present as larvae during winter through early spring (January through April) and during late spring through summer (May through July). Diversity and species richness within the rockfishes was highest in January and February, corroborating previous findings that the majority of rockfishes spawn in winter (Wyllie-Echevarria 1987). Low overall abundance and species richness during late summer and fall (August-December) in both the visual larval assemblage and the larval rockfish assemblage is consistent with previous findings in the CCS (Auth 2011, Brodeur et al. 2008, Thompson et al. 2014).

Such seasonal patterns are hypothesized to reflect stark differentiation among life histories that time spawning to the spring transition as an evolutionary strategy to maximize the likelihood of strong overlap with productive conditions, or forgo predictably reliable access to these conditions in order to reduce losses due to offshore transport (Cushing 1975, Parrish et al. 1981). However, these tradeoffs can be offset by larval behavior or maternal effects. The ability of larvae to control their vertical position

in the water column can reduce the effects of cross-shelf transport, while taking advantage of high productivity during the spring transition (Morgan 2014). Moreover, structure generated during the upwelling season, such as fronts and eddies, can retain and accumulate larvae and in turn help larvae avoid displacement into unfavorable habitat and close life cycle processes (Bjorkstedt et al. 2002, Nishimoto and Washburn 2002, Woodson et al. 2012, Morgan 2014). Some winter spawning rockfishes produce small and weak swimming larvae with enhanced energy reserves when productivity is low and offshore transport in the CCS is generally onshore, whereas spring spawners substantially reduce available energy reserves during the larval stage but produce large and strong swimming larvae when productivity is high and transport offshore is typically strongest (Fisher et al. 2007).

Several oceanic taxa (e.g., *P. crockeri* and *T. crenularis*) were observed to be present year-round with peaks between late summer and early winter. These taxa are associated with offshore waters that move closer to the coast when upwelling and offshore transport is weakest, reflecting seasonal oceanographic processes that affect availability of larvae to our sampling methods more so than seasonal variability in reproductive output or differentiation among life history strategies (Thompson et al. 2012).

Responses of Ichthyoplankton to Climate Variability: Patterns and Mechanisms

Analysis of the ichthyoplankton assemblage off northern California suggests a strong effect of climate forcing on assemblage composition and species-specific patterns

in abundance. The effect of climate variability was most apparent during the late 2014-16 MHW, during which numerous rare taxa were collected, common taxa were recorded at their highest densities, and several taxa with cool water affinities declined sharply or disappeared from our collections. Recall that this event is comprised of two phases (the warm ‘blob’ and the 2015-16 El Niño), which are distinct from one another with respect to physical dynamics. During the warm ‘blob’ phase in late 2014-15, anomalous onshore transport of warm offshore waters impinged on coastal areas and was followed by a brief upwelling season in mid-2015 (Chao et al. 2017), whereas the 2015-16 El Niño was characterized by reduced upwelling and poleward advection of warm waters from the south (Jacox et al. 2016, Chao et al. 2017). Changes in the larval fish assemblage are consistent with these patterns, specifically in the source of new (or newly abundant) taxa associated with each phase of the MHW. I examine the responses of the ichthyoplankton assemblage during each of these events separately.

Several non-exclusive mechanisms are likely responsible for the appearances of new taxa and the variations in abundance among species during both phases of the MHW. These mechanisms are likely related to anomalous currents that can affect the distribution of passively drifting larvae, the ability of fish to change their distribution in response to elevated temperatures, or changes in local processes that influence reproduction. These mechanisms are discussed in further detail below.

Late 2014-15 warm ‘blob’ impacts

In late 2014-15, unusual larval occurrences coincided with the arrival of the warm ‘blob’ in coastal waters. The most apparent changes during this phase were the presence

of rare oceanic and far-offshore species' larvae (e.g., *Cyclothone* spp., *I. lockingtoni*, and *E. bathybius*). Moreover, new (*Genyonemus lineatus*) and common (*Citharichthys* spp.) taxa with coastal affinities were collected in unusually high abundance in late 2014, following some of the highest recorded temperature anomalies in the CCE in late 2013-14 (Gentemann et al. 2017).

Changes in cross-shelf transport are, I believe, the primary cause for the changes in abundance among taxa and the appearance of several rare oceanic taxa during this time. It is clear that anomalous onshore advection associated with reduced upwelling during the warm 'blob' phase of the MHW were responsible for the sudden appearance of taxa that are distributed far-offshore in oceanic waters. The persistent occurrence of *I. lockingtoni* (medusafish) throughout the warm 'blob' and *E. bathybius* (deepsea sole) in early 2015 are indicators of anomalous onshore transport (Auth et al. 2015). This hypothesis is consistent with advection of warm water copepods from offshore sources and other zooplankton into coastal areas throughout the MHW (Hooff and Peterson 2006, Keister et al. 2011, Peterson et al. 2017, Robertson and Bjorkstedt 2020). Anomalous onshore transport also reduced the potential for offshore dispersion for many coastal species during the MHW, leading to the cosmopolitan distribution and increased abundance at nearshore stations of species that are typically restricted to offshore stations (e.g., *Citharichthys* spp., *L. exilis*, *S. entomelas*, and *B. ochotensis*; see Appendix E).

Some taxa did not always conform to patterns consistent with simple hypotheses linked to onshore transport of warm water into the region sampled by the TH-line in late 2014-15. Some of these patterns might reflect responses to weaker elements of the

climate forcing signal, or might be linked to changes in population productivity or distribution in response to anomalous warming. For example, the first recorded appearance of larval *G. lineatus* (white croaker) in September and October 2014 in advance of strong onshore or poleward transport suggests a northward expansion of the stock in response to elevated SST anomalies first observed in late 2013-14 (Bond et al. 2015, Gentemann et al. 2017). This hypothesis is consistent with generally few observations of adult white croaker north of San Francisco (CDFW 2013), while no records of their larvae exist this far north. Moreover, shifts in spawning stocks of *Doryteuthis opalescens* (market squid) to northern California in 2014 (Van Noord and Dorval 2017, Zander and Bjorkstedt unpublished data) and Alaska in 2015 (Miller 2015), well north of their normal range, corroborates the influence of warm ‘blob’ waters on species typically restricted to coastal waters off southern California.

2015-16 El Niño impacts

In 2015 and 2016, following the warm ‘blob’, several new (or more abundant) taxa appeared with the propagation of warm waters from the south associated with the development of the 2015-16 El Niño. Although several oceanic species continued to occur in our collections during the 2015-16 El Niño, presumably as a consequence of reduced upwelling, taxa observed during this time were predominantly coastal species with core distributions off central or southern California (e.g., *S. jordani*, *M. productus*, *S. sagax*, *T. symmetricus*). Appearances (or increased abundance) of these southern species during strong poleward advection of warm waters suggest some of the source of change within the ichthyoplankton assemblage was the result of alongshore rather than

cross-shelf shifts. This mechanism suggests that ichthyoplankton were either advected northward (Sanford et al. 2019) or adults responded by shifting poleward to spawn, a common response amongst marine fishes to warming events in the CCS (Lea and Rosenblatt 2000, Walker et al. 2020).

Several shared life history traits can provide support for the hypothesis that poleward shifts in the spawning distributions facilitated the unusual larval occurrences (or high abundances) during the 2015-16 El Niño. The appearance of several taxa along the TH-line that are generally restricted to or spawn off southern California is consistent with documented poleward shifts in distributions of numerous fish species in the CCS during the 2015-16 El Niño (Cavole et al. 2016, Walker et al. 2020). This hypothesis draws further support from observations that many of these species are pelagic or mid-water schooling fishes (e.g., Pacific hake, Pacific sardine, shortbelly rockfish, chilipepper rockfish) that are less attached to fixed habitats (e.g., reefs) and more likely to shift distributions as the CCE experienced warm water anomalies (Manderson et al. 2011). The presence of larvae of Pacific jack mackerel (2015) and Pacific mackerel (2016) along the Trinidad Head Line and off coastal Oregon are indicators of poleward spawning shifts (Auth et al. 2018).

Moreover, the larvae of most of these species are captured at a relatively young age and have short pelagic larval durations, thus hypotheses built solely on poleward advection of larvae have limited or no support. For example, if we assume that preflexion larvae are < 5-20 days old (Hitchman et al. 2012, Thompson et al. 2016) and an average poleward current of 10 cm/s (per observations during the strong 1997-98 El Niño; Kosro

2002), potential sources of larvae that could have been carried in to our sampling region are limited to areas just south of Cape Mendocino. Larvae could not have been carried over distances exceeding 200 km over a 10-20 day early larval period. This is consistent with the hypothesis that a larger part of the variability in the assemblage during the 2015-16 El Niño was driven by the poleward movement of adults and builds on previous work that ichthyoplankton can be used as indicators or proxies for the distribution of the adult spawning stock (Ralston et al. 2003, Ralston and Howard 2010).

Anomalous alongshore advection is, I believe, a plausible cause of unusual ichthyoplankton occurrences and, in some cases, high abundances of several taxa. Transport exerts a strong influence on plankton distributions, and for taxa with an extended pelagic larval duration (PLD) the potential for extensive transport increases. This is consistent with generally strong associations between water mass types and distinct zooplankton assemblages or indicator taxa (Hooff and Peterson 2006, Keister et al. 2005, 2011). Several warm water krill and copepod species that serve as indicators of poleward advection were present in coastal waters off northern California and elsewhere in the northern California Current during the 2015-16 El Niño (Peterson et al. 2017, Robertson and Bjorkstedt 2020). This hypothesis draws further support from studies documenting the sudden appearance of sessile invertebrates and *Pleuroncodes planipes* (pelagic red crabs) with an extended PLD off northern California associated with the 2015-16 El Niño that are typically restricted to subtropical areas (Sanford et al. 2019, Cimino et al. 2021). Similarly, Cowen (1985) hypothesized that unusual recruitment events of California Sheephead (*Semicossphus pulcher*) in Monterey, well north of their

normal range, was the result of anomalous poleward advection of eggs and larvae from sources south of Point Conception during the very strong 1983 El Niño.

Comparisons to the late 2009-10 and late 2018-19 El Niño

Similar events and responses in the ichthyoplankton assemblage along the TH-line were observed during the late 2009-10 and 2018-19 El Niño events. Consistent throughout these events is a general increase in species richness, higher abundance and representation of coastal taxa with southern distributions, and increased diversity, species richness, and abundance among the rockfishes. However, comparisons between these events suggests some differences. For example, the late 2009-10 El Niño was characterized by high species richness and abundance of larvae distributed in oceanic or far-offshore waters, whereas species richness during the late 2018-19 event was low, including oceanic taxa, but had high representation and abundance of southern coastal species (e.g., *M. productus*, *E. mordax*, *S. sagax*, *S. jordani*), which mirrored the assemblage during the 2015-16 El Niño. Changes in the assemblage during the 2009-10 El Niño event are consistent with anomalously strong downwelling and onshore transport in the northern California Current in winter 2009-10 (Bjorkstedt et al. 2010), whereas poleward shifts in the spawning stock may have contributed significantly to the observed patterns in winter 2019. For example, adult *S. jordani* (shortbelly rockfish) were highly abundant off Oregon and Washington during the 2018-19 El Niño where they historically do not occur in large numbers (Thompson et al. 2019).

Other patterns and mechanisms

Changes in reproductive output are not likely to have been a major driver of changes in larval fish assemblages, yet changes in condition or productivity are expected to occur in response to shifts in the ecosystem. Despite reduced energetics for reproduction in marine fishes during El Niño events (Harvey 2005), larval abundances of most taxa in this study increased markedly during the late 2014-16 MHW. However, the osmerids (e.g., smelts) declined at the onset of elevated SST anomalies in late 2013. Osmerid larvae are observed to decline during warm water events in the northern California Current, typically attributed to reduced offshore dispersion from nearshore spawning habitat and increased mortality due to reduced food availability (Richardson and Pearcy 1977, Brodeur et al. 1985, Brodeur et al. 2008). However, invoking cross-shelf transport and reduced food availability as sole drivers implies the assumption that adults were consistently present and successfully reproducing. Population trends and research suggests that some osmerids (e.g., surf smelt) have been in decline in the northern California Current since the 1980s and warming conditions may not be favorable to survival or energetics for reproduction (Russell 2020).

It is not clear why *Sebastes melanops* (black rockfish) and *Sebastes flavidus* (yellowtail rockfish), two coastal winter spawning species, were generally only present in the collection during warm water events (e.g., 2010, 2015-17, and 2019). At the onset of this study, I expected these species to occur consistently throughout the time series given that the adults of each species are common to the shelf waters off northern California. During warm water events, I suspect that larvae of *S. melanops* and *S. flavidus* are carried

into the survey from highly productive spawning areas that lie just south of the TH-line, around or just south of Cape Mendocino. During non-warming years, larvae from local sources are likely being retained inshore of the survey through larval behavior or interactions with hydrographic structure (e.g., coastal boundary layer, upwelling fronts, lee side of headlands) that enable larval retention (Bjorkstedt et al. 2002, Mace and Morgan 2006, Morgan and Fisher 2010, Morgan et al. 2011 Nickols et al. 2012, 2013). Regardless of the exact mechanism, these patterns demonstrate the sensitivity of larvae to climate forcing and highlights the need to continue long term monitoring to resolve such obscure patterns.

Value of Genetic Identification for Resolving Assemblage Variability in Response to Climate Forcing

The aggregate response in abundance of *Sebastes* to climate variability (i.e., increased abundance during the MHW) corroborates patterns in other components of the visual assemblage. However, resolution of rockfish to species (or species complexes) illustrates how the aggregate response obscures important variability in how rockfishes respond to climate forcing. For example, the arrival of new species during the 2015-16 El Niño would have remained poorly resolved without the use of genetic techniques. Moreover, these results identified shifts in seasonal occurrence of *S. diploproa* (splitnose rockfish) and the WEVZ complex from typically only occurring in late spring and summer months to unusual occurrences in winter months during years strongly affected by climate forcing (see Appendix E). These data cannot resolve whether this pattern is

the result of a phenological shift, repeat broods (Lefebvre et al. 2018, Holder and Field 2019), or the appearance of a winter spawning species within the WEVZ complex not previously sampled. Regardless of the exact mechanism, the occurrence of larvae outside of their typical seasonal range corroborates shifts previously reported in ichthyoplankton throughout the CCS in response to climate forcing (Asch 2015, Auth et al. 2018).

This is yet another demonstration of the power of resolving the rockfishes and other cryptic species in larval surveys. These methods are relatively inexpensive and have revealed previously unknown diversity, spatial patterns, spawning habitat, and sensitivity to climate change within the genus *Sebastes* (Taylor et al. 2004, Thompson et al. 2017, 2017, Johansson et al. 2018). For this reason, genetic techniques combined with sampling of biological data should continue and become more common place in ichthyoplankton surveys.

Ecosystem Implications

Warm water events are expected to increase in frequency and intensity, against a continuing background warming trend driven by climate change (Frölicher et al. 2018; Oliver et al. 2018). This study indicates that such warm water events can cause sharp transitions in larval fish assemblages (and presumably adult populations) in the coastal waters off northern California. More generally, these results complement shifts in species distributions in response to climate forcing (Cavole et al. 2016, Walker et al. 2020). As marine fish species are expected to shift their distributions north in response to climate induced warming (Pinsky et al. 2013, Jacox et al. 2020), and if warming events such as

the 2014-16 MHW become more frequent under climate change, we should expect to see these assemblage changes more frequently, which may have unknown consequences for the species settling into coastal ecosystems off Northern California. Moreover, these shifts have resulted in relatively low values of the Index of Coastal Prey Biomass used along the NH line (Daly et al. 2013), which suggests poor prey conditions for piscivorous juvenile salmon since 2012, particularly during the late 2014-16 MHW (Weber et al. 2021). This study confirms the value of larval fish surveys as a source of information regarding these changes and as indicators of ecosystem state (Brodeur et al. 2008, Hsieh et al. 2009, Asch 2015, Auth et al. 2018, Nielson et al. 2020).

Motivations for Future Work

This dataset provides a strong foundation for developing and exploring hypotheses regarding what drives ichthyoplankton assemblage variability in the context of climate forcing. In particular this study has drawn attention to developing accurate estimates of where and when adult fish populations spawn, the magnitude of larval displacement along the coast, and analysis of distributions relative to hydrographic structure. One way to enhance this data in the future is to provide both estimates of age of individual larvae and develop larval transport models in the study region. This would help elucidate questions relating to whether larvae captured in the study area are coming from other areas along the coast, the extent to which larvae are transported, and if alongshore transport of larvae is intensified during strong climate events when geographic barriers such as Cape Mendocino break down.

At the onset of this study, I expected to find higher densities of nearshore rockfishes from the subgenus *Pteropodus* (e.g., brown rockfish, china rockfish, grass rockfish, etc.). Focused studies should be developed to sample larval fish inshore of the TH-line to characterize nearshore assemblages, specifically with respect to the question of whether larvae of nearshore species remain close to the coast, and to determine whether these assemblages respond in similar ways to the ichthyoplankton assemblage analyzed in this study.

REFERENCES

- Allen, L.G., D.J. Pondella and M.H. Horn. 2006. The ecology of marine fishes: California and adjacent waters. University of California Press, Berkeley.
- Amaya, D., A.J. Miller, S. Xie and Y. Kosaka. 2020. Physical drivers of the summer 2019 North Pacific marine heatwave. *Nature Communications*, 11(1), 1–9.
- Asch, R.G. 2015. Climate change and decadal shifts in the phenology of larval fishes in the California Current ecosystem, *Proc Natl Acad Sci*.
- Austin, J. A. and S. J. Lentz. 2002. The inner shelf response to wind-driven upwelling and downwelling. *Journal of Physical Oceanography* 32: 2171–2193.
- Auth, T.D. and R. D. Brodeur. 2006. Distribution and community structure of ichthyoplankton off the Oregon coast, USA, in 2000 and 2002. *Mar. Ecol. Prog. Ser.* 319:199–213.
- Auth, T. D., R. D. Brodeur and K. M. Fisher. 2007. Diel variation in vertical distribution of an offshore ichthyoplankton community off the Oregon coast. *Fishery Bulletin*, vol. 105, no. 3, pp. 313– 326.
- Auth, T.D. 2008. Distribution and community structure of ichthyoplankton from the northern and central California Current in May 2004–06. *Fish Oceanogr* 17:316–331.
- Auth, T.D. 2011. Analysis of the spring–fall epipelagic ichthyoplankton community in the northern California Current in 2004–2009 and its relation to environmental factors. *Calif. Coop. Ocean. Fish. Invest. Rep.* 52, 148–166.
- Auth, T. D., R. D. Brodeur, H.L. Soulen, L. Ciannelli and W. T. Peterson. 2011. The response of fish larvae to decadal changes in environmental forcing factors off the Oregon coast. *Fisheries Oceanography*, 20, 314–328.
- Auth, T. D., R. D. Brodeur and J. O. Peterson. 2015. Anomalous ichthyoplankton distributions and concentrations in the Northern California Current during the 2010 El Niño and La Niña events. *Progress in Oceanography*, 137, 103–120.
- Auth, T., E. Daly, R. Brodeur and J. Fisher. 2018. Phenological and distributional shifts in ichthyoplankton associated with recent warming in the northeast Pacific Ocean. *Global Change Biology*, 24, 1–14.

- Barth, J. A., S. D. Pierce and R. L. Smith. 2000. A separating coastal upwelling jet at Cape Blanco, Oregon, and its connection to the California Current System, *Deep Sea Res., Part II*, 47, 783 – 810.
- Bizzarro, J.J., et al. 2020. Genetic identification of blue rockfish (*Sebastes mystinus*) and deacon rockfish (*S. diaconus*) to enable life history analyses for stock assessment. *Fishery Bulletin*, vol. 118, no. 1, 2020, p. 37.
- Bjorkstedt, E. P. 1998. Remote sensing and ichthyoplankton ecology of coastal upwelling fronts off central California. Doctoral dissertation. Department of Biological Sciences, Stanford University, Stanford, California.
- Bjorkstedt, E. P., L. K. Rosenfeld, B.A. Grantham, Y. Shkedy and J. Roughgarden. 2002. Distributions of larval rockfishes *Sebastes* spp. across nearshore fronts in a coastal upwelling region. *Marine Ecology Progress Series*, 242 (November), 215–228.
- Bjorkstedt, E. P., R. Goericke, S. McClatchie, E. Weber, W. Watson, N. Lo, et al. 2010. State of the California current 2009-2010: Regional variation persists through transition from la Niña to el Niño (and back?). *California Cooperative Oceanic Fisheries Investigations Reports*, 51, 39-69.
- Bjorkstedt, E. and W. Peterson. 2015. Zooplankton data from high-frequency coastal transects: enriching the contributions of ocean observing systems to ecosystem-based management in the northern California Current. In: Liu, Y., Kerkerling, H., Weisberg, R.H. (eds.). *Coastal Ocean Observing Systems: Advances and Syntheses*. Elsevier, pp. 199–142.
- Bond, N. A., M. F. Cronin, H. Freeland and N. Mantua. 2015. Causes and impacts of the 2014 warm anomaly in the NE Pacific, *Geophys. Res. Lett.*, 42, 3414–3420.
- Brinton, E. and A. Townsend. 2003. Decadal variability in abundances of the dominant euphausiid species in southern sectors of the California Current. *Deep-Sea Research II* 50, 2449–2472.
- Brodeur, R.D., D. M. Gadomski, W. G. Pearcy, H. P. Batchelder and C. B. Miller. 1985. Abundance and distribution of ichthyoplankton in the upwelling zone off Oregon during anomalous El Niño conditions. *Est. Coast. Shelf Sci.* 21:365– 378.
- Brodeur, R. D., W. T. Peterson, T. D. Auth, H. L. Soulen, M. M. Parnel, and A. A. Emerson. 2008. Abundance and diversity of coastal fish larvae as indicators of recent changes in ocean and climate conditions in the Oregon upwelling zone. *Marine Ecology Progress Series* 366:187–202.

- California Department of Fish and Wildlife. 2013. California Marine Sportfish Identification: Croakers. Web.
- Cavole, L. M., et al. 2016. Biological impacts of the 2013– 2015 warm-water anomaly in the Northeast Pacific: Winners, losers, and the future. *Oceanography* 29: 273–285.
- Chhak, K. and E. Di Lorenzo. 2007. Decadal variations in the California current upwelling cells. *Geophysical Research Letters*. 34(14): L14604.
- Chao, Y., J. D. Farrara, E. Bjorkstedt, F. Chai, F Chavez, D. L. Rudnick, W. Enright, J. L. Fisher, W. T. Peterson, G. F. Welch and C. O. Davis. 2017. The origins of the anomalous warming in the California coastal ocean and San Francisco Bay during 2014–2016. *J. Geophys. Res. Oceans* 122 (9), 7537–7557.
- Chavez, F. P., J. T. Pennington, C. G. Castro, J. P. Ryan, R. P. Michisaki, B. Schlining, ... and C. A. Collins. 2002. Biological and chemical consequences of the 1997–1998 El Niño in central California waters. *Progress in Oceanography*, 54(1-4), 205-232.
- Checkley, D. M. 1982. Selective feeding by Atlantic herring (*Clupea harengus*) larvae on zooplankton in natural assemblages. *Mar Ecol Prog Ser* 9:245–253.
- Checkley Jr., D. M and J. A. Barth. 2009. Patterns and processes in the California current system. *Progress in Oceanography* 83, 49–64.
- Chelton, D.B., Bernal, P.A., McGowan, J.A. (1982) Large-scale interannual physical and biological interaction in the California Current. *J. Mar. Res.* 40:1095–1123.
- Chenillat, F., P. Rivière, X. Capet, Di Lorenzo and B. Blanke. 2012. North Pacific Gyre Oscillation modulates seasonal timing and ecosystem functioning in the California Current upwelling system. *Geophysical Research Letters*, 39(1).
- Cimino, M. A., M. G. Jacox, S. J. Bograd, S. Brodie, G. Carroll, E. L. Hazen, B. E. Lavaniegos, M. M. Morales, E. Satterthwaite and R. R. Rykaczewski. 2021. Anomalous poleward advection facilitates episodic range expansions of pelagic red crabs in the eastern North Pacific. *Limnology and Oceanography*, 66(8), 3176-3189.
- Clarke, K.R. and R. M. Warwick. 2001. Change in marine communities: an approach to statistical analysis and interpretation. 2nd edn, PRIMER-E, Plymouth, UK.
- Cowen, R. K. 1985. Large scale pattern of recruitment by the labrid, *Semicossyphus pukher*: causes and implications. *J. Mar. Res.* 43:719-742.

- Cushing, D.H. 1975. Marine ecology and fisheries. Cambridge University Press, Cambridge.
- Daly, E. A., T. D. Auth, R. D. Brodeur and W. T. Peterson. 2013. Winter ichthyoplankton biomass as a predictor of early summer prey fields and survival of juvenile salmon in the northern California Current. *Marine Ecology Progress Series* 484:203–217.
- De Cáceres, M. and P. Legendre. 2012. Associations between species and groups of sites: indices and statistical inference. *Ecology*. 2009 Dec;90(12):3566-74.
- Di Lorenzo, E., et al. 2008. North Pacific Gyre Oscillation links ocean climate and ecosystem change, *Geophys. Res. Lett.*, 35, L08607.
- Di Lorenzo, E., V. Combes, J. E. Keister, P. T. Strub, A. C. Thomas, P. J. Franks, ... and W. T. Peterson. 2013. Synthesis of Pacific Ocean climate and ecosystem dynamics. *Oceanography*, 26(4), 68-81.
- Di Lorenzo, E. and N. Mantua. 2016. Multi-year persistence of the 2014/15 North Pacific marine heatwave, *Nat. Clim. Change*.
- Doney, S. C., et al. 2012. Climate change impacts on marine ecosystems. *Annu. Rev. Mar. Sci.* 4, 11–37.
- Doyle, M. J., K. L. Mier, M. S. Busby and R. D. Brodeur. 2002. Regional variation in springtime ichthyoplankton assemblages in the northwest Pacific. *Progress in Oceanography Special Issue* 53(2-4): 247-281.
- Fisher, R., S.M. Sogard and S.A. Berkeley. 2007. Trade-offs between size and energy reserves reflect alternative strategies for optimizing larval survival potential in rockfish. *Mar Ecol Prog Ser* 344:257–270.
- Flament, P. 2002. A state variable for characterizing water masses and their diffusive stability: spiciness. *Prog. Oceanogr.* **54**: 493–501.
- Frale, B. W., D. W. Wagman, T. N. Frierson, A. Aquilar and B. L. Sidlauskas. 2015. A new species of *Sebastes* (Scorpaeniformes: Sebastidae) from the northeastern Pacific, with a redescription of the blue rockfish, *S. mystinus* (Jordan and Gilbert, 1881). *Fish. Bull.* 113:355–377.
- Froese, R. and D. Pauly. 2010. A Global Information System on Fishes. Fishbase. <http://www.fishbase.org>.

- Frölicher, T.L., E. M. Fischer and N. Gruber. 2018. Marine heatwaves under global warming. *Nature* 560 (7718), 360.
- Fuiman, L. A. 2002. Special considerations of fish eggs and larvae. In *Fishery Science, The unique contributions of early life stages*. Edited by L.A. Fuiman and G.W. Robert. Blackwell Publishing. pp. 1–32.
- Garcia-Reyes, M. and J. L. Largier. 2012. Seasonality of coastal upwelling off central and northern California: New insights, including temporal and spatial variability. *Journal of Geophysical Research*.
- Gentemann, C. L., M. R. Fewings and M. García-Reyes. 2017. Satellite sea surface temperatures along the West Coast of the United States during the 2014–2016 northeast Pacific marine heat wave. *Geophysical Research Letters* 44(1):312–319.
- Hare, J.A. 2014. The future of fisheries oceanography lies in the pursuit of multiple hypotheses. *ICES Journal of Marine Science* 71:2,343–2,356.
- Harvey, C. J. 2005. Effects of El Niño events on energy demand and egg production of rockfish (Scorpaenidae: *Sebastes*): a bioenergetics approach. *Fish Bull* 103:71–83.
- Hebert, P. N., A. Cywinska, S. L. Ball and J. R. deWaard. 2003. Biological identifications through DNA barcodes. *Proc. R. Soc. Lond. B* 270, 313–322.
- Hickey, B. M. 1979. The California Current System— hypotheses and facts. *Prog Oceanogr* 8:191–279.
- Hickey, B. M. and N. S. Banas. 2009. Why is the north end of the California Current System so productive? *Oceanography*, 21(4), 90–107.
- Hitchman S. M., N. B. Reynolds and A. R. Thompson. 2012. Larvae define spawning habitat of bocaccio rockfish *Sebastes paucispinis* within and around a large southern California marine reserve. *Mar Ecol Prog Ser* 465:227–242.
- Hobday, A. J., E. Oliver, A. Sen Gupta, J. A. Benthuisen, M. T. Burrows, M. G. Donat, N. J. Holbrook, P. J. Moore, M. S. Thomsen, T. Wernberg, D. A. Smale. 2018. Categorizing and naming marine heatwaves. *Oceanography* 31 (2), 1–13.
- Holder, A. M. and J. C. Field. 2019. An exploration of factors that relate to the occurrence of multiple brooding in rockfishes (*Sebastes* spp.). *Fishery Bulletin*, 117(3), 180-189.

- Hooff, R.C. and W.T. Peterson. 2006. Copepod biodiversity as an indicator of changes in ocean and climate conditions of the northern California current ecosystem. *Limnol. Oceanogr.* 51 (6), 2607–2620.
- Houde, E. D. 1987. Fish early life dynamics and recruitment variability, *Am. Fish. Soc. Symp.*, 2, 17–29.
- Houde, E. D. 2002. Mortality. In *Fishery Science, The unique contributions of early life stages*. Edited by L.A. Fuiman and G.W. Robert. Blackwell Publishing. pp 64–87.
- Houde, E. D. 2008. Emerging from Hjort’s Shadow, *J. Northw. Atl. Fish. Sci.*, 41, 53–70.
- Hsieh C. H., C. Reiss, W. Watson, M. J. Allen et al. 2005. A comparison of long-term trends and variability in populations of larvae of exploited and unexploited fishes in the southern California region: a community approach. *Prog Oceanogr* 67:160–185.
- Hsieh, C. H., H. J. Kim, W. Watson, Di Lorenzo and G. Sugihara. 2009. Climate-driven changes in abundance and distribution of larvae of oceanic fishes in the southern California region. *Glob Change Biol* 15: 2137–2152.
- Huyer, A. 1983. Coastal upwelling in the California current system. *Prog. Oceanogr.* 112, 259–284.
- Jacox, M. G. and C. A. Edwards. 2011. Effects of stratification and shelf slope on nutrient supply in coastal upwelling regions, *J. Geophys. Res.*, 116, C03019.
- Jacox, M. G. and C. A. Edwards. 2012. Upwelling source depth in the presence of nearshore wind stress curl, *J. Geophys. Res.*, 117, C05008.
- Jacox, M. G., J. Fiechter, A. M. Moore and C. A. Edwards. 2015. ENSO and the California Current coastal upwelling response. *Journal of Geophysical Research: Oceans*, 120(3), 1691-1702.
- Jacox, M. G., E. L. Hazen, K. D. Zaba, D. L. Rudnick, C. A. Edwards, A. M. Moore, and S. J. Bograd. 2016. Impacts of the 2015–2016 El Niño on the California Current System: Early assessment and comparison to past events. *Geophys. Res. Lett.*
- Jacox, M.G., M.A. Alexander, N.J. Mantua, J.D.Scott, G. Hervieux, R.S. Webb and F.E. Werner, F.E. 2018a. Forcing of multiyear extreme ocean temperatures that impacted California current living marine resources in 2016. *Bull. Amer. Meteor. Soc.* 99 (1), S27–S33.

- Jacox, M.G., C.A. Edwards, E.L. Hazen and S.J. Bograd. 2018b. Coastal upwelling revisited: Ekman, Bakun, and improved upwelling indices for the U.S. west coast. *J. Geophys. Res.*
- Jacox, M. G., M.A. Alexander, S.J. Bograd and J.D. Scott. 2020. Thermal displacement by marine heatwaves. *Nature*, 584, 82–86.
- Johansson, M. L., M., N. C. Litz, R. D. Brodeur, T. A. Britt, C. A. Vanegas, J. R. Hyde, Banks and A. Michael. 2018. Seasonal distribution and environmental associations among late larval and juvenile rockfish (*Sebastes* spp.) off Oregon and Washington: new insights based on genetics. Oregon State University. *Fishery Bulletin*, vol. 116 no. 3-4, 2018, p.266.
- Keister, J.E., T. B. Johnson, C. A. Morgan and W. T. Peterson. 2005. Biological indicators of the timing and direction of warm-water advection during the 1997/1998 El Niño off the central Oregon coast, USA. *Mar. Ecol. Prog. Ser.* 295, 43–48.
- Keister, J. E., E. DiLorenzo, C. A. Morgan, V. Combes, and W. T. Peterson. 2011. Copepod species composition is linked to ocean transport in the northern California Current, *Global Change Biol.*, 17, 2498–2511.
- Koslow, A. J., R. Goericke and W. Watson. 2013. Fish assemblages in the southern California Current: Relationships with climate, 1951- 2008, *Fish. Oceanogr.*, 1–13.
- Koslow, J. A. and P. Davison. 2015. Productivity and biomass of fishes in the California Current large marine ecosystem: comparison of fishery-dependent and independent time series. *Environmental Development*, 17: 23–32.
- Koslow, J.A. and M. Wright. 2016. Ichthyoplankton sampling design to monitor marine fish populations and communities. *Mar. Policy* 68, 55–64.
- Koslow, J. A., H. McMonagle and W. Watson. 2017. Influence of climate on the biodiversity and community structure of fishes in the southern California Current. *Marine Ecology Progress Series*, 571, 193–206.
- Kosro, P. M. 2002. A poleward jet and an equatorward undercurrent observed off Oregon and northern California, during the 1997–98 El Niño. *Progress in Oceanography*, 54(1-4), 343-360.
- Kramer, D., M. J. Kalin, E. G. Stevens, J. R. Thrailkill and J. R. Zweifel. 1972. Collecting and processing data on fish eggs and larvae in the California Current region. NOAA Technical Report NMFS, Book CIRC-370.

- Laidig, T.E., K. M. Sakuma, and M. M. Nishimoto. 1996. Description of the pelagic larval and juvenile striptail rockfish, *Sebastes saxicola* (family Scorpaenidae), with an examination of larval growth. *Fish Bull* 94:289–299.
- Largier, J. L., B. A. Mangell, and C. D. Winant. 1993. Subtidal circulation over the Northern California Shelf, *J. Geophys. Res.*, 98(C10), 18,147– 18,179.
- Lea, R.N. and R.H. Rosenblatt. 2000. Observations on fishes associated with the 1997-98 El Niño off California Cal. Coop. Oceanic fish. Invest. Rep., 41, pp. 117-129.
- Lefebvre, L. S., S. G. Beyer, D. M. Stafford, N. S. Kashef, E. J. Dick, S. M. Sogard and J. C. Field. 2018. Double or nothing: Plasticity in reproductive output in the chilipepper rockfish (*Sebastes goodei*). *Fisheries Research*, 204, 258-268.
- Lilly, L. E., and M. D. Ohman. 2018. CCE IV: El Niño-related zooplankton variability in the southern California Current System. *Deep-Sea Res. Part I*.
- Love, M. S., M. Yoklavich and L. Thorsteinson. 2002. *The rockfishes of the northeast Pacific*. Berkeley, CA: University of California Press.
- Love, M.S., C.W. Mecklenburg, T.A. Mecklenburg and L.K. Thorsteinson. 2005. Resource Inventory of Marine and Estuarine Fishes of the West Coast and Alaska: A Checklist of North Pacific and Arctic Ocean Species from Baja California to the Alaska–Yukon Border. U. S. Department of the Interior, U. S. Geological Survey, Biological Resources Division, Seattle, Washington, p. 98104 OCS Study MMS 2005-030 and USGS/NBII 2005-00.
- Mace, A. J. and S. G. Morgan. 2006. Biological and physical coupling in the lee of a small headland: contrasting transport mechanisms for crab larvae in an upwelling region. *Mar Ecol Prog Ser* 324: 185–196.
- Mackas, D.L., W. T. Peterson, M. D. Ohman and B. E. Lavaniegos. 2006. Zooplankton anomalies in the California Current system before and during the warm ocean conditions of 2005. *Geophysical Research Letters* 33, L22S07.
- Manderson, J.P., L. Palamara, J. Kohut and M. J. Oliver. 2011. Ocean observatory data are useful for regional habitat modeling of species with different vertical habitat preferences. *Mar. Ecol. Prog. Ser.* 438, 1–17.
- Marliave, J. B. 1986. Lack of planktonic dispersal of rocky intertidal fish larvae. *Transactions of the American Fisheries Society* 115:149–154.

- Matarese, A. C., A. W. Kendall Jr., D. M. Blood, and B. M. Vinter. 1989. Laboratory guide to early life history stages of northeast Pacific fishes. NOAA Tech. Rep. NMFS 80, 652 p.
- McClatchie, S. 2014. Regional fisheries oceanography of the California Current System: the CalCOFI program. Springer. 235pp. ISBN 978-94- 007-7222-9.
- McClatchie, S., J. Gao, E. J. Drenkard, A. R. Thompson, W. Watson, L. Ciannelli, S. J. Bograd, and J. T. Thorson. 2018. Interannual and secular variability of larvae of mesopelagic and forage fishes in the southern California Current System. *Journal Geophysical Research Oceans*.
- McGurk., M. D. 1992. Avoidance of towed plankton nets by herring larvae: a model of night-day catch ratios based on larval length, net speed and mesh width. *J Plankton Res* 14:173–182
- Miller, M. 2015. Warm-water fish increasingly spotted in Alaska waters. KTOO Alaska Public Media, September 15, 2015, <http://www.alaskapublic.org/2015/09/15/warm-water-fish-increasinglyspotted-in-alaska-waters>.
- Miller, J. D. and R. N. Lea. 1972. Guide to the Coastal Marine Fishes of California, Fish Bulletin 157. Sacramento, California Department of Fish and Game.
- Miller, S.H. and S.G. Morgan. 2013. Interspecific differences in depth preference: regulation of larval transport in an upwelling system. *Mar Ecol Prog Ser* 476:301-306.
- Morgan, L. E., S. R. Wing, L. W. Botsford, C. J. Lundquist and J. M. Diehl. 2000. Spatial variability in red sea urchin (*Strongylocentrotus franciscanus*) recruitment in northern California. *Fisheries Oceanography*, 9(1), 83-98.
- Morgan, S.G. and J. L. Fisher. 2010. Larval behavior regulates nearshore retention and offshore migration in an upwelling shadow and along the open coast. *Marine Ecology Progress Series*, 404, pp.109-126.
- Morgan, S. G., J. L. Fisher and J. Largier. 2011. Larval retention, entrainment, and accumulation in the lee of a small headland. *Limnol. Oceanogr.* 56: 161–178.
- Morgan, S. G., J. L. Fisher, S. T. McAfee, J. L. Largier and C. M. Halle. 2012. Limited recruitment during relaxation events: larval advection and behavior in an upwelling system. *Limnol. Oceanogr.* 57, 457–470.
- Morgan, S.G. 2014. Behaviorally mediated larval transport in upwelling systems. *Advances in Oceanography*, 2014.

- Moser, H. G., R. L. Charter, P. E. Smith, D. A. Ambrose, S. R. Charter, C. A. Meyer, E. M. Sandknop, and W. Watson. 1993. Distributional atlas of fish larvae and eggs in the California Current region: taxa with 1000 or more total larvae, 1951-1984.
- Moser, H. G., R. L. Charter, P. E. Smith, D. A. Ambrose, S. R. Charter, C. A. Meyer, E. M. Sandknop, and W. Watson. 1994. Distributional atlas of fish larvae in the California Current region: taxa with less than 1000 total larvae, 1951-1984.
- Moser, H. G. 1996. The early stages of fishes in the California Current region. Calif Coop. Oceanic Fish. Invest. Atlas 33. 1505 pp.
- Moser, H. G., R. L. Charter, W. Watson, D. A. Ambrose, J. L. Butler, S. R. Charter and E. M. Sandknop. 2000. Abundance and distribution of rockfish (*Sebastes*) larvae in the Southern California Bight in relation to environmental conditions and fishery exploitation. Calif. Coop. Oceanic Fish. Invest. Rep. 41:132–148.
- Nickols, K. J., B. Gaylord and J. L. Largier. 2012. The coastal boundary layer: predictable current structure decreases alongshore transport and alters scales of dispersal. *Marine Ecology Progress Series* 464:17–35.
- Nickols, K. J., S. H. Miller, B. Gaylord, S. G. Morgan and J. L. Largier. 2013. Spatial differences in larval supply within the coastal boundary layer impact availability to shoreline habitats. *Mar. Ecol. Prog. Ser.* 494, 191–203.
- Nielsen, J.M., L. A., Rogers, R. D. Brodeur, et al. 2020. Responses of ichthyoplankton assemblages to the recent marine heatwave and previous climate fluctuations in several Northeast Pacific marine ecosystems. *Glob Change Biol.* 2021; 27: 506– 520.
- Van Noord, J.E. and E. Dorval 2017. Oceanographic influences on the distribution and relative abundance of market squid paralarvae (*Doryteuthis opalescens*) off the Southern and Central California coast. *Mar Ecol.* 2017; 38:e12433.
- Nishimoto, M. M and L. Washburn. 2002. Patterns of coastal eddy circulation and abundance of pelagic juvenile fish in the Santa Barbara Channel, California, USA. *Marine Ecology Progress Series* 241: 183-199.
- Oksanen, J., Blanchet, F.G., Friendly, M., Kindt, R., Legendre, P., McGlin, D., Minchin, P.R., O'Hara, R.B., Simpson, G.L., Solymos, P., Stevens, M.H., Szoecs, E., and H. Wagner. 2020. vegan: Community Ecology Package. R package version 2.5-7.
- Oliver, E.C., M.G. Donat, M.T. Burrows, P.J. Moore, D.A. Smale, L.V. Alexander, J.A. Benthuyssen, M. Feng, A.S. Gupta, A.J. Hobday and N.J. Holbrook. 2018. Longer and more frequent marine heatwaves over the past century. *Nat. Commun.* 9 (1),

1324.

- Parrish, R. H., C. S. Nelson and A. Bakun. 1981. Transport mechanisms and reproductive success of fishes in the California Current. *Biol. Oceanogr.* 1(2):175-203.
- Peterson, W. T., J. L. Fisher, P. T. Strub, X. Du, C. Risien, J. Peterson and C. T. Shaw. 2017. The pelagic ecosystem in the Northern California Current off Oregon during the 2014–2016 warm anomalies within the context of the past 20 years. *Journal of Geophysical Research: Oceans* 122(9):7267–7290.
- Pinsky, M.L., B. Worm, M.J Fogarty, J.L Sarmiento and S.A. Levin. 2013. Marine taxa track local climate velocities. *Science*, **341**(6151): 1239-1242.
- R Core Team. 2020. R: A language and environment for statistical computing. R Foundation for Statistical Computing, Vienna, Austria.
- Ralston, S., J. R. Bence, M. B. Eldridge and W. H. Lenarz. 2003. An approach to estimating rockfish biomass based on larval production, with application to *Sebastes jordani*. *Fish. Bull.* 101:129–146.
- Ralston, S. and B. R. MacFarlane. 2010. Population estimation of bocaccio (*Sebastes paucispinis*) based on larval production. *Can. J. Fish. Aquat. Sci.* 67:1005– 1020.
- Ralston, S., K. M. Sakuma and J.C. Field. 2013. Interannual variation in pelagic juvenile rockfish (*Sebastes* spp.) abundance: Going with the flow. *Fisheries Oceanography* 22:288–308.
- Richardson, S. and W. G. Pearcy. 1977. Coastal and oceanic larvae in an area of upwelling off Yaquina Bay, Oregon. *Fish Bull* 75:125 – 145.
- Robertson, R.R. and E.P. Bjorkstedt. 2020. Climate-driven variability in *Euphausia pacifica* size distributions off northern California. *Prog Oceanogr* 188: 102412.
- Russell, M. 2020. Investigating the effects of climate co-stressors on surf smelt energy demands. WWU Graduate School Collection. 967.
- Sabatès, A. and M. Masò. 1990. Effect of a shelf-slope front on the spatial distribution of mesopelagic fish larvae in the western Mediterranean. *Deep-Sea Res.*, 37, 1085–1098.
- Sadrozinski, A. 2008. Cross-shelf ichthyoplankton distributions in relation to hydrography off Northern California, with special attention to larval rockfishes. Thesis (M.S.)—Humboldt State University, Natural Resources: Fisheries Biology, 171 pp.

- Sakuma, K. M., S. Ralston and D. A. Roberts. 1999. Diel vertical distribution of postflexion larval *Citharichthys* spp. and *Sebastes* spp. off central California. *Fish. Oceanogr.* 8:68–76.
- Sanford, E., J. L. Sones, M. García-Reyes, J. R. Goddard and J. L. Largier. 2019. Widespread shifts in the coastal biota of northern California during the 2014-2016 marine heatwaves. *Sci Rep.* 2019;9(4216):1–14.
- Satterthwaite, E. V., J. P. Ryan, J. B. Harvey and S. G. Morgan. 2021. Invertebrate larval distributions influenced by adult habitat distribution, larval behavior, and hydrodynamics in the retentive upwelling shadow of Monterey Bay, California, USA. *Marine Ecology Progress Series*, 661, 35-47.
- Send, U., R. C. Beardsley and C. D. Winant. 1987. Relaxation from upwelling in the coastal ocean dynamics experiment. *Journal of Geophysical Research: Oceans*, 92(C2), 1683-1698.
- Shannon, C.E. and W. Weaver. 1949. *The Mathematical Theory of Communication*. University of Illinois Press, Urbana.
- Smith, K.A. and I.M. Suthers. 1999. Displacement of diverse ichthyoplankton assemblages by a coastal upwelling event on the Sydney shelf. *Mar. Ecol. Prog. Ser.* 176:49–62.
- Suntsov, A., J.A. Koslow and W. Watson. 2012. The spatial structure of coastal ichthyoplankton assemblages off central and southern California. *California Cooperative Oceanic Fisheries Investigations Reports* **53**, 153–170.
- Sydeman, W. J., J. A. Santora, S. A. Thompson, B. B. Marinovic, and E. Di Lorenzo. 2013. Increasing variance in North Pacific climate relates to unprecedented ecosystem variability off California. *Global Change Biology* 19:1662–1675. T
- Sydeman, W.J., M. García-Reyes, D.S. Schoeman, R.R. Rykaczewski, S.A. Thompson, B.A. Black BA, et al. 2014. Climate change and wind intensification in coastal upwelling ecosystems. *Science*. 345:77–80.
- Taylor, C. A., W. Watson, T. Chereskin, J. Hyde and R. Vetter. 2004. Retention of larval rockfishes, *Sebastes*, near natal habitat in the southern California bight, as indicated by molecular identification methods. *California Cooperative Oceanic Fisheries Investigations Reports*, 45(May 2015), 152–166.
- Taylor, C. A. and W. Watson. 2004. Utility of larval pigmentation to identify nearshore rockfishes of the *Sebastes* subgenus *Pteropodus* from Southern California. *Calif. Coop. Oceanic Fish. Invest. Rep.* 45:113–117.

- Thompson, A.R., W. Watson, S. McClatchie and E. D. Weber. 2012. Multi-scale sampling to evaluate assemblage dynamics in an oceanic marine reserve. *PLoS ONE* 7, e33131.
- Thompson, A. R., T. D. Auth, R. D. Brodeur, N. M. Bowlin, and W. Watson. 2014. Dynamics of larval fish assemblages in the California Current System: a comparative study between Oregon and southern California. *Mar. Ecol. Prog. Ser.* 506:193–212.
- Thompson, A. R., J. R. Hyde, W. Watson, D. C. Chen and L. W. Guo. 2016. Rockfish assemblage structure and spawning locations in southern California identified through larval sampling. *Marine Ecology Progress Series*, 547 (April), 177–192.
- Thompson, A. R., D. C Chen, L. W. Guo, J. R. Hyde and W. Watson. 2017. Larval abundances of rockfishes that were historically targeted by fishing increased over 16 years in association with a large marine protected area. *Royal Society Open Science*, 4(9).
- Thompson, A. R., I. Schroeder, S. Bograd, E. Hazen, M. Jacox, A. Leising, S. Melin, et al. 2019. State of the California Current: A new anchovy regime and marine heatwave? *California Cooperative Oceanic Fisheries Investigations Reports*, 61, 1–61.
- Walker, H. J. Jr, Hastings, P. A., Hyde, J. R., Lea, R. N., Snodgrass, O. E. and L. F. Bellquist. 2020. Unusual occurrences of fishes in the Southern California Current System during the warm water period of 2014– 2018. *Estuarine, Coastal and Shelf Science*, 236, 106634.
- Weber, E. D. et al. 2021. State of the California Current 2019–2020: Back to the Future With Marine Heatwaves? *Front. Mar. Sci.*, 1080.
- Wells, B. K., et al. 2017. State of the California Current 2016–17: Still anything but “normal” in the North. *CALCOFI Rep*, 58: 1–55.
- Welsh, A.H., R.B. Cunningham, C.F. Donnelly and D.B. Lindenmayer. 1996. Modelling the abundance of rare species: statistical models for counts with extra zeros. *Ecol. Model.* 88, 297–308.
- Wickham, H. 2016. *ggplot2: Elegant Graphics for Data Analysis*. Springer-Verlag New York.
- Williams, E. H. and S. Ralston. 2002. Distribution and co-occurrence of rockfishes (family: Sebastidae) over trawlable shelf and slope habitats of California and southern Oregon. *Fish. Bull.* 100:836–855.

- Wing, S. R., L. W. Botsford, J. L. Largier and L. E. Morgan. 1995. Spatial structure of relaxation events and crab settlement in the northern California upwelling system. *Marine Ecology Progress Series*, 128, 199-211.
- Wood, S.N. 2017. Generalized Additive Models: An Introduction with R (2nd edition). Chapman and Hall/CRC.
- Woodson, C. B., M. A. McManus, J. A. Tyburczy, J. A. Barth, L. Washburn, J. E. Caselle, M. H. Carr, D. P. Malone, P. T. Raimondi, B. A. Menge and S. R. Palumbi. 2012. Coastal fronts set recruitment and connectivity patterns across multiple taxa. *Limnology and Oceanography*, 57(2), 582-596.
- Wyllie-Echevarria, T. 1987. Thirty-four species of California rockfishes: maturity and seasonality of reproduction. *Fish Bull* 85:229–250.

APPENDIX A

Appendix A: Detailed methods for conducting genetic sequencing and identification on ethanol-preserved larval rockfishes (*Sebastes* spp.).

Genomic DNA was extracted from an eyeball or caudal fin tissue of each individual larvae using a chelex-based boiling protocol (Walsh et al. 1991). Polymerase chain reaction (PCR) was used to amplify a 625 base pair region of the mtDNA cytochrome *b* gene using the primers GLURF2 and CB3RF2 (Rocha-Olivares et al. 1999). Each PCR reaction was conducted with 6.25 µl of GoTaq Hotstart Master Mix (Promega), 0.5 µl of 10 µM of each primer, 4.25 µl of PCR clean water, and 1 µl of chelex supernatant containing DNA template. Thermal cycling conditions of PCR included an initial denaturation at 94° C for 2 min, followed by 35 cycles of 94° for 45 sec, 57° for 1.5 min, and 72° for 1.5 min. A final extension was carried out at 72° C for 3 min. A negative control was included in each PCR reaction to test for the possibility of contamination. PCR products were then sent to McLab Inc. (<https://www.mclab.com>) for PCR clean-up and sequencing. Cleaned PCR products were sequenced in one direction using the primer CBINR3.

Sequences were edited and aligned using either the DNA sequence analysis software Sequencher v.4.8 (GeneCodes) or finchTV v.1.5 (Geospiza). Unknown sequences were compared to a reference data set of 374 independent haplotype sequences representing 67 species of identified adult *Sebastes* (Hyde and Vetter 2007) and identified by creating Neighbor Joining phylogenetic trees with MEGA v.7.0.26 (Sudhir et al.

2015). The optimality criterion was set to distance (number of base pair differences divided by the total base pairs sequenced).

Within MEGA, nonparametric bootstrapping was used (1000 replicates) to cluster each unknown larval rockfish haplotype within the reference data set of 374 known adult *Sebastes* sequences. If an unknown sequence clustered within a single species monophyletic clade with a bootstrap value $\geq 80\%$, this was considered a high-confidence identification of that unknown sequence. If an unknown larval sequence clustered within a single species monophyletic clade with a bootstrap value $< 80\%$, the unknown sequence was directly compared to the three nearest reference adult species. Not all species successfully form single species monophyletic clades. Species complexes that fail to form single species monophyletic clades include the pygmy rockfish (*S. wilsoni*), Puget Sound rockfish (*S. emphaeus*), harlequin rockfish (*S. variegatus*), and sharpchin rockfish (*S. zacentrus*) complex (WEVZ complex), the blue rockfish (*S. mystinus*) and widow rockfish (*S. entomelas*) complex, the darkblotched rockfish (*S. crameri*), yellowmouth rockfish (*S. reedi*), dusky rockfish (*S. ciliatus*), light dusky rockfish (*S. variabilis*), and northern rockfish (*S. polyspinis*) complex, and the splitnose rockfish (*S. diploproa*), Cortez rockfish (*S. cortezi*), semaphore rockfish (*S. melanosema*), *S. peduncularis*, and blackmouth rockfish (*S. sinensis*) complex. Unknown sequences falling into the WEVZ complex could not be reliably differentiated between species based on the potential occurrence of all four species within the study area and the lack of nucleotide differences between species. All species falling into the WEVZ complex were given an identification as “WEVZ”. Unknown larval sequences falling into the *S. crameri*, *S. reedi*, *S. ciliatus*, *S.*

variabilis, and *S. polyspinis* complex were assumed to be either *S. crameri* or *S. reedi* based on adult distributions (Love et al. 2002). *S. ciliatus*, *S. variabilis*, and *S. polyspinis* adults do not occur off northern California and are primarily distributed from the Aleutian Islands south to southern British Columbia (Love et al. 2002). *S. crameri* and *S. reedi* consistently differ at two nucleotide sites (site 343 and 555) within the mtDNA cytochrome *b* gene, allowing all individuals except one to be identified as *S. crameri*. Unknown larval sequences falling into the *S. diploproa*, *S. cortezi*, *S. melanosema*, *S. peduncularis*, and *S. sinensis* complex were assumed to be *S. diploproa* based on adult distributions (Love et al. 2002). *S. diploproa* is a common species off northern California and *S. cortezi*, *S. melanosema*, *S. peduncularis*, and *S. sinensis* adults are either restricted to the Sea of Cortez or do not occur north of Baja California (Love et al. 2002). Unknown sequences falling into the *S. mystinus* and *S. entomelas* complex were differentiated on the basis of one nucleotide difference (site 627) between *S. entomelas* and *S. mystinus*. Although *S. mystinus* can be differentiated from *S. entomelas* at the cytochrome *b* gene, recent genetic analysis found *S. mystinus* (blue rockfish) is composed of two recently diverged but morphologically similar species that have a population break at Cape Mendocino: blue rockfish are distributed south of Cape Mendocino and *Sebastes diaconus* (deacon rockfish) distributed north of Cape Mendocino (Frale et al. 2015, Bizzarro et al. 2020). Due to the TH-line residing just north of Cape Mendocino in the transition zone between both populations, it is possible that larvae of both species are sampled. Unfortunately, references of the cytochrome *b* gene do not exist for deacon

rockfish, thus I cannot differentiate these species from one another and herein refer to individuals genetically identified as blue rockfish as the “MyDi” complex.

APPENDIX B

Appendix B. Taxonomic list of rare larval fishes within the visual assemblage, including corresponding adult biogeographic ranges in '()', mean areal density (No./m²), total areal density, percent of total areal density, maximum observed areal density in a sample, and percent positive tow. Adult spawning ranges are defined as: (C) coastal (typically occupy and spawn in habitat inshore of the upper slope), or (O) oceanic (mostly spawn offshore of the upper slope), crossed with species latitudinal ranges defined as: (CW) coastwide (typically found and spawn throughout the CCS), (N) northern (adults spawn mostly Monterey Bay and north), or (S) southern (adults spawn mostly Monterey Bay and south). Total areal density is calculated as the areal density summed across all samples. Percent positive tow is calculated as the number of tows in which a species was observed over the total number of tows. Mean areal density is calculated as the total areal density over the total number of tows. Percent of total density is calculated as the total areal density of an individual taxon over the total aggregate larval density summed across all samples.

Taxa	Common Name	Family	Mean density	Total density	Percent of total density	Percent Positive Tow
<i>Sebastolobus spp.</i> (CW-C)	Thornyheads	Sebastidae	0.066	36.8	0.49	2
<i>Clupea pallasii</i> (N-C)	Pacific herring	Clupeidae	0.065	36.3	0.48	4.5
<i>Genyonemus lineatus</i> (S-C)	White croaker	Sciaenidae	0.059	32.7	0.44	1.3
<i>Ammodytes hexapterus</i> (N-C)	Pacific sand lance	Ammodytidae	0.046	25.8	0.34	3.2
<i>Sardinops sagax</i> (S-C)	Pacific sardine	Clupeidae	0.037	20.3	0.27	3.6
<i>Ichthyos lockingtoni</i> (CW-O)	Medusafish	Centrolophidae	0.035	19.6	0.26	3.1
<i>Diaphus theta</i> (CW-O)	California headlightfish	Myctophidae	0.031	17.5	0.23	2.3
<i>Nannobranchium regale</i> (CW-O)	Pinpoint lampfish	Myctophidae	0.03	16.6	0.22	4.5
<i>Chauliodus macouni</i> (CW-O)	Pacific viperfish	Stomiidae	0.028	15.3	0.2	4.7
<i>Scorpaenichthys marmoratus</i> (CW-C)	Cabazon	Cottidae	0.027	14.8	0.2	4.1
<i>Microstomus pacificus</i> (CW-C)	Dover sole	Pleuronectidae	0.023	12.8	0.17	2.5
<i>Hemilepidotus spinosus</i> (N-C)	Brown Irish lord	Cottidae	0.022	12	0.16	2.7
<i>Lepidogobius lepidus</i> (CW-C)	Bay goby	Oxudercidae	0.022	11.9	0.16	3.2
<i>Lestidiops ringens</i> (CW-O)	Slender barracudina	Paralepididae	0.021	11.6	0.15	3.9
<i>Isopsetta isolepis</i> (N-C)	Butter sole	Pleuronectidae	0.02	11	0.15	2.3
<i>Protomyctophum thompsoni</i> (N-O)	Northern flashlightfish	Myctophidae	0.019	10.5	0.14	3.1

Taxa	Common Name	Family	Mean density	Total density	Percent of total density	Percent Positive Tow
Cottidae (CW-C)	Sculpins	Cottidae	0.018	10	0.13	2.7
<i>Lampadena urophaos</i> (S-O)	Sunbeam lampfish	Myctophidae	0.016	9.1	0.12	1.3
<i>Parvilux ingens</i> (S-O)	Giant lampfish	Myctophidae	0.016	9.07	0.12	2.3
<i>Leptocottus armatus</i> (CW-C)	Staghorn sculpin	Cottidae	0.016	8.95	0.12	1.8
<i>Tetragonurus cuvieri</i> (CW-O)	Smalleye squaretail	Tetragonuridae	0.016	8.74	0.12	2.3
<i>Radulinus asprellus</i> (N-C)	Slim sculpin	Cottidae	0.014	7.99	0.11	2.2
<i>Bathylagus pacificus</i> (N-O)	Pacific blacksmelt	Bathylagidae	0.014	7.85	0.1	2.3
<i>Hemilepidotus hemilepidotus</i> (N-C)	Red Irish lord	Cottidae	0.011	5.89	0.08	2
<i>Nannobranchium ritteri</i> (CW-O)	Broadfin lampfish	Myctophidae	0.01	5.38	0.07	1.4
<i>Cryptacanthodes aleutensis</i> (N-C)	Dwarf wrymouth	Cryptacanthodidae	0.008	4.58	0.06	1.6
<i>Hexagrammos decagrammus</i> (N-C)	Kelp greenling	Hexagrammidae	0.008	4.56	0.06	0.9
<i>Platichthys stellatus</i> (N-C)	Starry flounder	Pleuronectidae	0.008	4.35	0.06	0.5
<i>Embassichthys bathybius</i> (N-C)	Deepsea sole	Pleuronectidae	0.008	4.21	0.06	0.9
<i>Ruscarius meanyi</i> (N-C)	Puget Sound sculpin	Cottidae	0.007	3.74	0.05	1.4
<i>Trachurus symmetricus</i> (S-C)	Jack mackerel	Carangidae	0.006	3.29	0.04	0.4
<i>Loweina rara</i> (S-O)	Laura's lanternfish	Myctophidae	0.005	2.93	0.04	0.9

Taxa	Common Name	Family	Mean density	Total density	Percent of total density	Percent Positive Tow
<i>Ophiodon elongatus</i> (CW-C)	Lingcod	Hexagrammidae	0.005	2.83	0.04	0.7
<i>Hexagrammos stelleri</i> (N-C)	Whitespotted greenling	Hexagrammidae	0.005	2.66	0.04	0.9
<i>Anoplopoma fimbria</i> (CW-C)	Sablefish	Anoplopomatidae	0.005	2.61	0.03	0.7
<i>Clevelandia ios</i> (CW-C)	Arrow goby	Oxudercidae	0.005	2.55	0.03	0.7
<i>Hexagrammos lagocephalus</i> (N-C)	Rock greenling	Hexagrammidae	0.005	2.55	0.03	0.5
<i>Eopsetta jordani</i> (CW-C)	Petrable sole	Pleuronectidae	0.004	2.31	0.03	0.9
<i>Scomber japonicus</i> (S-C)	Pacific mackerel	Scombridae	0.004	2	0.03	0.2
<i>Pleuronichthys decurrens</i> (CW-C)	Curlfin sole	Pleuronectidae	0.003	1.88	0.03	0.7
<i>Trachipterus altivelis</i> (CW-O)	King-of-the-salmon	Trachipteridae	0.003	1.82	0.02	0.7
<i>Leuroglossus stilbius</i> (S-O)	California smoothtongue	Bathylagidae	0.003	1.78	0.02	0.9
<i>Myoxocephalus polyacanthocephalus</i> (N-C)	Great sculpin	Cottidae	0.003	1.75	0.02	0.7
<i>Melamphaes lugubris</i> (CW-O)	Highsnout ridgehead	Melamphaidae	0.003	1.71	0.02	0.7
<i>Hippoglossoides elassodon</i> (N-C)	Flathead sole	Pleuronectidae	0.002	1.35	0.02	0.5
<i>Bathylagus bericoides</i> (CW-O)	Bigscale deepsea smelt	Bathylagidae	0.002	1.06	0.01	0.2
<i>Lepidopsetta bilineata</i> (CW-C)	Rock sole	Pleuronectidae	0.002	1.03	0.01	0.5
<i>Gadus chalcogrammus</i> (N-C)	Alaska pollock	Gadidae	0.002	1	0.01	0.2

Taxa	Common Name	Family	Mean density	Total density	Percent of total density	Percent Positive Tow
<i>Leptagonus leptorhynchus</i> (N-C)	Longnose poacher	Agonidae	0.002	1	0.01	0.2
<i>Pallasina barbata</i> (N-C)	Tube-nose poacher	Agonidae	0.002	1	0.01	0.2
Stichaeidae (N-C)	Pricklebacks	Stichaeidae	0.002	1.0	0.01	0.2
<i>Tactostoma macropus</i> (CW-O)	Longfin dragonfish	Stomiidae	0.002	0.99	0.01	0.4
<i>Ceratoscopelus townsendi</i> (S-O)	Dogtooth lampfish	Myctophidae	0.002	0.98	0.01	0.4
<i>Melamphaes</i> spp. (CW-O)	Bigscales	Melamphaidae	0.002	0.96	0.01	0.4
<i>Electrona risso</i> (S-O)	Electric lanternfish	Myctophidae	0.002	0.94	0.01	0.4
<i>Nansenia candida</i> (N-O)	Bluethroat argentine	Microstomatidae	0.002	0.94	0.01	0.4
<i>Clinocottus globiceps</i> (N-C)	Mosshead sculpin	Cottidae	0.002	0.93	0.01	0.2
<i>Leuroglossus schmidtii</i> (N-O)	Northern smoothtongue	Bathylagidae	0.002	0.93	0.01	0.4
<i>Poromitra crassiceps</i> (CW-O)	Crested bigscale	Melamphaidae	0.002	0.93	0.01	0.4
<i>Brosmophycis marginata</i> (S-C)	Red brotula	Bythitidae	0.002	0.91	0.01	0.4
<i>Melamphaes parvus</i> (CW-O)	Little bigscale	Melamphaidae	0.002	0.9	0.01	0.2
<i>Limanda aspera</i> (N-C)	Yellowfin sole	Pleuronectidae	0.001	0.83	0.01	0.4
<i>Anoplarchus insignis</i> (N-C)	Slender cockscomb	Stichaeidae	0.001	0.7	0.01	0.4
<i>Enophris bison</i> (N-C)	Buffalo sculpin	Cottidae	0.001	0.7	0.01	0.2

Taxa	Common Name	Family	Mean density	Total density	Percent of total density	Percent Positive Tow
<i>Anoplarthus purpureus</i> (N-C)	High cockscomb	Stichaeidae	0.001	0.65	0.01	0.4
<i>Ronquilus jordani</i> (N-C)	Northern ronquil	Bathymasteridae	0.001	0.65	0.01	0.4
<i>Stellerina xyosterna</i> (CW-C)	Pricklebreast poacher	Agonidae	0.001	0.62	0.01	0.4
<i>Atheresthes stomias</i> (N-C)	Arrowtooth flounder	Pleuronectidae	0.001	0.6	0.01	0.2
<i>Rhamphocottus richardsonii</i> (N-C)	Grunt sculpin	Cottidae	0.001	0.58	0.01	0.4
<i>Cololabis saira</i> (S-O)	Pacific saury	Scomberesocidae	0.001	0.57	0.01	0.2
<i>Diogenichthys atlanticus</i> (S-O)	Longfin lanternfish	Myctophidae	0.001	0.53	0.01	0.2
<i>Bathylagus wesethi</i> (S-O)	Snubnose blacksmelt	Bathylagidae	0.001	0.52	0.01	0.2
<i>Pleuronectes quadrituberculatus</i> (N-C)	Alaska plaice	Pleuronectidae	0.001	0.52	0.01	0.2
Zoarcidae (CW-C)	Eelpouts	Zoarcidae	0.001	0.52	0.01	0.2
<i>Hypsagonus mozinoi</i> (N-C)	Kelp poacher	Agonidae	0.001	0.51	0.01	0.2
<i>Cyclothone pseudopallida</i> (CW-O)	Slender bristlemouth	Gonostomatidae	0.001	0.5	0.01	0.2
<i>Argentina sialis</i> (S-C)	Pacific argentine	Argentinidae	0.001	0.49	0.01	0.2
<i>Porichthys</i> spp. (CW-C)	Stargazers	Batrachoididae	0.001	0.46	0.01	0.2
<i>Xeneretmus leiops</i> (N-C)	Smooth-eye poacher	Agonidae	0.001	0.46	0.01	0.2
<i>Danophos oculatus</i> (CW-O)	Bottlelight	Myctophidae	0.001	0.45	0.01	0.2

Taxa	Common Name	Family	Mean density	Total density	Percent of total density	Percent Positive Tow
<i>Hippoglossina stomata</i> (S-C)	Bigmouth flounder	Pleuronectidae	0.001	0.45	0.01	0.2
<i>Symphurus atricaudus</i> (S-C)	California tonguefish	Cynoglossidae	0.001	0.45	0.01	0.2
<i>Cyclothone acclinidens</i> (CW-O)	Benttooth bristlemouth	Gonostomatidae	0.001	0.44	0.01	0.2
<i>Spectrunculus grandis</i> (CW-O)	Pudgy cuskeel	Ophidiidae	0.001	0.44	0.01	0.2
<i>Bathyagonus pentacanthus</i> (N-C)	Bigeye poacher	Agonidae	0.001	0.43	0.01	0.2
<i>Bathyagonus alascanus</i> (N-C)	Gray starsnout	Agonidae	0.001	0.43	0.01	0.2
<i>Bathyagonus infraspinus</i> (N-C)	Spinycheek starsnout	Agonidae	0.001	0.41	0.01	0.2
<i>Rathbunella</i> spp. (S-C)	Ronquils	Bathymasteridae	0.001	0.35	< 0.01	0.2
<i>Chitonotus pugentensis</i> (CW-C)	Roughback sculpin	Cottidae	0.001	0.35	< 0.01	0.2
<i>Microgadus proximus</i> (N-C)	Pacific tomcod	Gadidae	0.001	0.35	< 0.01	0.2
<i>Odontopyxis trispinosa</i> (CW-C)	Pygmy poacher	Agonidae	0.001	0.35	< 0.01	0.2
<i>Opisthocentrus ocellatus</i> (N-C)	Ocellated blenny	Callionymidae	0.001	0.35	< 0.01	0.2
Pholidae (N-C)	Gunnels	Pholidae	0.001	0.35	< 0.01	0.2
<i>Symbolophorus californiensis</i> (S-O)	Bigfin lanternfish	Myctophidae	0.001	0.35	< 0.01	0.2
<i>Zaniolepis frenata</i> (S-C)	Shortspine combfish	Zaniolepididae	0.001	0.35	< 0.01	0.2
<i>Lepidopsetta polyxystra</i> (N-C)	Northern rock sole	Pleuronectidae	0.001	0.33	< 0.01	0.2

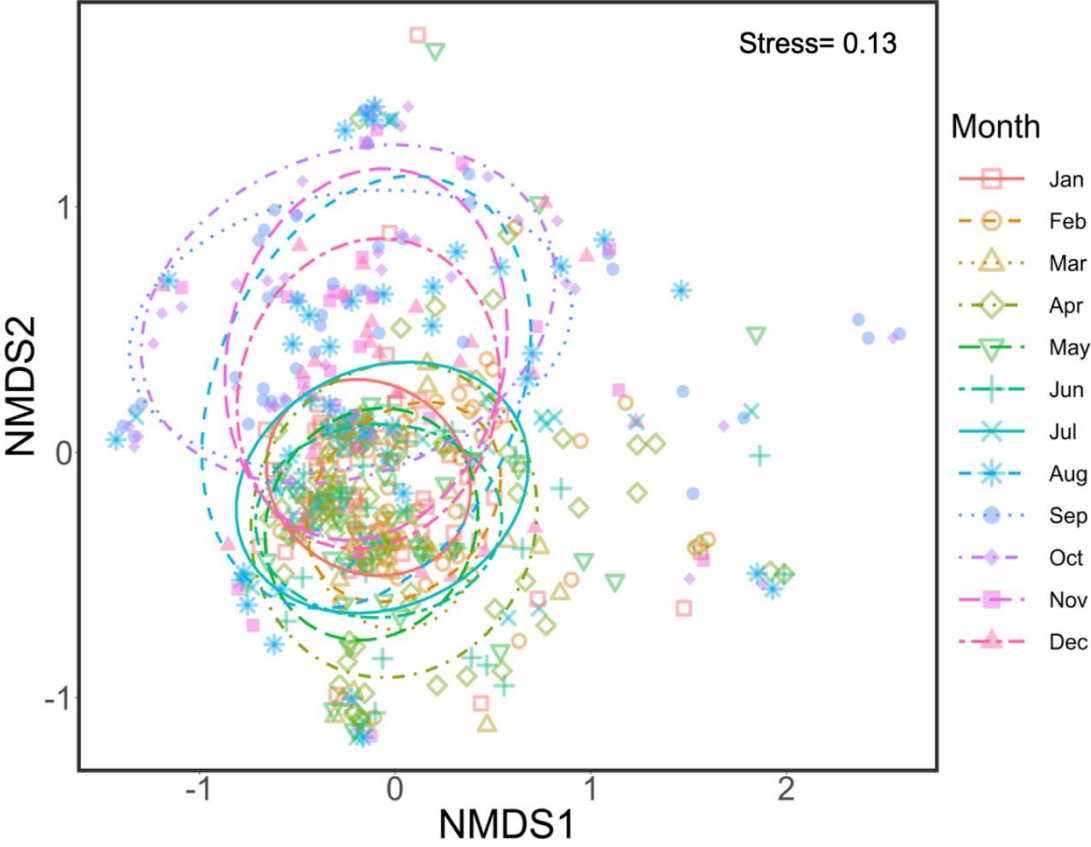
Taxa	Common Name	Family	Mean density	Total density	Percent of total density	Percent Positive Tow
<i>Bathylagus milleri</i> (N-O)	Robust blacksmelt	Bathylagidae	0.001	0.32	< 0.01	0.2
<i>Poroclinus rothrocki</i> (N-C)	Whitebarred prickleback	Lumpenidae	0.001	0.32	< 0.01	0.2
<i>Chirolophis nugator</i> (N-C)	Mosshead warbonnet	Stichaeidae	0.001	0.31	< 0.01	0.2
<i>Gadus macrocephalus</i> (N-C)	Pacific cod	Gadidae	0.001	0.31	< 0.01	0.2

APPENDIX C

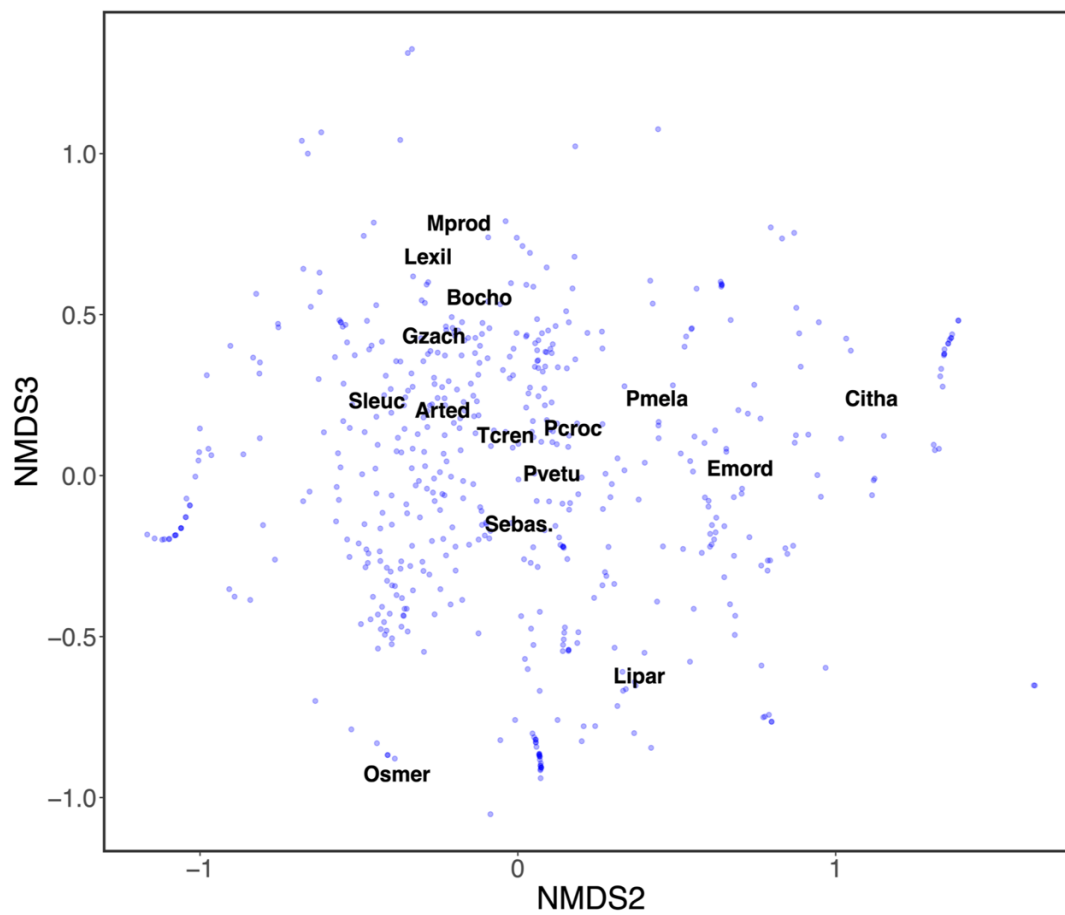
Appendix C. Ordination plots depicting (A) seasonal structure within the visual assemblage by individual months along NMDS1 and NMDS2, (B) assemblage structure within the visual assemblage along NMDS2 and NMDS3, and (C) seasonal structure within the rockfish assemblage by individual months along NMDS1 and NMDS2. In figures A and C, points and ellipses are color coded by the month a sample was collected. See Table 1 for species names corresponding to abbreviations in figure B.

Figure A (corroborating Figure 27) depicts strong differentiation between the months of January-July from the months of August-December but generally weak differentiation between months within the August-December and January-July period. Figure C (corroborating Figure 32) depicts strong differentiation between the months of January-March from the months of May-September but weak differentiation between months within January-March and May-September. Variability along NMDS3 within the visual assemblage (Figure B) appears to differentiate among assemblages that included *M. productus*, *L. exilis*, and *B. ochotensis* from those with substantial representation of osmerids and *Liparis* spp. at interannual scales.

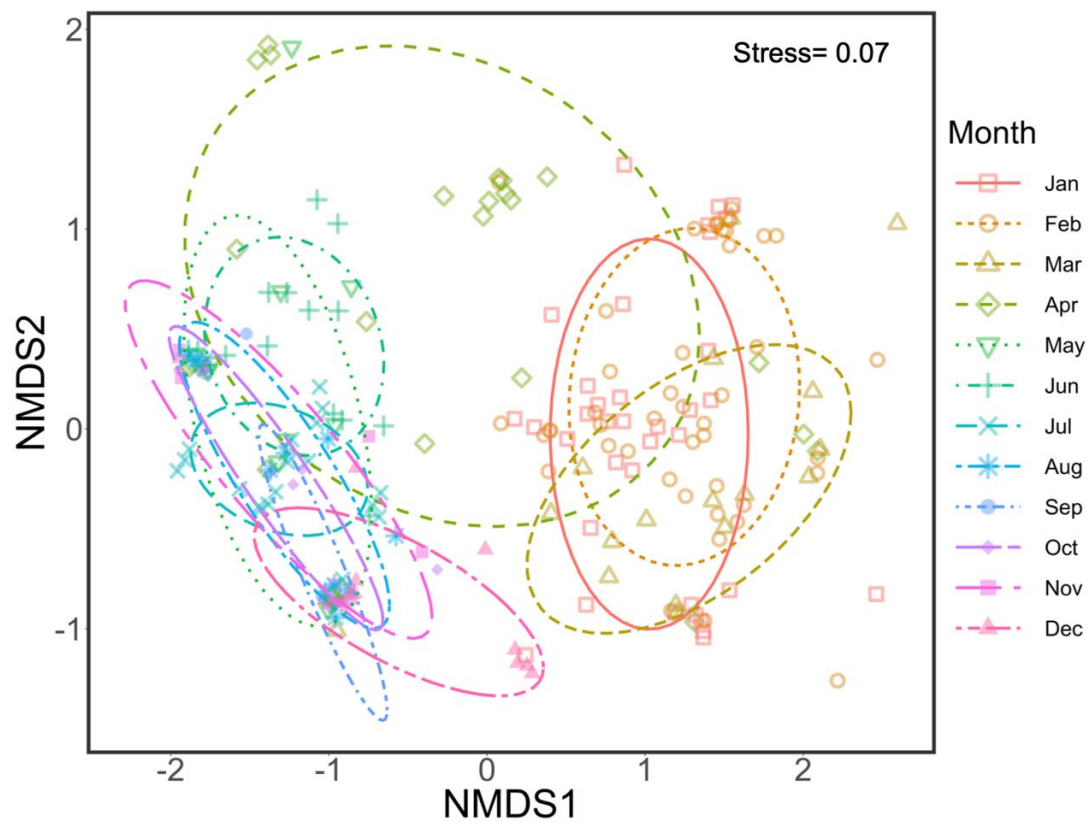
(A)



(B)



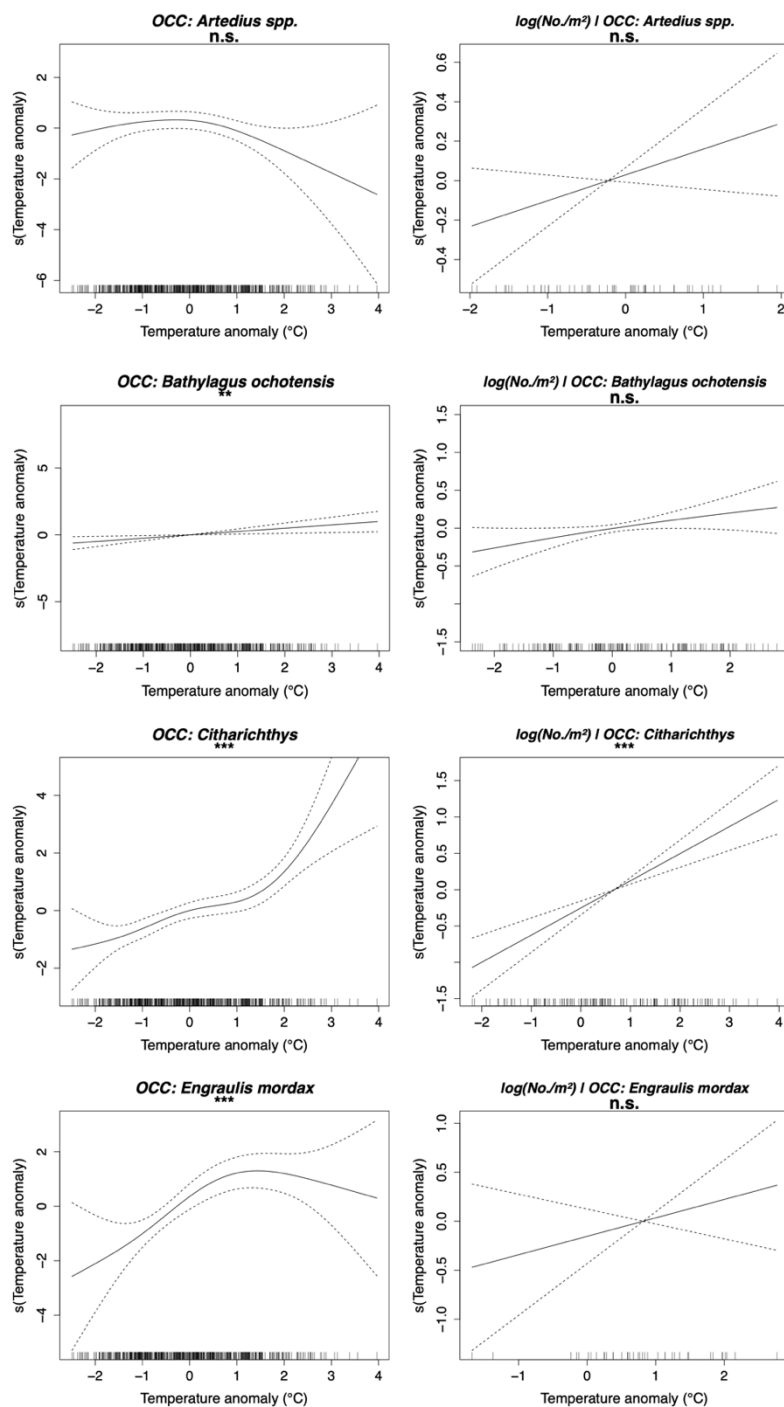
(C)



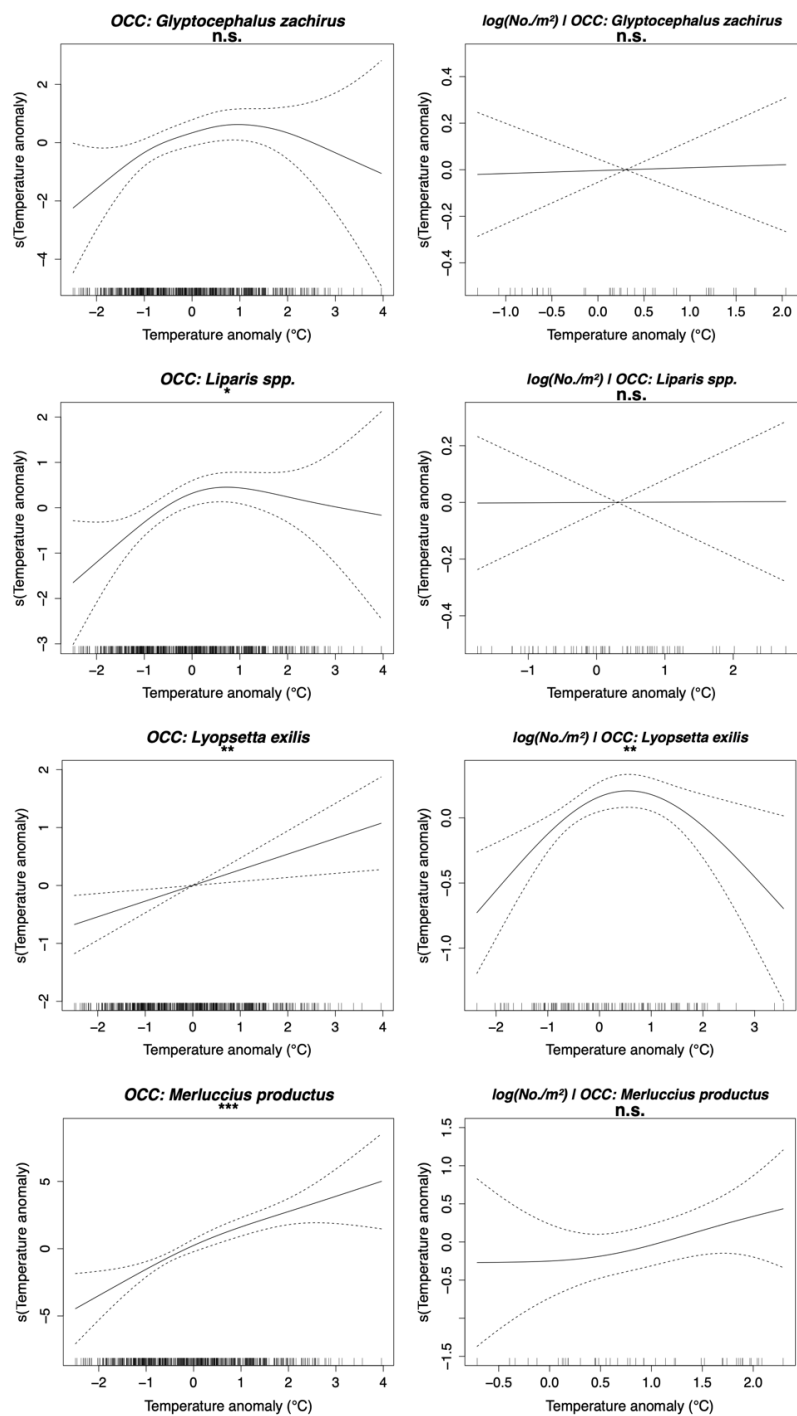
APPENDIX D

Appendix D. Fitted lines (solid) and 95% confidence intervals (dashed) for the additive effect of a seasonally corrected temperature anomaly in the upper 0-10 m of the water-column on larval abundance based on delta generalized additive models (delta-GAM) for common taxa included within the (A) visual assemblage and (B) rockfish assemblage. The binomial model (OCC; left hand column) estimates the probability of larval occurrence in relation to a temperature anomaly. The lognormal model ($\log_{10}(\text{No.}/\text{m}^2)$ | OCC; right hand column) estimates the magnitude of abundance for positive counts in relation to a temperature anomaly. Explanatory variables used to model both presence and abundance of positive counts were station, day of year, and a seasonally corrected temperature anomaly between 0 and 10 m (see methods for anomaly calculations). The significance of the temperature anomaly smooth term within each model is indicated for each taxon and set at: * = $p < 0.05$, ** = $p < 0.01$, *** = $p < 0.001$, and n. s. = not significant.

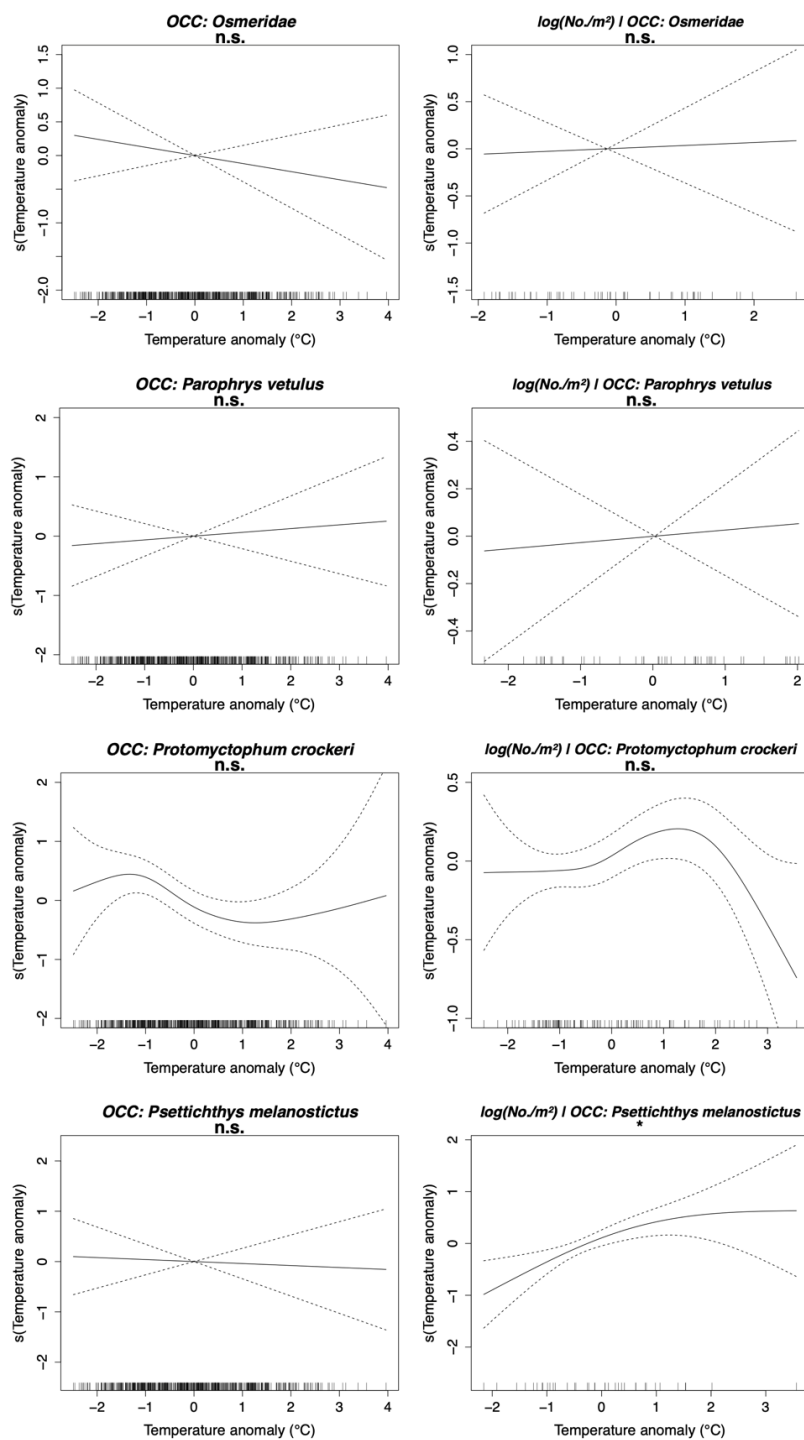
(A)



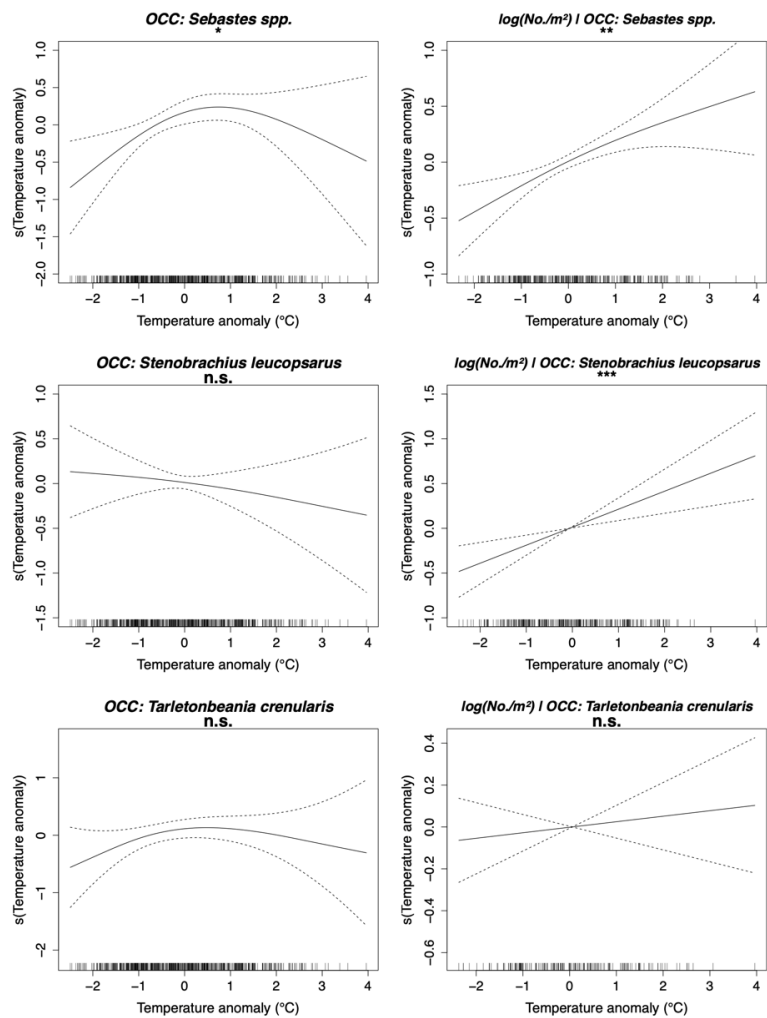
(A; continued)



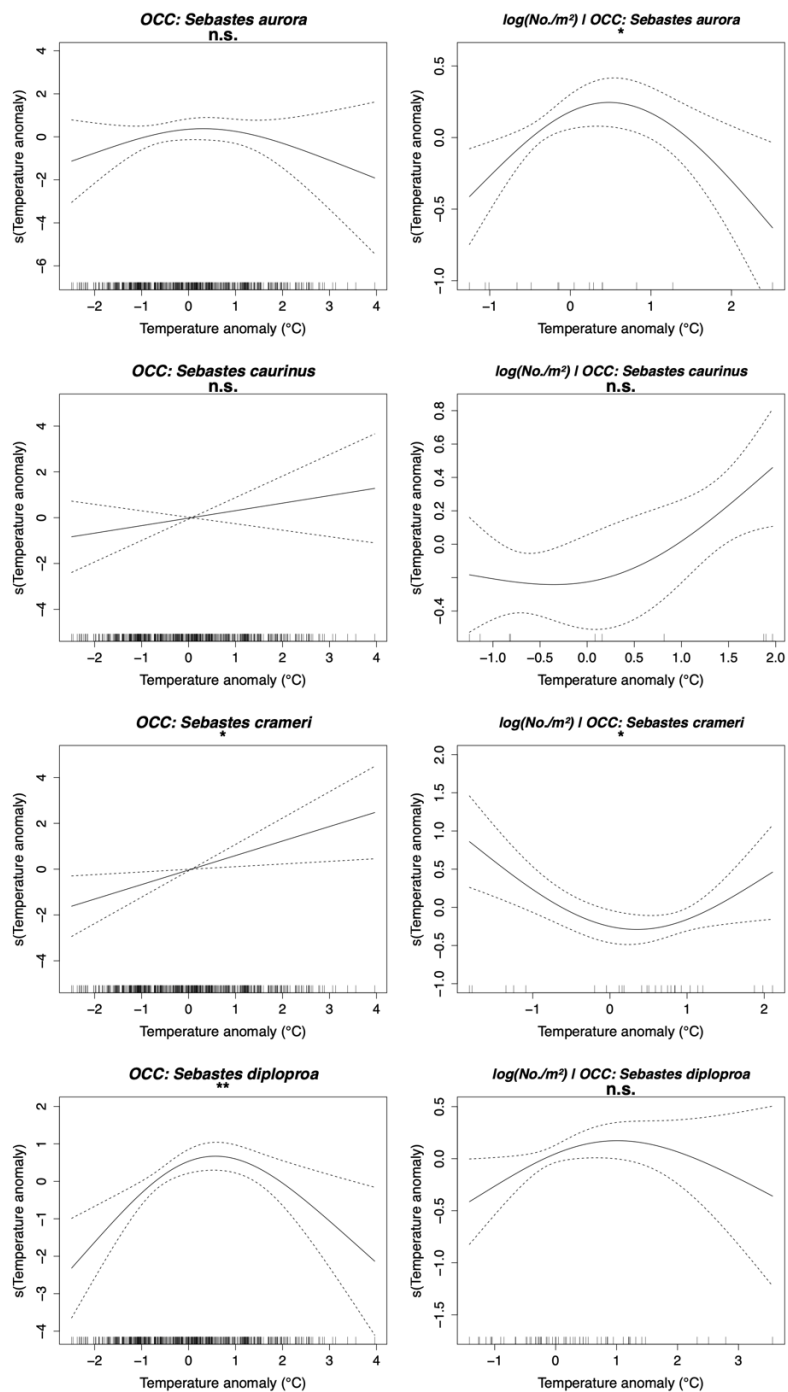
(A; continued)



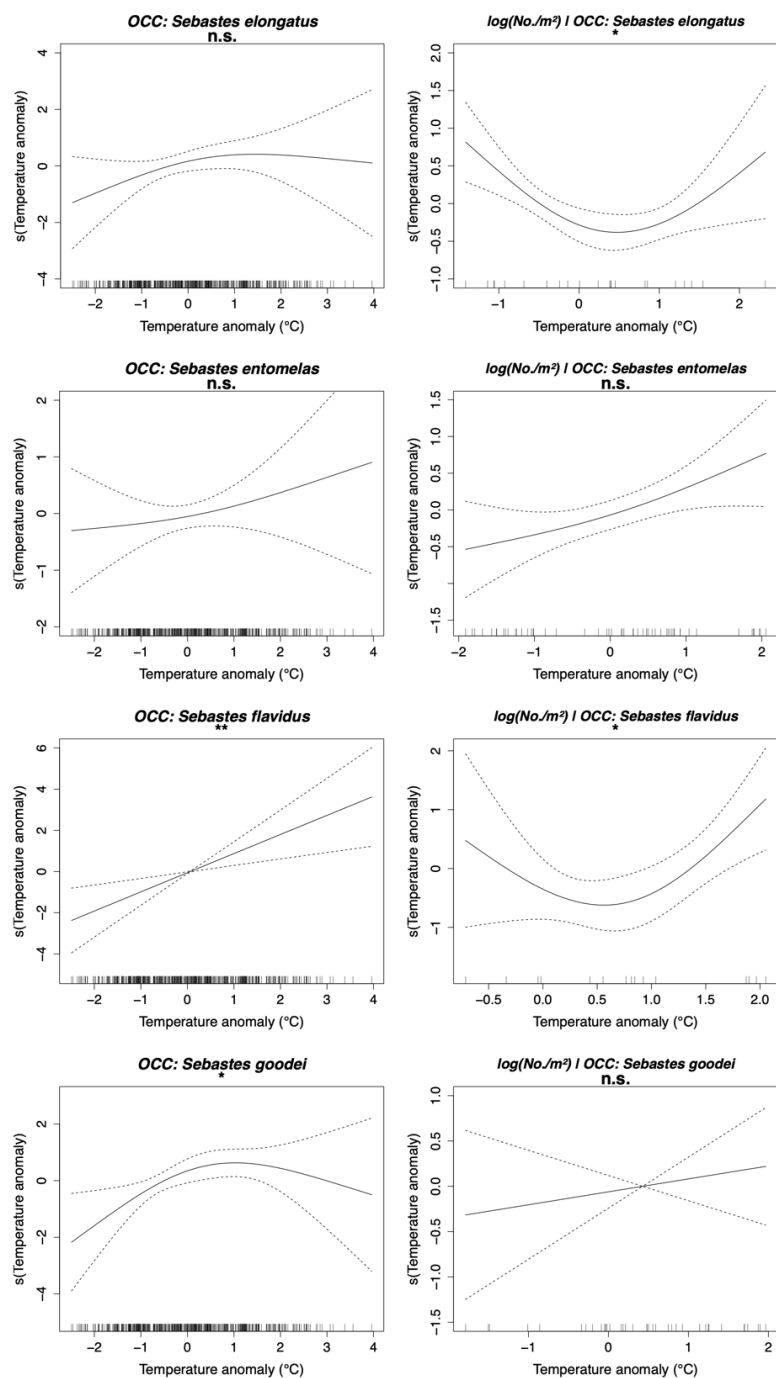
(A; continued)



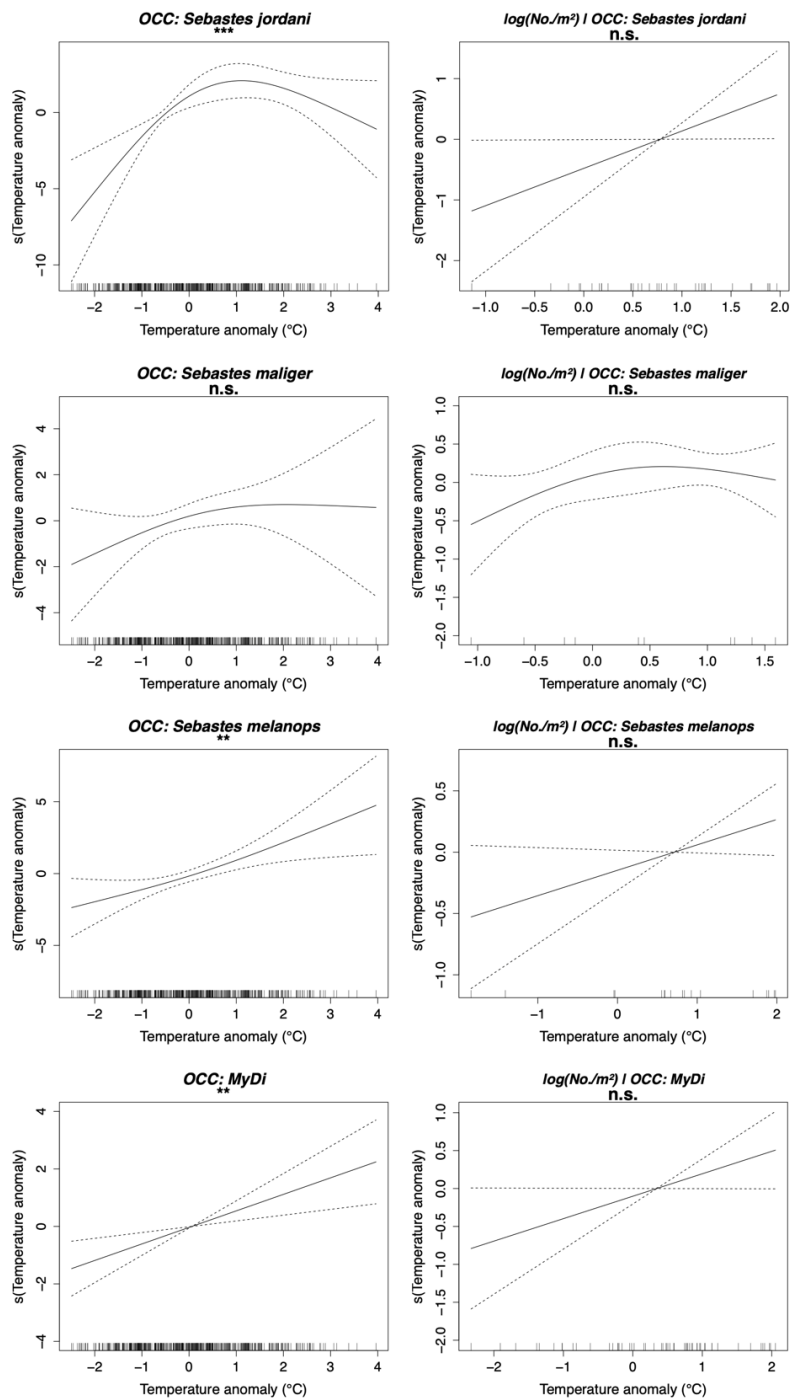
(B)



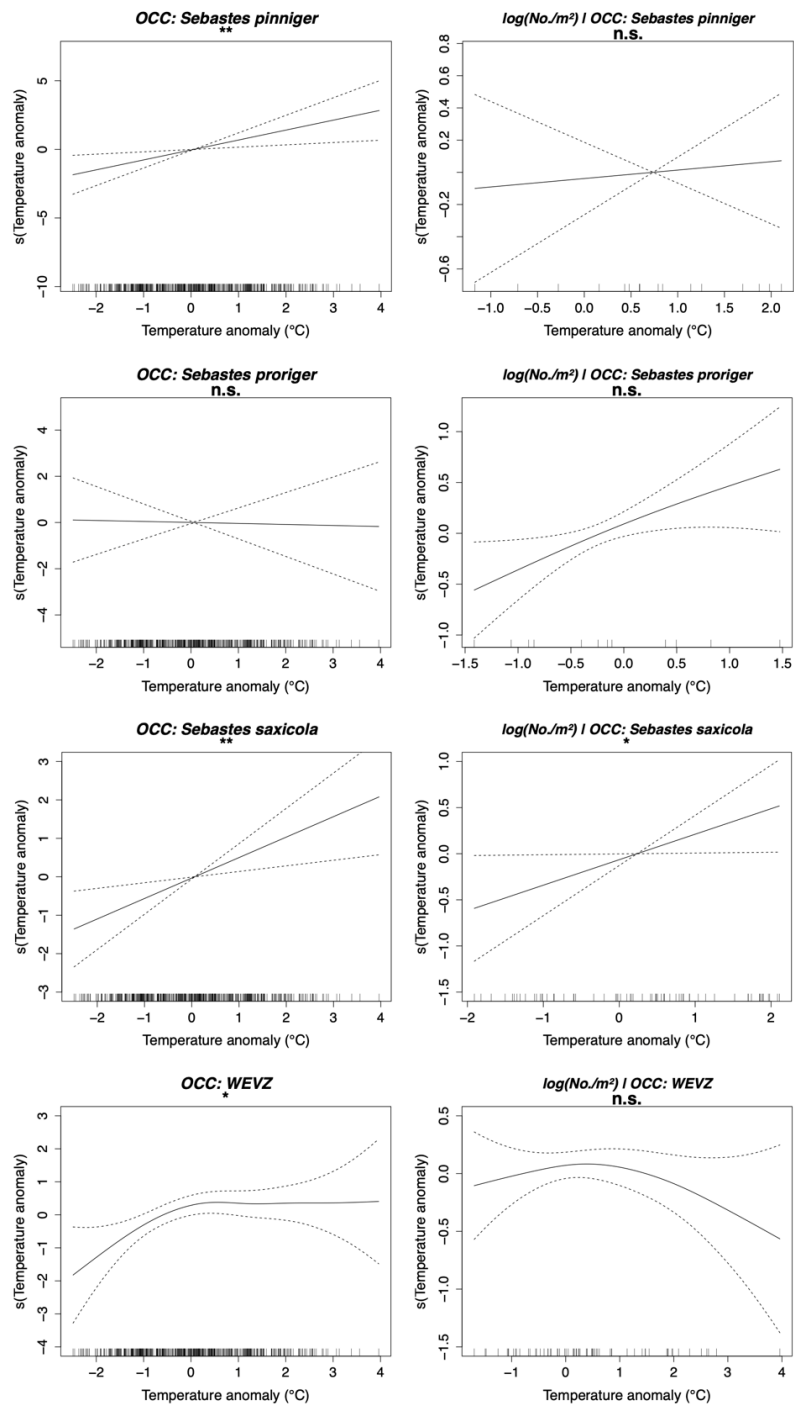
(B; continued)



(B; continued)



(B; continued)



APPENDIX E

Appendix E. Interannual variability in cross-shelf distributions and seasonal occurrence. Plots depict interannual variation in cross-shelf distributions by cruise date (x-axis) and station (y-axis) for common taxa within the (A) visual assemblage and (B) rockfish assemblage. Also included is interannual variation in seasonal occurrence by year (x-axis) and day of year (y-axis) for common taxa within the (C) visual assemblage and (E) rockfish assemblage. Circles scale with areal density (No./m²). Gray shading indicates extended observation gaps.

Despite the general patterns of individual taxa tending to be either broadly distributed or concentrated at nearshore (TH01-TH02) or offshore (TH03-TH05) stations, cross-shelf distributions were not static over the time series. For example, *E. mordax* was variable in cross-shelf distributions, shifting between inshore and offshore distributions between late 2014 and late 2017. In early 2019, *E. mordax* was distributed across most of the transect (stations TH01-TH04). Taxa that were generally restricted to nearshore (*P. melanostictus* and *Artedius* spp.) or offshore (e.g., *M. productus* and *B. ochotensis*) stations were more broadly distributed across the entire transect during the late 2014-2016 MHW. In contrast, *T. crenularis* and *P. crockeri*, two deep-water myctophids disappeared or declined in abundance at nearshore stations in mid 2014-15.

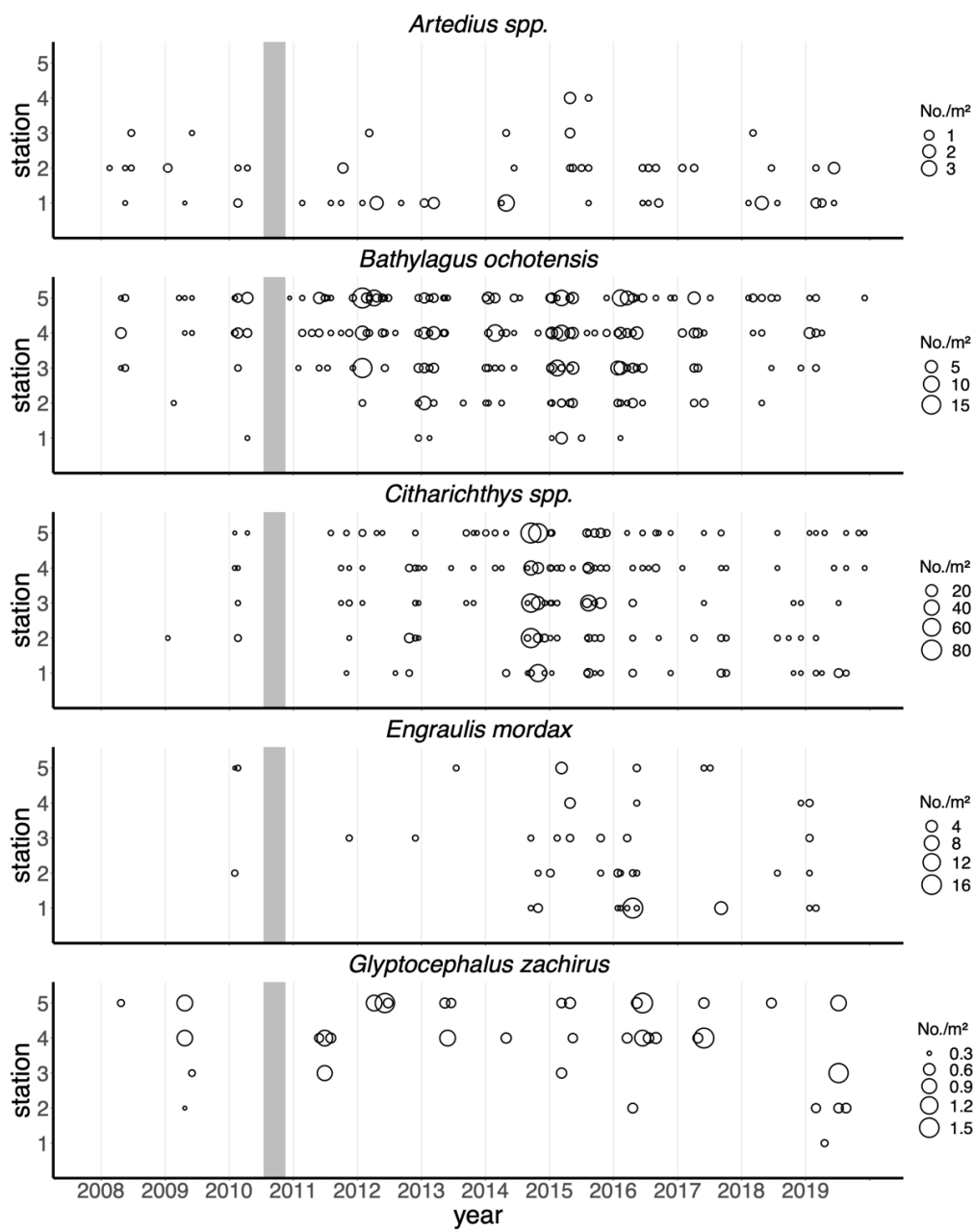
Average cross-shelf distributions within the rockfishes were mostly consistent throughout the time series, although some taxa increased in density nearshore during certain years. For example, *S. entomelas*, and *S. saxicola*, typically found to be distributed offshore, appeared at TH02 for the first time in winter during the mild 2009-10 El Niño and again in higher densities in 2015-17 during the MHW. Similarly, *S. crameri* appeared at TH01 in early 2015 and at TH03 in early 2016, 2017, and 2019.

The seasonal occurrence of most taxa was generally consistent across the TH-line time series, although some taxa occurred outside of their normal range during certain years. For example, *E. mordax* and *P. vetulus* deviated from their normal seasonal occurrence during warmer years. *E. mordax* was most often present in late summer and fall months but occurred in unusually high densities in winter and early spring in 2015-16. *P. vetulus* was most often present in winter and early spring but was captured in summer and fall in 2015-18 before returning to their normal seasonal occurrence in early 2019.

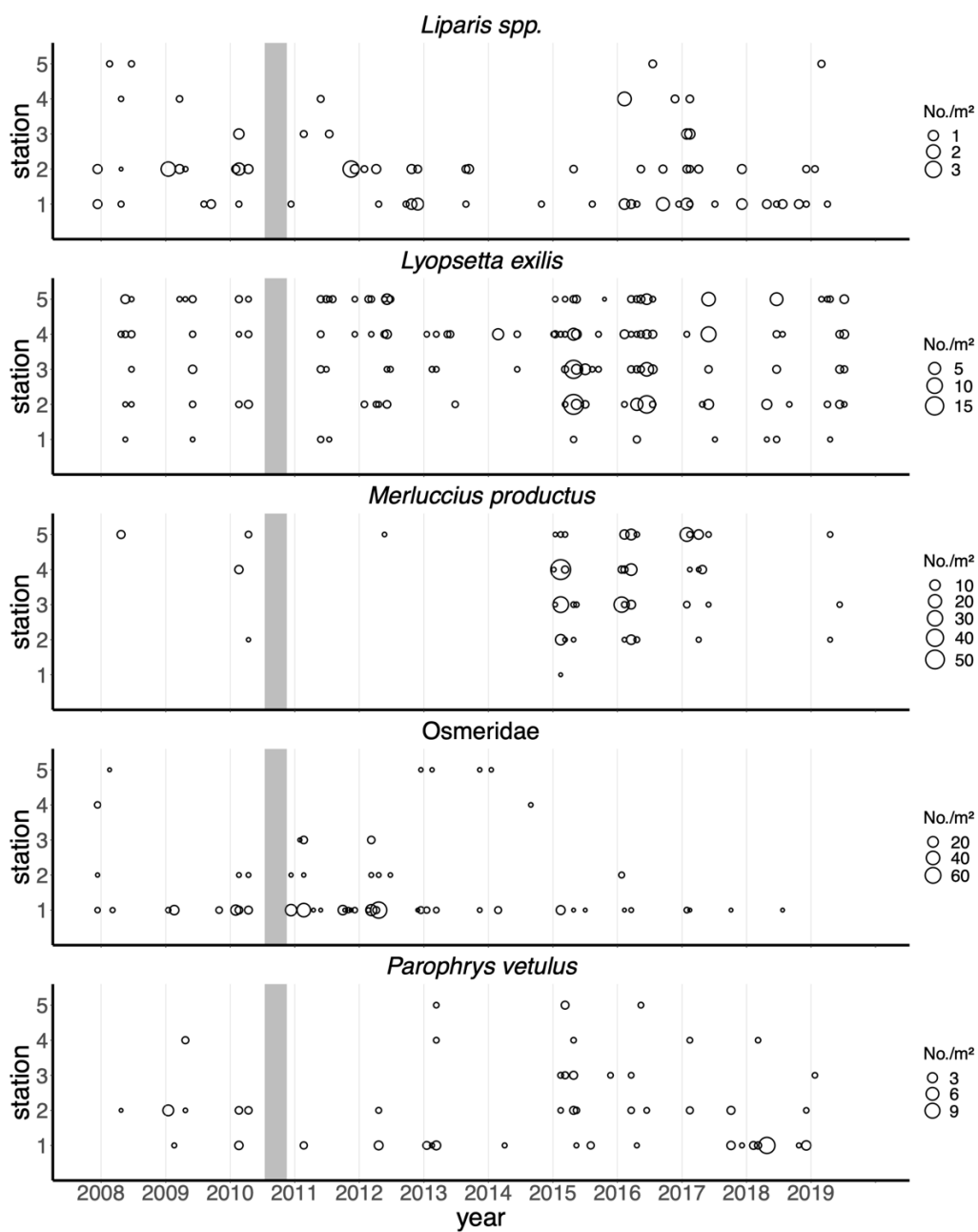
Most rockfishes were consistent with respect to their patterns of seasonal occurrence. Several summer spawning species (*S. aurora*, *S. diploproa*, WEVZ complex) were captured in winter months, well outside of their typical seasonal range: *S. aurora* was captured in January 2014, *S. diploproa* was captured in February 2016 and January 2017, and the WEVZ complex was captured in January 2017 and 2019 and February 2015 and

2016. No winter spawning rockfishes appeared to diverge substantially from their typical seasonal occurrence.

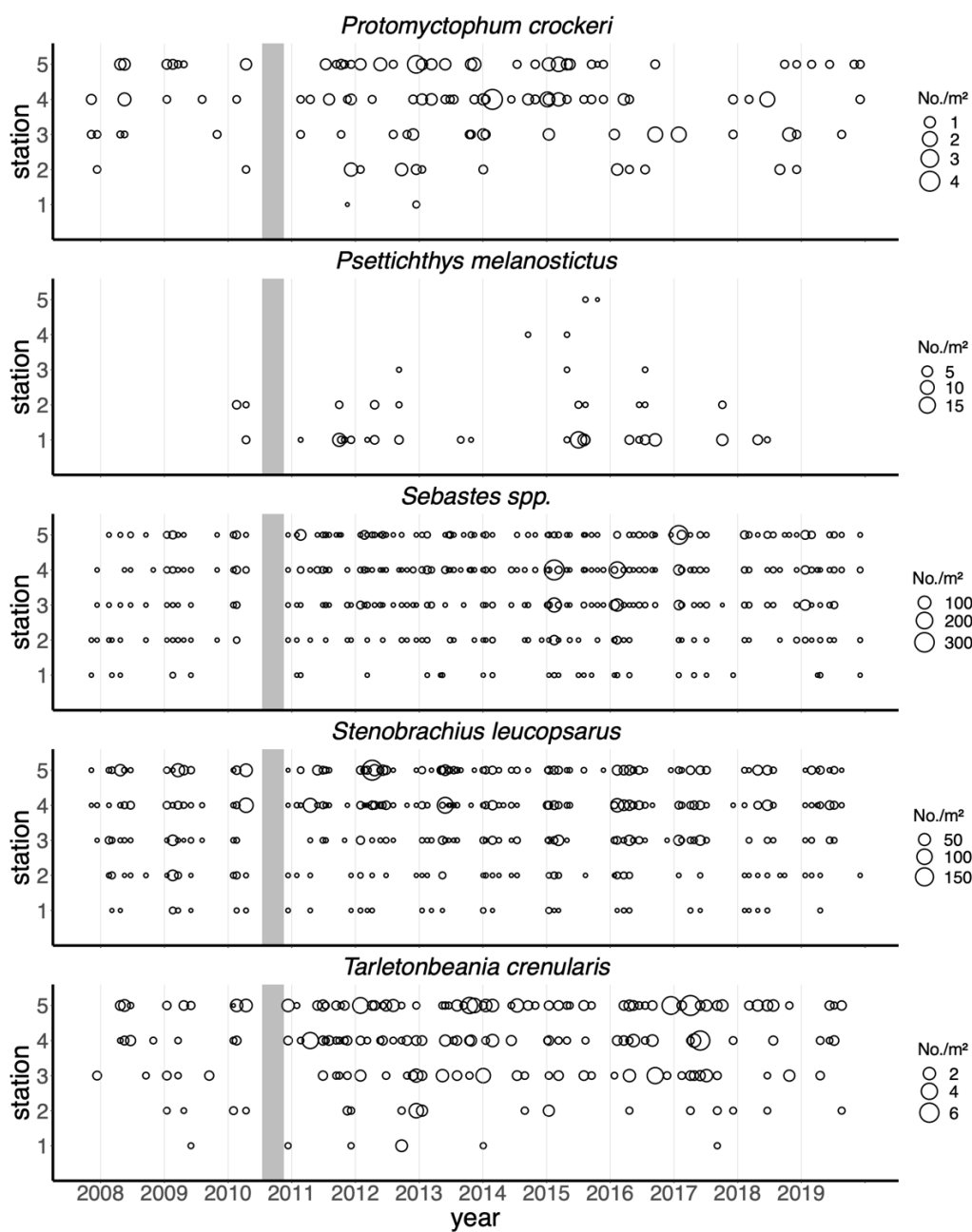
(A)



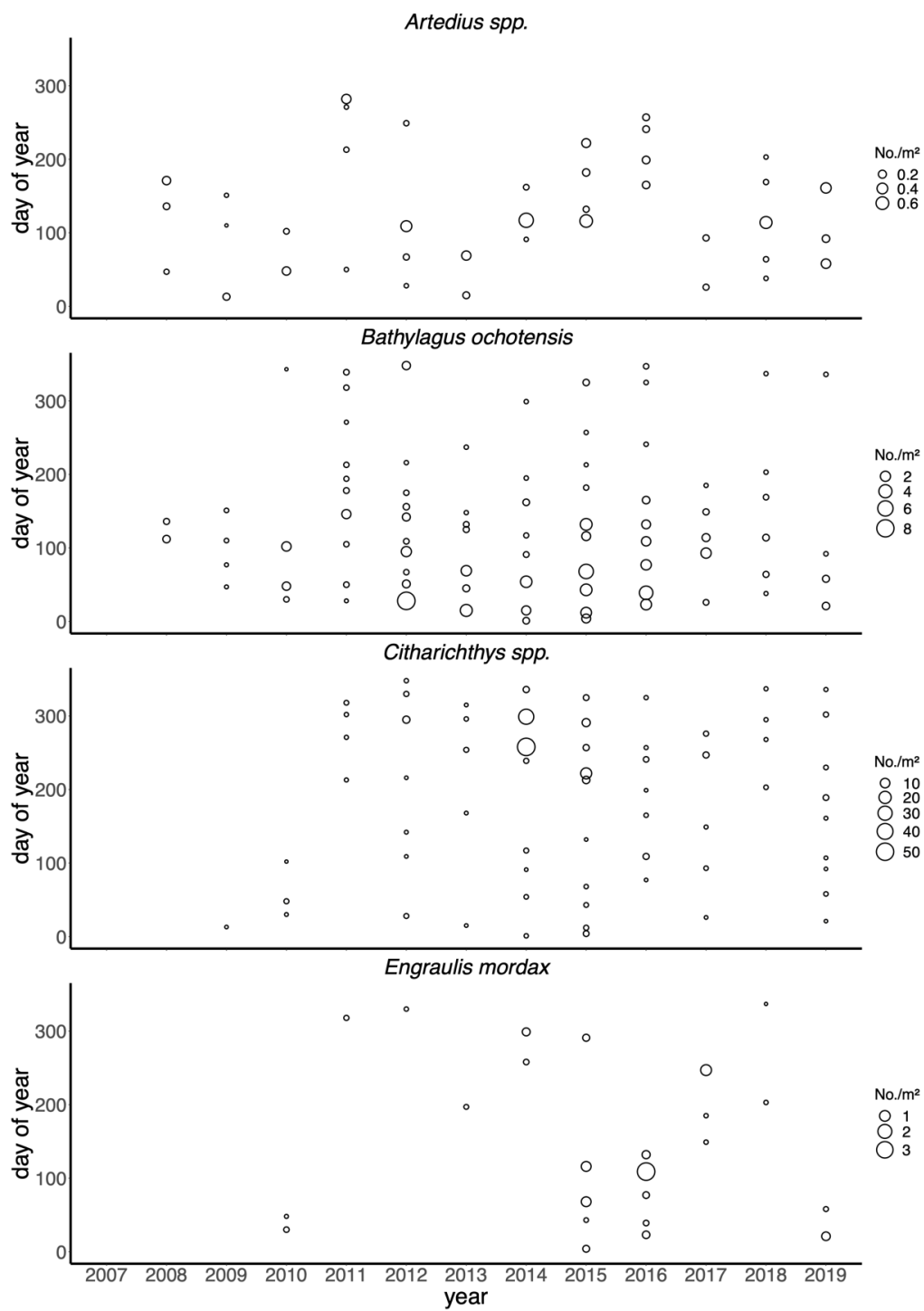
(A; continued)



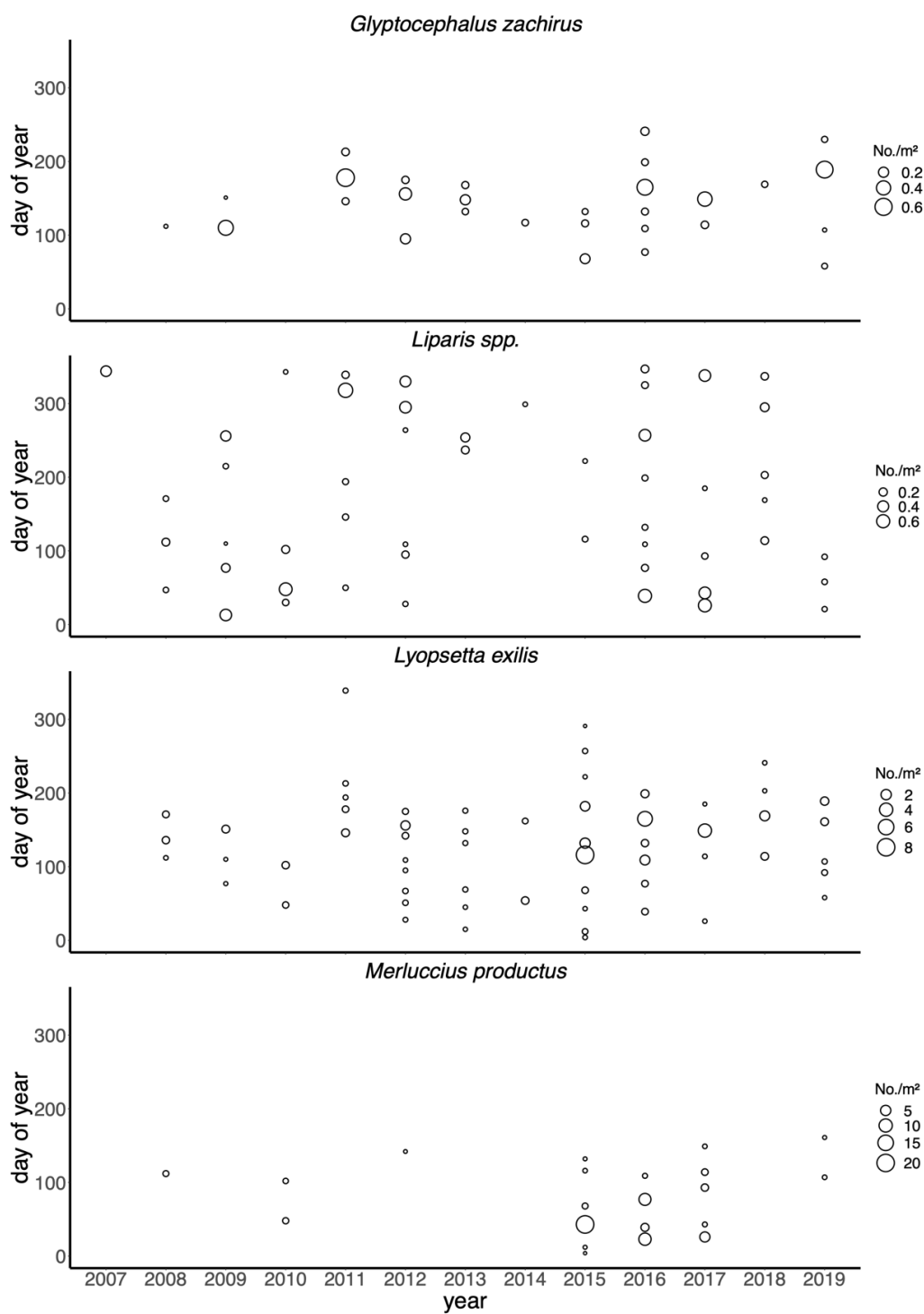
(A; continued)



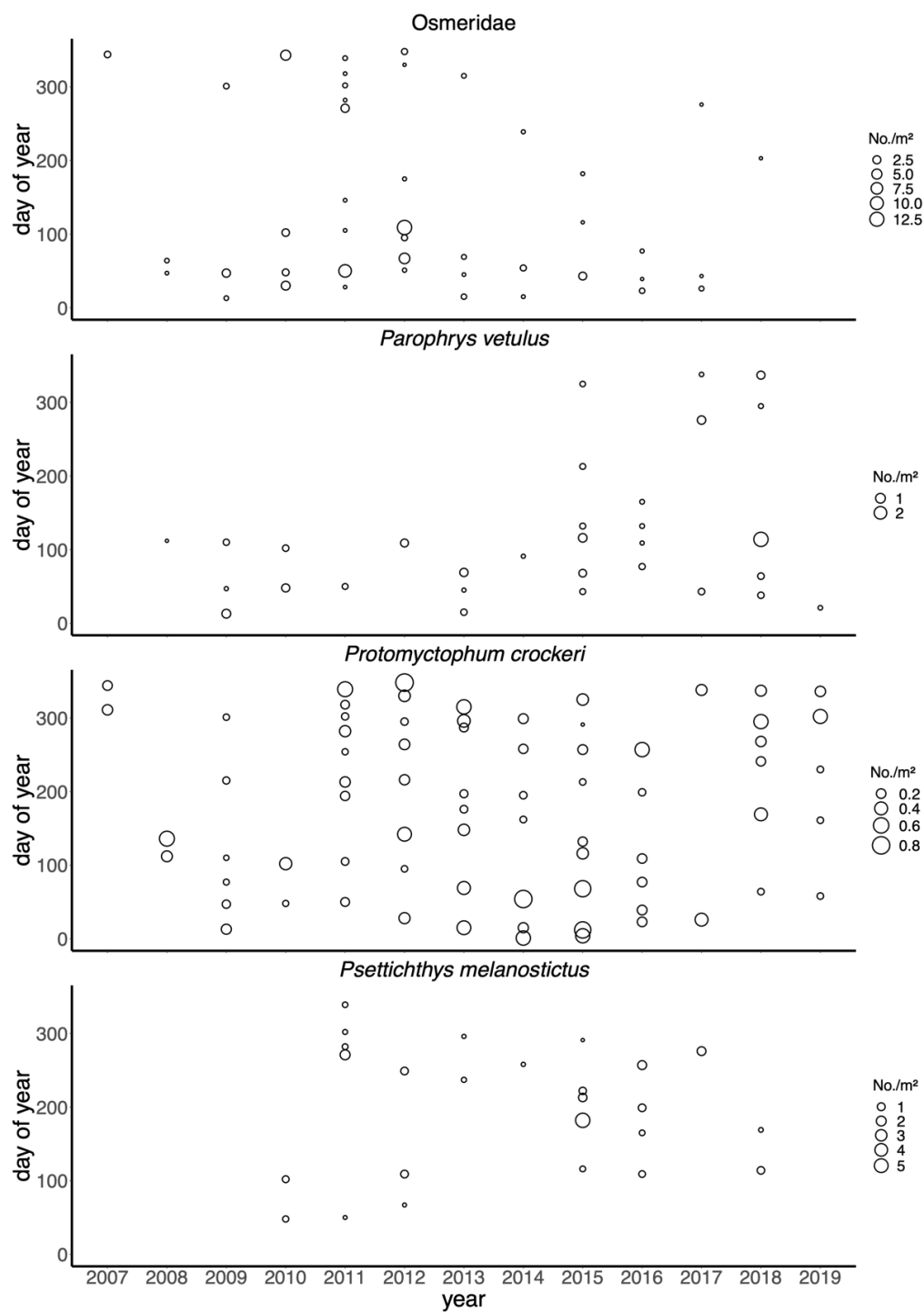
(B)



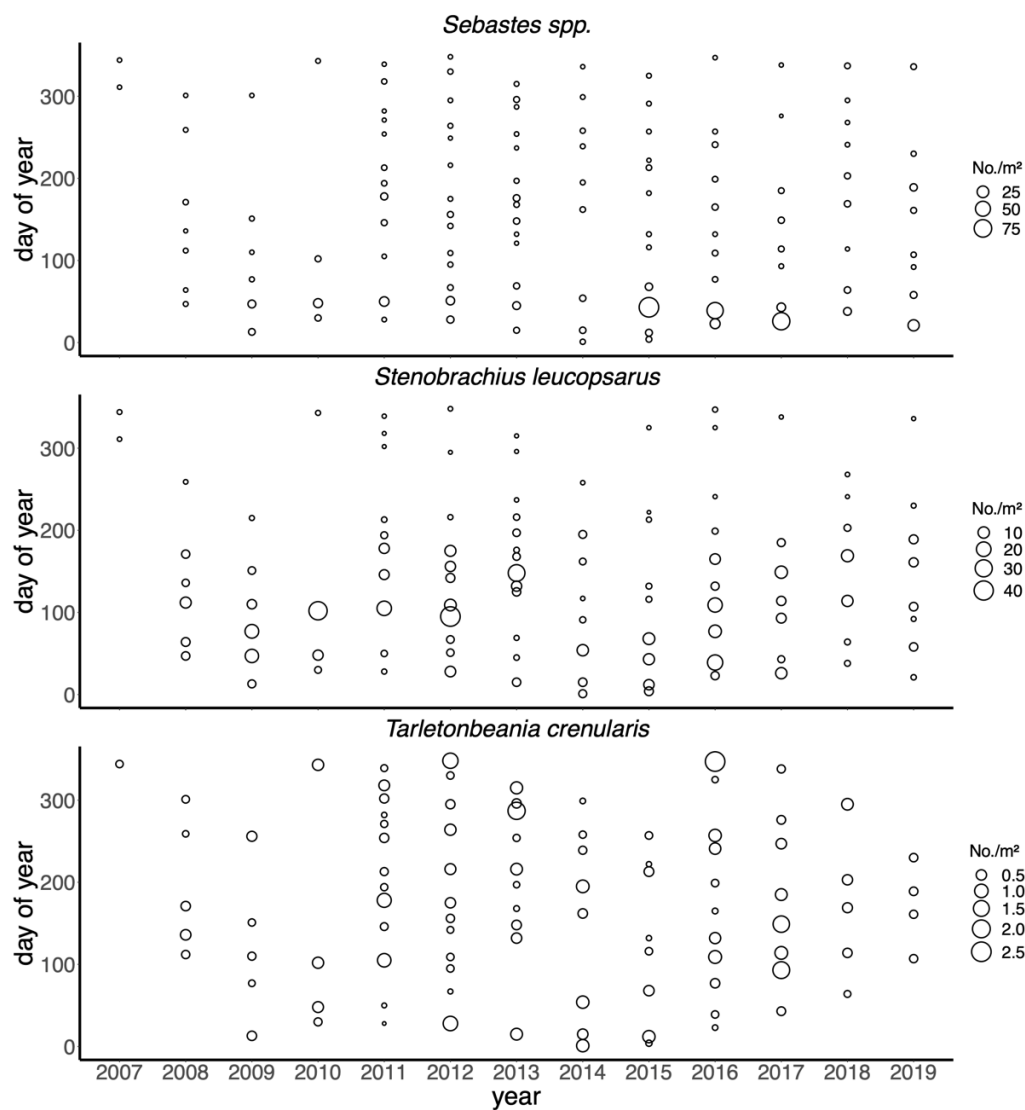
(B; continued)



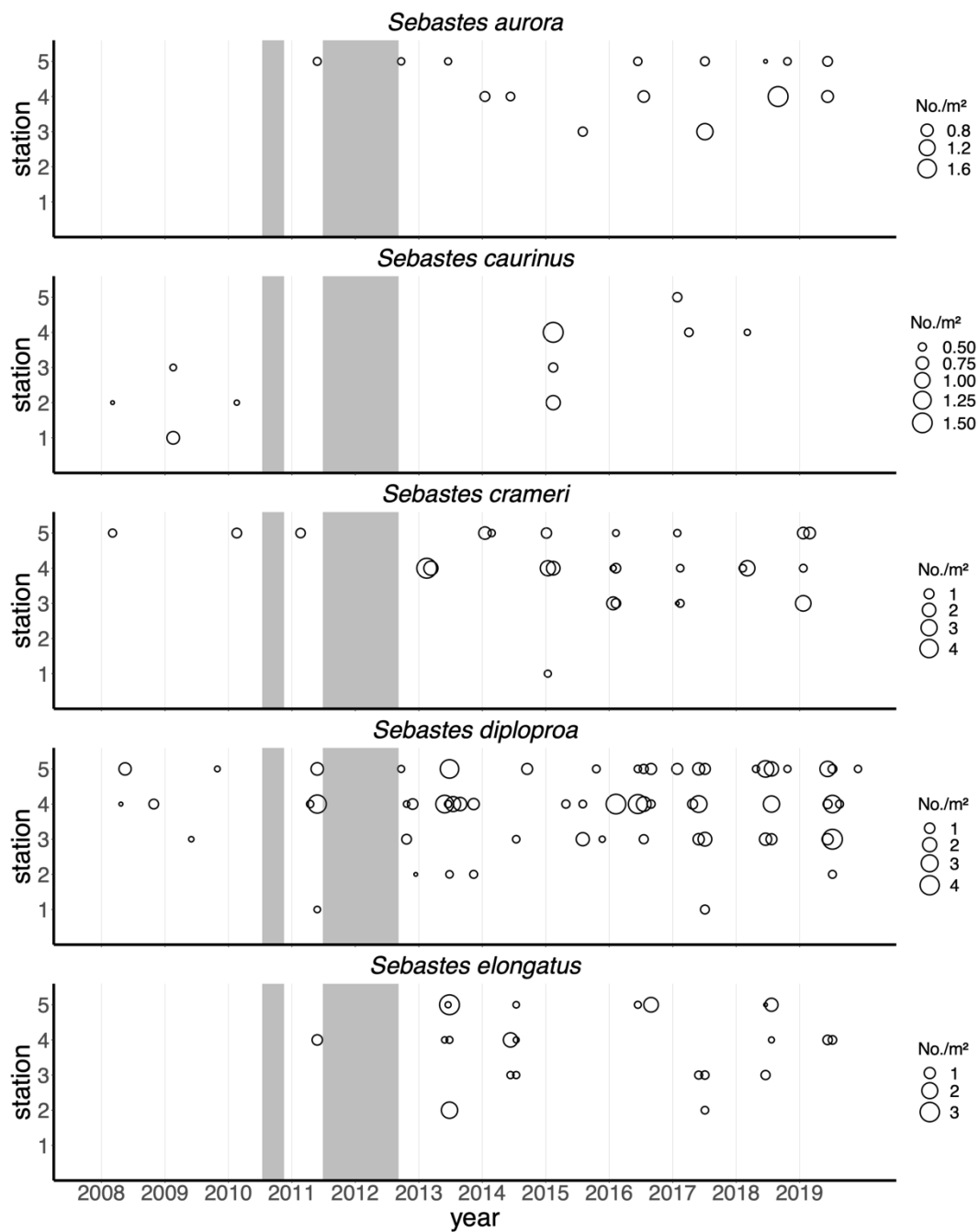
(B; continued)



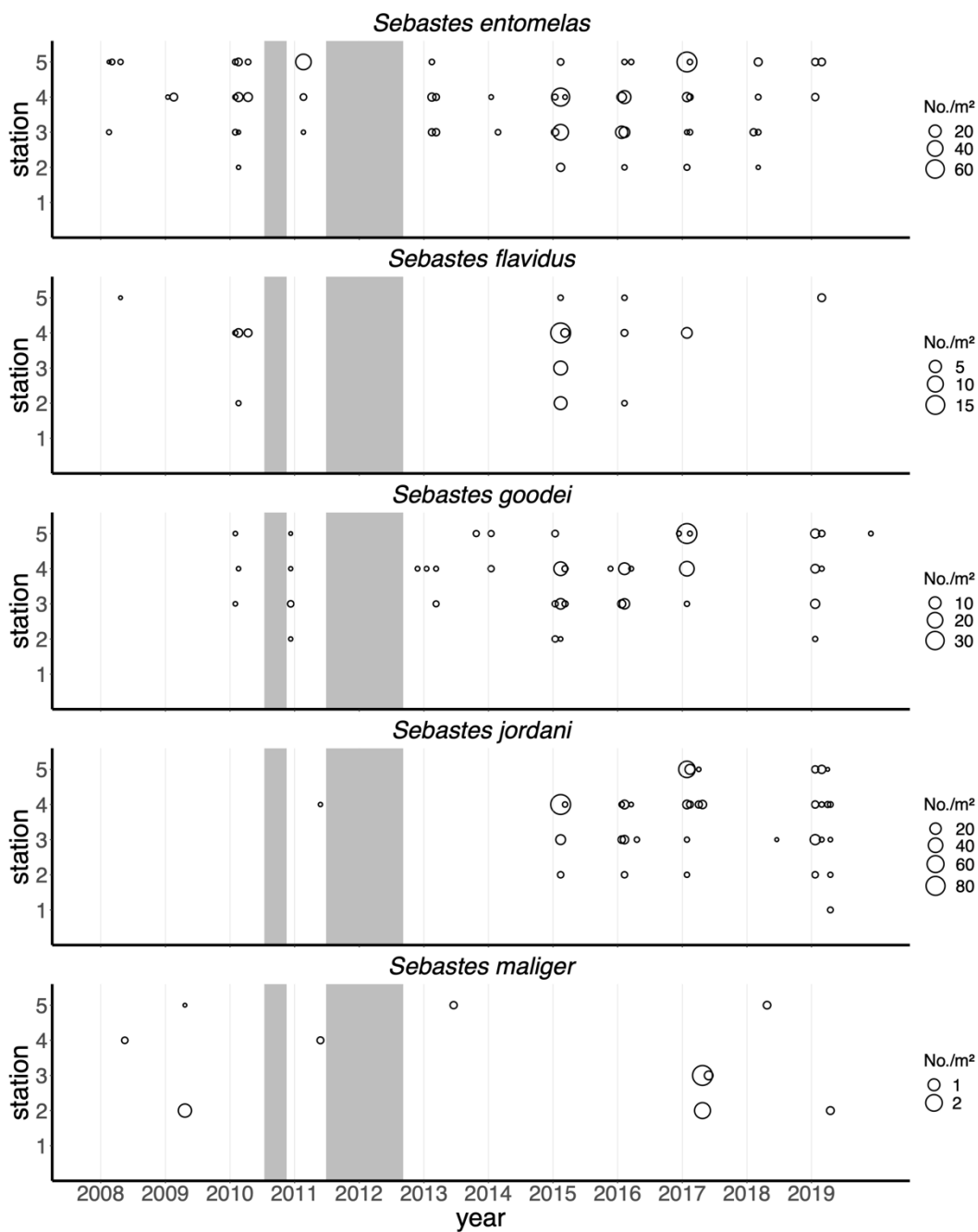
(B; continued)



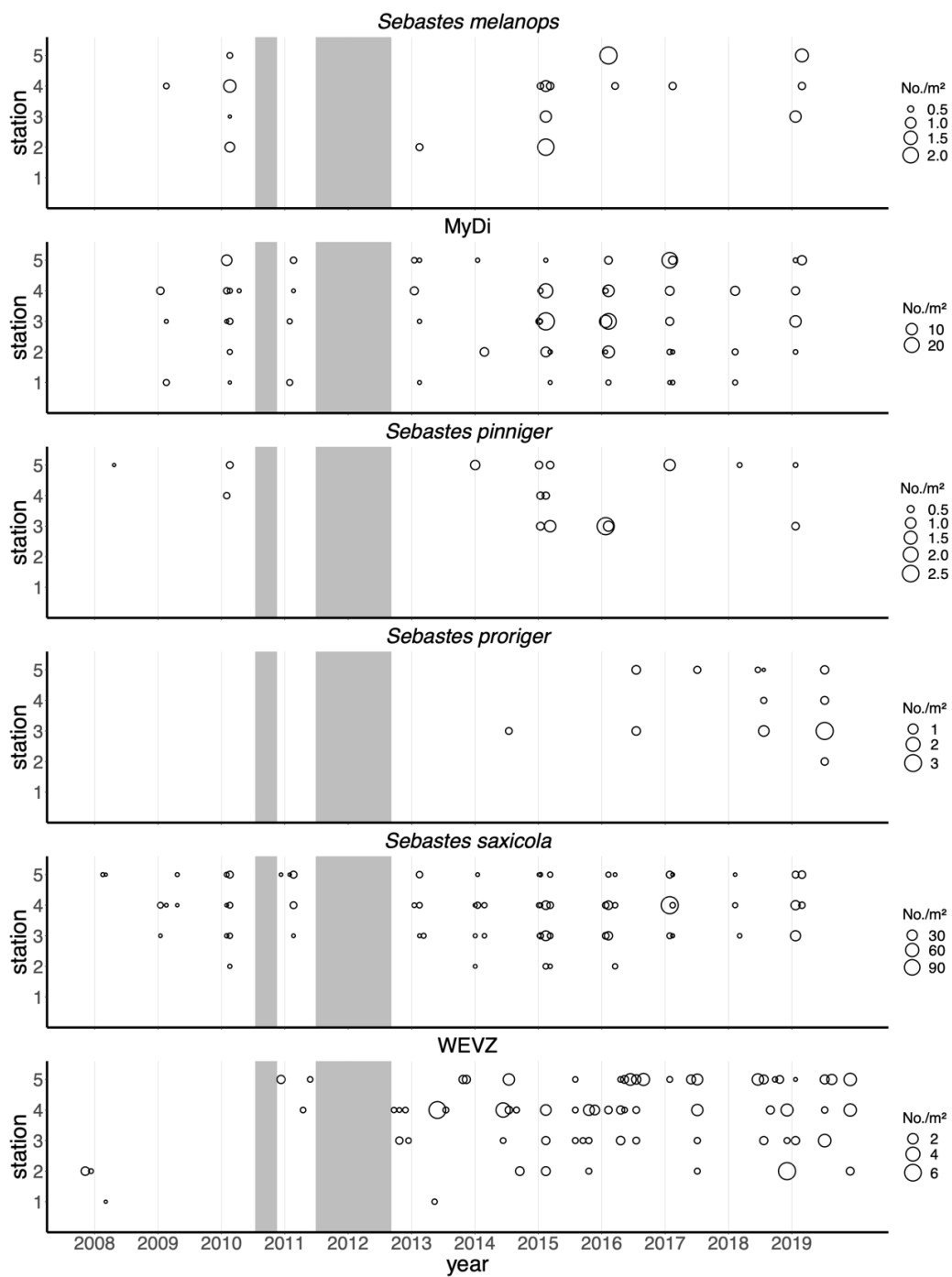
(C)



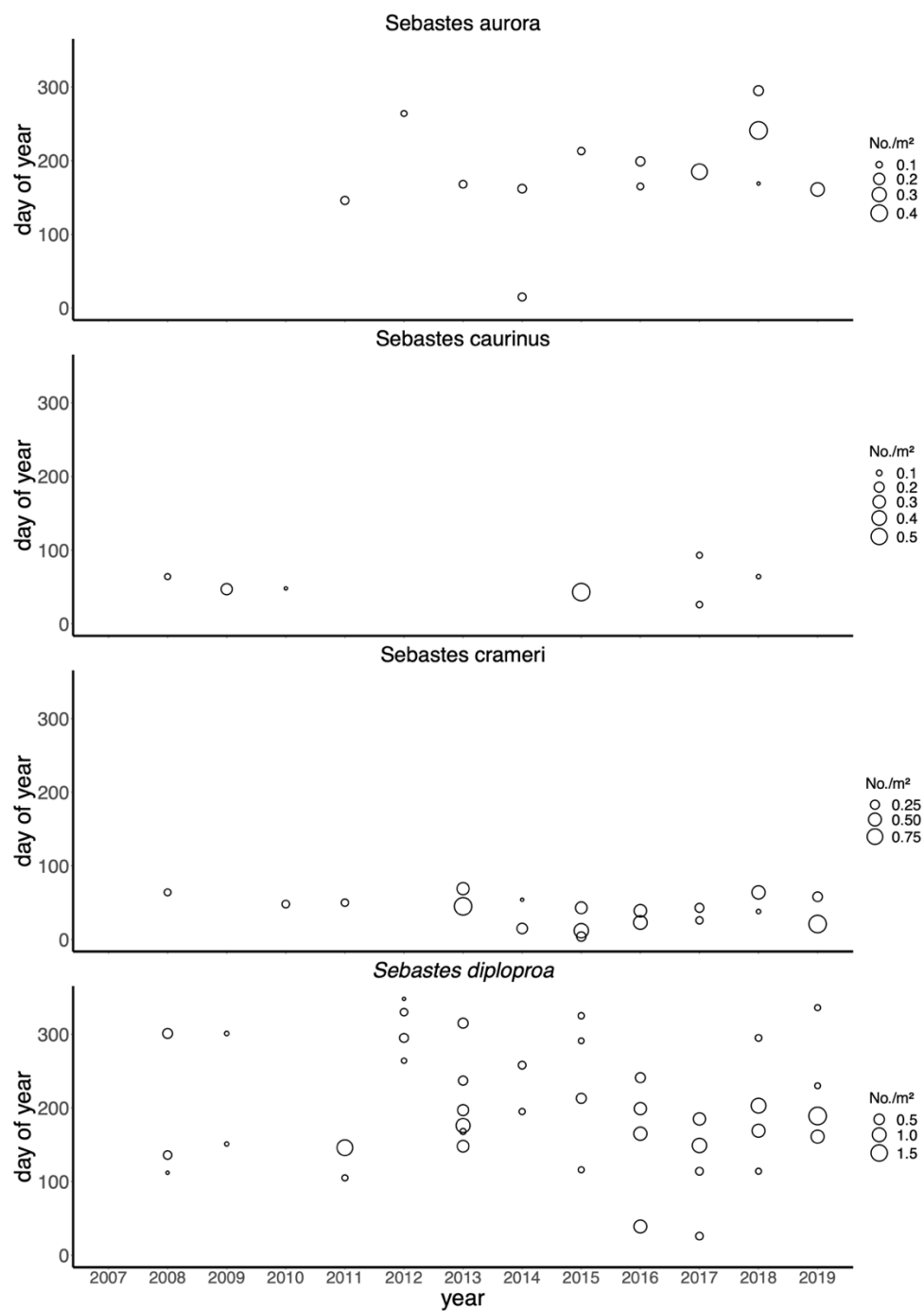
(C; continued)



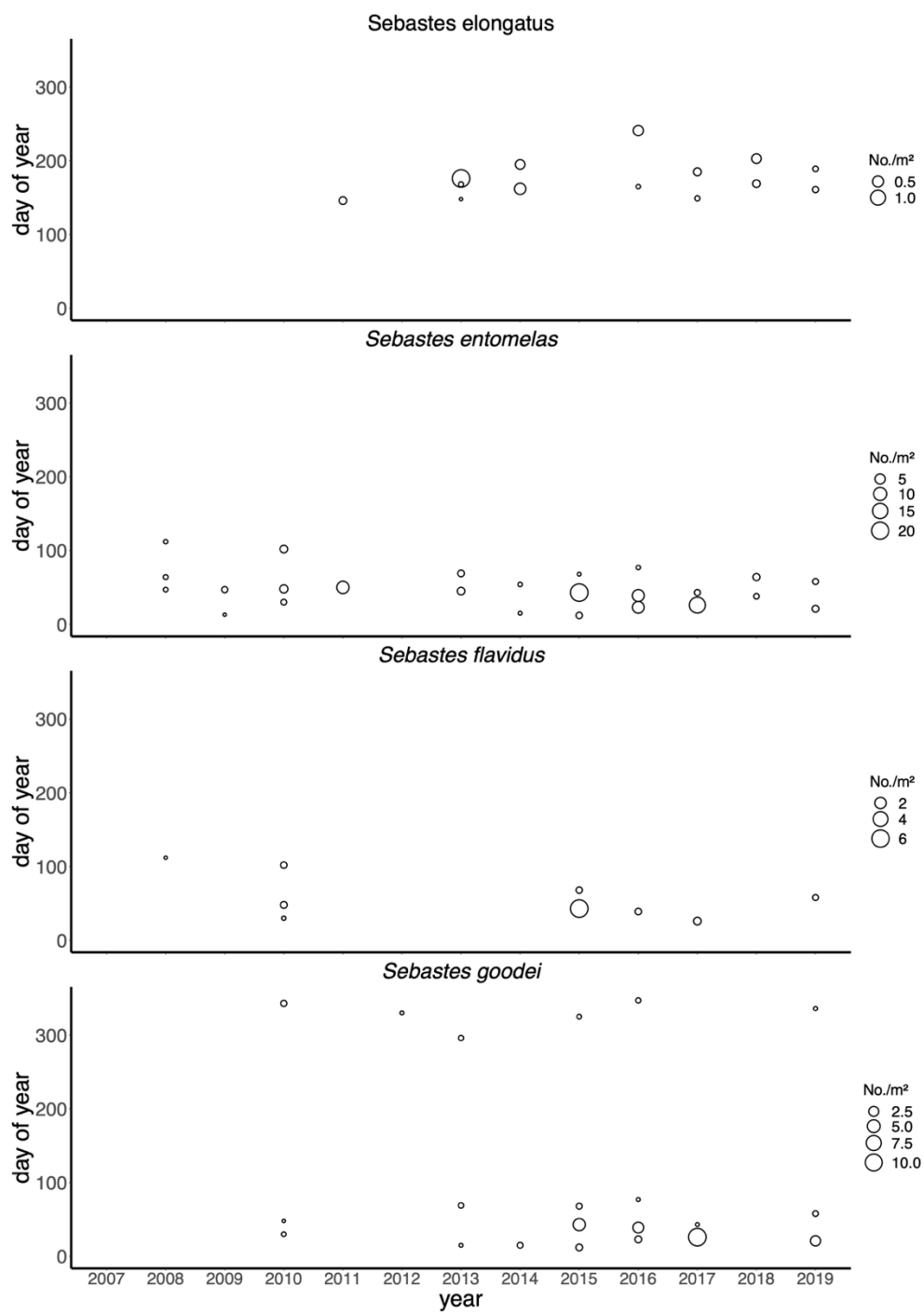
(C; continued)



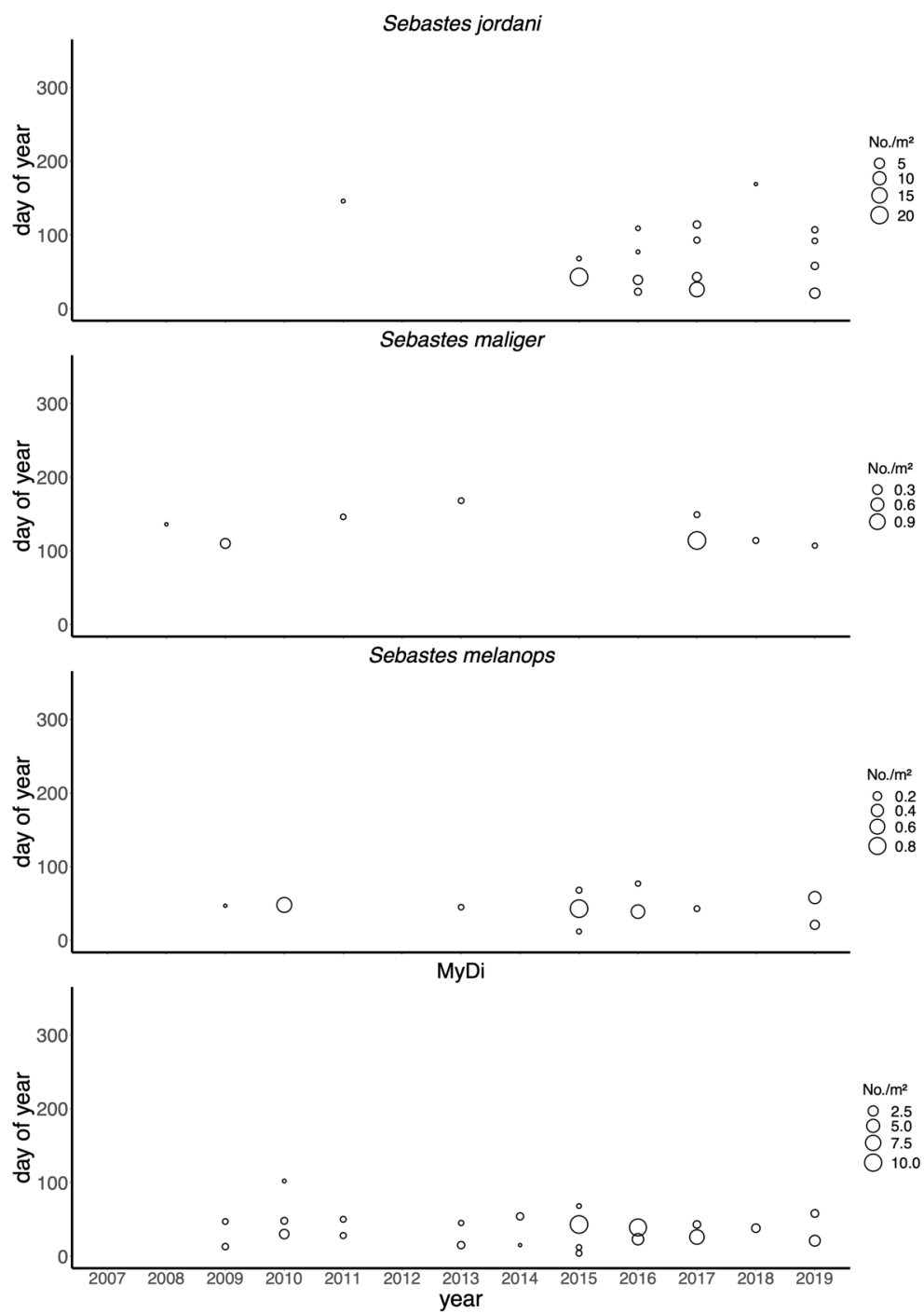
(D)



(D; continued)



(D; continued)



(D; continued)

